# Three-Dimensional Neural Differentiation of Mesenchymal Stem Cells.

---

Thesis submitted in fulfilment of the requirements for the degree of
Doctor of Philosophy (Science)

**Neus Gomila Pelegri**

October 2023

School of Life sciences
Faculty of Science
University of Technology Sydney

# Certificate of original authorship

I, Neus Gomila Pelegri, declare that this thesis is submitted in fulfilment of the requirements for the award of Doctor of Philosophy, in the Faculty of Science at the University of Technology Sydney.

This thesis is wholly my own work unless otherwise referenced or acknowledged. In addition, I certify that all information sources and literature used are indicated in the thesis.

This document has not been submitted for qualifications at any other academic institution.

This research is supported by the Australian Government Research Training Program.

Signature of candidate:

Production Note:
Signature removed prior to publication.

24th of October 2023

# Thesis format statement

In accordance with the University of Technology Sydney thesis committee 'Graduate Research Candidature Management, Thesis Preparation and Submission Procedures (Version 1.13, 2023)', this PhD thesis is presented by compilation. It is comprised of three chapters written in the traditional thesis format, one original research article submitted to a peer-reviewed journal and two original research articles published to peer-reviewed journals, of which I am the first author. I hereby declare that I have contributed significantly to these studies. For the Research articles, I carried out all experimental procedures and data analysis and drafted the first copy of the three research papers.

Production Note:
Signature removed prior to publication.

Neus Gomila Pelegri

24th of October 2023

# Acknowledgements

I would like to start by acknowledging the traditional custodians of the land where this research has been conducted, the Gadigal People of the Eora Nation. I pay respect to their Elders, past, present, and emerging, acknowledging them as the traditional custodians of knowledge for these lands.

Next, I would like to thank my supervisors, Cathy, Jerran, and Matt, who have helped me throughout this PhD, trusted my ability from the beginning and have kept sight of the finish line even when I couldn't see it. Thank you for everything you have taught me. Cathy, your patience, care, organisation, love for teaching and ability to troubleshoot anything and everything that comes your way has been inspirational. Thank you for teaching me that there is always a solution and to not let adversity get the best of me but rather grow from it. Jerran, your resourcefulness, and ability to always find funding and publications have been a great lesson on how to make the most of what we have. Matt, thank you for agreeing to become my supervisor halfway through. For helping me troubleshoot, listening to me every time I needed to talk things through and believing in me even when I didn't. I don't think I would have finished this PhD if it wasn't for you, and for that, I will forever be grateful. It has been incredibly beautiful to work alongside someone who loves what they do so much, who has so many students and people they help, and somehow, you always manage to do it all. Your work ethic and honesty have been so refreshing and inspiring. Thank you.

Thank you to Amy Bottomley and the Microbial Imaging Facility at UTS for their professional assistance and collaboration in several parts of this project.

Thank you to Aleksandra Stanczak for being the best intern I could have asked for. Your involvement in this PhD and ability to step in when needed was really helpful. Thank you for also becoming a good friend in the process, I will forever cherish our time working together.

Thank you to the NIRU group, especially to Reggie; thank you for being an incredible colleague to do a PhD along with. Your hard work and dedication have been inspirational. I still remember when I first taught you when you were finishing undergraduate, and I was fresh at teaching. I am very glad I now get to call you a friend. Caitlin, your support during this time has also been really appreciated. It has been great to have another crazy plant lady to share tips and obsess over plants with!

Thank you to the Proteomics core facility for their professional support during this candidature. Thanks for the best time in Lorne; that conference was by far the best I have been to, and it was thanks to you all.

Thank you to Max Cummins, for his professional support and input in this PhD. Your expertise has been invaluable in making this PhD the best it can be. At a personal level, thank you for the support and love you have given me for a large proportion of this endeavour. Thank you to the Cummins family as well for your love and support it has been really appreciated.

To Carolina and the Zajc family. Thank you for the support and advice you have always given me and for reminding me what I am made of and how hard I have worked for this every time I forgot and wanted to give up.

To my girlfriends Narina, Elise, Bianca, Emma, Bella, Adri, Cecilia, Silvia, Tegan, Caitlin who have been there through thick and thin and have consistently shown up for me and listened to me even if they didn't know what I was talking about. Thank you for holding space for me in the most beautiful way. Thank you for supporting me when things got tough and celebrating all my wins with me. I love you all so much, and while you are all scattered around the globe (and I can't hug you as much as I would like), I am grateful to have you in my life.

To Christine, Lynda and Alison, your love, support, and trust in me have been greatly appreciated. Thank you for helping me become the best version of myself, helping me grow through adversity, and helping me navigate my mental health through all the ups and downs. There has been a lot of it in these 5 years of PhD, and your support has been crucial.

To Elena, for always being there for me and giving me as many pep talks (and tarot readings) as I needed. To help me believe I would get it to the finish line even when I didn't. Thank you for not letting me fall through the cracks when things felt all too much and I just wanted to run away.
To Emy, I am not sure what I would have done without you. Thank you for always giving me advice and helping me find my light when everything seems dark. For making sure I stayed healthy and supporting me and my health when I got sick.

To my big sister Gloria for your unwavering trust in me and for being the best friend anyone could ask for. Thank you for always being there no matter what. I miss you terribly, but I know we will always be connected no matter how many kilometres separate us. Thank you for giving me the most beautiful niece I could have asked for, Elsa you always brighten my days, even if through a screen. Cannot wait to hug you both very soon.

Thank you to the most important person in my life. My mum. Thank you for giving me life and forever unconditionally loving me. Thank you for always supporting me financially and emotionally. Especially when 10 years ago I decided I wanted to leave Spain and move to Australia. Your unconditional love and support have made me who I am today. Thank you for being the person to always pick me up when I'm down, the unwavering support that never goes away. Thank you for showing me how to be a strong independent and loving person, full of integrity and grace despite the many challenges life throws at us. I will forever look up to you and to the calibre of a human you are. Your love and support will always be unmatched. Thank you for being the most supportive mother I could had ever asked for and always reminding me how proud you are of me. I miss you so much and I cannot wait to hug you again very soon and celebrate with you this massive achievement.

And lastly, I would like to dedicate this thesis to my maternal grandmother Margarita, a woman who was well ahead of her time, with a lot of grace and a big vision, who always carried forward no matter what and looked after all her loved ones. And to my maternal grandfather Jaume, who despite all the pain and suffering he went through in his lifetime, his heart never closed off. To whom I owe my love for creating with my hands and my ever-loving heart. Thank you both for showing me that the unseen world does indeed exist. You both will forever live through me. This thesis would have never happened if it wasn't for the sacrifices, you made and I hope it makes you proud.

And to all women who are doing hard things, breaking the rules, and challenging the system, Thank you. Thank you to all of you who have paved the way before me so that I could accomplish what I have accomplished.

Thank you to everyone who has been part of my life the last 10 years I have spent overall studying at UTS. This PhD marks the end of an era that, while really hard at times, I will forever cherish. It has shaped me into the resilient woman I am today, and for that, I will be forever grateful.

And thank you to you for reading this piece of work that has taken a lot of strength, dedication, resilience, and commitment to achieve.

# Publications

**The following publications have arisen directly from the work contained within this thesis.**

*Pelegri NG, Milthorpe BK, Gorrie CA, Santos J. Neurogenic marker expression in differentiating human adipose derived adult mesenchymal stem cells. Stem Cell Investig. 2023 Mar 23;10:7. doi: 10.21037/sci-2022-015. PMID: 37034185; PMCID: PMC10076228.*
Published in March 2023

*Gomila Pelegri, N.; Stanczak, A.M.; Bottomley, A.L.; Milthorpe, B.K.; Gorrie, C.A.; Padula, M.P.; Santos, J. Adipose-Derived Stem Cells Spontaneously Express Neural Markers When Grown in a PEG-Based 3D Matrix. Int. J. Mol. Sci. 2023, 24, 12139. https://doi.org/10.3390/ijms241512139*
Published in July 2023

*Gomila Pelegri, N.; Stanczak, A.M.; Bottomley, A.L.; Cummins, M.L.; Milthorpe, B.K.; Gorrie, C.A.; Padula, M.P.; Santos, J. Neural Marker Expression in Adipose-Derived Stem Cells Grown in PEG-Based 3D Matrix Is Enhanced in the Presence of B27 and CultureOne Supplements. Int. J. Mol. Sci. 2023, 24, 16269. https://doi.org/10.3390/ijms242216269*

# Conference Proceedings

Lorne Proteomics 2023 annual meeting, Victoria Australia – poster presentation
*Adipose-derived stem cells spontaneously express neural markers when grown in a PEG-based 3D matrix.*

# Funding and scholarships

This research was funded by:

Australian Government Research Training Program Stipend Funded by the Commonwealth Government Department of Education and Training.

Partially funded by the Schwartz Foundation philanthropic donation to support research.

# Table of Contents

# List of figures



***Please note that the Figures listed above include those in chapters one, three, and six only.**

# List of tables



***Please note that the Tables listed above include those in chapters one, three, and six only.**

# Abbreviations

% - Percentage

2D – Two dimensions

3D – Three dimensions

AD – Alzheimer's disease

ADSCs – Adipose-derived stem cells

ALS – Amyotrophic lateral sclerosis

ANOVA – Analysis of variance

BMSCs – Bone marrow stem cells

C1 – CultureOne

CNS – Central nervous system

$CO_2$ – Carbon dioxide

DMEM – Dulbecco's modified eagles' medium

DoS – Degrees of substitution

ECM – Extracellular matrix

ESCs – Embryonic stem cells

FBS – Foetal bovine serum

GBCs – Glioblastoma cells

GelMa – Gelatin Methacrylate

hADSCs – Human adipose derived stem cells

iPSCs – Induced pluripotent stem cells

kDa – Kilodalton

kPa – Kilopascal

LAP – Lithium acylphosphinate

MAA – Methacrylic anhydride

MSCs – Mesenchymal stem cells

MWCO – Molecular weight cut off

NBCs – Neuroblastoma cells

NIHR – National institute of health registry

nm – Nanometre

NPCs – Neural progenitor cells

NSCs – Neural stem cells

OaC – Organ on a chip

PBS – Phosphate-buffered solution

PEG – Polyethylene Glycol

PEGDA - Polyethylene Glycol Diacrylate

pH – Potential of hydrogen

PNS – Peripheral nervous system

RGD – Aginine-glycine-aspartic acid

SCI – Spinal cord injury

SGZ – Subgranular zone

UV – Ultraviolet light

V-SVZ – Ventricular-subventricular zone

w/v – Weight per volume

PBS – Phosphate buffered solution

µL – Microliter

***Please note that the abbreviations listed above include those in chapters one, three, five and six only.**

# Abstract

Neurological disorders are the leading cause of disability and death worldwide, with over 9 million deaths annually. They have a large socioeconomic impact for many countries with dementia generating costs of up to US$818 billion in 2015 alone. Living with neurological conditions also has a significant effect on people's lives, with many comorbidities associated with them. The complex and inaccessible nature of the nervous system, as well as its limited self-healing capacity, have made research translation challenging. To date, most neurological conditions remain poorly understood, incurable and difficult to treat, in spite of the considerable research that has been undertaken to better understand and treat them. The number of individuals affected by neurological conditions is growing yearly, and the need for more research that translates into clinical therapies has become unquestionable. Research translation has been limited by the lack of more physiologically relevant models. Animal models and traditional 2D tissue culture are the most widely used techniques to study neurological conditions and test potential therapeutic agents. However, they have proven to not be representative of *in vivo* conditions in humans. Particularly in 2D models, the cell architecture and arrangement are vastly different from the native tissue. To address these issues, tissue engineering and 3D culture models provide a new avenue to create a cell growth environment that better mimics the brain. However, healthy neural cells are still difficult to source for the creation of these 3D models. We may be able to overcome this issue by utilising human Adipose-derived stem cells (hADSCs). hADSCs are relatively easy to obtain and have the capacity to differentiate into neural cells and, therefore, may be an excellent source of cells for 3D models to study and treat neurological conditions.

This thesis describes the investigation of a suitable 3D model to efficiently differentiate hADSCs into neural cells. Chapter One is an introduction to the field. Chapter Two assesses the effects of commercially available neural supplements (B27, CultureOne and N2) on 2D-grown hADSCs. These experiments found that while the supplements had neurodifferentiation effects on the cells, the 2D environment was not suitable for long-term differentiations, with cells starting to detach from the tissue culture plate after 7 days. Chapter Three explored the use

of GelMa as a 3D matrix to mimic the brain environment. However, those experiments were not successful, and the focus moved to other matrices. Subsequently, Chapter Four explored the use of bioprinted PEG-based hydrogels at 1.1kPa with RGB and YIGSR peptides as a model to grow hADSCs for neural differentiation for 14 days. That research showed good cell viability as well as spontaneous neural marker expression from the cells, suggesting that the model was a suitable one to further explore neural differentiation of hADSCs in 3D matrices. Chapter Five explored the combination of the PEG-based 3D matrix studied in Chapter Four, together with the neural support supplements used in Chapter Two. Results showed that the addition of the supplements further enhanced neural differentiation marker expression in the hADSCs, suggesting that the use of both the PEG-based 3D matrix and the supplements are a good combination for ADSCs neural differentiation, warranting further research.

# Thesis Structure

This thesis has been structured by compilation, and there are numbered references at the end of each chapter.

**Chapter One:** Background and literature review.

**Chapter Two:** Neural differentiation of ADSCs grown in a 2D environment – Published work:
*Pelegri NG, Milthorpe BK, Gorrie CA, Santos J. Neurogenic marker expression in differentiating human adipose derived adult mesenchymal stem cells. Stem Cell Investig. 2023 Mar 23;10:7. doi: 10.21037/sci-2022-015. PMID: 37034185; PMCID: PMC10076228.*

**Chapter Three:** Will examine the use of GelMa hydrogel-based 3D matrixes as models for growing and differentiating ADSCs towards a neuronal lineage.
Unpublished work:
*ADSCs in 3D GelMa matrices*

**Chapter Four:** Will compare the growth and changes of ADSCs in 2D vs. 3D in PEG-based hydrogels.
Published work:
*Gomila Pelegri, N.; Stanczak, A.M.; Bottomley, A.L.; Milthorpe, B.K.; Gorrie, C.A.; Padula, M.P.; Santos, J. Adipose-Derived Stem Cells Spontaneously Express Neural Markers When Grown in a PEG-Based 3D Matrix. Int. J. Mol. Sci. 2023, 24, 12139. https://doi.org/10.3390/ijms241512139*

**Chapter Five:** Will compare the same 3 supplements used in Chapter Two using the same PEG-based matrix used in Chapter Four.
Published work:

*Gomila Pelegri, N.; Stanczak, A.M.; Bottomley, A.L.; Cummins, M.L.; Milthorpe, B.K.; Gorrie, C.A.; Padula, M.P.; Santos, J. Neural Marker Expression in Adipose-Derived Stem Cells Grown in PEG-Based 3D Matrix Is Enhanced in the Presence*

*of B27 and CultureOne Supplements. Int. J. Mol. Sci. 2023, 24, 16269. https://doi.org/10.3390/ijms242216269*

**Chapter Six:** Conclusions, limitations, and future directions.

# Chapter One: Background and literature review

## 1.1. Introduction

The nervous system is a complex and intricate network of organs, tissues and cells that are responsible for the coordination of all body activities. It facilitates communication between all bodily systems, governs all bodily functions from cognition and emotion, to movement, sensations (sight, hearing, taste, touch, and smell) and basic bodily functions including regulation of the circulatory, respiratory, renal, digestive, and reproductive functions [1].

There are two main parts to the nervous system: the central nervous system (CNS), which includes the brain and spinal cord; and the peripheral nervous system (PNS) which includes all the nerves that branch off from the spinal cord and extend to all parts of the body [2]. Disruption to the functions of either the CNS or PNS, either of traumatic or non-traumatic/degenerative nature, can lead to a wide range of neurological disorders such as Alzheimer's disease, motor neuron disease, multiple sclerosis, stroke, brain and spinal cord injuries, infections and neuroinflammation that lead to poor health outcomes and suffering in affected individuals [3]. Furthermore, the nervous system has limited self-repair capacity. Neurological conditions are the leading cause of disability and death worldwide with 9 million deaths per annum attributed to such conditions [4-6]. They have devastating socio-economic impact for many countries, with dementia alone generating costs up to US$ 818 billion in 2015 [7] and predicted to surpass US$ 2.8 trillion by 2030 [8] . While considerable research has been undertaken to understand each disorder and identify potential therapeutic agents [9-11] most remain poorly understood, incurable and difficult to treat. With a growing number of affected individuals, the need for research and translation into clinical therapies has become unquestionable [11, 12].

Unfortunately, studying the human nervous system *in vivo* is challenging due to the complex and inaccessible nature of the brain and spinal cord. Historically, researchers have been limited to studying these disorders using *in vivo* and *ex*

*vivo* animal models, and 2D culture models (Table 1), the results of which have proved to be ineffective in human clinical trials [11, 12]. This poor translation has been mainly attributed to the lack of an accurate *in vitro* model of the CNS to test treatments on human cells [10, 13-15], and highlights the need to develop a more suitable cell culture model for neurological diseases.

**Table 1** Current CNS modelling techniques: Advantages and disadvantages

| Model type | Advantages | Disadvantages | References |
|---|---|---|---|
| ***In vivo*** | - Complex; suitable to characterise pathological conditions.<br>- Fit for long term studies.<br>- Anatomically relevant | - Expensive<br>- Not always relevant to humans<br>- Limited sample size<br>- Low control over variables<br>- Challenging to quantify results | [16, 17] |
| **Ex vivo** tissue sections | - Complex structure<br>- All cell types present | - Loss of tissue function<br>- Short-term<br>- Limited access to human tissue | [18, 19] |
| **2D *in vitro*** | - Simple and Efficient<br>- Reproducible<br>- Low-cost<br>- High throughput<br>- Easily quantifiable<br>- High control over variables and environmental conditions | - Low complexity<br>- Short-term only<br>- Limited cell source availability<br>- Not always physiologically relevant. lacks the bigger picture of full organ or tissue<br>- Restricted insight into biological mechanisms and functions | [20, 21] |
| **3D *in vitro*** cell aggregates | - High throughput<br>- Quantifiable<br>- 3D environment – more physiologically relevant | - Restricted in variables vs complexity. Cannot have both high complexity and large amount of variables<br>- Shorter-term<br>- Cells become necrotic in the centre | [22] |
| **3D *in vitro*** scaffolds | - Reproducible<br>- Controlled complexity<br>- Suitable for long term studies<br>- Quantifiable<br>- Better understanding of biological mechanism<br>- Physiologically relevant | - Not well-established protocols<br>- Limited human cell sources<br>- Limited to tissue size<br>- Require bioreactors for long term experiments | [23, 24] |

This chapter will explore the different models and techniques being used to study the nervous system and its disorders. It will range from animal models, 2D tissue culture models and 3D tissue culture. It will touch on the different stem cells being looked at in the regenerative medicine field and their potential as treatment for

the multiple neurological disorders as well as the scaffolds and cells chosen for this research project.

## 1.2. Nervous system modelling techniques

*In vivo* animal models

*In vivo* animal models involve the use of a living organism to study pathologies, drug toxicity and efficacy, and more. Typically, they involve animals, which may be genetically modified and thus predisposed to the pathologies of research interest, subsequently exposed to traumas, infections, therapeutics and/or other experimental treatments [25]. Animal experiments are more complex and can be used to mimic pathological conditions more accurately than other models. They are suitable for long term studies to assess disease progression overtime, identify potential therapeutic targets, assess efficacy of potential treatments as well as to investigate and better understand pathogenesis [26, 27].

Common animal models for neurological conditions in vertebrates include rodents (mice and rats), monkeys and zebrafish. *In vivo* animal models have been used to study neurological disorders for decades and several animal models for diseases including Parkinson's Disease, Alzheimer's, epilepsy, stroke have been established [25, 28]. While these have provided invaluable insight into pathogenesis and potential treatment avenues [27], they imperfectly model human disease progression and systems and thus the observations often translate poorly. Host responses to disease and therapeutics can vary greatly between species and this can lead to expensive and unsuccessful clinical trials [29-33]. Additionally, experiments involving animal models typically run for long periods, are time consuming and costly. Sample sizes are often restricted for logistical and ethical reasons and such models provide researchers with limited ability to study specific cellular and molecular mechanisms, and control certain variables (i.e. animal behaviour). Behavioural studies of such animals are often semi-quantitative in nature, which can limit their utility. Using animals for research purposes also presents ethical concerns [34]. Animals are sentient and many

disease models can cause physical pain and psychological distress. Additionally, the captive living conditions of research animals are vastly different to their natural habitat which can add to the suffering and impact the reliability of the results. Contrary to human subjects, animals are also unable to consent to participate in a particular study or clearly articulate when a procedure is too painful or be able to cease their participation when they chose to [34]. It is important to note that there aren't always alternatives to animal models, highlighting the need to investigate and improve models to study the nervous system.

*Ex-vivo* models

*Ex-vivo* models are also commonly used to study the nervous system. This approach hybridises *in vivo* models and tissue culture through excising tissue sections from living organisms and maintaining them in *in vitro* conditions similar to the tissue of interest [35-37]. For example, thin slices of brain or spinal cord are commonly cultured and studied as neural models *in vitro* [38, 39]. A particular region of interest can be selected from a target organ, for example the hippocampus, excised from fresh tissue and used to assess effects of treatments or study the interactions of different cells in that area [39-42]. In *ex-vivo* slices, the cellular architecture as well as intercellular connections are retained providing a better representation of *in vivo* conditions allowing investigation of specific cellular interactions and molecular mechanisms of disease progression and development in neurological disorders such as spinal cord injury [43], Alzheimer's disease [44], and Parkinson's disease [45, 46]. These are also often used to study tumours and cancerous growth [47].

While *ex-vivo* models have the ability to maintain more complex cellular interactions than in 2D culture models, they do not retain the entirety of interactions and functions present *in vivo*. Additionally, *ex vivo* slices of brain can only be maintained in tissue culture for a short time with cell loss becoming apparent after only a few hours post extraction [39, 48] which limits their utility in disease progression or treatment studies which typically occur over longer

periods of time. They also have low reproducibility, especially for tumour and cancerous growth study given each tumour is different [47]. Furthermore, typically e*x vivo* models for the nervous system utilise animal tissues [40, 43-46] due to the limited accessibility of fresh human nervous system samples [39, 48]. Similarly, as with *in vivo* animal models, study findings from *ex vivo* animal models often translate poorly to human applications [39, 48].

*In vitro* tissue culture: 2D vs 3D models

Tissue culture is a widely used technique for understanding the mechanisms of cell behaviour *in vitro.* It has become a fundamental tool to examine the biophysical and biomolecular mechanisms and functions of how cells assemble into tissues and organs [49]. Tissue culture is also essential to understand the mechanisms that cause underlying conditions in a cost-effective manner [49], allowing for tests to be conducted on human cells rather than using cost-intensive animal testing that may or may not be suitable, while reducing the ethical implications of animal models [15]. However, traditionally tissue culture has been conducted in 2D conditions where the cells grow in a 2D plane and rely on cell adherence to a flat surface, commonly polystyrene or glass, for mechanical support (Figure 1). The stiffness of these materials is magnitudes higher than that seen in soft tissues, poorly representing the tissue of origin. It is known that stiffness has a direct effect on cell adhesion, spreading, migration and differentiation [50]. Furthermore, the monolayer arrangement creates an unnatural environment where homogenous growth occurs on an XY plane only and provides equal exposure to oxygen, nutrients, growth factors and waste products [49, 51] (Table 2), which is not the case in an organ. This XY arrangement also limits cell-cell interactions and cells lack the stimulation to self-organize and become incapable of producing a biochemically relevant, tissue-like environment [49, 51, 52].

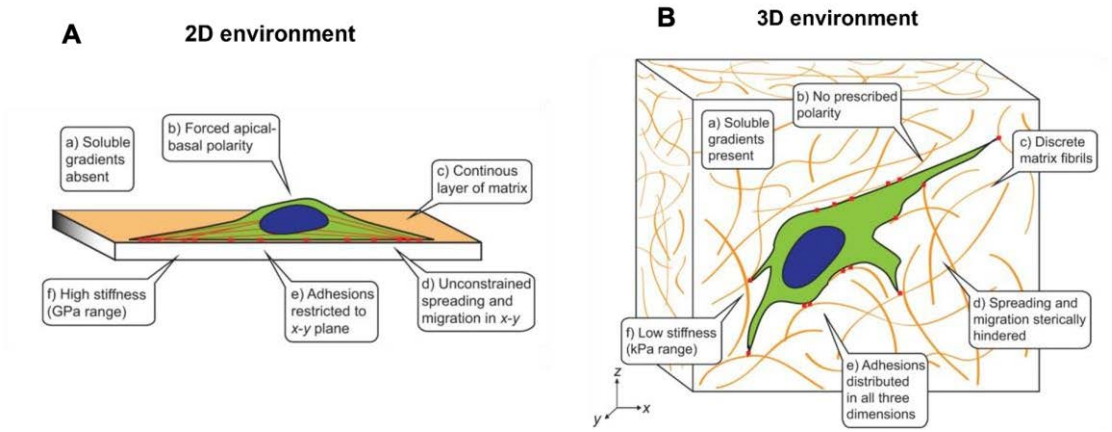


**Figure 1** Adhesive, topographical mechanical and soluble cues, which affect cellular development (A) in 2D (B) in 3D. Surface interactions in 2D and ECM interactions in 3D have been marked in red. Cell-to-cell interactions can be observed only on cell edges in 2D, as opposed to creating a complex network in 3D. Imaged adapted from Baker et al. 2012 [50]

**Table 2** A comparison of 2D and 3D tissue culture models

| Key Characteristics | 2D cell culture | 3D cell culture | References |
|---|---|---|---|
| **Cell Shape** | Flat and stretched (apical-basal polarity) | Natural shape retained (aggregate/spheroid structures) | [49, 51, 53, 54] |
| **Cell exposure to medium/drugs** | Cells have equal exposure to growth medium | Gradient of medium availability, resembling physiological conditions | [49, 51, 53] |
| **Cell differentiation** | Poor differentiation | Physical pressures can induce cell differentiation | [55] [56] [57] [58] |
| **Drug sensitivity** | Altered drug response due to unnatural microenvironment. Cells are equally exposed | Cells frequently more resilient, drugs show less potency. More accurate predictions of *in vivo* drug responses | [14, 15] [59] |
| **Cell proliferation** | Proliferation rate is higher than *in vivo* conditions | Proliferation rate depends on cell type and 3D cell culture technique. | [49, 51] |
| **Response to mechanical stimuli*** | Poor response | Well-established response | [60] [57] [58] |

*in this context, response to mechanical stimuli, refers to the cells actively interacting with the matrix provided

In addition to these physical spatial restrictions, numerous 2D models tend to consist of single cell type cultures (monocultures), which fail to allow investigations of interactions among different cell types [61]. Although 2D tissue culture is simple, reproducible and efficient, they are not a complete representation of *in* vivo processes [49] meaning the data obtained from 2D tissue culture experiments cannot be directly translated into clinical trials [15, 53, 61]

More recently, 3D *in vitro* models have shown promise in a breadth of disease models. 3D tissue culture aims to bridge the gap between whole-animal studies and the use of traditional 2D cell culture by creating an environment that is closer to the original tissue physiology and phenotype. Table 2 summarises the differences between 2D and 3D. 3D culture creates a more realistic physiological state by mimicking spatial organization and cell-cell interactions. It intends to accurately simulate the extracellular matrix (ECM) and the native tissue as closely as possible by enabling the cells to grow in a 3D structure, taking into account the original spatial organization of the cells in their native tissue environment and, therefore, mimicking the biological responses of these cells [15, 49, 52].

Additionally, the presence of ECM allows for accumulation of proteins and growth factors, which diffuse freely into the media in 2D conditions [52]. The cues encountered by the individual cells influence tissue development and homeostasis and, ultimately, regulate cell fate. There is increasing evidence that cells grown in 3D conformations show cell responses more comparable to *in vivo* behaviours with cells varying considerably both morphologically and physiologically from cells grown in 2D monolayers [15, 62-64]. Cells can be at various stages of the growth cycle; ranging from actively proliferating, quiescent, apoptotic, hypoxic and necrotic due to the heterogeneous exposure to nutrients and waste similar to *in vivo* conditions. They also retain their natural shape and proliferation capacity, and differentiation can be induced by the mechanical pressures of the scaffolds the cells are grown in [49, 55, 65]. Figure 1 and Table 2 illustrate the main differences that cells experience between 2D and 3D tissue culture, and the following section will describe the intricacies of 3D models and considerations regarding their use in neural cell culture.

### 1.3. 3D tissue culture

An ideal 3D culture model would simulate a tissue specific physiological microenvironment where cells can proliferate, aggregate, and differentiate [66]. The model would include cell to cell interactions as well as cell to ECM

interactions. The stiffness would resemble that of the tissue of origin, and there would be oxygen, nutrient, and metabolic waste gradients as well as tissue-specific scaffolding cells [67]. A variety of promising model techniques have been developed (Table 3) however, they do not meet all the criteria listed above and therefore researchers must choose the most appropriate model for the study being conducted. Additionally, there is a considerable breath of parameters that require optimisation specific to particular tissue types. These include the specific cell line, whether it needs to be a primary cell, the tissue of origin to be modelled and the final aim of the study. It is crucial to consider these parameters before choosing the 3D cell culture technique [66, 68].

Table 3: 3D tissue culture techniques advantages and disadvantages

| Model type | Advantages | Disadvantages | References |
|---|---|---|---|
| **Scaffold-free** E.g., Hanging drop, low attachment plate, magnetic levitation | - Cells self-assemble into spheroids.<br>- Does not require a scaffold.<br>- Mimics cell-cell interactions<br>- Simple<br>- Good for tumour reproduction | - Limited control of size and shape<br>- High variability between organoids<br>- May not represent mechanical properties of tissue.<br>- ECM-cell interactions not represented.<br>- Limit in size – difficult to scale up for high throughput applications.<br>- Necrotic centre | [51, 61, 66-69] |
| **Scaffold-based** | - Reproducible<br>- Tuneable environment<br>- Mimics ECM-cell and cell-cell interactions<br>- Suitable for long term studies<br>- Physiologically relevant | - Not well-established protocols<br>- Many variables to control/optimise.<br>- Limited in size<br>- High manufacturing complexity<br>- Downstream analysis difficulties | [66, 70] [71] [55, 61, 72, 73] |
| **Organ on a chip** | - Suitable for drug testing<br>- Physiologically relevant<br>- Suitable for long term studies | - High manufacturing complexity<br>- Higher need for expertise.<br>- Costly<br>- No standardised protocols<br>- Limited scalability | [74-76] |

3D models can be broadly divided into those with or without structural support, including scaffold-free and scaffold-based 3D culture systems [77]. Figure 2 visually represents the different methods available with and without scaffold.

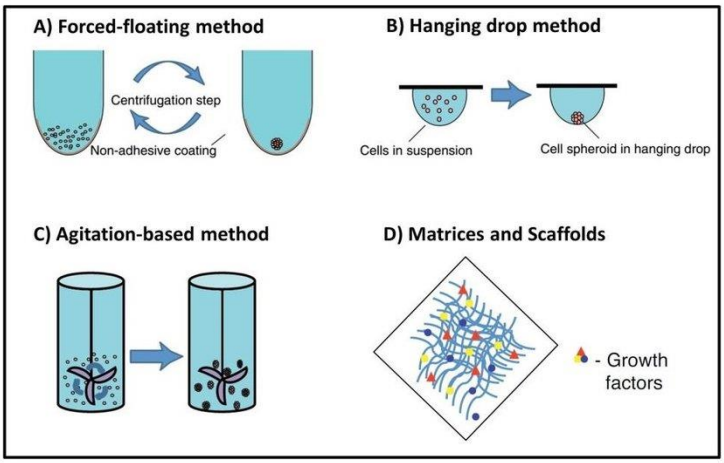


**Figure 2** Visual representation of the different 3D tissue culture methods with and without scaffold. Image reproduced from faCellitate [78]

Scaffold-free systems are anchorage independent and instead rely on the cells' ability to self-assemble and aggregate into non-adherent spheroids. Spheroids

enable for a better reproducibility of cell-to-cell physiology of tissues and tumours [66]. There are several approaches for spheroid formation (Figure 2). Forced floating methods (eg. low-adhesion plates; magnetic levitation technique) where cells are grown in conditions that prevent cell attachment and promote cell aggregation and spheroid formation. The use of low adhesion plates prevent cell attachment by using round bottom plates treated with hydrophilic or hydrophobic coating like the non-adherent polymer poly-HEMA while magnetic levitation forces the cells into floatation and aggregation by using an externally applied magnetic field to the magnetic nanoparticle preloaded cells [70]. Another spheroid formation approach is the hanging drop method (eg. hanging drop microplates) where cells are placed in specialized plates with open, bottomless wells that are designed for the formation of a small droplet that is big enough for cells to aggregate and become a spheroid. However, hanging drop method is limited by size, and spheroids need to be moved to low adhesion plates for analysis [53]. Agitation-based approaches (eg. bioreactors) are another technique used in scaffold-free tissue culture where cells are pushed to self-aggregate by creating dynamic culture conditions. This approach allows for large-scale production of spheroids; however, the cells are under shear stress and the spheroids are not always uniform in size [53].

So far, spheroids have successfully been used in modelling tumour growth and metastasis studies [79] and in the context of nervous system modelling, neurospheres or spheroids made from a mixed culture of progenitor, neuronal and glial cells, have been successfully used for the study of the interactions between the different cell types of the nervous system and their role in differentiation [80]. This has also been a promising model for drug testing as it is a more physiologically relevant culture system [69]. While scaffold-free tissue culture provides great insight into cell-cell interactions with highly reproducible results, cell aggregates require careful exchange of nutrients and gases and are only viable in small size. Cell death problems arise when the aggregates become larger than 1-2mm given the limited exchange of metabolites and waste products. The centres can easily become hypoxic past a certain size and cells become

necrotic. Additionally, they also do not represent the interactions with the ECM and lack the mechanical effects from the external environment. So, as the size and complexity of the 3D model increases, the need for a scaffold becomes unquestionable [51, 61, 66-69].

Scaffold-based systems are anchorage-dependent and involve the presence of a scaffold that provides a physical support element. Scaffolds can be defined as synthetic 3D structures made of various materials that have different porosities, permeability, chemical composition, and mechanical properties. These are designed to mimic the environment of specific tissues [70]. In scaffold-based cell culture, the cells are embedded within the matrix and are affected by the chemical and physical properties of the material. Scaffold porosity facilitates oxygen, nutrient and waste transportation as well as allowing for cell's proliferation, migration, and interaction with the scaffold and each other [66, 70].
The scaffolds can be polymeric hard scaffolds or hydrogel-based scaffolds and can be of natural origin or synthetically engineered to mimic ECM properties like stiffness, charge, or adhesive motifs. In some synthetic scaffolds, growth factors, hormones and other biologically active molecules can be added to enhance proliferation, attachment, and specific cell phenotype [71] (Figure 2).

When selecting a scaffold, researchers will need to carefully consider the tissue of origin and the material properties of the scaffold of choice as scaffold and material properties can regulate cell adhesion, proliferation activation and differentiation, as well as requirements for the intended application and use [55, 61, 72, 73]. For example, if the intended use is for transplantation, the scaffold will need to be biodegradable and easily remodelled by the body and replaced by native tissue to restore original function. In this case, the scaffold needs to support growth and differentiation. Additionally, the scaffold needs to disintegrate without toxic or immunogenic reactions. On the other hand, if a scaffold is intended as an *in vitro* model for treatment testing or disease modelling, the scaffold will need to closely mimic the native tissue structure [61].

Furthermore, the stem cell-material interface is a complex and dynamic environment. The cell and the material interact with one another and dictate their fate. The cells remodel the scaffold and the material through its properties (stiffness, adhesivity, degradability, porosity, permeability etc.) affects the cells' fate. Hard polymers are a suitable scaffold for specialised tissues such as skin, tendons or bone and softer scaffolds and hydrogels are good for softer tissues like brain, [66, 70]. For example, mesenchymal stem cells (MSCs) are known to be extremely sensitive to substrate stiffness. MSCs were neurogenic on soft matrices but myogenic on matrices with muscle stiffness and osteogenic on rigid matrices that mimic collagenous bone [55].

Organ-on-a-chip (OaC) are another 3D culture model currently used in bioengineering and drug discovery where artificial models of human organs are created using microfluidic cell culture chips [75]. The microfluidic chips have really well-defined structures, patterns or scaffolds that are generated using microfabrication techniques like soft lithography, photolithography and contact printing [74]. OaC is designed to mimic the key structural environment and complexity of organs at a smaller scale where the position, shape, chemical and physical environment of the cells in culture can be controlled to reproduce key organ functions and physiology using microfluidics [76]. These can contain an array of channels, valves and pumps that offer precise control over fluid flow [75, 81]. The key functions and structure of major organs such as lung, gut, liver, kidney and more recently brain are being developed using OaC method [82-86].

OaC are a great tool to explore drug efficacy and toxicity on cell and are the perfect next step after having a 3D structure and cell population to test on.
However, while they are starting to become commercially available, OaC are not easily accessible to all researchers as they require specialised knowledge and equipment. They are technically challenging and time consuming to create. Furthermore, they are also expensive to develop and maintain given the specialised equipment and materials required. Additionally, while some platforms are being designed for high-scale, overall, they can have limited scalability and

protocols need to be further validated and standardised [75, 76]. Amirifar et al. 2022 has written an in depth review about organ-on-a-chip models for neural studies and the nervous system [87].

With all this information in mind, the current research project will be using scaffold-based 3D techniques. The cells and matrix of choice to develop the model will be further discussed in the following sections.

## 1.4. Stem Cells used for nervous system modelling.

Stem cells have been widely used for research purposes as they have considerable capacity to be of clinical benefit. In research, stem cells can be used for two main types of research: as a research model to further understand disease processes, disease modelling, cell metabolism, differentiation potential, drug testing among others, or to develop therapeutic treatments like transplants and transfusions. [88]. Stem cells are the backbone of regenerative medicine, the field that merges tissue engineering and cell therapies with the aim to harness and improve the human body's self-healing capacity, to heal and restore damage caused by age, disease, trauma, or congenital disorders [89-92].

Stem cells have two main characteristics: they self-renew (i.e. they have the ability to divide and form another stem cell), and they can differentiate into different cell types and give rise to different tissues [93]. Depending on their origin and potency, stem cells can be classified into two main types: embryonic stem cells (ESCs) and adult stem cells [94, 95]. ESCs are pluripotent stem cells that originate from the blastocyst of an embryo and they were first isolated from humans in 1998 [96]. They can self-renew and can differentiate into every somatic tissue, however these have ethical concerns given the embryo death during cell isolation [97]. Adult stem cells, also known as somatic stem cells or non-embryonic stem cells, are multipotent cells and can be isolated from many different adult tissues including blood, bone, and adipose tissue, among others [98]. They can self-renew but their differentiation potential is limited when

compared to ESCs however, they do not have the same ethical concerns as ESCs and do not have the same immune rejection concerns as ESCs if returned to the host they were isolated from [95].

The CNS is composed of neurons, astrocytes, and oligodendrocytes as well as other non-neural cells. Neurons process the information entering and leaving the CNS; astrocytes are the support cells [99] and oligodendrocytes are responsible for myelinating axons [100]. In the adult human brain, neurogenesis occurs in two regions: the ventricular-subventricular zone (V-SVZ) and the subgranular zone (SGZ) in the hippocampus. These are the only regions where neural stem cells (NSCs) and neural progenitor cells (NPCs) can be found in the adult brain. Oligodendrocyte progenitor cells (OPCs) on the other hand, can be found in the corpus callosum where oligodendrogenesis occurs in in the adult brain. [18, 101, 102].

Neural tissue culture models of the nervous system have been established using an array of different stem cells ranging from animal cells to human cells and immortalised cell lines. Table 3 summarises the advantages and disadvantages of the different cell types that will be discussed.

**Table 3** Stem cells used for nervous system regeneration. Advantages and disadvantages. ESCs = Embryonic stem cells; NSCs = Neural stem cells; iPSCs = induced pluripotent stem cells; MSCs = Mesenchymal stem cells

| | **ESCs** | **NSCs** | **Immortalised cells** | **iPSCs** | **MSCs** |
|---|---|---|---|---|---|
| **Differentiation capacity** | Very good | Good | Low | Very good | Good |
| **Harvest/access** | Controversial | Difficult | NA | Easy | Easy |
| **Tumorigenicity** | High | Low | High | High | Low |
| **Suitability for stem cell therapy** | Moderate | Moderate | No | Low | Moderate |
| **Immune complications** | High | High | NA | Moderate | Low |

Neural stem cells (NSCs) and Neural progenitor cells (NPCs) are commonly used primary cells for the study of the nervous system. While they can be obtained

from both human and animal origin, human cells are difficult to source and most of these studies are done in neural primary cells from animal origin [103, 104]. While these cells offer important insight into the disease mechanisms and drug responses, they suffer from some of the same limitations as animal models, like costs, ethical implications, and obvious inter-species differences as they do not always reflect the cellular interactions and responses comparable to human cells. Additionally, human sourced NSCs and NPCs transplants would be faced with potential immune rejection.[104-107].

Immortalised cell lines have also been widely used to create nervous system models [105, 108]. The first immortalised neuronal line was derived from lymph node, bone marrow and liver tissue that was infiltrated with neuroblastoma cancer [109]. From this, SK-N-SH neuroblastoma cell line was isolated from metastatic bone tumour [110] which was then further subcloned to establish the now widely used SH-SY5Y neuroblastoma cell line [111]. NT2 Is another human neuronally committed teratocarcinoma immortalised cell line used to create neuronal cultures [108]. This cell line was originally derived from a malignant pluripotent embryonal carcinoma isolated from the testicles of a 20-year-old male [112]. While these cells are widely used in *in vitro* neural models [103] like traumatic brain injury models [113, 114], cigarette effect models [115], Parkinson disease models [116] among others, the main concern with the use of these cell lines is their genetic and metabolic abnormalities as well as their oncogenic nature which may not represent normal human cell proliferation and interactions accurately [105, 108, 117] furthermore, these cells are not suitable for potential transplants and regenerative medicine purposes given their cancerous nature.

ESCs are another commonly used cell source as they are pluripotent cells. They can be isolated from the blastocyst from an embryo and can differentiate into neural cells [95]. Motor neurons have been successfully generated from both rodent [118] and human ESCs [119, 120] and *in vitro* differentiated ESCs are able to quite accurately reproduce neuroectoderm formation with structures and cellular organisation similar to the ventricular and sub-ventricular zones [121-

124]. While these cells have provided invaluable information in the process of neural differentiation and neuron formation, these cells have well documented ethical concerns; ESCs originate from the blastocyst of a 5-day embryo and in the process of generating the cells, the embryo dies. Furthermore, there are also concerns around potential immune rejection as well as possible tumorous growth given their fast uninhibited proliferative nature which can hinder their use in transplants and regenerative medicine [95, 125].

Induced pluripotent stem cells (iPSCs) are another type of widely used cells for the study of the nervous system. These cells have been genetically reprogrammed from adult somatic cells into ESCs-like cells. iPSCs were first generated in 2006 from mouse fibroblasts by genetically modifying the cells to pluripotent stem cells [126]. In 2007, the same was achieved for the first time in human adult fibroblasts [127]. These cells are remarkably similar to ESCs however they are generated in a completely different way. While ESCs are isolated from an embryo [95], iPSCs are adult somatic cells that have been reprogrammed into an embryonic-like state [127, 128]. iPSCs have shown great potential as a treatment avenue for neurological disorders, having been successfully differentiated into oligodendrocytes, glial cells, neurons and astrocytes [129, 130]. They have served as a source of much information for disease modelling and have enabled the use of cells from patients with particular diseases like Parkinson's disease so that genetic code is in the cells [131]. However, their genetic reprogramming, as well as their high proliferation, are a concern when applied as stem cell therapies or transplants, as there can be immunogenic issues, as well as tumorigenic growth and more work, is required to see if these would become problematic (cancerous or otherwise) [132]. Additionally, iPSCs are notoriously time-consuming to maintain and require significant optimisation [133].

Mesenchymal stem cells (MSCs) are another cell type that have been researched in the field of nervous system repair. MSCs are multipotent adult stem cells that can self-renew and differentiate into tissues from mesenchymal and non-

mesenchymal origin [134]. These multipotent cells have the capacity to differentiate into cells from the mesodermal lineage (adipose, chondrogenic and osteogenic cells) and transdifferentiate into cells from the ectodermal (neurogenic and epithelial cells) and the endodermal lineages (myogenic cells). [135-143]

While adult stem cells have restricted growth potential when compared to ESCs they do not have the same ethical concerns. Furthermore, they can be isolated with minimal complications meaning they are ideal for autologous transplants reducing the potential immune rejection [144-149]. Additionally, adult stem cells proliferate at slower rates than pluripotent stem cells and are less prone to unrestrained proliferation and hence are less tumorigenic [125].
MSCs can be isolated from different tissues such as bone marrow, adipose tissue, and foetal tissue [150]. Bone Marrow stem cells (BMSCs) are extracted from the central region of the bone marrow, a process that is painful and has significant risk of morbidity [151]. Furthermore, the number of MSCs in the bone marrow is low, meaning that they yield low numbers of stem cells and need to be expanded *in vitro* [150]. On the other hand, adipose derived stem cells (ADSCs) are obtained via tissue liposuction which has low invasiveness and risk and the number of stem cells obtained from adipose tissue is significantly higher than those obtained from bone marrow reducing the need to expand *in vitro* [144-149]. Additionally, there are minimal differences in morphology, immune phenotype, and differentiation capacity between BMSCs and ADSCs. Lastly, ADSCs can be maintained *in* vitro for longer periods with higher proliferation rates and low levels of senescence when compared to BMSCs [149, 152, 153] making ADSCs a superior candidate for regenerative medicine and clinical applications.

Given the easy accessibility, differentiation potential, few ethical concerns, potential for autologous transplants and the low risk of tumorous growth in transplants, ADSCs were the cells chosen for this research project and will be further explored in more detail in the following section.

## 1.5. Adipose-derived stem cells

ADSCs were first introduced in the early 2000s when Zuk et al [154] characterised a multipotent, undifferentiated, self-renewing cell population isolated from adipose tissue that exhibited similar morphology and phenotype to MSCs. These newly isolated stem cells also displayed similar differentiation capacity and stem cell marker expression to MSCs [154]. ADSCs can be repeatedly harvested, with more ease, with higher stem cell yield, quality, and proliferation capacity via a far less invasive procedure with low morbidity from subcutaneous adipose tissue, making them a superior alternative cell source for regenerative medicine to BMSCs [144-149, 152, 153].

ADSCs are commonly isolated from adipose tissue lipoaspirates via collagenase digestion followed by centrifugal density gradient separation [155]. *In vitro* the cells are plastic adherent and can be expanded as monolayers on plastic displaying spindle-shape morphology and lacking intracellular lipid droplets seen in adipocytes [155]. Moreover, these cells are further characterised by the expression of the stem cell-specific surface markers CD90, CD105, CD73, CD44 and CD166 and the lack of hematopoietic markers CD45 and CD34 expression [156].

ADSCs are a great candidate for regenerative medicine and cell therapy not only because of their differentiation potential; ADSCs have been differentiated towards the mesodermal lineage (adipose, chondrogenic and osteogenic cells) and transdifferentiated into cells from the ectodermal (neurogenic and epithelial cells) and the endodermal lineages (myogenic cells) [135-143] but also because of their self-renewal capacity, their low immunogenicity, their capacity to migrate to damaged sites, their autocrine and paracrine secretion capacity of a broad selection of cytokines, chemokines and growth factors, as well as for their anti-apoptotic, anti-inflammatory, proangiogenic, immunomodulatory and anti-scarring effects [157-159].

To date, according to the National Institute of health registry (NIHR), there have been over 400 human clinical using ADSCs in regenerative medicine for an array of conditions, including respiratory conditions, arthritis, connective tissue disease, joint diseases, bone fractures, musculoskeletal diseases, central nervous system disorders among others [160]. It is important to note, however, that there is a shortage of easily accessible clinical trial results to assess the success rate of these experiments[161]. Results of clinical trials are not always reported on the NIHR website, and there is no easy access database to find them, making it hard for researchers to track down the results and make solid conclusions to pivot, adapt and improve bench-based research. Furthermore, there is no regulation or standardisation for isolation procedures for clinical application which can lead to inconsistencies [159, 161]. There is also a lack of standardisation for adipose-derived stem cell nomenclature; there are many different names used to refer to the same cells in the literature making it difficult to collate all research currently available [162]. All these issues complicate research as it creates barriers to faster advancements, highlighting the need to standardise nomenclature and methods for clinical purposes. All these issues are covered in depth in Koh-Belic (2020) doctoral dissertation [162].

Nevertheless, the therapeutic potential of ADSCs is vast, and while there is a need for improved clinical protocols and standardisation, ADSCs hold genuine potential in the clinic. ADSCs have been used in animals and humans for bone regeneration [163-166] as well as for cartilage and interverbal disc regeneration [167-172]. Fat reconstruction is also an area where ADSCs have been successfully used to treat soft tissue defects in humans [173-176]. The cardiovascular and myocardial regeneration potential of ADSCs has also been investigated and has shown positive outcomes by other researchers. ADSCs have improved regeneration of ischemic myocardium, reduced apoptosis of cardiomyocytes and improved cardiac function, perfusion and remodelling after acute myocardial infarction in animal models [177, 178] and in human trials using autologous ADSCs in patients with ischemic cardiomyopathy ADSCs seemed to play a role in preserving ventricular function, myocardial perfusion and exercise

capacity of patients treated [179]. Furthermore, animal models have also revealed the hepatic regeneration potential of ADSCs [180, 181].

In the context of neural regeneration, there are several clinical trials currently listed in the NIHR [160], and many animal models using ADSCs for nervous system regeneration showing promising results, adding to the evidence that ADSCs could be an ideal candidate to treat neurological diseases such as Alzheimer's disease (AD), amyotrophic lateral sclerosis (ALS), Huntington's disease, stroke, Parkinson's disease among other neurological conditions [182, 183]. Animal models of AD using ADSCs have shown memory deficit restoration, reduction of Aβ deposition and restoration of learning and memory functions [184, 185]. ALS rodent models showed that ADSCs treated mouse showed a delay in motor deterioration and an increase in glial-derived neurotrophic factor and basic fibroblast growth factor as well as increased number of lumbar motor neurons [186]. Huntington's disease models also show significant improvement of lesions, improved rotarod performance, increased survival, diminished loss of neurons and reduced huntingtin aggregates suggesting ADSCs slow disease progression [187, 188]. In Ischemic stroke animal models, ADSCs administration improved functional recovery, reduced cell death and reduced reactive gliosis [189-193] and in Parkinson's rodent model ADSCs also showed to have neurogenic and anti-inflammatory effects as well as improving cognitive performance after administration [194].

While there is a need for more research into the use of ADSCs as a treatment for neuroregeneration, and better standardisation of procedures for clinical studies and reporting of clinical trials results is required, the potential of these cells as a therapeutic avenue for neurological disorders and for personalised medicine is strong, and it is worth pursuing.

In this project, we will be focusing on studying the neural development on ADSCs in 2D and 3D cell culture models. The 3D model of choice will be further explained below.

## 1.6. Choosing a Scaffold

The brain is a complex and intricate organ made of billions of cells, including neurons, astrocytes and oligodendrocytes, each with unique functions and spatial arrangements. The organisation and structure of the brain plays a critical role in its function as it allows for the formation of complex networks and interactions of cells for information processing learning, and memory. When selecting scaffolds to create a nervous system model, the brain structure needs to be taken into consideration. Other tissues with simpler arrangements or different tissue stiffness will require a different scaffold with different properties.

Three main requirements need to be taken into consideration when selecting a scaffold for tissue engineering; the physical properties of the scaffold (stiffness, pore size and degradation rate); the biochemical properties (biological activity and toxicity) and practicality (cost and reproducibility) [10]. A balance is required between competing constraints and limiting factors.

Scaffolds need to be designed and customised for each tissue of interest and by the desired end use of the model (i.e. for clinical applications or drug testing). The brain and brain cells have a low elastic modulus (stiffness) ranging from 0.1 kPa to 1.6 kPa [195, 196] (Figure 3) whereas the spinal cord, surprisingly, has a high elastic modulus that ranges from 100-1000 kPa [197-200]. Brain and spinal cord are naturally softer than bone ($10^6$- $10^7$ kPa)[201]. Therefore, a softer and more porous material is required for neural tissue engineering, whereas for the growth of bone tissue, a stiffer more compact scaffold may be more realistic [61]. Consequently, the scaffold of choice for a 3D model of the brain should ideally have an elastic modulus of <2 kPa, resembling the softness of the brain tissue.

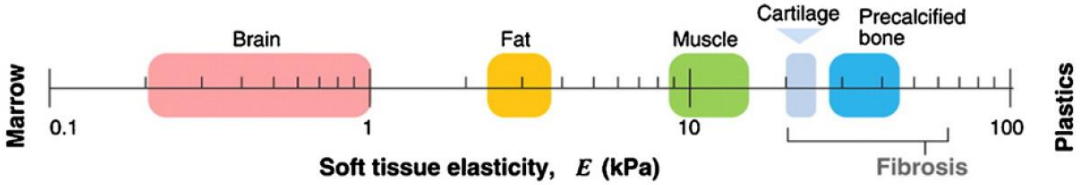

**Figure 3** Stiffness of different tissues. Reproduced from Liu et al. 2015 [202]

Stem cell growth and differentiation to differing lineages can be influenced by different factors including physical, chemical, and biological signals, such as the use of growth factors to drive neural stem cell differentiation [203-212]. ADSCs have been previously differentiated towards osteogenic, chondrogenic and neural lineages using different chemical and biological factors [135-137, 155, 213-219]. Physical signals seem play an important role in stem cell differentiation, such as MSCs undergoing osteogenesis when placed in stiffer substrates [220-222], and there is increasing evidence that MSCs differentiate towards neural lineages when placed in softer matrices [55, 57]. Her et al., (2013) demonstrated that MSCs fate could be manipulated towards the neuronal lineage when placed in a soft matrix (~1 kPa) and towards a glial lineage when placed in a stiffer substrate (~10 kPa) [57], showing that substrate stiffness can direct neural stem cell attachment, survival, growth and differentiation [57]. It has also been previously shown that substrates with an elastic modulus closer to brain tissue positively affects and supports neuronal attachment, growth, and expansion [58, 223]. When neurons are placed in soft hydrogels, they present typical neuron morphology, penetrating the hydrogel and forming a neurite meshwork, expressing neuronal markers like β-tubulin III [58, 223-225]. Neural stem cell (NSC) proliferation has been previously observed in soft (1kPa) hydrogels with neuronal differentiation being favoured [226, 227] while harder gels (>7kPa) seem to promote glial cultures [226, 227].

## 1.7. Hydrogels

Hydrogels have become of great interest for 3D tissue-engineered constructs due to their tuneable chemical and mechanical properties, their biocompatibility and they how they mimic the ECM [58, 228] and thus are an ideal candidate for CNS 3D modelling. Hydrogels are solid gels of cross-linked polymer networks that expand when immersed in aqueous solutions, allowing them to easily transport oxygen, nutrients, waste and biological factors [229] and are currently used in biomedical scenarios such as contact lenses and wound dressings [230]. They

are simple to use, non-toxic, non-immunogenic, have a high degree of biocompatibility, and are biodegradable, being able to be tuned to have a low degradation rate, which makes them ideal for long-term use [231]. Furthermore, the stiffness of the hydrogel can be adjusted to match the original tissue by controlling the mechanical properties [231]. Hydrogels have been successfully characterized and used in medical applications for bone and cartilage reconstruction, heart tissue regeneration, angiogenesis and drug delivery [232-235] and to a certain extent in developing 3D neural models with different stem cell types [129, 236-240]

### 1.7.1. Selected hydrogels: GelMa and PEG

Two types of hydrogels that are currently on the market and are considered highly used hydrogels for developing neural 3D models using different types of stem cells are gelatin-methacrylate (GelMa) and Polyethylene glycol (PEG) based hydrogels [239, 241-252]. GelMa and PEG will be the focus of this study and are discussed further below.

**GELMA**

GelMa hydrogels have suitable biological properties for tissue engineering and are highly biocompatible, biodegradable, non-cytotoxic, non-immunogenic, inexpensive and a cell-responsive biomaterial [253, 254]. GelMa hydrogels have been previously used in muscle [255, 256], epidermal [257], cardiovascular [258] and cartilage [259, 260] tissue engineering. However, neural tissue engineering models using GelMa hydrogels are still in early stages of development [253, 254]. GelMa hydrogels are reported to have versatile physical characteristics that closely mimic properties of the ECM; Gelatin contains many RGD (arginine-glycine-aspartic acid) sequences found in ECM proteins that allow for attachment of cells [256]. It also contains matrix metalloproteinases that aid in cell remodelling [261], allowing cells to attach, proliferate and spread within the scaffold [253, 254]. GelMa hydrogels also covalently crosslink when exposed to UV light (365-405nm) in the presence of a photo-initiator, and its physical and

mechanical properties can be tuned by varying its synthesis process, making it reportedly one of the most versatile hydrogels for a 3D culture that is currently being used [262-264].

Stiffness can be controlled by the degree of methacrylate substitution [262-264] where the number of methacrylate groups bound to an individual gelatin molecule proportionally controls the number of inter-gelatin crosslinks, and therefore, the stiffness of the hydrogel [253]. GelMa stiffness can also be tailored by selecting higher gelatin concentrations leading to higher stiffness and should be selected based on the desired tissue of interest [241, 265].

Studies have shown GelMa hydrogels are a suitable candidate for human ADSC growth in several models [263, 266-268]; with cells expanding to higher yields at lower stiffness (50% degrees of substitution) while stiffer substrates reduced the cell spreading and viability [263]. This could be attributed to the smaller hydrogel pore size in stiffer gels [263].

GelMa hydrogels have been reported as a promising hydrogel for neural cell culture models. NSCs have been shown to differentiate towards neuronal lineage expressing β-tubulin III and extending neurites when GelMa stiffness and concentration was low [241]. Furthermore, low GelMa stiffness and concentration has also allowed for neural cell growth, adhesion, proliferation and phenotype stability [242]. In contrast, if stiffness increases, neuronal outgrowth, viability, spreading and neurite length decrease [243]. GelMa has also been successfully used with other polymer composites for nerve tissue engineering [244] and for *in vivo* testing in traumatic brain injury models and Spinal Cord Injury (SCI), models showing no immune reaction or inflammation when implanted [242, 245].

**PEG**

PEG is highly biocompatible, non-immunogenic and resistant to protein adsorption. Its chemical structure is versatile and can be chemically modified, enabling it to form a hydrogel and bind to biomolecules, with its degradation rate

able to be controlled [269]. PEG hydrogels are made using photo-polymerisation that uses UV light (365-405nm) to convert a liquid PEG macromer solution into a solid gel at physiological temperature and pH allowing the hydrogel fabrication to occur *in situ* with spatial and temporal control and encapsulation of cells and biological agents. PEG alone is not bioactive, and therefore it requires other cell-adhesive molecules like diacrylate to form Polyethylene Glycol Diacrylate (PEGDA), or GelMa to form a PEG-GelMa composites. This process is important to obtain cell-attachment onto the hydrogel [269, 270].

PEG-based hydrogels have previously been used to differentiate MSCs into bone [271, 272], cartilage [273] and culture human organoids [274, 275]. When neural cells have been encapsulated in a PEG-based 3D polymer network, they created their own microenvironment for survival, proliferation and differentiation, forming electro-physiologically responsive neurons and glia [246]. Furthermore, by varying the degradation rate of the polymer, the time-scale over which neural cells extend their processes can be regulated [246]. Additionally, cross-linked PEG-based hydrogels have been shown to promote neuronal survival and axon outgrowth via cell-ECM interactions and allowed neurons to remodel their extracellular environment [239], demonstrating that PEG-based hydrogels permit cell survival for over a week and allow for strong motor axon extensions [239]. Compared to 2D cultures, cells grown in 3D PEG hydrogels cultures are reported to demonstrate higher metabolic activity, lower apoptotic activity and higher cell proliferation [247]. Furthermore, PEG hydrogels maintain increased neural progenitor cell (NPC) numbers and a decreased number of glial cells compared to monolayer cultures [248] and enhance NSC survival, proliferation and differentiation [252].

This information in a rapidly growing new field shows that hydrogels, with GelMa and PEG-based hydrogels, are a promising avenue for supporting neural regeneration and should be further explored using ADSCs and considering the endpoint applications.

For this project, **I hypothesise** that ADSCs will show enhanced neural differentiation in 3D environments that mimic neural tissue stiffness and that differentiation will be enhanced by the addition of neural growth supplements in the 3D environments. The supplements that will be used will be the commercially available B27, CultureOne (C1) and N2 from Gibco (Life Technologies). C1 is a supplement designed to support the differentiation of NSCs to neurons [276], while B27 and N2 are designed to support mature neural cells [277, 278].

The **aims** of this thesis are to:

1. Differentiate of ADSCs towards neural cells under 2D conditions using the neural supplements B27, C1 and N2. (Chapter Two)
2. Culture undifferentiated ADSCs in a 3D environment that mimics brain stiffness using
    a. GelMa (Chapter Three)
    b. PEG-based hydrogels (Chapter Four)
3. Differentiate of the ADSCs towards a neural lineage under the optimised 3D conditions (PEG-based hydrogels) using neural growth supplements B27, C1 and N2 (Chapter 5)

## 1.8. References


1. Health, N.I.o. *What does the nervous system do?* 2018 10/1/2018 [cited 2023; Available from: https://www.nichd.nih.gov/health/topics/neuro/conditioninfo/functions.
2. Health, N.I.o. *What are the parts of the nervous system*. 2018 [cited 2023; Available from: https://www.nichd.nih.gov/health/topics/neuro/conditioninfo/parts.
3. Organization, W.H. *Mental Health: Neurological disorders*. 2016 May 2016 [cited 2018 21st of October]; Available from: http://www.who.int/features/qa/55/en/.
4. Carroll, W.M., *The global burden of neurological disorders.* The Lancet. Neurology, 2019. **18**(5): p. 418-19.
5. Feigin, V.L., et al., *Global, regional, and national burden of neurological disorders, 1990–2016: a systematic analysis for the Global Burden of Disease Study 2016.* The Lancet. Neurology, 2019. **18**(5): p. 459-80.
6. Feigin, V.L., et al., *The global burden of neurological disorders: translating evidence into policy.* The Lancet. Neurology, 2020. **19**(3): p. 255-65.
7. Prince, M.J., et al., *World Alzheimer Report 2015 -The Global Impact of Dementia: An analysis of prevalence, incidence, cost and trends*. 2015, Alzheimers disease international.
8. Organisation, W.H., *Global action plan on the public health response to dementia 2017–2025*. 2017.
9. Organization, W.H., *Neurological disorders: public health challenges*. 2006: World Health Organization.
10. Hopkins, A.M., et al., *3D in vitro modeling of the central nervous system.* Progress in neurobiology, 2015. **125**: p. 1-25.
11. Pankevich, D.E., et al., *Improving and accelerating drug development for nervous system disorders.* Neuron, 2014. **84**(3): p. 546-53.
12. Massey, T.H. and N.P. Robertson, *Repurposing drugs to treat neurological diseases.* Journal of neurology, 2018. **265**(2): p. 446-8.
13. Wegener, G. and D. Rujescu, *The current development of CNS drug research.* The international journal of neuropsychopharmacology, 2013. **16**(7): p. 1687-93.
14. Hongisto, V., et al., *High-throughput 3D screening reveals differences in drug sensitivities between culture models of JIMT1 breast cancer cells.* PLoS One, 2013. **8**(10): p. e77232.
15. Edmondson, R., et al., *Three-dimensional cell culture systems and their applications in drug discovery and cell-based biosensors.* Assay and drug development technologies, 2014. **12**(4): p. 207-18.
16. Cernak, I., *Animal models of head trauma.* NeuroRx: : the journal of the American Society for Experimental NeuroTherapeutics, 2005. **2**(3): p. 410-22.
17. Götz, J. and L.M. Ittner, *Animal models of Alzheimer's disease and frontotemporal dementia.* Nature Reviews Neuroscience, 2008. **9**(7): p. 532.
18. Hansen, D.V., et al., *Neurogenic radial glia in the outer subventricular zone of human neocortex.* Nature, 2010. **464**(7288): p. 554-61.

19. Morrison, B., 3rd, et al., *An in vitro model of traumatic brain injury utilising two-dimensional stretch of organotypic hippocampal slice cultures.* Journal of Neuroscience Methods, 2006. **150**(2): p. 192-201.
20. Dubois-Dauphin, M.L., et al., *The long-term survival of in vitro engineered nervous tissue derived from the specific neural differentiation of mouse embryonic stem cells.* Biomaterials, 2010. **31**(27): p. 7032-42.
21. Blain, M., et al., *Isolation and culture of primary human CNS neural cells*, in *Protocols for neural cell culture*. 2009, Humana Press -Springer Protocols. p. 87-104.
22. Lancaster, M.A., et al., *Cerebral organoids model human brain development and microcephaly.* Nature, 2013. **501**(7467): p. 373-9.
23. Ogunshola, O.O., *In vitro modeling of the blood-brain barrier: simplicity versus complexity.* Current Pharmaceutical Design, 2011. **17**(26): p. 2755-61.
24. Cecchelli, R., et al., *Modelling of the blood–brain barrier in drug discovery and development.* Nature reviews Drug discovery, 2007. **6**(8): p. 650-61.
25. Khan, A., et al., *In vitro and in vivo animal models: The engineering towards understanding human diseases and therapeutic interventions*, in *Omics Technologies and Bio-Engineering*. 2018, Elsevier. p. 431-48.
26. Barré-Sinoussi, F. and X. Montagutelli, *Animal models are essential to biological research: issues and perspectives.* Future science OA, 2015. **1**(4): p. FSO63.
27. Institute of, M. and C. National Research, *The National Academies Collection: Reports funded by National Institutes of Health*, in *International Animal Research Regulations: Impact on Neuroscience Research: Workshop Summary*. 2012, National Academies Press (US)
Copyright © 2012, National Academy of Sciences.: Washington (DC).
28. Casals, J.B., et al., *The use of animal models for stroke research: a review.* Comparative medicine, 2011. **61**(4): p. 305-13.
29. Zhao, X. and A. Bhattacharyya, *Human models are needed for studying human neurodevelopmental disorders.* The American Journal of Human Genetics, 2018. **103**(6): p. 829-57.
30. Herson, P.S. and R.J. Traystman, *Animal models of stroke: translational potential at present and in 2050.* Future neurology, 2014. **9**(5): p. 541-51.
31. Chesselet, M.-F. and S.T. Carmichael, *Animal models of neurological disorders.* Neurotherapeutics 2012. **9**(2): p. 241-4.
32. Pound, P. and R. Ram, *Are researchers moving away from animal models as a result of poor clinical translation in the field of stroke? An analysis of opinion papers.* BMJ Open Science, 2020. **4**(1): p. e100041.
33. Van Norman, G.A., *Limitations of animal studies for predicting toxicity in clinical trials: is it time to rethink our current approach?* JACC: Basic to Translational Science, 2019. **4**(7): p. 845-54.
34. Andersen, M.L. and L.M. Winter, *Animal models in biological and biomedical research-experimental and ethical concerns.* Anais da Academia Brasileira de Ciências, 2017. **91**: p. e20170238.
35. Dusinska, M., et al., *Toxicity tests: In vitro and in vivo*, in *Adverse effects of engineered nanomaterials*. 2017, Elsevier. p. 51-82.

36. Wang, X., K.-F. So, and X.-M. Xu, *Advances and challenges for neural regeneration research*, in *Neural Regeneration*. 2015, Elsevier Inc. p. 3-17.
37. Runden, E., et al., *Regional selective neuronal degeneration after protein phosphatase inhibition in hippocampal slice cultures: evidence for a MAP kinase-dependent mechanism.* The Journal of neuroscience, 1998. **18**(18): p. 7296-305.
38. Pettigrew, D.B., K.P. Shockley, and K.A. Crutcher, *Disruption of spinal cord white matter and sciatic nerve geometry inhibits axonal growth in vitro in the absence of glial scarring.* BMC Neuroscience, 2001. **2**: p. 8.
39. Croft, C., et al., *Organotypic brain slice cultures to model neurodegenerative proteinopathies.* Molecular Neurodegeneration, 2019. **14**: p. 1-11.
40. Pérez-Rodríguez, D., et al., *Hippocampus and cerebral cortex present a different autophagic response after oxygen and glucose deprivation in an ex vivo rat brain slice model.* Neuropathology and Applied Neurobiology, 2015. **41**(4): p. e68-e79.
41. Kann, O., et al., *Metabolic dysfunction during neuronal activation in the ex vivo hippocampus from chronic epileptic rats and humans.* Brain, 2005. **128**(10): p. 2396-407.
42. Iglesias, J.E., et al., *A computational atlas of the hippocampal formation using ex vivo, ultra-high resolution MRI: application to adaptive segmentation of in vivo MRI.* Neuroimage, 2015. **115**: p. 117-37.
43. Fernandez-Zafra, T., S. Codeluppi, and P. Uhlén, *An ex vivo spinal cord injury model to study ependymal cells in adult mouse tissue.* Experimental Cell Research, 2017. **357**(2): p. 236-42.
44. Jang, S., et al., *Long-term culture of organotypic hippocampal slice from old 3xTg-AD mouse: An ex vivo model of Alzheimer's disease.* Psychiatry investigation, 2018. **15**(2): p. 205.
45. Daviaud, N., et al., *Modeling nigrostriatal degeneration in organotypic cultures, a new ex vivo model of Parkinson's disease.* Neuroscience, 2014. **256**: p. 10-22.
46. Dal Ben, M., et al., *Earliest mechanisms of dopaminergic neurons sufferance in a novel slow progressing ex vivo model of parkinson disease in rat organotypic cultures of substantia nigra.* International Journal of Molecular Sciences, 2019. **20**(9): p. 2224.
47. Hickman, J.A., et al., *Three-dimensional models of cancer for pharmacology and cancer cell biology: capturing tumor complexity in vitro/ex vivo.* Biotechnology journal, 2014. **9**(9): p. 1115-28.
48. Nogueira, G.O., et al., *Modeling the human brain with ex vivo slices and in vitro organoids for translational neuroscience.* Frontiers in Neuroscience, 2022. **16**: p. 838594.
49. Duval, K., et al., *Modeling Physiological Events in 2D vs. 3D Cell Culture.* Physiology, 2017. **32**(4): p. 266-77.
50. Baker, B.M. and C.S. Chen, *Deconstructing the third dimension: how 3D culture microenvironments alter cellular cues.* Journal of Cell Science, 2012. **125**(13): p. 3015-24.

51. Antoni, D., et al., *Three-dimensional cell culture: a breakthrough in vivo.* International Journal of Molecular Sciences, 2015. **16**(3): p. 5517-27.
52. Muncie, J.M. and V.M. Weaver, *The Physical and Biochemical Properties of the Extracellular Matrix Regulate Cell Fate.* Current topics in developmental biology, 2018. **130**: p. 1-37.
53. Kim, J.B., *Three-dimensional tissue culture models in cancer biology.* Seminars in Cancer Biology, 2005. **15**(5): p. 365-77.
54. Huang, H., et al., *Peptide hydrogelation and cell encapsulation for 3D culture of MCF-7 breast cancer cells.* PLoS One, 2013. **8**(3): p. e59482.
55. Engler, A.J., et al., *Matrix elasticity directs stem cell lineage specification.* Cell, 2006. **126**(4): p. 677-89.
56. Hopkins, A.M., et al., *Silk hydrogels as soft substrates for neural tissue engineering.* Advanced functional materials, 2013. **23**(41): p. 5140-49.
57. Her, G.J., et al., *Control of three-dimensional substrate stiffness to manipulate mesenchymal stem cell fate toward neuronal or glial lineages.* Acta biomaterialia, 2013. **9**(2): p. 5170-80.
58. Matyash, M., et al., *Novel soft alginate hydrogel strongly supports neurite growth and protects neurons against oxidative stress.* Tissue Engineering. Part A, 2012. **18**(1-2): p. 55-66.
59. Weaver, V.M., et al., *Reversion of the malignant phenotype of human breast cells in three-dimensional culture and in vivo by integrin blocking antibodies.* The Journal of cell biology, 1997. **137**(1): p. 231-45.
60. Li, Y., et al., *An approach to quantifying 3D responses of cells to extreme strain.* Scientific reports, 2016. **6**: p. 19550.
61. Haycock, J.W., *3D cell culture: a review of current approaches and techniques.* Methods in molecular biology, 2011. **695**: p. 1-15.
62. Baharvand, H., et al., *Differentiation of human embryonic stem cells into hepatocytes in 2D and 3D culture systems in vitro.* The International journal of developmental biology, 2006. **50**(7): p. 645-52.
63. Benya, P.D. and J.D. Shaffer, *Dedifferentiated chondrocytes reexpress the differentiated collagen phenotype when cultured in agarose gels.* Cell, 1982. **30**(1): p. 215-24.
64. Zietarska, M., et al., *Molecular description of a 3D in vitro model for the study of epithelial ovarian cancer (EOC).* Molecular carcinogenesis, 2007. **46**(10): p. 872-85.
65. Streuli, C., *Extracellular matrix remodelling and cellular differentiation.* Current opinion in cell biology, 1999. **11**(5): p. 634-40.
66. Langhans, S.A., *Three-dimensional in vitro cell culture models in drug discovery and drug repositioning.* Frontiers in pharmacology, 2018. **9**: p. 6.
67. Griffith, L.G. and M.A. Swartz, *Capturing complex 3D tissue physiology in vitro.* Nature reviews Molecular cell biology, 2006. **7**(3): p. 211-24.
68. Pampaloni, F., E.G. Reynaud, and E.H. Stelzer, *The third dimension bridges the gap between cell culture and live tissue.* Nature reviews Molecular cell biology, 2007. **8**(10): p. 839-45.

69. Moors, M., et al., *Human neurospheres as three-dimensional cellular systems for developmental neurotoxicity testing.* Environmental health perspectives, 2009. **117**(7): p. 1131-8.
70. Fang, Y. and R.M. Eglen, *Three-Dimensional Cell Cultures in Drug Discovery and Development.* SLAS Discovery: Advancing the Science of Drug Discovery, 2017. **22**(5): p. 456-72.
71. Caliari, S.R. and J.A. Burdick, *A practical guide to hydrogels for cell culture.* Nature methods, 2016. **13**(5): p. 405-14.
72. Murphy, W.L., T.C. McDevitt, and A.J. Engler, *Materials as stem cell regulators.* Nature materials, 2014. **13**(6): p. 547-57.
73. Benoit, D.S., et al., *Small functional groups for controlled differentiation of hydrogel-encapsulated human mesenchymal stem cells.* Nature materials, 2008. **7**(10): p. 816-23.
74. Wang, Z., et al., *Organ-on-a-chip platforms for drug delivery and cell characterization: A review.* Sensors and Materials, 2015. **27**(6): p. 487-506.
75. Bhatia, S.N. and D.E. Ingber, *Microfluidic organs-on-chips.* Nature biotechnology, 2014. **32**(8): p. 760-72.
76. Leung, C.M., et al., *A guide to the organ-on-a-chip.* Nature Reviews Methods Primers, 2022. **2**(1): p. 33.
77. Ho, W.J., et al., *Incorporation of multicellular spheroids into 3-D polymeric scaffolds provides an improved tumor model for screening anticancer drugs.* Cancer science, 2010. **101**(12): p. 2637-43.
78. faCellitate. *Effect of culture methods on multicellular tumor mct spheroid formation*. 2022 [cited 2023; Available from: https://facellitate.com/effect-of-culture-methods-on-multicellular-tumor-mct-spheroid-formation/.
79. Ivascu, A. and M. Kubbies, *Rapid generation of single-tumor spheroids for high-throughput cell function and toxicity analysis.* Journal of Biomolecular Screening, 2006. **11**(8): p. 922-32.
80. Campos, L.S., *Neurospheres: insights into neural stem cell biology.* Journal of neuroscience research, 2004. **78**(6): p. 761-69.
81. Koyilot, M.C., et al., *Breakthroughs and applications of organ-on-a-chip technology.* Cells, 2022. **11**(11): p. 1828.
82. Huh, D., et al., *Reconstituting organ-level lung functions on a chip.* Science, 2010. **328**(5986): p. 1662-68.
83. Kim, H.J., et al., *Human gut-on-a-chip inhabited by microbial flora that experiences intestinal peristalsis-like motions and flow.* Lab on a Chip, 2012. **12**(12): p. 2165-74.
84. Beckwitt, C.H., et al., *Liver 'organ on a chip'.* Experimental cell research, 2018. **363**(1): p. 15-25.
85. Ashammakhi, N., et al., *Kidney-on-a-chip: untapped opportunities.* Kidney international, 2018. **94**(6): p. 1073-86.
86. Haring, A.P., H. Sontheimer, and B.N. Johnson, *Microphysiological human brain and neural systems-on-a-chip: potential alternatives to small animal models and emerging platforms for drug discovery and personalized medicine.* Stem cell reviews and reports, 2017. **13**: p. 381-406.

87. Amirifar, L., et al., *Brain-on-a-chip: Recent advances in design and techniques for microfluidic models of the brain in health and disease.* Biomaterials, 2022. **285**: p. 121531.
88. Council, N.H.a.M.R., *National Statement on Ethical Conduct in Human Research 2007 (Updated 2018)*. 2007, The National Health and Medical Research
Council, the Australian Research Council and Universities Australia.
89. Cossu, G., et al., *Lancet Commission: Stem cells and regenerative medicine.* Lancet, 2018. **391**(10123): p. 883-910.
90. Akter, F., *Chapter 2 - Principles of Tissue Engineering*, in *Tissue Engineering Made Easy*. 2016, Academic Press. p. 3-16.
91. Akter, F., *Chapter 1 - What is Tissue Engineering*, in *Tissue Engineering Made Easy*. 2016, Academic Press. p. 1-2.
92. Schenke-Layland, K., *From tissue engineering to regenerative medicine--the potential and the pitfalls.* Advanced Drug Delivery Reviews, 2011. **63**(4-5): p. 193-4.
93. Lan, M.L., et al., *Characterizing the radioresponse of pluripotent and multipotent human stem cells.* PLoS One, 2012. **7**(12): p. e50048.
94. Singh, V., et al., *Induced pluripotent stem cells: applications in regenerative medicine, disease modeling, and drug discovery.* Frontiers in cell and developmental biology, 2015. **3**(2).
95. Rippon, H. and A. Bishop, *Embryonic stem cells.* Cell proliferation, 2004. **37**(1): p. 23-34.
96. Thomson, J.A., et al., *Embryonic stem cell lines derived from human blastocysts.* science, 1998. **282**(5391): p. 1145-7.
97. Guenther, M.G., *Transcriptional control of embryonic and induced pluripotent stem cells.* Epigenomics, 2011. **3**(3): p. 323-43.
98. Young, H.E. and A.C. Black Jr, *Adult stem cells.* The Anatomical Record Part A: Discoveries in Molecular, Cellular, and Evolutionary Biology, 2004. **276**(1): p. 75-102.
99. Molofsky, A.V., et al., *Astrocytes and disease: a neurodevelopmental perspective.* Genes & development, 2012. **26**(9): p. 891-907.
100. Barres, B.A., *The mystery and magic of glia: a perspective on their roles in health and disease.* Neuron, 2008. **60**(3): p. 430-40.
101. Maldonado-Soto, A.R., et al., *Stem cells in the nervous system.* American journal of physical medicine & rehabilitation/Association of Academic Physiatrists, 2014. **93**(11): p. S132.
102. Kriegstein, A. and A. Alvarez-Buylla, *The glial nature of embryonic and adult neural stem cells.* Annual review of neuroscience, 2009. **32**: p. 149-84.
103. Shipley, M.M., C.A. Mangold, and M.L. Szpara, *Differentiation of the SH-SY5Y human neuroblastoma cell line.* Journal of Visualized Experiments, 2016(108): p. e53193.
104. Ko, K.R. and J.P. Frampton, *Developments in 3D neural cell culture models: the future of neurotherapeutics testing?* Expert Review of Neurotherapeutics, 2016. **16**(7): p. 739-41.

105. Pacitti, D., R. Privolizzi, and B.E. Bax, *Organs to cells and cells to organoids: the evolution of in vitro central nervous system modelling.* Frontiers in cellular neuroscience, 2019. **13**: p. 129.
106. Hartung, T., *Thoughts on limitations of animal models.* Parkinsonism & related disorders, 2008. **14**: p. S81-S83.
107. Gharib, W.H. and M. Robinson-Rechavi, *When orthologs diverge between human and mouse.* Briefings in bioinformatics, 2011. **12**(5): p. 436-41.
108. Pilipović, K., et al., *Modeling Central Nervous System Injury In Vitro: Current Status and Promising Future Strategies.* Biomedicines, 2023. **11**(1): p. 94.
109. Goldstein, M.N., J.A. Burdman, and L. Journey, *Long-term tissue culture of neuroblastomas. II. Morphologic evidence for differentiation and maturation.* Journal of the National Cancer Institute, 1964. **32**(1): p. 165-99.
110. Biedler, J.L., L. Helson, and B.A. Spengler, *Morphology and growth, tumorigenicity, and cytogenetics of human neuroblastoma cells in continuous culture.* Cancer research, 1973. **33**(11): p. 2643-52.
111. Biedler, J.L., et al., *Multiple neurotransmitter synthesis by human neuroblastoma cell lines and clones.* Cancer research, 1978. **38**(11_Part_1): p. 3751-57.
112. Andrews, P.W., *Human teratocarcinomas.* Biochimica et Biophysica Acta (BBA)-Reviews on Cancer, 1988. **948**(1): p. 17-36.
113. Juntunen, M., et al., *In vitro oxygen-glucose deprivation-induced stroke models with human neuroblastoma cell-and induced pluripotent stem cell-derived neurons.* Stem Cells International, 2020. **2020**: p. 8841026.
114. Lockhart, E.M., et al., *Allopregnanolone attenuates N-methyl-D-aspartate-induced excitotoxicity and apoptosis in the human NT2 cell line in culture.* Neuroscience letters, 2002. **328**(1): p. 33-6.
115. Riveles, K., L.Z. Huang, and M. Quik, *Cigarette smoke, nicotine and cotinine protect against 6-hydroxydopamine-induced toxicity in SH-SY5Y cells.* Neurotoxicology, 2008. **29**(3): p. 421-27.
116. Nakaso, K., S. Ito, and K. Nakashima, *Caffeine activates the PI3K/Akt pathway and prevents apoptotic cell death in a Parkinson's disease model of SH-SY5Y cells.* Neuroscience letters, 2008. **432**(2): p. 146-50.
117. Gordon, J. and S. Amini, *General overview of neuronal cell culture*, in *Neuronal Cell Culture: Methods and Protocols*, S. Amini and M.K. White, Editors. 2021: Humana Totowa, NJ. p. 1-8.
118. Wichterle, H., et al., *Directed differentiation of embryonic stem cells into motor neurons.* Cell, 2002. **110**(3): p. 385-97.
119. Amoroso, M.W., et al., *Accelerated high-yield generation of limb-innervating motor neurons from human stem cells.* Journal of Neuroscience, 2013. **33**(2): p. 574-86.
120. Li, X.-J., et al., *Specification of motoneurons from human embryonic stem cells.* Nature biotechnology, 2005. **23**(2): p. 215-21.
121. Wu, J.Q., et al., *Dynamic transcriptomes during neural differentiation of human embryonic stem cells revealed by short, long, and paired-end*

*sequencing.* Proceedings of the National Academy of Sciences, 2010. **107**(11): p. 5254-9.
122. Zhang, S.-C., et al., *In vitro differentiation of transplantable neural precursors from human embryonic stem cells.* Nature biotechnology, 2001. **19**(12): p. 1129-33.
123. Curchoe, C.L., J. Russo, and A.V. Terskikh, *hESC derived neuro-epithelial rosettes recapitulate early mammalian neurulation events; an in vitro model.* Stem cell research, 2012. **8**(2): p. 239-46.
124. Shi, Y., et al., *Human cerebral cortex development from pluripotent stem cells to functional excitatory synapses.* Nature neuroscience, 2012. **15**(3): p. 477-86.
125. Ritfeld, G.J., R.A. Roos, and M. Oudega, *Stem cells for central nervous system repair and rehabilitation.* Physical Medicine & Rehabilitation : the journal of injury, function, and rehabilitation, 2011. **3**(6): p. S117-S122.
126. Takahashi, K. and S. Yamanaka, *Induction of pluripotent stem cells from mouse embryonic and adult fibroblast cultures by defined factors.* cell, 2006. **126**(4): p. 663-76.
127. Takahashi, K., et al., *Induction of pluripotent stem cells from adult human fibroblasts by defined factors.* cell, 2007. **131**(5): p. 861-72.
128. Avior, Y., I. Sagi, and N. Benvenisty, *Pluripotent stem cells in disease modelling and drug discovery.* Nature reviews Molecular cell biology, 2016. **17**(3): p. 170-82.
129. Bordoni, M., et al., *From Neuronal Differentiation of iPSCs to 3D Neuro-Organoids: Modelling and Therapy of Neurodegenerative Diseases.* International Journal of Molecular Sciences, 2018. **19**(12): p. 3972.
130. Bellin, M., et al., *Induced pluripotent stem cells: the new patient?* Nature reviews Molecular cell biology, 2012. **13**(11): p. 713-26.
131. Peng, J. and X. Zeng, *The role of induced pluripotent stem cells in regenerative medicine: neurodegenerative diseases.* Stem cell research & therapy, 2011. **2**(32): p. 1-6.
132. Liang, G. and Y. Zhang, *Genetic and epigenetic variations in iPSCs: potential causes and implications for application.* Cell stem cell, 2013. **13**(2): p. 149-59.
133. Santostefano, K.E., et al., *A practical guide to induced pluripotent stem cell research using patient samples.* Laboratory investigation, 2015. **95**(1): p. 4-13.
134. Rastegar, F., et al., *Mesenchymal stem cells: Molecular characteristics and clinical applications.* World journal of stem cells, 2010. **2**(4): p. 67.
135. Gimble, J. and F. Guilak, *Adipose-derived adult stem cells: isolation, characterization, and differentiation potential.* Cytotherapy, 2003. **5**(5): p. 362-9.
136. Jang, S., et al., *Functional neural differentiation of human adipose tissue-derived stem cells using bFGF and forskolin.* BMC Cell Biology, 2010. **11**: p. 25.
137. Park, J., et al., *Small molecule-based lineage switch of human adipose-derived stem cells into neural stem cells and functional GABAergic neurons.* Scientific reports, 2017. **7**(1): p. 10166.

138. Wislet-Gendebien, S., et al., *Astrocytic and neuronal fate of mesenchymal stem cells expressing nestin.* Brain research bulletin, 2005. **68**(1-2): p. 95-102.
139. Prabhakaran, M.P., J.R. Venugopal, and S. Ramakrishna, *Mesenchymal stem cell differentiation to neuronal cells on electrospun nanofibrous substrates for nerve tissue engineering.* Biomaterials, 2009. **30**(28): p. 4996-5003.
140. Ma, K., et al., *Generation of neural stem cell-like cells from bone marrow-derived human mesenchymal stem cells.* Neurological research, 2011. **33**(10): p. 1083-93.
141. Long, X., et al., *Neural cell differentiation in vitro from adult human bone marrow mesenchymal stem cells.* Stem cells and development, 2005. **14**(1): p. 65-9.
142. Scuteri, A., et al., *Mesenchymal stem cells neuronal differentiation ability: a real perspective for nervous system repair?* Current stem cell research & therapy, 2011. **6**(2): p. 82-92.
143. Takeda, Y.S. and Q. Xu, *Neuronal differentiation of human mesenchymal stem cells using exosomes derived from differentiating neuronal cells.* PloS one, 2015. **10**(8): p. e0135111.
144. Tsuji, W., J.P. Rubin, and K.G. Marra, *Adipose-derived stem cells: Implications in tissue regeneration.* World journal of stem cells, 2014. **6**(3): p. 312-21.
145. Raposio, E., S. Bonomini, and F. Calderazzi, *Isolation of autologous adipose tissue-derived mesenchymal stem cells for bone repair.* Orthopaedics & traumatology, surgery & research, 2016. **102**(7): p. 909-12.
146. Wankhade, U.D., et al., *Advances in Adipose-Derived Stem Cells Isolation, Characterization, and Application in Regenerative Tissue Engineering.* Stem Cells International, 2016. **2016**: p. 3206807.
147. Raposio, E., F. Simonacci, and R.E. Perrotta, *Adipose-derived stem cells: comparison between two methods of isolation for clinical applications.* Annals of medicine and surgery, 2017. **20**: p. 87-91.
148. Zuk, P.A., et al., *Multilineage cells from human adipose tissue: implications for cell-based therapies.* Tissue Engineering, 2001. **7**(2): p. 211-28.
149. Strioga, M., et al., *Same or not the same? Comparison of adipose tissue-derived versus bone marrow-derived mesenchymal stem and stromal cells.* Stem cells and development, 2012. **21**(14): p. 2724-52.
150. de Souza Fernandez, T. and C. de Souza Fernandez, *Mesenchymal stem cells: biological characteristics and potential clinical applications for haematopoietic stem cell transplantation*, in *Pluripotent Stem Cells - From the Bench to the Clinic*. 2016, IntechOpen.
151. Liao, H.-T. and C.-T. Chen, *Osteogenic potential: Comparison between bone marrow and adipose-derived mesenchymal stem cells.* World journal of stem cells, 2014. **6**(3): p. 288-95.
152. Kern, S., et al., *Comparative analysis of mesenchymal stem cells from bone marrow, umbilical cord blood, or adipose tissue.* Stem cells, 2006. **24**(5): p. 1294-301.

153. Izadpanah, R., et al., *Biologic properties of mesenchymal stem cells derived from bone marrow and adipose tissue.* Journal of cellular biochemistry, 2006. **99**(5): p. 1285-97.
154. Zuk, P.A., et al., *Human adipose tissue is a source of multipotent stem cells.* Molecular biology of the cell, 2002. **13**(12): p. 4279-95.
155. Bunnell, B.A., et al., *Adipose-derived stem cells: isolation, expansion and differentiation.* Methods, 2008. **45**(2): p. 115-20.
156. Bourin, P., et al., *Stromal cells from the adipose tissue-derived stromal vascular fraction and culture expanded adipose tissue-derived stromal/stem cells: a joint statement of the International Federation for Adipose Therapeutics and Science (IFATS) and the International Society for Cellular Therapy (ISCT).* Cytotherapy, 2013. **15**(6): p. 641-48.
157. Shingyochi, Y., H. Orbay, and H. Mizuno, *Adipose-derived stem cells for wound repair and regeneration.* Expert opinion on biological therapy, 2015. **15**(9): p. 1285-92
158. Frese, L., P.E. Dijkman, and S.P. Hoerstrup, *Adipose Tissue-Derived Stem Cells in Regenerative Medicine.* Transfusion medicine and hemotherapy : offizielles Organ der Deutschen Gesellschaft fur Transfusionsmedizin und Immunhamatologie, 2016. **43**(4): p. 268-274.
159. Mazini, L., M. Ezzoubi, and G. Malka, *Overview of current adipose-derived stem cell (ADSCs) processing involved in therapeutic advancements: flow chart and regulation updates before and after COVID-19.* Stem Cell Research & Therapy, 2021. **12**(1): p. 1.
160. Health, N.I.o., *Clinical trials containing the phrase 'adipose derived stem cell'*. 2023.
161. Raposio, E. and R. Ciliberti, *Clinical use of adipose-derived stem cells: European legislative issues.* Annals of medicine and surgery, 2017. **24**: p. 61-4.
162. belic, N.K., *New Stemsation: A Comprehensive Analysis of Adipose Stem Cells*. 2020, University of Technology Sydney.
163. Lu, W., et al., *Bone tissue engineering by using a combination of polymer/Bioglass composites with human adipose-derived stem cells.* Cell and tissue research, 2014. **356**(1): p. 97-107.
164. Godoy Zanicotti, D., D.E. Coates, and W.J. Duncan, *In vivo bone regeneration on titanium devices using serum-free grown adipose-derived stem cells, in a sheep femur model.* Clinical oral implants research, 2017. **28**(1): p. 64-75.
165. Abudusaimi, A., et al., *Adipose-derived stem cells enhance bone regeneration in vascular necrosis of the femoral head in the rabbit.* The Journal of International Medical Research, 2011. **39**(5): p. 1852-60.
166. Lendeckel, S., et al., *Autologous stem cells (adipose) and fibrin glue used to treat widespread traumatic calvarial defects: case report.* Journal of Cranio-Maxillofacial Surgery, 2004. **32**(6): p. 370-3.
167. Li, G., et al., *Poly (3-hydroxybutyrate-co-4-hydroxybutyrate) based electrospun 3D scaffolds for delivery of autogeneic chondrocytes and adipose-derived stem cells: evaluation of cartilage defects in rabbit.* Journal of Biomedical Nanotechnology, 2015. **11**(1): p. 105-16.

168. Latief, N., et al., *Adipose stem cells differentiated chondrocytes regenerate damaged cartilage in rat model of osteoarthritis.* Cell Biology International, 2016. **40**(5): p. 579-88.
169. Kasir, R., V.N. Vernekar, and C.T. Laurencin, *Regenerative engineering of cartilage using adipose-derived stem cells.* Regenerative engineering and translational medicine, 2015. **1**(1): p. 42-49.
170. Pak, J., *Regeneration of human bones in hip osteonecrosis and human cartilage in knee osteoarthritis with autologous adipose-tissue-derived stem cells: a case series.* Journal of medical case reports, 2011. **5**(1): p. 296.
171. Koh, Y.-G. and Y.-J. Choi, *Infrapatellar fat pad-derived mesenchymal stem cell therapy for knee osteoarthritis.* The Knee, 2012. **19**(6): p. 902-7.
172. Pak, J., J.H. Lee, and S.H. Lee, *A novel biological approach to treat chondromalacia patellae.* PLoS One, 2013. **8**(5): p. e64569.
173. Sterodimas, A., et al., *Tissue engineering with adipose-derived stem cells (ADSCs): current and future applications.* Journal of Plastic, Reconstructive & Aesthetic Surgery, 2010. **63**(11): p. 1886-92.
174. Yoshimura, K., et al., *Cell-assisted lipotransfer for facial lipoatrophy: efficacy of clinical use of adipose-derived stem cells.* Dermatologic Surgery, 2008. **34**(9): p. 1178-85.
175. Rigotti, G., et al., *Clinical treatment of radiotherapy tissue damage by lipoaspirate transplant: a healing process mediated by adipose-derived adult stem cells.* Plastic and reconstructive surgery, 2007. **119**(5): p. 1409-22.
176. Tiryaki, T., N. Findikli, and D. Tiryaki, *Staged stem cell-enriched tissue (SET) injections for soft tissue augmentation in hostile recipient areas: a preliminary report.* Aesthetic Plastic Surgery, 2011. **35**: p. 965-71.
177. Valina, C., et al., *Intracoronary administration of autologous adipose tissue-derived stem cells improves left ventricular function, perfusion, and remodelling after acute myocardial infarction.* European heart journal, 2007. **28**(21): p. 2667-77.
178. Schaun, M.I., et al., *Cell therapy in ischemic heart disease: interventions that modulate cardiac regeneration.* Stem cells international, 2016. **2016**.
179. Perin, E.C., et al., *Adipose-derived regenerative cells in patients with ischemic cardiomyopathy: The PRECISE Trial.* American heart journal, 2014. **168**(1): p. 88-95. e2.
180. Suga, H., et al., *IFATS collection: Fibroblast growth factor-2-induced hepatocyte growth factor secretion by adipose-derived stromal cells inhibits postinjury fibrogenesis through a c-Jun N-terminal kinase-dependent mechanism.* Stem cells, 2009. **27**(1): p. 238-49.
181. Seo, M.J., et al., *Differentiation of human adipose stromal cells into hepatic lineage in vitro and in vivo.* Biochemical and biophysical research communications, 2005. **328**(1): p. 258-64.
182. Gutierrez-Fernandez, M., et al., *Adipose tissue-derived mesenchymal stem cells as a strategy to improve recovery after stroke.* Expert opinion on biological therapy, 2015. **15**(6): p. 873-881.

183. Chang, K.-A., J.-H. Lee, and Y.-H. Suh, *Therapeutic potential of human adipose-derived stem cells in neurological disorders.* Journal of pharmacological sciences, 2014. **126**(4): p. 293-301.
184. Kim, S., et al., *The preventive and therapeutic effects of intravenous human adipose-derived stem cells in Alzheimer's disease mice.* PLoS One, 2012. **7**(9): p. e45757.
185. Ma, T., et al., *Intracerebral transplantation of adipose-derived mesenchymal stem cells alternatively activates microglia and ameliorates neuropathological deficits in Alzheimer's disease mice.* Cell transplantation, 2013. **22**: p. S113-26.
186. Lee, J.K., H.K. Jin, and J.-s. Bae, *Bone marrow-derived mesenchymal stem cells reduce brain amyloid-β deposition and accelerate the activation of microglia in an acutely induced Alzheimer's disease mouse model.* Neuroscience letters, 2009. **450**(2): p. 136-41.
187. Lee, S.T., et al., *Slowed progression in models of Huntington disease by adipose stem cell transplantation.* Annals of Neurology, 2009. **66**(5): p. 671-81.
188. Im, W., et al., *Extracts of adipose derived stem cells slows progression in the R6/2 model of Huntington's disease.* PloS one, 2013. **8**(4): p. e59438.
189. Gutiérrez-Fernández, M., et al., *Effects of intravenous administration of allogenic bone marrow-and adipose tissue-derived mesenchymal stem cells on functional recovery and brain repair markers in experimental ischemic stroke.* Stem cell research & therapy, 2013. **4**(1): p. 1-12.
190. Leu, S., et al., *Adipose-derived mesenchymal stem cells markedly attenuate brain infarct size and improve neurological function in rats.* Journal of translational medicine, 2010. **8**(63): p. 1-16.
191. Gutiérrez-Fernández, M., et al., *Trophic factors and cell therapy to stimulate brain repair after ischaemic stroke.* Journal of cellular and molecular medicine, 2012. **16**(10): p. 2280-90.
192. Gutiérrez-Fernández, M., et al., *Comparison between xenogeneic and allogeneic adipose mesenchymal stem cells in the treatment of acute cerebral infarct: proof of concept in rats.* Journal of translational medicine, 2015. **13**: p. 1-10.
193. Ikegame, Y., et al., *Comparison of mesenchymal stem cells from adipose tissue and bone marrow for ischemic stroke therapy.* Cytotherapy, 2011. **13**(6): p. 675-85.
194. Schwerk, A., et al., *Adipose-derived human mesenchymal stem cells induce long-term neurogenic and anti-inflammatory effects and improve cognitive but not motor performance in a rat model of Parkinson's disease.* Regenerative medicine, 2015. **10**(4): p. 431-46.
195. Elkin, B.S., et al., *Mechanical heterogeneity of the rat hippocampus measured by atomic force microscope indentation.* Journal of neurotrauma, 2007. **24**(5): p. 812-22.
196. Lu, Y.B., et al., *Viscoelastic properties of individual glial cells and neurons in the CNS.* Proceedings of the National Academy of Sciences, 2006. **103**(47): p. 17759-64.

197. Mazuchowski, E.L., A Thibault, Lawrence E. *BIOMECHANICAL PROPERTIES OF THE HUMAN SPINAL CORD AND PIA MATER*. in *2003 Summer Bioengineering Conference* 2003. Florida.
198. Bilston, L.E. and L.E. Thibault, *The mechanical properties of the human cervical spinal cord in vitro.* Annals of biomedical engineering, 1996. **24**(1): p. 67-74.
199. Bertram, C.D., L.E. Bilston, and M.A. Stoodley, *Tensile radial stress in the spinal cord related to arachnoiditis or tethering: a numerical model.* Medical & biological engineering & computing, 2008. **46**(7): p. 701-7.
200. Maikos, J.T., R.A. Elias, and D.I. Shreiber, *Mechanical properties of dura mater from the rat brain and spinal cord.* Journal of Neurotrauma, 2008. **25**(1): p. 38-51.
201. Rho, J.Y., R.B. Ashman, and C.H. Turner, *Young's modulus of trabecular and cortical bone material: ultrasonic and microtensile measurements.* Journal of Biomechanics, 1993. **26**(2): p. 111-9.
202. Liu, J., et al., *Hydrogels for Engineering of Perfusable Vascular Networks.* International journal of molecular sciences, 2015. **16**(7): p. 15997-6016.
203. Pelegri, N.G., C.A. Gorrie, and J. Santos, *Rat Hippocampal Neural Stem Cell Modulation Using PDGF, VEGF, PDGF/VEGF, and BDNF.* Stem cells international, 2019. **2019**: p. 4978917.
204. Hachem, L.D., A.J. Mothe, and C.H. Tator, *Effect of BDNF and Other Potential Survival Factors in Models of In Vitro Oxidative Stress on Adult Spinal Cord-Derived Neural Stem/Progenitor Cells.* Bioresearch Open Access, 2015. **4**(1): p. 146-59.
205. Mothe, A.J., et al., *Neural stem/progenitor cells from the adult human spinal cord are multipotent and self-renewing and differentiate after transplantation.* PLoS One, 2011. **6**(11): p. e27079.
206. Ahmed, S., B.A. Reynolds, and S. Weiss, *BDNF enhances the differentiation but not the survival of CNS stem cell-derived neuronal precursors.* The Journal of Neuroscience, 1995. **15**(8): p. 5765-78.
207. Jin, K., et al., *Vascular endothelial growth factor (VEGF) stimulates neurogenesis in vitro and in vivo.* Proceedings of the National Academy of Sciences of the United States of America, 2002. **99**(18): p. 11946-50.
208. Sun, Y., et al., *Vascular endothelial growth factor-B (VEGFB) stimulates neurogenesis: evidence from knockout mice and growth factor administration.* Developmental biology, 2006. **289**(2): p. 329-35.
209. Khaibullina, A.A., J.M. Rosenstein, and J.M. Krum, *Vascular endothelial growth factor promotes neurite maturation in primary CNS neuronal cultures.* Brain research. Developmental brain research, 2004. **148**(1): p. 59-68.
210. Chen, B.Y., et al., *Brain-derived neurotrophic factor stimulates proliferation and differentiation of neural stem cells, possibly by triggering the Wnt/beta-catenin signaling pathway.* Journal of neuroscience research, 2013. **91**(1): p. 30-41.
211. Cattaneo, E. and R. McKay, *Proliferation and differentiation of neuronal stem cells regulated by nerve growth factor.* Nature, 1990. **347**(6295): p. 762-65.

212. Schanzer, A., et al., *Direct stimulation of adult neural stem cells in vitro and neurogenesis in vivo by vascular endothelial growth factor.* Brain Pathology, 2004. **14**(3): p. 237-48.
213. Georgiou, M., et al., *Engineered neural tissue with aligned, differentiated adipose-derived stem cells promotes peripheral nerve regeneration across a critical sized defect in rat sciatic nerve.* Biomaterials, 2015. **37**: p. 242-51.
214. Anghileri, E., et al., *Neuronal differentiation potential of human adipose-derived mesenchymal stem cells.* Stem cells and development, 2008. **17**(5): p. 909-16.
215. Xu, Y., et al., *Myelin-forming ability of Schwann cell-like cells induced from rat adipose-derived stem cells in vitro.* Brain Research, 2008. **1239**: p. 49-55.
216. Xu, Y., et al., *Neurospheres from rat adipose-derived stem cells could be induced into functional Schwann cell-like cells in vitro.* BMC neuroscience, 2008. **9**: p. 21.
217. Fujimura, J., et al., *Neural differentiation of adipose-derived stem cells isolated from GFP transgenic mice.* Biochemical and biophysical research communications, 2005. **333**(1): p. 116-21.
218. Santos, J., B.K. Milthorpe, and M.P. Padula, *Proteomic Analysis of Cyclic Ketamine Compounds Ability to Induce Neural Differentiation in Human Adult Mesenchymal Stem Cells.* International journal of stem cells, 2019. **20**(3).
219. Santos, J., et al., *Proteomic Analysis of Human Adipose Derived Stem Cells during Small Molecule Chemical Stimulated Pre-neuronal Differentiation.* International journal of stem cells, 2017. **10**(2): p. 193-217.
220. Li, X., et al., *Effect of substrate stiffness on the functions of rat bone marrow and adipose tissue derived mesenchymal stem cells in vitro.* Journal of Biomedical Materials Research Part A 2014. **102**(4): p. 1092-101.
221. Mao, A.S., J.W. Shin, and D.J. Mooney, *Effects of substrate stiffness and cell-cell contact on mesenchymal stem cell differentiation.* Biomaterials, 2016. **98**: p. 184-91.
222. Shih, Y.R., et al., *Matrix stiffness regulation of integrin-mediated mechanotransduction during osteogenic differentiation of human mesenchymal stem cells.* Journal of bone and mineral research, 2011. **26**(4): p. 730-8.
223. Flanagan, L.A., et al., *Neurite branching on deformable substrates.* Neuroreport, 2002. **13**(18): p. 2411-15.
224. Koch, D., et al., *Strength in the periphery: growth cone biomechanics and substrate rigidity response in peripheral and central nervous system neurons.* Biophysical journal, 2012. **102**(3): p. 452-60.
225. Man, A.J., et al., *Neurite outgrowth in fibrin gels is regulated by substrate stiffness.* Tissue Engineering. Part A, 2011. **17**(23-24): p. 2931-42.
226. Leipzig, N.D. and M.S. Shoichet, *The effect of substrate stiffness on adult neural stem cell behavior.* Biomaterials, 2009. **30**(36): p. 6867-78.

227. Saha, K., et al., *Substrate modulus directs neural stem cell behavior.* Biophysical journal, 2008. **95**(9): p. 4426-38.
228. Hoffman, A.S., *Hydrogels for biomedical applications.* Advanced Drug Delivery Reviews, 2012. **64**: p. 18-23.
229. Tibbitt, M.W. and K.S. Anseth, *Hydrogels as extracellular matrix mimics for 3D cell culture.* Biotechnology and bioengineering, 2009. **103**(4): p. 655-63.
230. Caló, E. and V. Khutoryanskiy, *Biomedical applications of hydrogels: A review of patents and commercial products.* European Polymer Journal, 2015. **65**: p. 252-267.
231. Koutsopoulos, S., *Self-assembling peptide nanofiber hydrogels in tissue engineering and regenerative medicine: Progress, design guidelines, and applications.* Journal of biomedical materials research. Part A, 2016. **104**(4): p. 1002-16.
232. Koutsopoulos, S., et al., *Controlled release of functional proteins through designer self-assembling peptide nanofiber hydrogel scaffold.* Proceedings of the National Academy of Sciences of the United States of America, 2009. **106**(12): p. 4623-8.
233. Koutsopoulos, S. and S. Zhang, *Two-layered injectable self-assembling peptide scaffold hydrogels for long-term sustained release of human antibodies.* Journal of controlled release : official journal of the Controlled Release Society, 2012. **160**(3): p. 451-8.
234. Kisiday, J., et al., *Self-assembling peptide hydrogel fosters chondrocyte extracellular matrix production and cell division: implications for cartilage tissue repair.* Proceedings of the National Academy of Sciences of the United States of America, 2002. **99**(15): p. 9996-10001.
235. Nagai, Y., et al., *Slow release of molecules in self-assembling peptide nanofiber scaffold.* Journal of controlled release : official journal of the Controlled Release Society, 2006. **115**(1): p. 18-25.
236. Marchini, A., et al., *Multifunctionalized hydrogels foster hNSC maturation in 3D cultures and neural regeneration in spinal cord injuries.* Proceedings of the national academy of sciences, 2019. **116**(15): p. 7483-92.
237. Aurand, E.R., et al., *Hydrogel formulation determines cell fate of fetal and adult neural progenitor cells.* Stem cell research, 2014. **12**(1): p. 11-23.
238. Zychowicz, M., et al., *The collagen scaffold supports hiPSC-derived NSC growth and restricts hiPSC.* Frontiers in bioscience (Scholar edition), 2019. **11**: p. 105-21.
239. McKinnon, D.D., A.M. Kloxin, and K.S. Anseth, *Synthetic hydrogel platform for three-dimensional culture of embryonic stem cell-derived motor neurons.* Biomaterial science, 2013. **1**(5): p. 460-69.
240. Daud, M.F., et al., *An aligned 3D neuronal-glial co-culture model for peripheral nerve studies.* Biomaterials, 2012. **33**(25): p. 5901-13.
241. Wei, Z., B.T. Harris, and L.G. Zhang. *Gelatin methacrylamide hydrogel with graphene nanoplatelets for neural cell-laden 3D bioprinting*. in *Annual International Conference of the IEEE Engineering in Medicine and Biology Society (EMBC)*. 2016. Orlando, FL, USA: IEEE.

242. Al Rifai, N., et al. *Culture of PC12 neuronal cells in GelMA hydrogel for brain tissue engineering*. in *2015 International Conference on Advances in Biomedical Engineering (ICABME)*. 2015. Beirut, Lebanon: Institute of Electrical and Electronic Engineers.
243. Wu, Y., et al., *The influence of the stiffness of GelMA substrate on the outgrowth of PC12 cells.* Bioscience reports, 2019. **39**(1).
244. Dursun Usal, T., D. Yucel, and V. Hasirci, *A novel GelMA-pHEMA hydrogel nerve guide for the treatment of peripheral nerve damages.* International journal of biological macromolecules, 2019. **121**: p. 699-706.
245. Koffler, J., et al., *Biomimetic 3D-printed scaffolds for spinal cord injury repair.* Nature Medicine, 2019. **25**(2): p. 263-269.
246. Mahoney, M.J. and K.S. Anseth, *Three-dimensional growth and function of neural tissue in degradable polyethylene glycol hydrogels.* Biomaterials, 2006. **27**(10): p. 2265-74.
247. Lampe, K.J., et al., *Effect of macromer weight percent on neural cell growth in 2D and 3D nondegradable PEG hydrogel culture.* Journal of biomedical materials research. Part A, 2010. **94**(4): p. 1162-71.
248. Mooney, R., et al., *Control of neural cell composition in poly(ethylene glycol) hydrogel culture with soluble factors.* Tissue Engineering. Part A, 2011. **17**(21-2): p. 2805-15.
249. Lampe, K.J., K.B. Bjugstad, and M.J. Mahoney, *Impact of degradable macromer content in a poly(ethylene glycol) hydrogel on neural cell metabolic activity, redox state, proliferation, and differentiation.* Tissue Engineering Part A, 2010. **16**(6): p. 1857-66.
250. Namba, R.M., et al., *Development of porous PEG hydrogels that enable efficient, uniform cell-seeding and permit early neural process extension.* Acta biomaterialia, 2009. **5**(6): p. 1884-97.
251. Freudenberg, U., et al., *A star-PEG-heparin hydrogel platform to aid cell replacement therapies for neurodegenerative diseases.* Biomaterials, 2009. **30**(28): p. 5049-60.
252. Naghdi, P., et al., *Survival, proliferation and differentiation enhancement of neural stem cells cultured in three-dimensional polyethylene glycol-RGD hydrogel with tenascin.* Journal of Tissue Engineering and Regenerative Medicine, 2016. **10**(3): p. 199-208.
253. Yue, K., et al., *Synthesis, properties, and biomedical applications of gelatin methacryloyl (GelMA) hydrogels.* Biomaterials, 2015. **73**: p. 254-71.
254. Nichol, J.W., et al., *Cell-laden microengineered gelatin methacrylate hydrogels.* Biomaterials, 2010. **31**(21): p. 5536-44.
255. Hosseini, V., et al., *Engineered contractile skeletal muscle tissue on a microgrooved methacrylated gelatin substrate.* Tissue Engineering Part A, 2012. **18**(23-24): p. 2453-65.
256. Liu, Y. and M.B. Chan-Park, *A biomimetic hydrogel based on methacrylated dextran-graft-lysine and gelatin for 3D smooth muscle cell culture.* Biomaterials, 2010. **31**(6): p. 1158-70.
257. Zhao, X., et al., *Photocrosslinkable Gelatin Hydrogel for Epidermal Tissue Engineering.* Advanced healthcare materials, 2016. **5**(1): p. 108-18.

258. Chen, M.B., et al., *A 3D microfluidic platform incorporating methacrylated gelatin hydrogels to study physiological cardiovascular cell-cell interactions.* Lab Chip, 2013. **13**(13): p. 2591-8.
259. Li, X., et al., *3D Culture of Chondrocytes in Gelatin Hydrogels with Different Stiffness.* Polymers (Basel), 2016. **8**(8).
260. Schuurman, W., et al., *Gelatin-methacrylamide hydrogels as potential biomaterials for fabrication of tissue-engineered cartilage constructs.* Macromolecular bioscience, 2013. **13**(5): p. 551-61.
261. Van den Steen, P.E., et al., *Biochemistry and molecular biology of gelatinase B or matrix metalloproteinase-9 (MMP-9).* Critical reviews in biochemistry and molecular biology, 2002. **37**(6): p. 375-536.
262. Van Den Bulcke, A.I., et al., *Structural and rheological properties of methacrylamide modified gelatin hydrogels.* Biomacromolecules, 2000. **1**(1): p. 31-8.
263. Pepelanova, I., et al., *Gelatin-Methacryloyl (GelMA) Hydrogels with Defined Degree of Functionalization as a Versatile Toolkit for 3D Cell Culture and Extrusion Bioprinting.* Bioengineering (Basel), 2018. **5**(3): p. 55.
264. Shirahama, H., et al., *Precise Tuning of Facile One-Pot Gelatin Methacryloyl (GelMA) Synthesis.* Scientific reports, 2016. **6**: p. 31036.
265. Bertassoni, L.E., et al., *Direct-write bioprinting of cell-laden methacrylated gelatin hydrogels.* Biofabrication, 2014. **6**(2): p. 024105.
266. Eke, G., et al., *Development of a UV crosslinked biodegradable hydrogel containing adipose derived stem cells to promote vascularization for skin wounds and tissue engineering.* Biomaterials, 2017. **129**: p. 188-98.
267. Salamon, A., et al., *Gelatin-Based Hydrogels Promote Chondrogenic Differentiation of Human Adipose Tissue-Derived Mesenchymal Stem Cells In Vitro.* Materials (Basel), 2014. **7**(2): p. 1342-59.
268. Hu, Y., et al., *3D-engineering of Cellularized Conduits for Peripheral Nerve Regeneration.* Scientific reports, 2016. **6**: p. 32184.
269. Zhu, J., *Bioactive modification of poly(ethylene glycol) hydrogels for tissue engineering.* Biomaterials, 2010. **31**(17): p. 4639-56.
270. Hutson, C.B., et al., *Synthesis and characterization of tunable poly(ethylene glycol): gelatin methacrylate composite hydrogels.* Tissue Engineering Part A, 2011. **17**(13-14): p. 1713-23.
271. Nuttelman, C.R., M.C. Tripodi, and K.S. Anseth, *In vitro osteogenic differentiation of human mesenchymal stem cells photoencapsulated in PEG hydrogels.* J Biomed Mater Res A, 2004. **68**(4): p. 773-82.
272. Whitehead, A.K., et al., *Poly (ethylene glycol) hydrogel elasticity influences human mesenchymal stem cell behavior.* Regenerative Biomaterials, 2018. **5**(3): p. 167-75.
273. Schneider, M.C., et al., *An in vitro and in vivo comparison of cartilage growth in chondrocyte-laden matrix metalloproteinase-sensitive poly(ethylene glycol) hydrogels with localized transforming growth factor beta3.* Acta biomaterialia, 2019. **93**.

274. Cruz-Acuña, R., et al., *PEG-4MAL hydrogels for human organoid generation, culture, and in vivo delivery.* Nature protocols, 2018. **13**(9): p. 2102-119.
275. Cruz-Acuna, R., et al., *PEG-4MAL hydrogels for in vitro culture of human organoids and in vivo delivery to sites of injury.* Protocol exchange, 2017.
276. Scientific, T.F. *CultureOne™ Supplement (100X)*. 2023 [cited 2023 10th October]; Available from: https://www.thermofisher.com/order/catalog/product/A3320201.
277. Scientific, T.F. *B-27™ Supplement (50X), serum free*. 2023 [cited 2023 10th October]; Available from: https://www.thermofisher.com/order/catalog/product/17504044.
278. Scientific, T.F. *N-2 Supplement (100X)*. 2023 [cited 2023 10th October]; Available from: https://www.thermofisher.com/order/catalog/product/17502048.

# Chapter Two: Neurogenic marker expression in differentiating human adipose-derived adult mesenchymal stem cells.

**Submitted as:**
*Pelegri NG, Milthorpe BK, Gorrie CA, Santos J. Neurogenic marker expression in differentiating human adipose derived adult mesenchymal stem cells. Stem Cell Investig. 2023 Mar 23;10:7. doi: 10.21037/sci-2022-015. PMID: 37034185; PMCID: PMC10076228.*

Published on 23rd of March 2023

I certify that the work present in chapter two of this thesis has not been previously submitted as part of the requirements for a degree. I also certify that I carried out more than 70% of the experimental work, analysis and interpretation of the data presented in this paper.

**Author's contributions:**

Conceptualization, J.S., N.G.P. and C.A.G.; methodology, J.S., N.G.P. and C.A.G.; formal analysis, N.G.P.; investigation, N.G.P.; resources, J.S., B.K.M.; data curation, N.G.P.; writing—original draft preparation, N.G.P.; writing—review and editing, NGP; visualization, N.G.P.; supervision J.S. and C.A.G.; project administration, J.S.; funding acquisition, J.S. and B.K.M. All authors have read and agreed to the published version of the manuscript.

| | |
|---|---|
| Neus Gomila Pelegri | Production Note:<br>Signature removed prior to publication. |
| Bruce K. Milthorpe | Production Note:<br>Signature removed prior to publication. |
| Catherine A. Gorrie | Production Note:<br>Signature removed prior to publication. |
| Jerran Santos | Production Note:<br>Signature removed prior to publication. |

Original Article



# Neurogenic marker expression in differentiating human adipose derived adult mesenchymal stem cells

**Neus Gomila Pelegri[1,2], Bruce K. Milthorpe[1], Catherine A. Gorrie[2], Jerran Santos[1]**

[1]Advanced Tissue Engineering and Stem Cell Biology Group, School of Life Sciences, University of Technology Sydney, Sydney, NSW, Australia; [2]Neural Injury Research Unit, School of Life Sciences, University of Technology Sydney, Sydney, NSW, Australia

*Contributions:* (I) Conception and design: J Santos, BK Milthorpe, NG Pelegri; (II) Administrative support: CA Gorrie; (III) Provision of study materials: J Santos; (IV) Collection and assembly of data: NG Pelegri; (V) Data analysis and interpretation: NG Pelegri; (VI) Manuscript writing: All authors; (VII) Final approval of manuscript: All authors.

*Correspondence to:* Jerran Santos, PhD. Advanced Tissue Engineering and Stem Cell Biology Group, School of Life Sciences, University of Technology Sydney, Sydney, NSW, Australia. Email: Jerran.Santos@uts.edu.au.

**Background:** Adipose-derived stem cells (ADSCs) are increasingly utilised in the field of neural regeneration due to their high accessibility and capacity for differentiation into neural like cells. Culturing ADSCs in the presence of various growth factors, small molecules and combinations thereof have shown promise in this regard; however, these protocols are generally complex, time-consuming and costly. The need for commercially available and chemically defined growth media/supplements is required to facilitate further developments in this area.

**Methods:** In this study, we have examined the neural differentiation and proliferation potential of the commercially available supplements B27, CultureOne (C1) and N2 on human ADSCs (hADSCs). Through a combination of immunocytochemistry, cytokine analysis, and CNPase enzymatic assays, we provide novel insight into the neural differentiation effects of B27, C1 and N2 on hADSCs.

**Results:** The study found that C1 and N2 supplements initiated neural differentiation of the cells, with C1 pushing differentiation towards an oligodendrocytic lineage and N2 initiating neuronal differentiation. This suggests that C1 and N2 supplements can be used to drive neural differentiation in hADSCs. However, B27 did not show significant differentiation in the time frame in which the experiments took place and therefore is unsuitable for this purpose.

**Conclusions:** These findings highlight the utility of commercially available supplements in the neural differentiation of ADSCs and may assist in establishing simpler, more affordable differentiation protocols.

**Keywords:** CNPase; neurogenesis; oligodendrocytes; neurons; adipose-derived stem cells (ADSCs)

Received: 21 June 2022; Accepted: 16 February 2023; Published online: 23 March 2023.

doi: 10.21037/sci-2022-015

**View this article at:** https://dx.doi.org/10.21037/sci-2022-015

## Introduction

Adipose-derived stem cells (ADSCs), a mesenchymal stem cell (MSC) type, are of particular interest given that they are multipotent *in vitro* and are easily obtained via subcutaneous adipose tissue liposuction. This is a less invasive procedure compared to other common stem cell collection methods like bone marrow aspirates but still yields high cell numbers (1-6). ADSCs have the potential to differentiate into adipogenic, chondrogenic, osteogenic, myogenic, and neurogenic like cell lineages (7-10), making them suitable for many applications. Additionally, ADSCs have also been found to express b-III tubulin and NeuN in their undifferentiated state, two well-known markers of neuronal differentiation, hinting at their potential to become neural-like cells (11).

The differentiation of ADSCs into neural-like cells challenges the dogma that adult stem cells are multipotent and are restricted to differentiating into cell types derived

from the same embryonic germ layer; ADSCs are derived from the mesoderm while neural cells are derived from the ectoderm (12,13). Stem cell phenotypic signatures can be mapped out through several analytical techniques. These result in the identification of molecular and cellular markers, including surface makers, secreted proteins, and cytokines. These types of analyses highlight aspects of the cells' differentiation potential, while others suggest functions of specific molecules during the various differentiation states. To date, several different growth factors and chemicals have been explored to induce neural differentiation in ADSCs; rodent ADSCs have been successfully differentiated into neural stem cells (NSCs) and dopaminergic neurons following a two-step protocol of overnight pre-induction with basic fibroblast growth factor (bFGF), butylated hydroxyanisole (BHA), and B27 supplement followed by a 14-day treatment with sonic hedgehog (SHH), fibroblast growth factor 8 (FGF8) and B27 supplement over 14 days (14).

Human ADSCs (hADSCs) have been successfully differentiated towards neuronal lineages and into neurospheres by using a mixture of B27 supplement, bFGF and human epidermal growth factor (hEGF) for a week and then further differentiated into neuron-like cells by following treatment with a mixture of by L-glutamine, non-essential amino acids, N2 supplement and B27 supplement for another week (15). hADSCs have also been differentiated into dopamine-secreting cells using a growth factor cocktail composed of SHH, bFGF, FGF8, and brain derived neurotrophic factor (BDNF) in low-serum conditions (16) and in B27 supplemented serum-free conditions (17). Neural differentiation in hADSCs has also been induced with valproic acid (18) and isobutylmethyl xanthine (IBMX) (19). MSCs have also shown to differentiate towards neural stem cells (NSCs) and neurons and increase the secretion of BDNF and nerve growth factor (NGF) when co-cultured with NSCs (20). Additionally, ADSC transplants with or without prior differentiation have been reported to be beneficial in animal models of neuronal disorders such as Parkinson's disease, (21) peripheral nerve injury (22), epilepsy (23) and stroke (24), indicating their neuroregenerative potential.

A great variety of growth factors and chemicals are being studied alone or in combination as potential protocols for hADSCs differentiation into neural-like cells. Here, we will explore three readily available media supplements in isolation to distinguish the effects of the supplements on the hADSC differentiation process. In this current study, the potential of B27, CultureOne (C1) and N2 will be examined for neural differentiation of hADSCs *in vitro* using microscopic analysis to track morphological changes and cell numbers, immunocytochemistry to detect changes in neural marker expression and Bioplex analysis to investigate the changes in cytokine and chemokine secretion levels by the cells. Cytokines and chemokines investigation provides valuable insight into the secreted cytokines and their role in activating differentiation pathways in cells (25). As per the manufacturer's descriptions, these are commercially available neural differentiation and proliferation supplements and have been used for maintenance, maturation, proliferation and differentiation of neuronal stem cells (26,27).

## Methods

### *Cell culture*

#### Maintenance

hADSCs from a single donor were isolated and expanded as previously described (28) with approval from the UTS Human Research Ethics Committee (Ethics No. 2013000437). The study was conducted in accordance with the Declaration of Helsinki (as revised in 2013). Written informed consent was acquired for donor lipoaspirate release for research purposes only. After isolation, hADSCs were maintained in control media [Dulbecco's Modified Eagle medium (DMEM)/F12 + Glutamax media] (Gibco, Life Technologies, Carlsbad, CA, USA) with 10% heat inactivated foetal bovine serum (FBS, Gibco, Life Technologies, Carlsbad, CA, USA) and 1% Antibiotics/Antimycotics (ABAM, Gibco, Life Technologies, Carlsbad, CA, USA) and incubated at 37 ℃ at 5% $CO_2$. hADSCs were passaged five to seven times post isolation by stripping cells with TrypLE Express (12604 Gibco, Life Technologies, Roskilde, Denmark) before being cryostored by storing the cells in 90% FBS/10% DMSO v/v at –80 ℃.

#### Differentiation

Cells were revived from cryostorage under sterile conditions at passage 7 into control media DMEM/F12 + Glutamax media with 10% FBS and incubated at 37 ℃ with 5% $CO_2$. Cells were expanded until passage 9, and when they reached 80% confluency, they were seeded into either 6 well plates at 40,000 cells/mL or 24-well plates at 20,000 cells/mL for molecular or imaging analysis, respectively. Once cells reached 95%±2% confluence, treatment commenced. There were 3 biological replicates.

hADSCs were treated under sterile conditions at all

**Table 1** Treatment groups

| Treatment | Cell type | Base media | Supplement |
|---|---|---|---|
| B27 | hADSC | Neurobasal media | B27 supplement (50×) #17504-001 (Gibco, Life Technologies) |
| N2 | hADSC | Neurobasal media | N2 supplement (100×) #17502-048 (Gibco, Life Technologies) |
| CultureOne | hADSC | Neurobasal media | CultureOne (C1) supplement (100×) #A33202-01 (Gibco, Life Technologies) |
| DMEM (undifferentiated control) | hADSC | DMEM/F12 + Glutamax—control media | 10% FBS (Gibco, Life Technologies) |
| Staining controls | SHSY-5Y (NBCs) or U87MG (GBCs) | DMEM/F12 + Glutamax—control media | 10% FBS (Gibco, Life Technologies) |

DMEM, Dulbecco's Modified Eagle medium; hADSC, human adipose-derived stem cell; FBS, foetal bovine serum; NBC, neuroblastoma cell; GBC, glioblastoma cell.

times, and media were changed every 84 hours for 7 days. All cells were treated with either control media DMEM (DMEM/F12 + Glutamax + 10% FBS) (Gibco, Life Technologies, Carlsbad, CA, USA) or with Neurobasal media (Gibco, Life Technologies, Carlsbad, CA, USA) with 1% abam [antibiotic-antimycotic (100×) #15240-062 Invitrogen, CA, USA] and the addition of supplements shown in *Table 1*. The treatments used are commercially available media supplements for the purpose of neuronal cell maintenance, survival and differentiation *in vitro*. During treatment, at every media change, conditioned media were collected for further testing, and phase images at 10x magnification were taken of each treatment condition on the same marked area using the EVOS XL Core microscope (Thermofisher, Massachusetts, USA).

After 7 days of treatment, cells were either fixed for immunocytochemistry with 10% formalin for 30 min at room temperature, or they were harvested using a cell scraper and frozen at –80 ℃ for further testing.

### *Cytokine analysis*

#### Bioplex

The Bioplex assay is a commercially available immunoassay kit (Bio-plex Pro human cytokine 27-plex, M50-0KCAF0Y BioRad Laboratories, Hercules, CA, USA) for investigating and quantitating cytokine concentration changes relative to the baseline levels of up to 27 cytokines across multiple sample types simultaneously.

During treatment, 500 µL aliquots of conditioned media from each treatment group were collected at time 0 h and after every 84 h and stored at –80 ℃ until the assay was conducted. Concentrations of 27 cytokines consisting of interlukins IL-1b, IL-1ra, IL-2, IL-4, IL-5, IL-6, IL-7, IL-8, IL-9, IL-10, IL-12, IL-13, IL-15, IL-17A, Eotaxin, fibroblast growth factor (FGF) basic, granulocyte colony-stimulating factor (G-CSF), granulocyte-macrophage colony-stimulating factor (GM-CSF), interferon (IFN)-g, interferon gamma induced protein-10 (IP-10), monocyte chemoattractant protein-1 (MCP-1), macrophage inflammatory protein-1a (MIP-1a), platelet derived growth factor-bb (PDGF-bb), macrophage inflammatory protein-1b (MIP-1b), RANTES, tumor necrosis factor (TNF)-α and vascular endothelial growth factor (VEGF)] were simultaneously assessed using the Bioplex kit. Assays were performed according to the manufacturer's instructions.

### *Protein analysis*

#### Immunocytochemistry

After a primary wash with phosphate-buffered saline (PBS 0.01 M), fixed cells underwent a second wash step for 15 minutes in phosphate buffered saline triton-x (PBST) [0.01 M PBS and 0.1% Triton X-100 (BDH #30632) at pH 7.4]. They were then blocked in 5% normal goat serum (NGS) (Sigma-Aldrich #G9023) in PBST for 30 minutes. Primary antibodies were diluted in PBG [0.1 M PBS, pH 7.4, 0.1% Triton-X, 2% NGS, 1% bovine serum albumin (BSA) (Sigma-Aldrich #A9647)] and were added to the relevant wells and incubated overnight at room temperature with gentle agitation. Primary antibodies were rabbit anti-glial fibrillary acidic protein (GFAP) (1:1,000, Dako, Denmark #Z0334) as an astrocyte marker; rabbit anti-β-III tubulin (1:500, Abcam, Cambridge, UK #ab18207) as an

early neuronal marker; mouse anti-CNPase (1:200 Abcam, #ab6319-100) as an oligodendrocyte marker; rabbit anti-Ki67 (1/50 Abcam, #ab833) as a proliferation marker; and rabbit anti-DoubleCortin (1:1,000 Abcam, #ab18723) as a neuron developing maker. Cells were then washed with three changes of PBST and incubated with goat anti-mouse AF488 (1:200, Invitrogen, #A11001) or goat anti-rabbit AF488 (1:200, Invitrogen, #A11008) secondary antibodies in PBG for two hours at room temperature with gentle agitation. Following an additional wash with PBST, and counterstained with Hoechst (1:5,000 Invitrogen) for 30 minutes to stain the nuclei and finally washed twice with PBST. Plates were imaged using an IN Cell Analyzer 2200 high-content cellular analysis system (GE Healthcare Life Sciences, UK). Positive staining control cells were included in all staining runs. Glioblastoma U87MG cells were used for GFAP, 2',3' cyclic-nucleotide 3' phosphodiesterase (CNPase), and Ki67 positive staining controls. Neuroblastoma SHSY-5Y cells were used for β-III tubulin positive staining controls. Both U87MG and SHSY-5Y cells were grown in separate plates from the experimental cells; however, the cells were stained in parallel with the experimental plates for each antibody and were fixed and stained following the same protocol as the experimental cells. U87MG and SHSY-5Y cells were grown in a 24-well plate with DMEM/F12 + Glutamax media (Gibco, MA, USA) enriched with 10% heat-inactivated FBS (Sigma-Aldrich, MO, USA) until confluent.

**Image analysis**

For each stained plate, 10 randomised immunofluorescent images of each well were taken with a 20× objective using the GE Healthcare Life Sciences-IN Cell analyser 2200 high-content cellular analysis system. ImageJ 1.52p software was used for automated unbiased image analysis to count stained nuclei and positive stained area using threshold and analyse particles functions in a macro and create a ratio of stained area to number of nuclei. False positives and low-quality images (e.g., out of field, out of focus) were manually excluded from the analysis. Cell counts at each treatment were conducted using the same automated image analysis to count for cell nuclei for 20 fields of view at 20×.

### *Enzyme analysis*

**Protein extraction**

Cell protein extraction protocol was adapted from Santos *et al.* 2017 (28). Cells were harvested by decanting culture media, rinsed twice in sterile 1× PBS and detached using a cell scraper and 1× PBS. The detached cells were then collected and centrifuged at 1,000 relative centrifugal force (rcf) for 5 minutes. The supernatant was decanted, and the cell pellet was frozen at −80 ℃ until ready for testing. Samples were defrosted on ice and resuspended in 10 µL of 1.5 M tris-HCL (hydrochloric acid) buffer. They were then pipette lysed on ice following 1min sonication in the sonicator bath.

**Dot blots**

CNPase plays an important role in myelin formation and oligodendrocyte development (29,30). To detect the presence of CNPase enzymes in the conditioned media, circles of 2 mm in diameter were drawn on the polyvinylidene difluoride (PVDF) membrane with graphite pencil, and the membrane was activated by wetting in methanol. It was then rinsed twice with 0.5 M Tris and then air dried. Subsequently, 2 µL of sample were added to the marked area and left to bind to the PVDF membrane. Once dry, it was rinsed in Tris-buffered saline, pH 7 (TBS) and blocked by washing 3 times, for 5–10 min each wash, in a solution of skim milk powder and MilliQ water (0.1% w/v). Then 2 µL of mouse anti-CNPase (1/200 Abcam, #ab6319) and rabbit anti-Glutaminase (1:1,000 Abcam, # ab156876) primary antibodies diluted in PBS was added to the respective marked areas and incubated at room temperature until absorbed. After, PVDF was rinsed 3 times for 5–10 min each wash with TBS; 2 µL of secondary antibody anti-mouse immunoglobulin G (IgG) alkaline phosphatase (1:30,000 A4312 Sigma-Aldrich) and Anti-rabbit IgG peroxidase (1:6,000 A6154 Sigma-Aldrich) was added to the marked areas and incubated at room temperature until absorbed. The PVDF was then collected and rinsed 3 times for 5–10 min each wash with TBS. The blot was then developed appropriately with 3',3-Diaminobenzidine tablets for developing peroxidase (D4293 Sigma-Aldrich) and BCIP/NBT for alkaline phosphatase (B5655 Sigma-Aldrich) and the blot was imaged.

**CNPase enzyme assay**

CNPase catalyses the hydrolysis of 2'3'-cAMP to 2'AMP (30,31). This reaction can be used to test for the presence or absence of functional CNPase enzyme secreted by the cells (*Figure 1*).

The methodology used was adapted from Dreiling and Mattson [1980], where CNPase + 2'3'-cAMP + Water + phenol red = 2'AMP + $H^+$ causing a decrease in pH that can be detected using a colourimetric assay (32). When

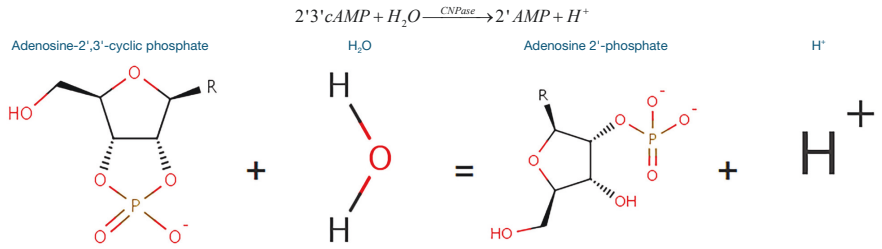


**Figure 1** Chemical reaction used to detect the presence of functional CNPase. 2'3' cAMP and water in the presence of CNPase will be hydrolised to 2' AMP and hydrogen. AMP, adenosine 2'-phosphate.

CNPase activity increases, pH will decrease (32), and when measuring that pH change with phenol red at 560 nm, it will result in a drop in absorbance (33).

Cells were first lysed on ice by adding equal parts by volume of buffer (1.5 M tris-HCL buffer at pH 8.8) and cells with gentle pipetting. Following a subsequent sonication, 5 µL of cells were loaded into a 96 well plate with 5 µL of Phenol red at 1 mM in NaOH pH 8.4 with 40 µL of 2'3'-cAMP (Sigma-Aldrich) 15 mM in MiliQ water. Test samples consisted of cells treated with either B27, N2, C1 or DMEM and of conditioned media following 84 hrs incubation of ADSC with either B27, N2, C1, or DMEM. Absorbance was measured at 560 nm for 90 min with 30 min interval reads and then during a further overnight incubation with reads every hour in the TECAN Infinity 200 plate reader. The blanks included consisted of Phenol red at pH 8.4 + substrate for the cell blanks and of Phenol red at pH 8.4 + substrate + clean media (B27, N2, C1, DMEM). A colourimetric result indicates the presence of CNPase secreted by the ADSC. An increase from the baseline DMEM sample indicates that the cells are differentiating towards an oligodendrocytic cell lineage in the presence of a growth factor.

### *Statistical analysis*

Data analysis for the raw imaging data was conducted using GraphPad Prism 8 using One-way analysis of variance (ANOVA), with a P value of <0.05 being considered statistically significant. Data analysis for Bioplex results was completed in R studio (version 1.3.959), where a single tail dendrogram heatmap was generated using Euclidean hierarchical clustering using R software for grouping cytokines trends over the different time points within each treatment.

## Results

### *Cell culture*

#### Cell morphology and survival

Morphological changes were observed between the treatments and the DMEM (undifferentiated control) (*Figure 2*) on both days 3.5 and 7. Individual cell morphology in the treatment groups becomes more polarised, and cells align more with each other in parallel bundles compared to the undifferentiated control cell organisation, specifically for B27 and N2 treatments. Cell counts did not significantly change between the treatments and the undifferentiated control DMEM (*Figure 2I*).

#### Immunocytochemistry and cellular differentiation

CNPase was not detected in undifferentiated cells and was expressed in all treatment groups (*Figures 3*,*4*), with the highest expression levels seen in the C1 group (*Figure 4A*) (P≤0.0001) and N2 group (*Figure 4B*) (P≤0.01). Doublecortin expression was absent in the undifferentiated ADSCs (*Figure 3B1*, *Figure 4B*) and only seen at low levels in the B27 and C1 treatment groups and significantly increased in the N2 treatment group (*Figure 3B3*, *Figure 4B*) (P≤0.0001). GFAP was absent in the undifferentiated ADSCs (*Figure 3C1*, *Figure 4C*), and GFAP levels were significantly increased in all treatment groups compared to the undifferentiated control (*Figure 3C2-C4*, *Figure 4C*) (P≤0.0001); however, these levels were lower than CNPase and Doublecortin expression levels in each treatment. b-III tubulin was expressed in the undifferentiated ADSCs (*Figure 3E1*) and did not significantly

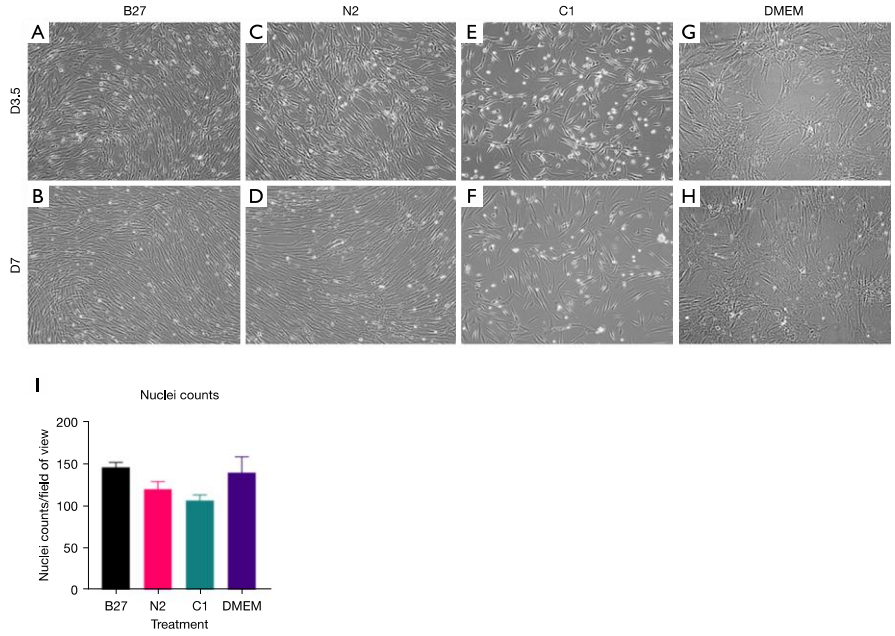


**Figure 2** Cell morphology and nuclei analysis (A-H) phase images 10× at day 3.5 and day 7 of treatment with either; (A,B) B27; (C,D) N2; (E,F) C1; (G,H) DMEM (undifferentiated control). Representative of the 3 biological replicates. (I) Nuclei counts/field of view for each treatment group and DMEM (undifferentiated control) at D7 after treatment completion of the 3 biological triplicates. DMEM, Dulbecco's Modified Eagle medium.

increase following differentiation with any treatment (*Figure 3E2-E4*, *Figure 4D*) (P>0.05). Undifferentiated cells expressed high levels of Ki67 and are undergoing proliferation (*Figure 3D1*). This was similar to the proliferation levels seen in all treatment groups (*Figure 3D1-D4*, *Figure 4E*). Overall, immunocytochemistry results (*Figure 4*) show that while all treatments co-express all markers, C1 is the treatment that shows the highest levels of CNPase, followed by N2 with CNPase expression and the highest levels of Doublecortin.

### *Cytokine analysis*

#### Bioplex

Bioplex assay was utilised to simultaneously investigate relative quantitative changes of 27 human cytokines across the different treatments and time points (*Figure 5*). The hierarchical clustering groups the cytokines with similar concentration trends over the treatment time points. Changes in cytokine levels for each treatment are shown as heatmaps in *Figure 4*. The heatmap provides an overview of all cytokines in relation to each other for each specific treatment over the two time points, day 3 and day 7, within each treatment.

The changes within each treatment can be observed on the heat maps (*Figure 5*). Overall, we find that IL-6, VEGF, and IL-8 cytokines continued to be the highest expressed cytokines regardless of treatment and IL-5 remained the cytokine with the lowest concentration across all treatments. However, when we look at differences between treatments on day 7 (*Figure 6*), it can be observed

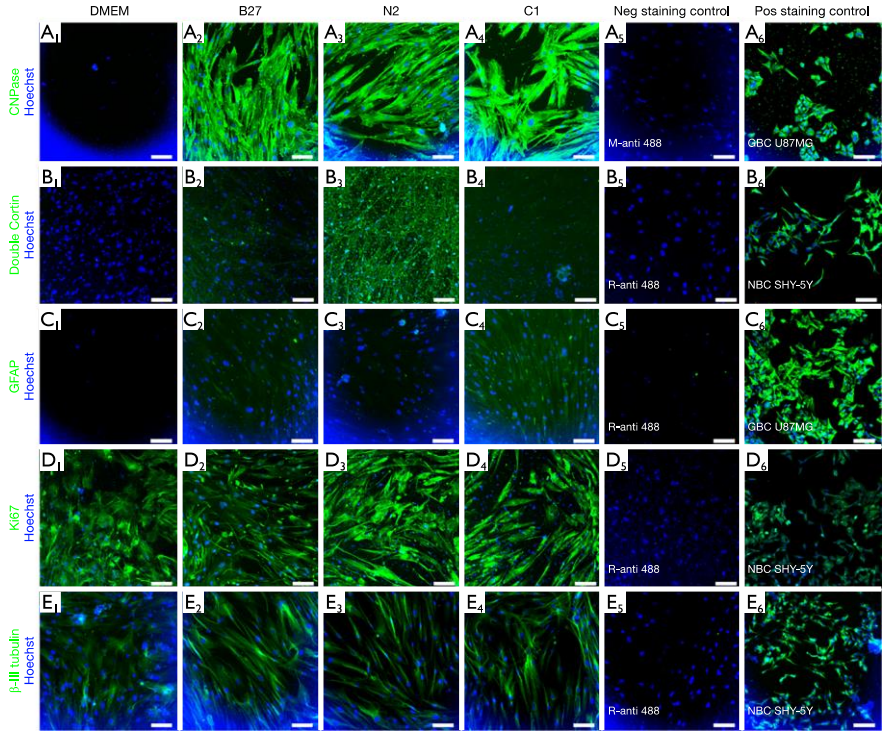


**Figure 3** Immunocytochemistry staining for (A) CNPase, (B) DoubleCortin, (C) GFAP, (D) Ki67 and (E) β-III tubulin, and following 7-day differentiation using B27, N2, C1 *vs.* DMEM (undifferentiated control). Scale bars =100 μm. GFAP, glial fibrillary acidic protein; DMEM, Dulbecco's Modified Eagle medium.

that while the cytokines that were originally secreted in the highest concentrations in DMEM undifferentiated control stayed the highest secreted cytokine within each treatment when comparing treatments, C1 treatment had the lowest concentration of those cytokines. C1 treatment also showed a decrease in all cytokines compared to DMEM except in MCP-1, IL-8 G-CSF and GM-CSF cytokines, which showed an increase compared to DMEM. N2 treatment showed a similar cytokine expression pattern with several upregulated cytokines compared to undifferentiated hADSCs. N2 expressed increased GM-CSF, IL-8, GM-CSF, MCP-1, IL-7, IP-10, PDGF-BB, IL-17A, VEGF, MIP-1b, IL-2 and FGF basic.

The cytokines secreted in untreated ADSCs (DMEM control) stayed the highest within each treatment; however, the treatment that secreted the least of those cytokines was C1. Cytokines in C1 treatment decreased to those compared in DMEM. Additionally, when looking at the cytokine secretion trends, C1 and N2 treatments have a similar pattern, whereas B27 has an entirely different pattern of secretions.

In summary, a clear trend can be seen, with C1 being the treatment with an overall decrease in cytokine concentration over the 7-day treatment compared to DMEM.

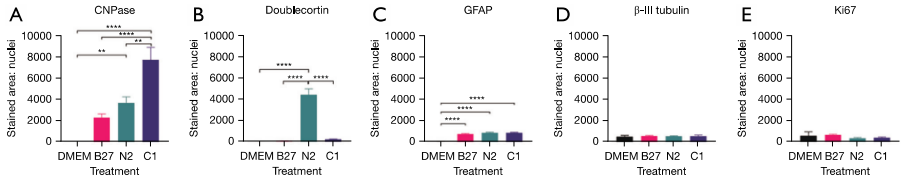


**Figure 4** Immunocytochemistry marker expression by treatments DMEM, B27, N2, C1 following 7 days of treatment for (A) CNPase immunocytochemistry marker. All treatments showed increased CNPase compared to DMEM. However, only N2 and C1 showed to be significantly increased with **, P≤0.01 for N2 and ****, P≤0.0001. Overall, C1 treatment had the highest expression of CNPase (****, P≤0.0001 between C1 and b27, C1 and DMEM and **, P≤0.01 for C1 and N2). (B) Doublecortin immunocytochemistry maker. N2 treatment showed a significant increase of Doublecortin compared to all other treatments (****, P≤0.0001) (C) GFAP immunocytochemistry marker. All treatments showed significant increase in GFAP compared to DMEM (****, P≤0.0001) (D) β-III tubulin immunocytochemistry marker. There was no significant change between treatments. (E) Ki67 marker. There was no significant change between treatments. No statistical significance P>0.05; statistical significance *, P≤0.05; statistical significance **, P≤0.01; statistical significance ***, P≤0.001; statistical significance ****, P≤0.0001. DMEM, Dulbecco's Modified Eagle medium; GFAP, glial fibrillary acidic protein.

### *Enzyme analysis*

#### Dot blot

The dot blot was used to detect any CNPase present in the media after treatment, indicative of CNPase secretion. *Figure 6* shows that there was little difference in CNPase secretion between all treatments. Day 3 (*Figure 7*) shows all treatments had higher CNPase secretion than DMEM undifferentiated control, whereas on day 7 (*Figure 8*), B27 and N2 CNPase secretion increased and C1 decreased by half.

#### CNPase assay

CNPase assay was conducted to detect the functionality of the CNPase enzyme present inside the cells as well as the CNPase enzyme secreted by the cells. When CNPase activity increases, it results in more H+ and, therefore, a drop in pH. The pH decrease changes phenol red from fuchsia to yellow, and that results in a descending gradient on the graphs (*Figure 8*).

In *Figure 6*, CNPase activity can be observed in both intercellular CNPase (*Figure 8A*) as well as extracellular CNPase (*Figure 8B*). C1 treatment shows the highest activity of CNPase over time intracellularly, while DMEM shows the highest activity of CNPase over time extracellularly.

## Discussion

This study's hypothesis was that MSCs would commence differentiation towards neuronal-like lineage in all three treatments, given that B27, N2 and C1 are commercially available supplements used for neuronal differentiation and maintenance in neural cultures. However, when using these treatments on hADSCs, the results indicate that the cells may be differentiating towards different neural cell types under different growth conditions. Following treatment of hADSCs with B27, N2 and to a lesser extent C1, cells became polarised and aligned with one another; morphological changes indicative of neural differentiation. Additionally, cells survived and continued to proliferate as all cells were found to express Ki67 proliferation marker. Furthermore, immunocytochemistry results showed that cells in all treatments expressed some level of CNPase, a well-known oligodendrocyte marker, with C1 treatment expressing the highest levels of CNPase and all treatments increased GFAP to a lesser extent. N2 treated cells also expressed the neuronal marker doublecortin. Additionally, all cells, including undifferentiated hADSCs, expressed B-tubulin marker, a well-known early neuronal marker; however, the levels between undifferentiated cells and treated cells did not increase significantly. Cytokine levels following C1 treatment were reduced compared to the DMEM undifferentiated control in all cases but four: GM-CSF, IL-8, G-CSF and MCP-1. N2 showed a similar but reduced change compared to C1 except for FGF basic and IL-8. On the other hand, B27 presented a distinct cytokine expression pattern whereby most cytokines are upregulated except for RANTES, IL-12, 1L-13, IFN-g, IL-1ra, IL-10 and Eotaxin and where the upregulation or downregulation compared to DMEM undifferentiated control is not as

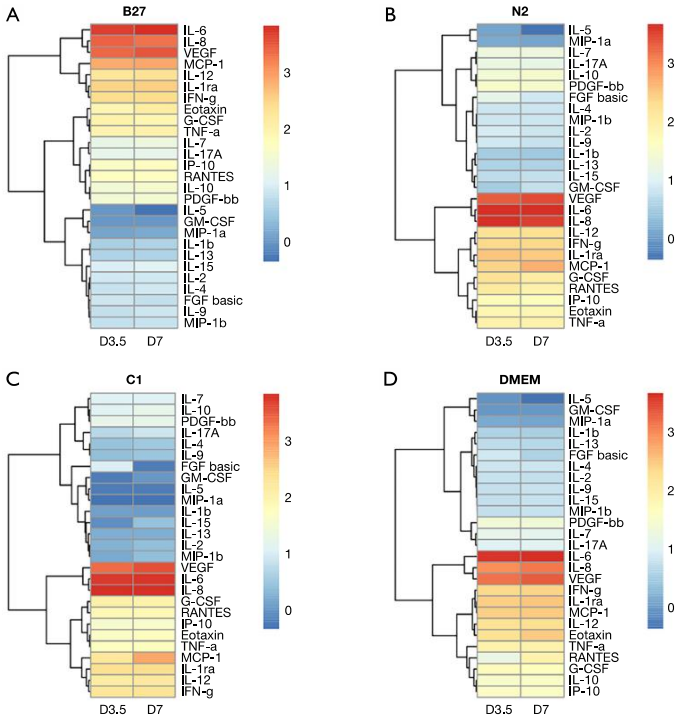


**Figure 5** Hierarchical correlation and grouping of up/down regulated cytokines and interleukins from ADSCs temporal differentiation with B27, N2, C1 and DMEM (undifferentiated control). Cytokine concentration values were transformed to common logarithm values to normalize the data distribution. Values shown are Log [cytokine]. Cytokine expression trends were clustered using Hierarchical clustering by Euclidean test. Red: expression above median indicative of high cytokine concentration; blue: expression below the median indicative of lower cytokine concentration; yellow: median expression across all samples indicative of no change. All three relative to each other within that treatment. (A) Heatmap collecting Log10 of cytokine concentration and cytokine trends in B27. (B) Heatmap collecting Log10 of cytokine concentration and cytokine trends in N2. (C) Heatmap collecting Log10 of cytokine concentration and cytokine trends in C1. (D) Heatmap collecting Log10 of cytokine concentration and cytokine trends in DMEM (undifferentiated control). ADSCs, adipose-derived stem cell; IL, interlukine; VEGF vascular endothelial growth factor; MCP-1, monocyte chemoattractant protein-1; IFN-g, interferon gamma; G-CSF, granulocyte colony-stimulating factor; TNF-a, tumour necrosis factor alpha; IP-10, interferon gamma induced protein-10; PDGF, platelet-derived growth factor; GM-CSF, granulocyte-macrophage colony-stimulating factor; MIP, macrophage inflammatory protein; FGF basic, fibroblast growth factor basic; DMEM, Dulbecco's Modified Eagle medium.

notable as C1. The most notable finding of this study was the presence of high intracellular and extracellular levels of functional CNPase after a 7-day treatment with C1 and N2, and to a notable but lesser extent with B27.

### *CNPase expression is increased in hADSCs following C1, N2 and B27 treatment*

Intracellular and extracellular functional CNPase was detected in all three treatments, with C1 having the

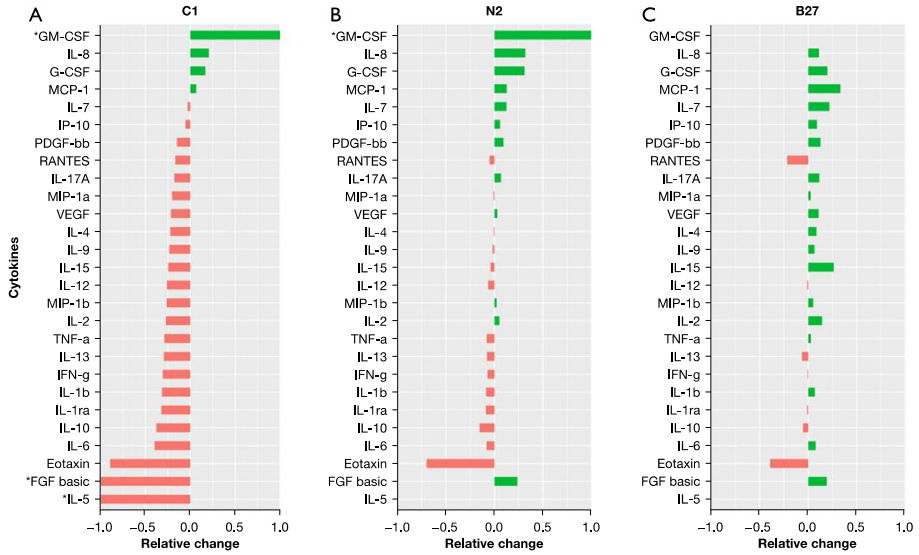


**Figure 6** Cytokines' log10 concentration change relative to DMEM (negative control) at day 7. Grouped by treatment. Values were transformed into Log10 to graph the data. Cytokines marked with * resulted in -infinite and + infinite values when transformed as they showed a decrease to zero or an increase from zero. The graph correctly displays an increase or a decrease from baseline. Raw value concentration can be found in the supplementary data. (A) Log10 concentration change at day 7 for C1 treatment compared to DMEM; (B) Log10 concentration change at day 7 for N2 treatment compared to DMEM; (C) Log10 concentration change at day 7 for B27 treatment compared to DMEM. DMEM, Dulbecco's Modified Eagle medium.

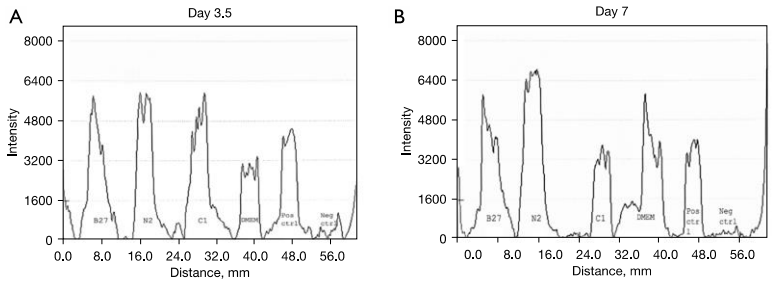


**Figure 7** CNPase expression in treatment media supernatant. (A) CNPase expression in media supernatant at day 3.5 compared to DMEM undifferentiated control, a positive control, and a negative control (B) CNPase expression in media supernatant at day 7 compared to DMEM undifferentiated control, a positive control and a negative control. DMEM, Dulbecco's Modified Eagle medium.

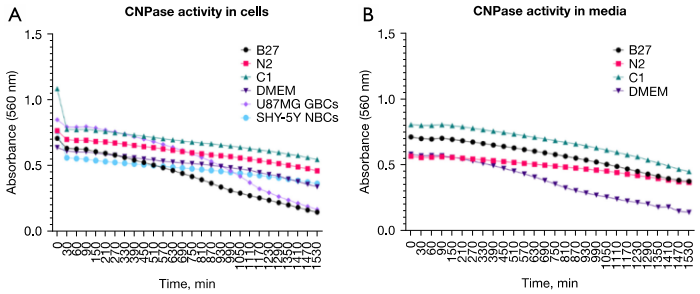


**Figure 8** CNPase assay activity (A) CNPase activity in cells over 25 h. (B) CNPase activity in media over 25 h. Time intervals were first every 30 minutes for 90 minutes, and then every 60 minutes. DMEM, Dulbecco's Modified Eagle medium; GBC, glioblastoma cell; NBC, neuroblastoma cell.

highest expression of CNPase. Immunocytochemistry (*Figures 2,3*) showed that all treatments being investigated expressed markers indicative of commencement of neural differentiation. As seen in *Figures 2,3*, this change is most pronounced in C1, with the highest expression of CNPase and low levels of any other marker. Additionally, CNPase enzymatic assay results (*Figure 7*) showed that the cells expressed intracellular and secreted extracellular functional CNPase. CNPase is a well-established oligodendrocyte marker (29,30) that is mainly expressed in glial cells, with oligodendrocytes having the highest expression of this enzyme of the four major CNS cell types. This enzyme is necessary for oligodendrocyte development and branching and plays a critical role in early myelin formation (29) and neuronal health more generally (34). CNPase deficiency in the brain has been associated with multiple neurological diseases (31), including Down syndrome, Alzheimer's disease (35), and Multiple Sclerosis (36). Furthermore, it is a key component of the 2'3'-cAMP-Adenosine pathway responsible for the production of adenosine (30). Adenosine is a neuromodulator that increases significantly following injury and plays a role in neuroprotection post CNS injury (30,37-40). In the 2'3'-cAMP-Adenosine pathway, this occurs largely via CNPase present in the oligodendrocytes suggesting that oligodendrocytes have a role protecting the axons making CNPase a necessary enzyme for sustained function of the axon-myelin unit and for long-term axonal health (30). Furthermore, CNPase expression in MSCs has been previously seen in rodent cells. Rat ADSCs expressed CNPase marker after being treated with isobutylmethylxanthine (IBMX) induction (41). IBMX is a small molecule chemical that has since been successfully used in hADSCs neurodifferentiation inductions (19). Additionally, it has been observed that human foetal MSCs upregulate CNPase expression after exposure to oligodendrocyte differentiation medium (42) and that rat MSCs have a strong oligodendrogenic effect on rat neural progenitor cells (NPCs) (43). hADSCs have also shown increased CNPase expression after 2 week neural differentiation treatment with bFGF and forskolin (8), suggestive of the capacity for hADSCs to express CNPase marker as a sign of neuronal differentiation and supporting the idea that CNPase expression in hADSCs following treatment with B27, C1 and N2 is indicative of neural like differentiations especially oligodendrocytic lineage following C1 treatment.

### *CNPase expression is influenced by the presence of different cytokines*

Cytokine changes are commonly seen following ADSC differentiation in a number of conditions (18,44,45). CNPase expression can also be influenced by the presence of different cytokines. Both IL-1b and TNF-a have been shown to inhibit the expression of CNPase in human oligodendrocytes (46). These two cytokines have been downregulated in C1 and N2, while they were upregulated in B27, consistent with the different levels of CNPase expression in the different treatments, with C1 having the highest expression and B27 having the least CNPase expression (*Figure 3*). Additionally, IL-8 has been shown to increase mouse oligodendrocyte

precursor proliferation as well as stimulate myelin basic protein *in vitro* (47), and this cytokine was upregulated in all treatments but particularly in C1 and N2 (*Figure 5*). G-CSF is another cytokine that was also found to be upregulated in all three treatments. Normally considered a growth factor for haematopoietic progenitor cells and neutrophils, it can also potentially be used for neural injury treatment such as spinal cord injury (48). G-CSF has been shown to protect oligodendrocytes from SCI-induced death by attenuating white matter loss and promoting functional recovery (49). G-CSF also has been shown to suppress the expression of pro-inflammatory cytokines IL-1b and TNF-a both *in vitro* (50,51) and *in vivo* (49,52); Therefore, G-CSF may have a role in upregulating CNPase expression indirectly through suppressing IL-1b and TNF-a given IL-1b, and TNF-a have been linked to CNPase expression suppression in human oligodendrocytes (46). Another cytokine that was upregulated in C1 and N2 is GM-CSF, generally associated with macrophage and eosinophil proliferation and maturation. This cytokine has also been shown to have neuroprotective effects in CNS diseases (53,54) and plays a role in NPC activation both *in vitro* and *in vivo* (55). Eotaxin-1 was found to be downregulated in all three treatments, with the most notable decrease in C1; Eotaxin is usually an immune modulator associated with the recruitment of eosinophils into inflammatory sites and is high in conditions such as asthma (56). It has recently been found to influence NPCs and microglia and can be secreted by several central nervous system cells (57). It is increased in neurodegenerative conditions such as schizophrenia and Alzheimer's disease (57,58) but appears to be active during accelerated aging and is stimulated by IL-4 and IL-13 (58), both of which are also downregulated in C1 and N2 treated ADSCs.

### *hADSCs differentiation differs following C1, N2 and B27 treatment*

In the current experiments, the analysis showed that C1-treated hADSCs had the highest levels of functional intracellular CNPase, suggesting that they were actually differentiating towards the oligodendrocytic lineage. However, according to the manufacturer, C1 is reported to inhibit glial cell proliferation in primary neural cell cultures. hADSCs are of mesenchymal cell origin rather than nervous system origin. When treated with C1, they appear to downregulate common haemopoietic cytokines that are normally present in mesenchymal cell lines (as seen by a downregulation from the untreated cells in *Figure 6*), suggesting that the cells may be reverting from the mesenchymal to a less differentiated or neural-like lineage.

hADSCs treated with B27 presented the lowest expression of all immunocytochemistry markers (*Figures 2,3*) as well as the least CNPase activity in the CNPase enzymatic assay (*Figure 7*), indicative of the least neural differentiation. B27 is a very commonly used neural supplement; however, it is generally used for the long-term survival of neurons rather than initial commitment and differentiation (26,27). The hADSC treated with B27 did not express significantly higher levels of CNPase and doublecortin than the undifferentiated control cells and may not have developed expression of neural cell markers (CNPase and doublecortin) at these early time points. In contrast, N2 treatment showed mixed levels of neural differentiation, with similar levels of both CNPase and doublecortin. Doublecortin is a well-established marker for immature neurons and for neurogenesis (59-61). It is possible that N2 is showing a mixed population of cells given the expression of both CNPase and doublecortin markers or that the cells are co-expressing both markers; however, the co-expression of both CNPase and doublecortin has not been reported before. There were small increases of GFAP following incubation with all three supplements compared to the non-differentiated ADSCs. GFAP is typically used to identify mature astrocytes but in this short time frame and in the absence of large fold change it is unclear whether there is a robust differentiation pathway towards astrocytic lineage. However, GFAP expression even at low levels, in these mesenchymal ADSC does indicate an early neural differentiation, possible towards a more glial lineage (62).

## Conclusions

Neural differentiation of hADSC can be successfully initiated using commonly available neuronal cell supplements C1 and N2. Although each supplement is usually used for neuronal differentiation and maintenance, we have shown that neural differentiation of hADSC can be initiated by these supplements with C1 pushing cells towards an oligodendrocytic lineage (increased CNPase) and N2 supporting neuronal differentiation (increased Doublecortin). B27 does not have a strong differentiating effect on hADSC at these early time points. Future work may investigate longer time intervals with further supplementation to further elucidate hADSC neural differentiation and would need to be

demonstrated in additional patient samples.

## Acknowledgments

The authors would like to appreciate the Schwartz Foundation philanthropic donation to support research for partly funding the project, as well as Dr. Max L. Cummins for proofreading the article and helping with data visualisation and Carolina Zajc for proofreading the article.
*Funding:* This research was partially funded by the Schwartz Foundation philanthropic donation to support research.

## Footnote

*Conflicts of Interest:* All authors have completed the ICMJE uniform disclosure form (available at https://sci.amegroups.com/article/view/10.21037/sci-2022-015/coif). The authors have no conflicts of interest to declare.

*Ethical Statement:* The authors are accountable for all aspects of the work in ensuring that questions related to the accuracy or integrity of any part of the work are appropriately investigated and resolved. The study was conducted in accordance with the Declaration of Helsinki (as revised in 2013). hADSCs from a single donor waste lipoaspirate were isolated and expanded with approval from the UTS Human Research Ethics Committee (Ethics No. 2013000437). Written informed consent was acquired for donor lipoaspirate release for research purposes only.



## References

1. Tsuji W, Rubin JP, Marra KG. Adipose-derived stem cells: Implications in tissue regeneration. World J Stem Cells 2014;6:312-21.
2. Raposio E, Bonomini S, Calderazzi F. Isolation of autologous adipose tissue-derived mesenchymal stem cells for bone repair. Orthop Traumatol Surg Res 2016;102:909-12.
3. Wankhade UD, Shen M, Kolhe R, et al. Advances in Adipose-Derived Stem Cells Isolation, Characterization, and Application in Regenerative Tissue Engineering. Stem Cells Int 2016;2016:3206807.
4. Raposio E, Simonacci F, Perrotta RE. Adipose-derived stem cells: Comparison between two methods of isolation for clinical applications. Ann Med Surg (Lond) 2017;20:87-91.
5. Zuk PA, Zhu M, Mizuno H, et al. Multilineage cells from human adipose tissue: implications for cell-based therapies. Tissue Eng 2001;7:211-28.
6. Strioga M, Viswanathan S, Darinskas A, et al. Same or not the same? Comparison of adipose tissue-derived versus bone marrow-derived mesenchymal stem and stromal cells. Stem Cells Dev 2012;21:2724-52.
7. Gimble J, Guilak F. Adipose-derived adult stem cells: isolation, characterization, and differentiation potential. Cytotherapy 2003;5:362-9.
8. Jang S, Cho HH, Cho YB, et al. Functional neural differentiation of human adipose tissue-derived stem cells using bFGF and forskolin. BMC Cell Biol 2010;11:25.
9. Park J, Lee N, Lee J, et al. Small molecule-based lineage switch of human adipose-derived stem cells into neural stem cells and functional GABAergic neurons. Sci Rep 2017;7:10166.
10. Wislet-Gendebien S, Wautier F, Leprince P, et al. Astrocytic and neuronal fate of mesenchymal stem cells expressing nestin. Brain Res Bull 2005;68:95-102.
11. Foudah D, Monfrini M, Donzelli E, et al. Expression of neural markers by undifferentiated mesenchymal-like stem cells from different sources. J Immunol Res 2014;2014:987678.
12. Miwa H, Era T. Tracing the destiny of mesenchymal stem cells from embryo to adult bone marrow and white adipose tissue via Pdgfrα expression. Development 2018;145:dev155879.
13. Frese L, Dijkman PE, Hoerstrup SP. Adipose Tissue-Derived Stem Cells in Regenerative Medicine. Transfus Med Hemother 2016;43:268-74.
14. Rad AA, Heidari MH, Aliaghaei A, et al. In vitro differentiation of adipose derived stem cells into functional dopaminergic neurons. Biomedical and Pharmacology Journal. 2017;10:595-605.
15. Ahmadi N, Razavi S, Kazemi M, et al. Stability of neural differentiation in human adipose derived stem cells by two induction protocols. Tissue Cell 2012;44:87-94.
16. Soheilifar MH, Javeri A, Amini H, et al. Generation

of Dopamine-Secreting Cells from Human Adipose Tissue-Derived Stem Cells In Vitro. Rejuvenation Res 2018;21:360-8.
17. Faghih H, Javeri A, Amini H, et al. Directed differentiation of human adipose tissue-derived stem cells to dopaminergic neurons in low-serum and serum-free conditions. Neurosci Lett 2019;708:134353.
18. Santos J, Hubert T, Milthorpe BK. Valproic Acid Promotes Early Neural Differentiation in Adult Mesenchymal Stem Cells Through Protein Signalling Pathways. Cells 2020;9:619.
19. Fajardo J, Milthorpe BK, Santos J. Molecular Mechanisms Involved in Neural Substructure Development during Phosphodiesterase Inhibitor Treatment of Mesenchymal Stem Cells. Int J Mol Sci 2020;21:4867.
20. Rong JU, Wen Z, Rong WU, et al. Interaction between neural stem cells and bone marrow derived-mesenchymal stem cells during differentiation. Biomed Rep 2015;3:242-6.
21. Chi K, Fu RH, Huang YC, et al. Adipose-derived Stem Cells Stimulated with n-Butylidenephthalide Exhibit Therapeutic Effects in a Mouse Model of Parkinson's Disease. Cell Transplant 2018;27:456-70.
22. Carlson KB, Singh P, Feaster MM, et al. Mesenchymal stem cells facilitate axon sorting, myelination, and functional recovery in paralyzed mice deficient in Schwann cell-derived laminin. Glia 2011;59:267-77.
23. Wang L, Zhao Y, Pan X, et al. Adipose-derived stem cell transplantation improves learning and memory via releasing neurotrophins in rat model of temporal lobe epilepsy. Brain Res 2021;1750:147121.
24. Zhou F, Gao S, Wang L, et al. Human adipose-derived stem cells partially rescue the stroke syndromes by promoting spatial learning and memory in mouse middle cerebral artery occlusion model. Stem Cell Res Ther 2015;6:92.
25. Galindo LT, Filippo TR, Semedo P, et al. Mesenchymal stem cell therapy modulates the inflammatory response in experimental traumatic brain injury. Neurol Res Int 2011;2011:564089.
26. Brewer GJ, Torricelli J, Evege EK, et al. Neurobasal medium/B27 supplement: A new serum-free medium combination for survival of neurons. Focus 1994;16:6-9.
27. Brewer GJ, Torricelli JR, Evege EK, et al. Optimized survival of hippocampal neurons in B27-supplemented Neurobasal, a new serum-free medium combination. J Neurosci Res 1993;35:567-76.
28. Santos J, Milthorpe BK, Herbert BR, et al. Proteomic Analysis of Human Adipose Derived Stem Cells during Small Molecule Chemical Stimulated Pre-neuronal Differentiation. Int J Stem Cells 2017;10:193-217.
29. Raasakka A, Kursula P. The myelin membrane-associated enzyme 2',3'-cyclic nucleotide 3'-phosphodiesterase: on a highway to structure and function. Neurosci Bull 2014;30:956-66.
30. Verrier JD, Jackson TC, Gillespie DG, et al. Role of CNPase in the oligodendrocytic extracellular 2',3'-cAMP-adenosine pathway. Glia 2013;61:1595-606.
31. Jackson EK. Discovery and Roles of 2',3'-cAMP in Biological Systems. Handb Exp Pharmacol 2017;238:229-52.
32. Dreiling CE, Mattson C. A new spectrophotometric assay for 2',3'-cyclic nucleotide 3'-phosphohydrolase activity in nervous tissue. Anal Biochem 1980;102:304-9.
33. Rovati L, Fabbri P, Ferrari L, et al. Plastic Optical Fiber pH Sensor Using a Sol-Gel Sensing Matrix. Fiber Optic Sensors 2012:415-39.
34. Lappe-Siefke C, Goebbels S, Gravel M, et al. Disruption of Cnp1 uncouples oligodendroglial functions in axonal support and myelination. Nat Genet 2003;33:366-74.
35. Vlkolinský R, Cairns N, Fountoulakis M, et al. Decreased brain levels of 2',3'-cyclic nucleotide-3'-phosphodiesterase in Down syndrome and Alzheimer's disease. Neurobiol Aging 2001;22:547-53.
36. Walsh MJ, Murray JM. Dual implication of 2',3'-cyclic nucleotide 3' phosphodiesterase as major autoantigen and C3 complement-binding protein in the pathogenesis of multiple sclerosis. J Clin Invest 1998;101:1923-31.
37. Stone TW, Ceruti S, Abbracchio MP. Adenosine receptors and neurological disease: neuroprotection and neurodegeneration. Handb Exp Pharmacol 2009;(193):535-87.
38. Bell MJ, Kochanek PM, Carcillo JA, et al. Interstitial adenosine, inosine, and hypoxanthine are increased after experimental traumatic brain injury in the rat. J Neurotrauma 1998;15:163-70.
39. Robertson CL, Bell MJ, Kochanek PM, et al. Increased adenosine in cerebrospinal fluid after severe traumatic brain injury in infants and children: association with severity of injury and excitotoxicity. Crit Care Med 2001;29:2287-93.
40. Lauro C, Cipriani R, Catalano M, et al. Adenosine A1 receptors and microglial cells mediate CX3CL1-induced protection of hippocampal neurons against Glu-induced death. Neuropsychopharmacology 2010;35:1550-9.
41. Ning H, Lin G, Lue TF, et al. Neuron-like differentiation of adipose tissue-derived stromal cells and vascular smooth muscle cells. Differentiation 2006;74:510-8.

42. Kennea NL, Waddington SN, Chan J, et al. Differentiation of human fetal mesenchymal stem cells into cells with an oligodendrocyte phenotype. Cell Cycle 2009;8:1069-79.
43. Steffenhagen C, Dechant FX, Oberbauer E, et al. Mesenchymal stem cells prime proliferating adult neural progenitors toward an oligodendrocyte fate. Stem Cells Dev 2012;21:1838-51.
44. Santos J, Dalla PV, Milthorpe BK. Molecular Dynamics of Cytokine Interactions and Signalling of Mesenchymal Stem Cells Undergoing Directed Neural-like Differentiation. Life (Basel) 2022;12:392.
45. Razavi S, Razavi MR, Kheirollahi-Kouhestani M, et al. Co-culture with neurotrophic factor secreting cells induced from adipose-derived stem cells: promotes neurogenic differentiation. Biochem Biophys Res Commun 2013;440:381-7.
46. Jana M, Pahan K. Redox regulation of cytokine-mediated inhibition of myelin gene expression in human primary oligodendrocytes. Free Radic Biol Med 2005;39:823-31.
47. Kadi L, Selvaraju R, de Lys P, et al. Differential effects of chemokines on oligodendrocyte precursor proliferation and myelin formation in vitro. J Neuroimmunol 2006;174:133-46.
48. Takahashi H, Yamazaki M, Okawa A, et al. Neuroprotective therapy using granulocyte colony-stimulating factor for acute spinal cord injury: a phase I/IIa clinical trial. Eur Spine J 2012;21:2580-7.
49. Kadota R, Koda M, Kawabe J, et al. Granulocyte colony-stimulating factor (G-CSF) protects oligodendrocyte and promotes hindlimb functional recovery after spinal cord injury in rats. PLoS One 2012;7:e50391.
50. Nishiki S, Hato F, Kamata N, et al. Selective activation of STAT3 in human monocytes stimulated by G-CSF: implication in inhibition of LPS-induced TNF-alpha production. Am J Physiol Cell Physiol 2004;286:C1302-11.
51. Boneberg EM, Hareng L, Gantner F, et al. Human monocytes express functional receptors for granulocyte colony-stimulating factor that mediate suppression of monokines and interferon-gamma. Blood 2000;95:270-6.
52. Zavala F, Abad S, Ezine S, et al. G-CSF therapy of ongoing experimental allergic encephalomyelitis via chemokine- and cytokine-based immune deviation. J Immunol 2002;168:2011-9.
53. Bouhy D, Malgrange B, Multon S, et al. Delayed GM-CSF treatment stimulates axonal regeneration and functional recovery in paraplegic rats via an increased BDNF expression by endogenous macrophages. FASEB J 2006;20:1239-41.
54. Nakagawa T, Suga S, Kawase T, et al. Intracarotid injection of granulocyte-macrophage colony-stimulating factor induces neuroprotection in a rat transient middle cerebral artery occlusion model. Brain Res 2006;1089:179-85.
55. Hayashi K, Ohta S, Kawakami Y, et al. Activation of dendritic-like cells and neural stem/progenitor cells in injured spinal cord by GM-CSF. Neurosci Res 2009;64:96-103.
56. Conroy DM, Williams TJ. Eotaxin and the attraction of eosinophils to the asthmatic lung. Respir Res 2001;2:150-6.
57. Teixeira AL, Gama CS, Rocha NP, et al. Revisiting the Role of Eotaxin-1/CCL11 in Psychiatric Disorders. Front Psychiatry 2018;9:241.
58. Ivanovska M, Abdi Z, Murdjeva M, et al. CCL-11 or Eotaxin-1: An Immune Marker for Ageing and Accelerated Ageing in Neuro-Psychiatric Disorders. Pharmaceuticals (Basel) 2020;13:230.
59. Walker TL, Yasuda T, Adams DJ, et al. The doublecortin-expressing population in the developing and adult brain contains multipotential precursors in addition to neuronal-lineage cells. J Neurosci 2007;27:3734-42.
60. Vukovic J, Borlikova GG, Ruitenberg MJ, et al. Immature doublecortin-positive hippocampal neurons are important for learning but not for remembering. J Neurosci 2013;33:6603-13.
61. Couillard-Despres S, Winner B, Schaubeck S, et al. Doublecortin expression levels in adult brain reflect neurogenesis. Eur J Neurosci 2005;21:1-14.
62. Safford KM, Hicok KC, Safford SD, et al. Neurogenic differentiation of murine and human adipose-derived stromal cells. Biochem Biophys Res Commun 2002;294:371-9.

doi: 10.21037/sci-2022-015
**Cite this article as:** Pelegri NG, Milthorpe BK, Gorrie CA, Santos J. Neurogenic marker expression in differentiating human adipose derived adult mesenchymal stem cells. Stem Cell Investig 2023;10:7.

The worked published in the article included in this chapter only comprised of the first 7 days of the experiment. The experiment was initially designed, and cell culture was completed for 42 days and had 4 time points (D7, D14, D28 and D42) at which the differentiation of the cells was going to be assessed. One of the key problems that was encountered was the significant amount of cell detachment that occurred during the differentiations, which led to cell loss. Additionally, the cells also started to form sheets/aggregates that lifted when we attempted to fix the cells in formalin at the endpoint times. That increased as the treatments proceeded, and by day 42, the cells were not able to be fixed to the plate, and staining could not be performed in a way that was able to be quantified. Different ways to try to mitigate those problems were tried. Gelatine was added on top of the remaining cells in the wells after fixing to try to keep them in place; however, that interfered with the staining protocol and the diffusion of the antibodies to reach the cells at the bottom of the plate. The staining protocol was not able to be optimised to image the cells in the environment they were in, and only week 1 of the experiments was suitable for performing downstream analysis. This led to the design of the following experiments presented in this thesis, looking at creating a suitable 3D model for neural differentiation of ADSCs.

# Chapter Three: ADSCs in 3D GelMa matrices

## 3.1. Introduction

In this work, Gelatin Methacrylate (GelMa) was the first hydrogel selected for exploring neural differentiation of ADSCs in 3D matrices. GelMa was chosen as it is a highly desirable biomaterial for tissue engineering and 3D cell culture, given it is reported to be a highly biocompatible, biodegradable, non-cytotoxic, non-immunogenic, inexpensive, and a cell-responsive biomaterial [1, 2]. Additionally, GelMa has versatile physical and chemical characteristics that are reported as being tuneable to closely resemble the properties of the extracellular matrix (ECM) [1-4]. GelMa contains many RGD (arginine-glycine-aspartic acid) sequences found in ECM proteins that allow for cell attachment and contains matrix metalloproteinases that aid in cell remodelling [1, 3, 4]; these allow cells to attach, proliferate and spread within the scaffold [1-4]. Modification of gelatin with methacrylate to create GelMa allows it to be covalently crosslinked via UV light (365-400nm) exposure with the addition of a photo-initiator. Some commonly used photoinitiators are Irgacure 2959 and lithium acylphosphinate (LAP) [5]. Furthermore, GelMa's physical and mechanical properties can be modified by varying its synthesis process, making it a tuneable hydrogel for a 3D culture [6-8]. Stiffness can be controlled by changing the degree of the methacrylate substitution [6-8], where the number of methacrylate groups bound to an individual gelatin molecule proportionally controls the number of inter-gelatin crosslinks, and therefore, the stiffness of the hydrogel [1]. GelMa stiffness can also be tailored by selecting higher gelatin concentrations, leading to higher stiffness allowing the parameters to be modified based on the desired outcome and based on the mechanical properties of the tissue that is being studied [9, 10]. In the case of this project, brain stiffness will be mimicked by creating <2kPa hydrogels [11].

GelMa has been reported to be successfully used in creating muscle [3, 12], epidermal [13], cardiovascular [14] and cartilage [15, 16] tissue models. While neural tissue engineering models using GelMa hydrogels may be a promising

avenue for neural cell culture models, these models remain in the early stages of development [1, 2]. Neural stem cells (NSCs) have been shown to differentiate towards neuronal lineage expressing β-tubulin III and extending neurites when GelMa stiffness and concentration were low [10]. Furthermore, low GelMa stiffness and concentration have also allowed for neural cell growth, adhesion, proliferation and phenotype stability [17]. In contrast, if stiffness increases, neuronal outgrowth, viability, spreading, and neurite length decrease [18]. GelMa has also been successfully used with other polymer composites for nerve tissue engineering [19] and for *in vivo* testing in traumatic brain injury models and Spinal Cord Injury (SCI), with models showing no immune reaction or inflammation when implanted [17, 20].

Additionally, studies have also shown that similar to NSCs, ADSCs expand to higher yields at lower stiffness (50% degrees of substitution (DoS)) while stiffer substrates reduce the cell spreading and viability [7]. This could be attributed to the smaller hydrogel pore size in stiffer gels [7]. With ADSCs having been successfully grown in GelMa in the past, [7, 21-23] and its tuneable characteristics, GelMa seemed a promising material for the development of a 3D model for neural differentiation of ADSCs.

The following chapter will detail the approaches used to cast low-stiffness GelMa hydrogels based on the hypothesis that GelMa hydrogels can be optimised to develop a 3D neural model for neural differentiation of hADSCs.

GelMa hydrogels have not been used in this context previously, and the goal is to explore and change different parameters in order to create a suitable low-stiffness 3D matrix in which to grow and differentiate hADSC.

## 3.2. Materials, Methods

### 3.2.1. GelMa synthesis

GelMa synthesis was performed using the protocol for GelMa type A from Lee et al. (2016). In brief, 10% (w/v) gelatin solution of type A (porcine, Bloom strength

175, Sigma-Aldrich) or gelatin solution of type A (porcine, Bloom strength 300, Sigma-Aldrich) was dissolved under stirring in 0.1 M carbonate-bicarbonate buffer pH 9 at 60°C. The derivatisation of gelatin proteins was performed by the addition of methacrylic anhydride (MAA) at 50°C with rigorous stirring at 500 rpm. MAA was added in sequential steps, giving a total MAA amount equal to the defined ratio in each recipe (x mL MAA/g gel,). (Table 4).

**Table 4** Table showing the different amounts of MMA added for each recipe.

| Product | Gelatin Type | Ratio (MMA (ml/gel (g)) | CB-Buffer | pH control | DoS (%) | Name |
|---|---|---|---|---|---|---|
| GelMA A1 | A | 0.05 | 0.1M | Sequential | 71.2 | A70 |
| GelMA A2 | A | 0.0375 | 0.1M | Sequential | 45.3 | A50 |
| GelMA A3 | A | 0.025 | 0.1M | Sequential | 39.7 | A40 |

The pH was adjusted back to 9 after each methacrylate addition and the reaction was carried out for 60 min and terminated by pH adjustment to 7.4. After completion, the reaction mixture was filtered using standard paper filters (Whatman™, 90 mm diameter) and dialyzed with a 14 kDa molecular-weight-cut-off (MWCO) membrane at 40°C for 36 h against ultrapure water. GelMA solution after dialysis was frozen and lyophilized before being used for GelMa hydrogel casting.

GelMa hydrogels were cast using 2.5% and 5% w/v GelMa and 0.5% of the photoinitiator Irgacure 2959 and crosslinked under 360nm UV for 1min and 1.5min. This protocol was repeated using the same ingredients and two different gelatin bloom strengths, 175 and 300. Bloom is a measure of gelatin strength and stiffness [24]

### 3.2.2. Commercially available GelMa hydrogels casting

#### *3.2.2.1. Manual casting*

GelMa (300 bloom 60% degrees of substitution; Sigma- Aldrich #900622) was mixed with 0.5% Irgacure 2959 photoinitiator in PBS at different concentrations

and crosslinked using 365nm UV light for different time lengths. All parameters were tested in triplicate. All parameters tested can be found below in Table 5. Irgacure concentration and gelatin setting time parameters were left unchanged at 0.5% w/v for Irgacure and 20 minutes at 5°C setting time for GelMa. Irgacure concentration was not changed as it is known to be toxic to cells and to significantly decrease cell viability when used above 0.5% w/v concentration [5, 25].

**Table 5** Variables tested to cast commercially available GelMa hydrogels.

| Percentage | UV exposure time | Crosslinking check |
|---|---|---|
| 3% | 30sec | 1hr at 37°C |
| 5% | 30sec | 1hr at 37°C |
| 10% | 30sec | 1hr at 37°C |
| 3% | 60sec | 1hr at 37°C |
| 5% | 60sec | 1hr at 37°C |
| 10% | 60sec | 1hr at 37°C |
| 3% | 90sec | 1hr at 37°C |
| 5% | 90sec | 1hr at 37°C |
| 10% | 90sec | 1hr at 37°C |
| 3% | 5min | 1hr at 37°C |
| 5% | 5min | 1hr at 37°C |
| 10% | 5min | 1hr at 37°C |
| 3% | 10min | 1hr at 37°C* |
| 5% | 10min | 1hr at 37°C |
| 10% | 10min | 1hr at 37°C |

*Parameters used for subsequent experiments

After GelMa crosslinking optimisation, 3% GelMa (300 bloom 60% degrees of substitution Sigma- Aldrich #900622) with 0.5% Irgacure 2959 crosslinked for 10min at 365nm UV light was the selected parameters to use with cells. See Table 6 in results section 3.3.2 for results on GelMa crosslinking optimisation and why those were the selected parameters.

*3.2.2.2. Cell culture*

150uL of GelMa at 3% GelMa (300 bloom 60% degrees of substitution Sigma-Aldrich #900622) with 0.5% Irgacure 2959 was crosslinked in a 24 well plate for 10min at 365nm UV light. Once GelMa discs were crosslinked, given that the GelMa only cross-linked at high exposure to UV light (see results table 3), the cells were seeded on top of the gels to avoid prolonged UV exposure as it is known to cause cell damage [26, 27]. Previous studies using mesenchymal stem cells showed that higher UV light exposure and increased Irgacure concentration were linked to reduced cell viability [25].

ADSCs, Glioblastoma cells (GBCs) U87MGs and neuroblastoma cells (NBCs) SHSY5Y cells were seeded at 30,000 cells/mL on top of the GelMa discs in a 24-well plate. A control plate was also set up where cells grew on plastic. Cells were maintained in media mixture containing DMEM/F12 + Glutamax media (Gibco, Life Technologies, Carlsbad, CA, USA) with 10% heat inactivated FBS (Gibco, Life Technologies, Carlsbad, CA, USA) and incubated at 37°C at 5% $CO_2$ for 10 days with media changes every 84hrs.

*3.2.2.3. Cell viability & proliferation: Alamar blue*

Alamar blue cell viability assay was performed at the endpoint time at day 10 on both plates. Alamar blue is a non-toxic cell viability assay that detects metabolically active cells. When Alamar blue is added to cells, the main active ingredient is reduced by metabolically active cells, and the solution becomes red in colour and highly fluorescent.

Alamar blue was added to the same media mixture described above to yield a 10% concentration of alamar blue to media ratio. The Alamar blue and media mixture was added to the cells and left to incubate for 16hrs to allow enough time to penetrate through the 3D matrices. To minimise variability between treatments, the same was done on the 2D cells. Negative control wells were included, containing alamar blue and media mixture only. After the incubation period, the alamar blue and media mixture was transferred to a different 24-well plate to keep the cellular growth environment as undisturbed as possible from outside factors

and new fresh media was added to remaining cells before terminating experiments. The collected Alamar blue media was then measured using the fluorescence bottom-up mode in a Tecan M200Plate Reader using 530-560nm excitation and 590nm emission wavelengths. The results were averaged for both test samples and negative controls and compared to each other. The data were analysed as absolute fluorescence values.

#### *3.2.2.4. Phase Imaging*

Phase images at 10x magnification were taken of each cell type at every media change, D3.5, D7 and D10 on the same marked area using the EVOS XL Core microscope (Thermofisher, Massachusetts, USA).

#### *3.2.2.5. Bioprinting – CELLINK*

A CELLINK bioprinter (BIO X pneumatically driven extrusion 3D bioprinter CELLINK Life Sciences, Boston, MA, USA) was also used to cast GelMa hydrogels. The CELLINK GelMa casting protocol was followed [28]. In brief, GelMa at 300 bloom and 60% degrees of substitution (Sigma- Aldrich #900622) was mixed with Irgacure 2959 in PBS to obtain a final concentration of 7% GelMa and 0.5% Irgacure 2959. After, 9 million U87MG cells/mL were added to the GelMa mixture before bioprinting. Once the cells were evenly suspended in the GelMa solution, it was transferred to the bioprinter, and bioprinting commenced on a 24-well plate. The following parameter combinations were tested for GelMa bioprinting:

1. Bed base plate temperature 10°C; Pinter head temperature 24°C; printing pressure 25kPa, extrusion time: 1s, needle gage 25G. UV exposure time 30s.
2. Bed base plate temperature 10°C; Pinter head temperature 24°C; printing pressure 25kPa, extrusion time: 1s, needle gage 25G. UV exposure time 2min.

3. Bed base plate temperature 10°C; Pinter head temperature: 7°C; printing pressure 55kPa, extrusion time: 1s, needle gage 25G. UV exposure time 1.5min
4. Bed base plate temperature 10°C; Pinter head temperature 27°C; printing pressure 55kPa, extrusion time: 1s, needle gage 25G. UV exposure time 2min.

After the gels were bioprinted, they were checked under the microscope to assess hydrogel structure and cell spread. After, the cells were maintained in DMEM/F12 + Glutamax media (Gibco, Life Technologies, Carlsbad, CA, USA) with 10% heat inactivated FBS (Gibco, Life Technologies, Carlsbad, CA, USA) and incubated at 37°C at 5% $CO_2$ overnight. The following day, the 3D constructs were checked under the microscope, and the media was removed.

## 3.3. Results

### 3.3.1. GelMa synthesis

On all occasions, after crosslinking the GelMa at different percentages and for different amounts of time, the GelMa mixture was placed at 37°C to assess its crosslinking. GelMa went back into solution every time, indicating a lack of crosslinking by the methacrylate, making the synthesised GelMa unsuitable to use for tissue culture. This could be due to a lack of derivatisation of the gelatin with the methacrylate, but this was not able to be investigated with the resources and expertise available.

### 3.3.2. GelMa hydrogel manual casting

In order to reduce variability in the gels and assess if the synthesised GelMa was not crosslinking due to synthesis methodology or due to crosslinking methodology, commercially available GelMa was also tested. Manual casting of the GelMa hydrogel using commercially available GelMa mixture only worked for GelMa exposed to UV light for 10 minutes, suggesting that the crosslinking methodology was not robust enough. Different 360nm UV light sources were

tested, and a new Irgacure 2959 reagent was also purchased to investigate the reason for failed crosslinking however, the results remained the same. All results of the different parameters tested can be found in Table 6. The lowest stiffness matrix that crosslinked was 3% commercially available GelMa exposed to 10min of UV. That was the selected matrix to test with cells.

**Table 6** Results for each set of parameters tested using commercially available GelMa.

| Percentage | UV exposure time | Crosslinking check | Crosslinking |
|---|---|---|---|
| 3% | 30sec | 1hr at 37°C | No |
| 5% | 30sec | 1hr at 37°C | No |
| 10% | 30sec | 1hr at 37°C | No |
| 3% | 60sec | 1hr at 37°C | No |
| 5% | 60sec | 1hr at 37°C | No |
| 10% | 60sec | 1hr at 37°C | No |
| 3% | 90sec | 1hr at 37°C | No |
| 5% | 90sec | 1hr at 37°C | No |
| 10% | 90sec | 1hr at 37°C | No |
| 3% | 5min | 1hr at 37°C | Partial crosslinking Meniscus formation |
| 5% | 5min | 1hr at 37°C | Partial crosslinking Meniscus formation |
| 10% | 5min | 1hr at 37°C | Partial crosslinking Meniscus formation |
| **3%** | **10min** | **1hr at 37°C** | **Yes*** |
| 5% | 10min | 1hr at 37°C | Yes |
| 10% | 10min | 1hr at 37°C | Yes |

*Parameters used for subsequent experiments

### *3.3.2.1. Cell viability & proliferation: Alamar blue*

Alamar blue results (Figure 4) showed that after 10 days in culture, ADSCs, GBCs and NBCs viability decreased significantly (p-value <0.001) compared to the respective 2D-grown control cells. ADSCs had a viability 2/3 lower than their 2D control counterparts and NBCs being ½ lower than the control cells.

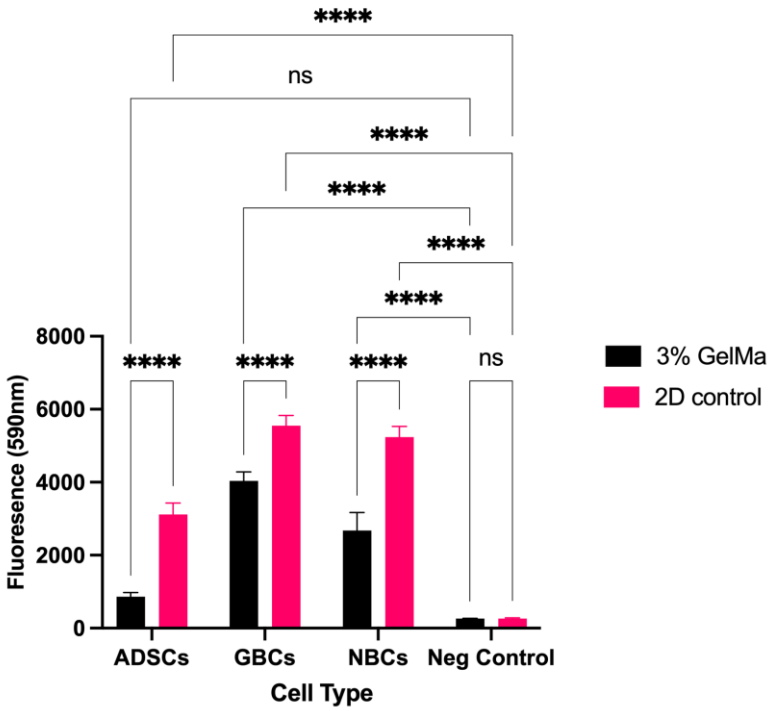


**Figure 4** Alamar blue results at day 10 comparing GelMa grown cells vs. 2D grown cells.

### *3.3.2.2. Phase Imaging*

Phase imaging revealed noteworthy variability in the gel construct appearance between replicates and between cell lines (Figure 5). Broken pieces of hydrogel can be observed in many of the 3D constructs (Figure 5). Additionally, cell numbers appear much lower compared to the 2D controls. When doing media changes and assessing the cells visually under the microscope, many cells were observed floating and therefore, are likely lost during media changes. Furthermore, the integrity of the gel can be seen to deteriorate over time.

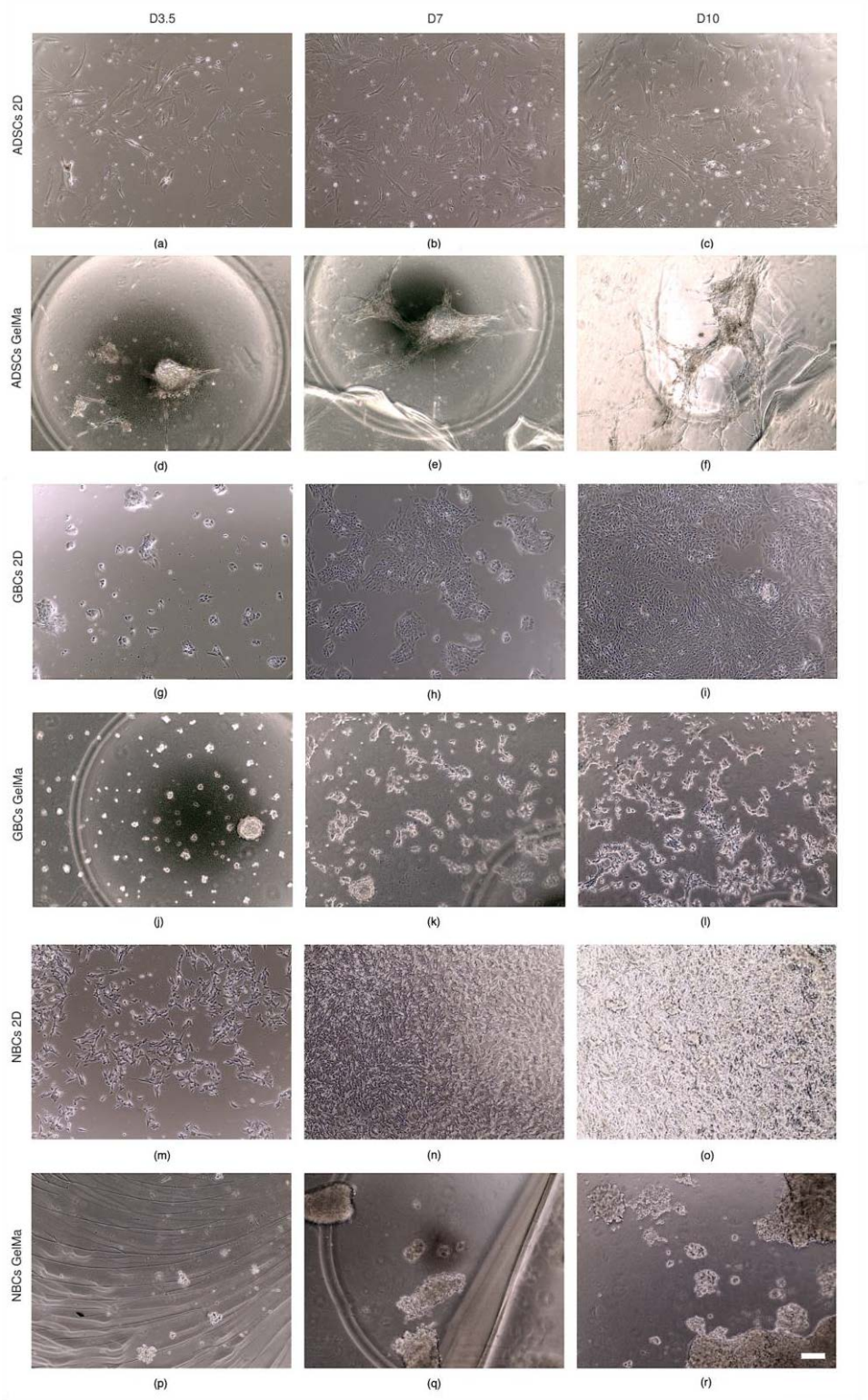


**Figure 5** Phase imaging at 10x magnification for cells grown in either GelMa or 2D conditions over time at time points D3.5, D7 and D10. (a-c): ADSCs grown in 2D conditions; (d-f) ADSCs grown on GelMa; (g-i) GBCs grown in 2D conditions; (j-l) GBCs grown on GelMa; (m-o) NBCs grown in 2D conditions; (p-r) NBCs grown on GelMa. Scale bar 100um.

### 3.3.3. GelMa hydrogel bioprinting

To further reduce GelMa variability and optimise structural gel integrity, GelMa was tested using the CELLINK bioprinter. In all instances tested, when the 3D constructs were checked under the microscope 24 hours after bioprinting, the cells were in suspension in the media, and the GelMa had dissolved, meaning the GelMa hydrogels were not crosslinked correctly.

**Figure 6** schematic summarises the methodology used for all experiments and outcomes in all instances.

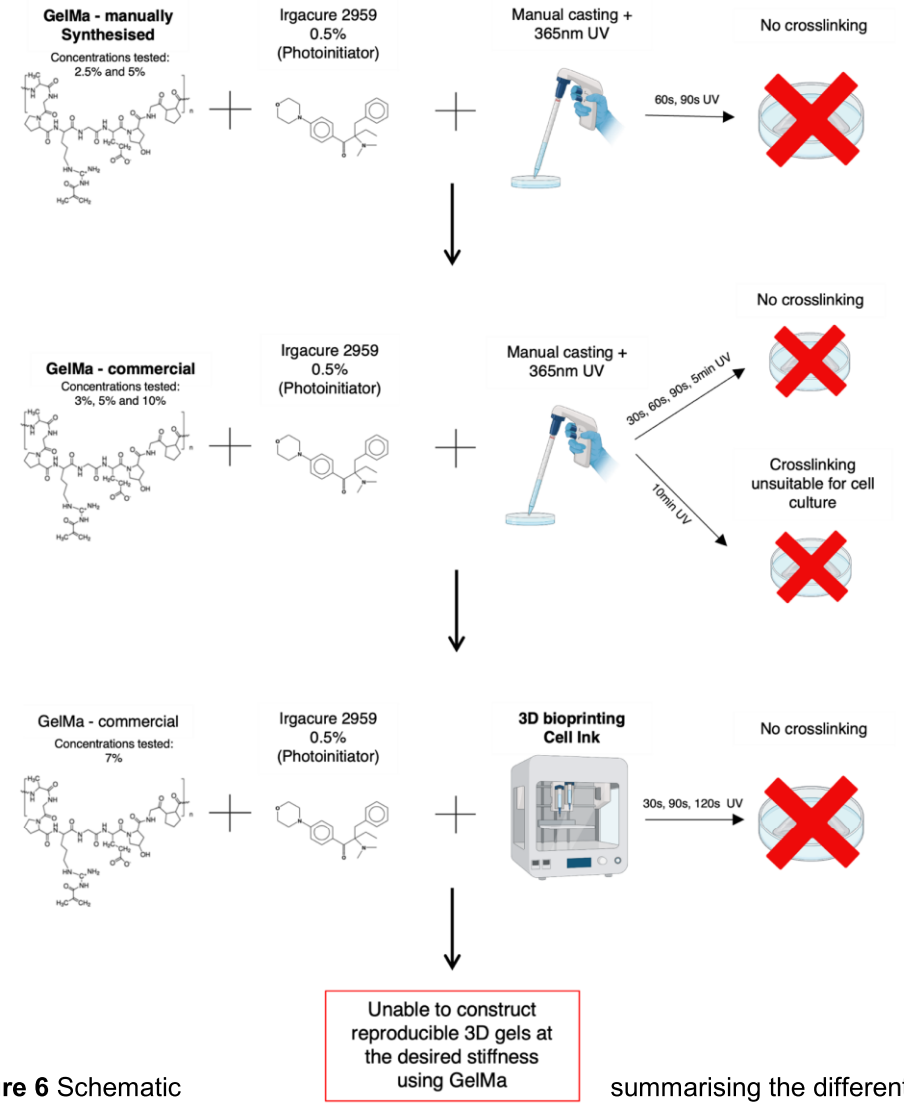


**Figure 6** Schematic summarising the different methodologies used to create GelMa hydrogels and respective outcomes.

## 3.4. Discussion

GelMa was the hydrogel of choice to test with ADSCs due to its reported success with other cell types [3, 12-16]. Unfortunately, a 3D environment with the characteristics desired to create a 3D ADSCs neural differentiation model was not able to be created. Throughout the experiment stages, attempts to reduce variables as much as possible were made by purchasing commercially available synthesised GelMa, using different UV lamps, purchasing new reagents, and using a bioprinter to reduce manual casting gel variability. Nevertheless, the key issue remained the same: the GelMa crosslinking did not work to the required standards to encapsulate cells in a low stiffness (1kPa) matrix that mimicked the brain.

A possible reason for the crosslinking problems could be due to UV light's tissue and hydrogel penetration limits [29] however, negative results are not well documented or communicated in the literature, making it hard to conclude what the problem in crosslinking has been. Furthermore, the caveats and difficulties encountered while attempting to make the hydrogel work in a reproducible manner were more than anticipated. It was found that the reproducibility of a GelMa protocol was low, likely due to the number of variables influencing the process of casting GelMa hydrogels, especially when bioprinting GelMa. It was found that to cast GelMa hydrogels and keep them at the required stiffness, there are many variables that need to be accounted for that are not always clearly listed in published protocols: Gelatin bloom will impact gel stiffness, as it is a measure of gelatin strength and stiffness [24], gelatin's degrees of substitution with methacrylate will affect gel stiffness, the photoinitiator type used will affect gel structure and crosslinking; Irgacure 2959 uses a different UV wavelength compared to LAP and Irgacure 2959 has been reported to generate GelMa gels that have larger pore size and faster degradation rate than those crosslinked with LAP [5]), The photoinitiator amount will impact GelMa stiffness and the gels' ability to fully crosslink. However too high amounts can cause toxicity for the cells [25]); GelMa concentration, UV wavelength, UV intensity and UV exposure time will also impact gel stiffness and crosslinking [30]. GelMa distance from the UV

source will impact UV intensity which in turn affects crosslinking and stiffness. Furthermore, we also found that GelMa polymerisation prior to crosslinking, and the temperature at which the GelMa is polymerised prior to crosslinking will also affect crosslinking [30]. These are the major variables that need to be accounted for when creating GelMa hydrogels. Additionally, when manually casting gels, manual pipetting adds variability from gel to gel.

For GelMa bioprinting, the variables increase. In addition to those listed above, when bioprinting one needs to also account for bed base plate temperature, printer head temperature, printing pressure, extrusion time and needle gauge. It was observed when using the bioprinter that, due to the nature of the machine and where the UV lamp is located relative to the 24-well plate, the UV exposure varied between wells; the ones right below the lamp would get higher, more direct exposure to UV than those in the edges of the plate meaning all variables were not kept stable for all wells. Additionally, plate height could not be automatically set to a particular height which meant that one had to manually adjust the distance each time, adding human error and bringing more variability between runs.

In conclusion, we were unable to optimize a robust enough protocol to create the neural model to study the cells' neural development potential. Through this research, it has become apparent that 3D culturing with GelMa requires substantial expertise due to the high variability in products. Additionally, the current methodologies found in the literature differ significantly from one another. For example, some methodologies using Irgacure 2959 photoinitiator, crosslink the gels using 365nm UV light exposure for 1minute and 30 seconds [31] while others use 15minutes of UV light exposure to crosslink the gels [32].

Further advice was sought from the engineering department at the University of Technology Sydney to improve the quality and reproducibility of the GelMa casting; however, we were unable to optimise a viable and robust method within a reasonable timeframe. The testing of different GelMa crosslinking methodologies using different photoinitiation systems like LAP, Ribofablin,

carboxylated camphorquinone, Eosin Y [29, 33-35] would have been the next best option. However, the time and costs involved in acquiring the necessary reagents and technical expertise (i.e., paid labour from biomaterials experts), as well as the additional equipment required for precision engineering of GelMa casts, were excessive. To ensure the timeliness of project progression, we identified a more user-friendly and streamlined approach to casting hydrogels using a RASTRUM bioprinter (Inventia, Sydney, Australia) which removed all variability in the hydrogel casting side and allowed for the focus to be solely on the biology. Rastrum provided ready-to-go optimised mixtures to create PEG-based hydrogels at the stiffness required, as well as ongoing support for troubleshooting at no extra cost. That work will comprise the remaining chapters of this thesis.

## 3.5. References


1. Yue, K., et al., *Synthesis, properties, and biomedical applications of gelatin methacryloyl (GelMA) hydrogels.* Biomaterials, 2015. **73**: p. 254-71.
2. Nichol, J.W., et al., *Cell-laden microengineered gelatin methacrylate hydrogels.* Biomaterials, 2010. **31**(21): p. 5536-44.
3. Liu, Y. and M.B. Chan-Park, *A biomimetic hydrogel based on methacrylated dextran-graft-lysine and gelatin for 3D smooth muscle cell culture.* Biomaterials, 2010. **31**(6): p. 1158-70.
4. Van den Steen, P.E., et al., *Biochemistry and molecular biology of gelatinase B or matrix metalloproteinase-9 (MMP-9).* Crit Rev Biochem Mol Biol, 2002. **37**(6): p. 375-536.
5. Xu, H., et al., *Effects of Irgacure 2959 and lithium phenyl-2, 4, 6-trimethylbenzoylphosphinate on cell viability, physical properties, and microstructure in 3D bioprinting of vascular-like constructs.* Biomedical Materials, 2020. **15**(5): p. 055021.
6. Van Den Bulcke, A.I., et al., *Structural and rheological properties of methacrylamide modified gelatin hydrogels.* Biomacromolecules, 2000. **1**(1): p. 31-8.
7. Pepelanova, I., et al., *Gelatin-Methacryloyl (GelMA) Hydrogels with Defined Degree of Functionalization as a Versatile Toolkit for 3D Cell Culture and Extrusion Bioprinting.* Bioengineering (Basel), 2018. **5**(3).
8. Shirahama, H., et al., *Precise Tuning of Facile One-Pot Gelatin Methacryloyl (GelMA) Synthesis.* Sci Rep, 2016. **6**: p. 31036.
9. Bertassoni, L.E., et al., *Direct-write bioprinting of cell-laden methacrylated gelatin hydrogels.* Biofabrication, 2014. **6**(2): p. 024105.
10. Wei, Z., B.T. Harris, and L.G. Zhang, *Gelatin methacrylamide hydrogel with graphene nanoplatelets for neural cell-laden 3D bioprinting.* Conf Proc IEEE Eng Med Biol Soc, 2016. **2016**: p. 4185-4188.
11. Liu, J., et al., *Hydrogels for Engineering of Perfusable Vascular Networks.* Int J Mol Sci, 2015. **16**(7): p. 15997-6016.
12. Hosseini, V., et al., *Engineered contractile skeletal muscle tissue on a microgrooved methacrylated gelatin substrate.* Tissue Eng Part A, 2012. **18**(23-24): p. 2453-65.
13. Zhao, X., et al., *Photocrosslinkable Gelatin Hydrogel for Epidermal Tissue Engineering.* Adv Healthc Mater, 2016. **5**(1): p. 108-18.
14. Chen, M.B., et al., *A 3D microfluidic platform incorporating methacrylated gelatin hydrogels to study physiological cardiovascular cell-cell interactions.* Lab Chip, 2013. **13**(13): p. 2591-8.
15. Li, X., et al., *3D Culture of Chondrocytes in Gelatin Hydrogels with Different Stiffness.* Polymers (Basel), 2016. **8**(8).
16. Schuurman, W., et al., *Gelatin-methacrylamide hydrogels as potential biomaterials for fabrication of tissue-engineered cartilage constructs.* Macromol Biosci, 2013. **13**(5): p. 551-61.

17. Al Rifai, N., et al. *Culture of PC12 neuronal cells in GelMA hydrogel for brain tissue engineering*. in *2015 International Conference on Advances in Biomedical Engineering (ICABME)*. 2015. IEEE.
18. Wu, Y., et al., *The influence of the stiffness of GelMA substrate on the outgrowth of PC12 cells.* Biosci Rep, 2019. **39**(1).
19. Dursun Usal, T., D. Yucel, and V. Hasirci, *A novel GelMA-pHEMA hydrogel nerve guide for the treatment of peripheral nerve damages.* Int J Biol Macromol, 2019. **121**: p. 699-706.
20. Koffler, J., et al., *Biomimetic 3D-printed scaffolds for spinal cord injury repair.* Nat Med, 2019. **25**(2): p. 263-269.
21. Eke, G., et al., *Development of a UV crosslinked biodegradable hydrogel containing adipose derived stem cells to promote vascularization for skin wounds and tissue engineering.* Biomaterials, 2017. **129**: p. 188-198.
22. Salamon, A., et al., *Gelatin-Based Hydrogels Promote Chondrogenic Differentiation of Human Adipose Tissue-Derived Mesenchymal Stem Cells In Vitro.* Materials (Basel), 2014. **7**(2): p. 1342-1359.
23. Hu, Y., et al., *3D-engineering of Cellularized Conduits for Peripheral Nerve Regeneration.* Sci Rep, 2016. **6**: p. 32184.
24. Hanani, Z.A.N., *Gelatin*, in *Encyclopedia of Food and Health*, B. Caballero, P.M. Finglas, and F. Toldrá, Editors. 2016, Academic Press: Oxford. p. 191-195.
25. Stratesteffen, H., et al., *GelMA-collagen blends enable drop-on-demand 3D printablility and promote angiogenesis.* Biofabrication, 2017. **9**(4): p. 045002.
26. Kielbassa, C., L. Roza, and B. Epe, *Wavelength dependence of oxidative DNA damage induced by UV and visible light.* Carcinogenesis, 1997. **18**(4): p. 811-816.
27. Sato, R., R. Harada, and Y. Shigeta, *Theoretical analyses on a flipping mechanism of UV-induced DNA damage.* Biophysics and Physicobiology, 2016. **13**: p. 311-319.
28. CELLINK. *GelMa casting protocol*. 2018 [cited 2022 15/04/2022]; Available from: https://www.cellink.com/wp-content/uploads/2018/04/GelMACastingProtocolver1.pdf.
29. Sharifi, S., et al., *Systematic optimization of visible light-induced crosslinking conditions of gelatin methacryloyl (GelMA).* Scientific Reports, 2021. **11**(1): p. 23276.
30. Leijten, J., et al., *Spatially and temporally controlled hydrogels for tissue engineering.* Materials Science and Engineering: R: Reports, 2017. **119**: p. 1-35.
31. Kim, C., et al., *Stem cell mechanosensation on gelatin methacryloyl (GelMA) stiffness gradient hydrogels.* Annals of biomedical engineering, 2020. **48**: p. 893-902.
32. Bock, N., et al., *GelMA, Click-Chemistry Gelatin and Bioprinted Polyethylene Glycol-Based Hydrogels as 3D Ex Vivo Drug Testing Platforms for Patient-Derived Breast Cancer Organoids.* Pharmaceutics, 2023. **15**(1): p. 261.

33. Monteiro, N., et al., *Photopolymerization of cell-laden gelatin methacryloyl hydrogels using a dental curing light for regenerative dentistry.* Dental materials, 2018. **34**(3): p. 389-399.
34. Tomal, W. and J. Ortyl, *Water-soluble photoinitiators in biomedical applications.* Polymers, 2020. **12**(5): p. 1073.
35. Nakayama, Y., et al., *Enhancement of visible light-induced gelation of photocurable gelatin by addition of polymeric amine.* Journal of Photochemistry and Photobiology A: Chemistry, 2006. **177**(2-3): p. 205-211.

# Chapter Four: Adipose-derived stem cells spontaneously express neural markers when grown in a PEG-Based 3D matrix.

**Submitted as:**
*Gomila Pelegri, N.; Stanczak, A.M.; Bottomley, A.L.; Milthorpe, B.K.; Gorrie, C.A.; Padula, M.P.; Santos, J. Adipose-Derived Stem Cells Spontaneously Express Neural Markers When Grown in a PEG-Based 3D Matrix. Int. J. Mol. Sci. 2023, 24, 12139. https://doi.org/10.3390/ijms241512139*

Published on 28th of July 2023

I certify that the work present in chapter four of this thesis has not been previously submitted as part of the requirements for a degree. I also certify that I carried out over 70% of the experimental work, analysis and interpretation of the data presented in this paper.

**Author's contributions:**

Conceptualization, J.S., N.G.P. and C.A.G.; methodology, J.S., N.G.P., M.P.P. and C.A.G.; formal analysis, N.G.P. and A.L.B.; investigation, N.G.P.; resources, J.S., B.K.M. and M.P.P.; data curation, N.G.P., A.M.S. and A.L.B.; writing—original draft preparation, N.G.P.; writing—review and editing, All; visualization, N.G.P. and A.M.S.; supervision J.S., M.P.P. and C.A.G.; project administration, J.S.; funding acquisition, J.S. and B.K.M. All authors have read and agreed to the published version of the manuscript.

| | |
|---|---|
| Neus Gomila Pelegri | Production Note: Signature removed prior to publication. |
| Aleksandra M. Stanczak | Production Note: Signature removed prior to publication. |
| Amy L. Bottomley | Production Note: Signature removed prior to publication. |
| Bruce K. Milthorpe | Production Note: Signature removed prior to publication. |
| Catherine A. Gorrie | Production Note: Signature removed prior to publication. |
| Matthew P. Padula | Production Note: Signature removed prior to publication. |
| Jerran Santos | Production Note: Signature removed prior to publication. |

International Journal of
*Molecular Sciences*

MDPI

*Article*

# Adipose-Derived Stem Cells Spontaneously Express Neural Markers When Grown in a PEG-Based 3D Matrix

**Neus Gomila Pelegri [1,2], Aleksandra M. Stanczak [3], Amy L. Bottomley [4], Bruce K. Milthorpe [1], Catherine A. Gorrie [2], Matthew P. Padula [3] and Jerran Santos [1,*]**

[1] Advanced Tissue Engineering and Stem Cell Biology Group, School of Life Sciences, University of Technology Sydney, Ultimo, NSW 2007, Australia; neus.gomilapelegri@uts.edu.au (N.G.P.); bruce.milthorpe@uts.edu.au (B.K.M.)
[2] Neural Injury Research Unit, School of Life Sciences, University of Technology Sydney, Ultimo, NSW 2007, Australia; catherine.gorrie@uts.edu.au
[3] School of Life Sciences, University of Technology Sydney, Ultimo, NSW 2007, Australia; aleksandra.m.stanczak@student.uts.edu.au (A.M.S.); matthew.padula@uts.edu.au (M.P.P.)
[4] Microbial Imaging Facility, University of Technology Sydney, Ultimo, NSW 2007, Australia; amy.bottomley@uts.edu.au
* Correspondence: jerran.santos@uts.edu.au

**Abstract:** Neurological diseases are among the leading causes of disability and death worldwide and remain difficult to treat. Tissue engineering offers avenues to test potential treatments; however, the development of biologically accurate models of brain tissues remains challenging. Given their neurogenic potential and availability, adipose-derived stem cells (ADSCs) are of interest for creating neural models. While progress has been made in differentiating ADSCs into neural cells, their differentiation in 3D environments, which are more representative of the in vivo physiological conditions of the nervous system, is crucial. This can be achieved by modulating the 3D matrix composition and stiffness. Human ADSCs were cultured for 14 days in a 1.1 kPa polyethylene glycol-based 3D hydrogel matrix to assess effects on cell morphology, cell viability, proteome changes and spontaneous neural differentiation. Results showed that cells continued to proliferate over the 14-day period and presented a different morphology to 2D cultures, with the cells elongating and aligning with one another. The proteome analysis revealed 439 proteins changed in abundance by >1.5 fold. Cyclic nucleotide 3′-phosphodiesterase (CNPase) markers were identified using immunocytochemistry and confirmed with proteomics. Findings indicate that ADSCs spontaneously increase neural marker expression when grown in an environment with similar mechanical properties to the central nervous system.

**Keywords:** tissue engineering; bioprinting; polyethylene glycol; PEG; neural differentiation; adipose-derived stem cells; hydrogels; immunocytochemistry; CNPase; proteomics

check for updates

**Citation:** Gomila Pelegri, N.; Stanczak, A.M.; Bottomley, A.L.; Milthorpe, B.K.; Gorrie, C.A.; Padula, M.P.; Santos, J. Adipose-Derived Stem Cells Spontaneously Express Neural Markers When Grown in a PEG-Based 3D Matrix. *Int. J. Mol. Sci.* **2023**, *24*, 12139. https://doi.org/10.3390/ijms241512139

Academic Editor: Agatina Campisi

Received: 3 July 2023
Revised: 21 July 2023
Accepted: 24 July 2023
Published: 28 July 2023



## 1. Introduction

Neurological disorders affect the body's peripheral and central nervous systems [1] and are among the leading causes of disability and death worldwide [2]. For most nervous system disorders, such as spinal cord injury, traumatic brain injury, stroke, multiple sclerosis and Alzheimer's disease, cures are unavailable, and treatment remains complex and can result in morbidity as well as significant social and economic impact [1–3].

Significant effort has been made to further understand and treat these and other neurological disorders; however, the gold standard in such research involves animal models, ex vivo samples or 2D cell culture models. Results from such studies typically translate poorly from animal models to the clinic, which has been attributed to the lack of accurate in vitro models of the nervous system [4–6].

The human brain is one of the most complex biological systems and, as such, is poorly replicated in animal models as well as in in vitro systems. Contrary to other simpler

organs, the cellular organisation and structure of the brain contains a high density of many cell types with diverse synaptic connections and interactions forming large and complex neural circuits. It is composed of cells like neurons, oligodendrocytes, glial cells, astrocytes, and other support cells, as well as an extracellular matrix (ECM). The brain ECM represents 20–30% of the brain occupying the space between neural cells and mainly formed of glycosaminoglycans like hyaluronic acid, proteoglycans like neurocan, glycoproteins like tenascin-R and fibrous proteins like collagen and fibronectin (Figure 1) [4,5,7–10]. The ECM is a physical barrier that assists in diffusion within the brain and has a role in neural development, including neurite outgrowth, synaptogenesis and plasticity [11–13]. Additionally, the brain is the softest tissue in the body, with an elastic modulus that ranges from 0.1 kPa to 1.6 kPa [14,15], making it even more challenging to replicate in vitro. Figure 1 shows a visual representation of the differences between brain structure compared to the epithelial tissue that lines different organs like lungs.

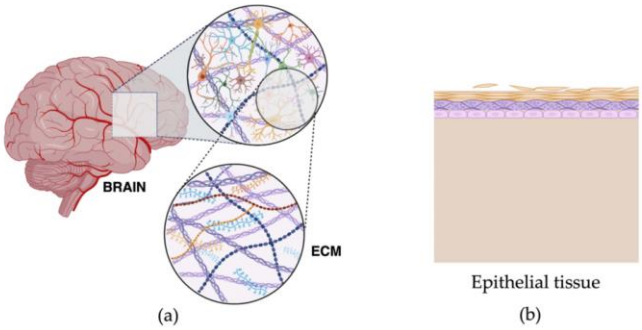


**Figure 1.** Diagrams showing the complex 3D brain structure versus squamous epithelium that might be modelled by 2D cell culture. (**a**) Brain structure and composition showing different cell types including glia, neurons, astrocytes, microglia, oligodendrocytes and other support cells. It also depicts the ECM and the different components of brain ECM like laminins, proteoglycans, collagen and hyaluronic acid. (**b**) Structure and composition of simple epithelial tissue with epithelial cells and basal membrane. Created with BioRender.com, accessed 23 June 2023.

There are considerable challenges in sourcing healthy human brain tissue or cells for experimental research due to the physical inaccessibility and high risk of damage, which makes it difficult to investigate the normal properties and behaviours of these cells in vitro. Without a complete understanding of the pathophysiology of neurological conditions, it is challenging to identify and validate potential therapeutic targets [5].

Adipose-derived stem cells (ADSCs) are an ideal candidate to develop disease models, as well as investigating potential treatment avenues due to their neurogenic potential, abundance and accessibility [16,17]. Not only are they highly abundant in the human body, they are also relatively easily accessible through subcutaneous adipose tissue liposuction, minimizing potential collection complications from more invasive cell collection methods like bone marrow aspirates [18]. Additionally, significant progress has been made in differentiating ADSCs toward neural cells; however, the most common method of differentiation is with 2D chemical inductions, which are not always stable [19–26]. Ahmadi et al. [27] compared the stability of ADSCs neural differentiation between a 2D chemical induction protocol and a sphere formation protocol. The results showed that while treated ADSCs from both protocols had large expression of neural-specific markers, and 2D chemical induction showed a rapid differentiation, it also led to further cell death and the neural-like state appeared to be reversible. On the other hand, the neurosphere formation protocol was slower, it had better cell viability and the neural-like state was more stable [27]. Dif-

ferentiation in 3D matrices that are more representative of the natural physiology of the nervous system may present benefits and yield higher translation to the clinic.

Tissue engineering offers a potential avenue to create a more accurate/representative in vitro model and take into consideration the effects of environmental and mechanical cues on cell differentiation [28,29].

There is increasing evidence that cells grown in 3D conformations show responses more comparable to in vivo behaviours while varying considerably both morphologically and physiologically from cells grown in 2D monolayers. In 3D culture models, cells replicate the shape and organization found in tissue as cells are allowed to grow in aggregates or spheroids containing multiple layers [28,30–34]. Additionally, cell exposure to nutrients and waste is also closer to in vivo conditions, where nutrients and growth factors/drug treatments are not equally distributed among all cells, which means cells are often more resistant to drug treatments and have higher rates of resistance to drug-induced apoptosis providing a more accurate prediction of in vivo drug response [28,33,35–39]. Furthermore, cell proliferation is also more realistic in 3D cultures compared to the unnatural rapid pace at which cells grow in 2D [34–36,40], while gene expression and protein abundance better resemble levels observed in in vivo tissues [33,34,40]. Cells also respond more accurately to the mechanical stimuli of the 3D environment, where cell differentiation can be induced by the mechanical pressures and composition of the scaffold that mimics the natural interactions of the cells with the ECM [41–45]. It is known that the ECM plays a critical role in determining cellular phenotype not only through mechanical cues but also by the direct interaction of proteins with the cell surface receptors [41–44,46]. For example, human-derived Mesenchymal Stem Cells (hMSCs) have been shown to differentiate towards a neural lineage when grown in scaffolds of a stiffness of ~1 kPa [44].

One way to achieve this is by modulating the 3D matrix composition and stiffness that the cells are grown in to resemble the tissue of origin better. In this study, we looked at the neuro-differentiation effects of PEG-based hydrogels at 1.1 kPa on ADSCs for 14 days with the added adhesion motifs such as arginylglycylaspartic acid, the peptide trimer RGD found in collagen, laminin and fibronectin, which mediates the adhesion of many cells including neurons [47], and laminin-derived (YIGSR) peptide, which promotes neuronal cell binding [48].

## 2. Results

### *2.1. Cell Proliferation, Viability and Morphology*

#### 2.1.1. ADSCs Proliferated in Both 2D and 3D Culture Conditions

Alamar blue viability assay showed that ADSCs remained viable and continued to proliferate in both 2D and 3D cultures for both the imaging plug (Figure 2a) and the large plug (Figure 2b), with 3D cultures showing higher proliferation rates in 3D than in 2D (Figure 2b). The imaging plug and large plug differences are further explained in the methods Section 4.1, but in brief, the imaging plug is the small version of the 3D construct, while the large plug is for proteome analysis. The concentration of cells was kept the same; however, the total number of cells differs depending on the size of the construct.

Live cell imaging analysis demonstrated that the staining control cells, U87MG glioblastoma cells (GBCs) and SHY5Y neuroblastoma cells (NBCs), proliferated over the 14-day period in both 2D (Figure 3a) and 3D (Figure 3b) conditions. There was a modest increase in ADSC numbers over 14 days in the 2D construct and a significant increase was seen in the 3D culture conditions, with a greater proliferation observed in the 3D construct at 14 days (Figure 3b,c).

Additionally, when looking at confluence data (Figure 3), an increase in total area covered by cells can be seen. 3D cells increased in area covered significantly over time between D1 and D14 in 3D ($p \leq 0.01$) while the increase in 2D is not significant (Figure 3c).

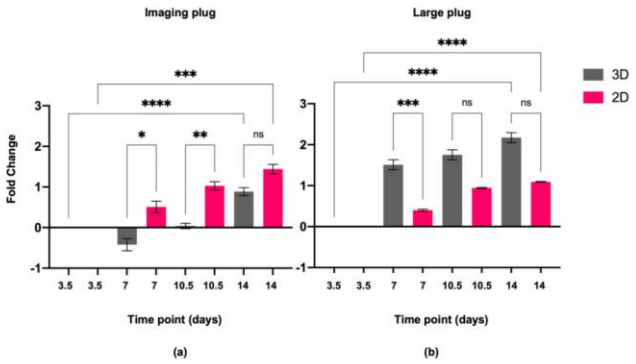


**Figure 2.** Fold change in cell activity over time relative to day 3.5 measured using alamar blue assay. Log2 scale has been used where the initial measurement obtained on day 3.5 equals zero, and the increase or decrease in measured parameters falls on the respective side of the *x*-axis. (**a**) Imaging plug; (**b**) large plug. Statistical significance defined as * = $p \leq 0.05$, ** = $p \leq 0.01$, *** = $p \leq 0.001$ and **** = $p \leq 0.0001$, ns: not significant.

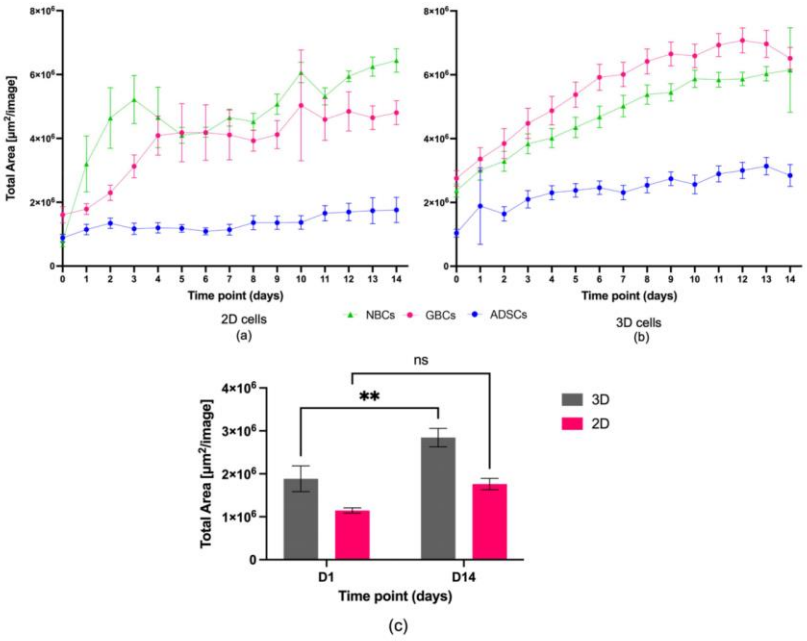


**Figure 3.** Graph showing the proliferation of cells over time as measured by total cell area for staining control cells GBC and NBC and for the ADSCs in (**a**) 2D and (**b**) 3D cultures (large plug). Error bars represent standard deviation. Green triangles—NBCs, pink circles—GBCs, and blue circles—ADSCs. (**c**) Graph showing the proliferation changes of ADSCs measured as total cell area comparing D1 and D14 when grown in 2D and 3D cultures (large plug). Statistical significance defined as ** = $p \leq 0.01$, ns: not significant.

#### 2.1.2. ADSCs Cell Morphology Changed in 3D Conditions

Cell morphology is an important aspect to consider in cell culture, particularly when comparing a 2D growth environment to a 3D one. Clear morphological changes can be seen from Day 1 where ADSCs in 2D cell culture had an irregular fibroblastic-like structure, appearing as large, flattened cells with obvious centrally located nuclei (Figure 4a–c,g). In contrast, ADSCs grown in 3D constructs displayed changes in the membrane giving the cells a narrower appearance. The cells looked more spindly, with elongated profiles and cytoplasm less spread out, darker in colour, and overall taking up less area in the XY plane. Clear networks and branching out can also be seen between cells (Figure 4d–f,h). Additionally, in 2D, as the cells become more confluent, it becomes harder to distinguish morphologically individual cells, and instead, cells become a homogenous monolayer, while in 3D, the cells expand but retain their respective individual morphology.

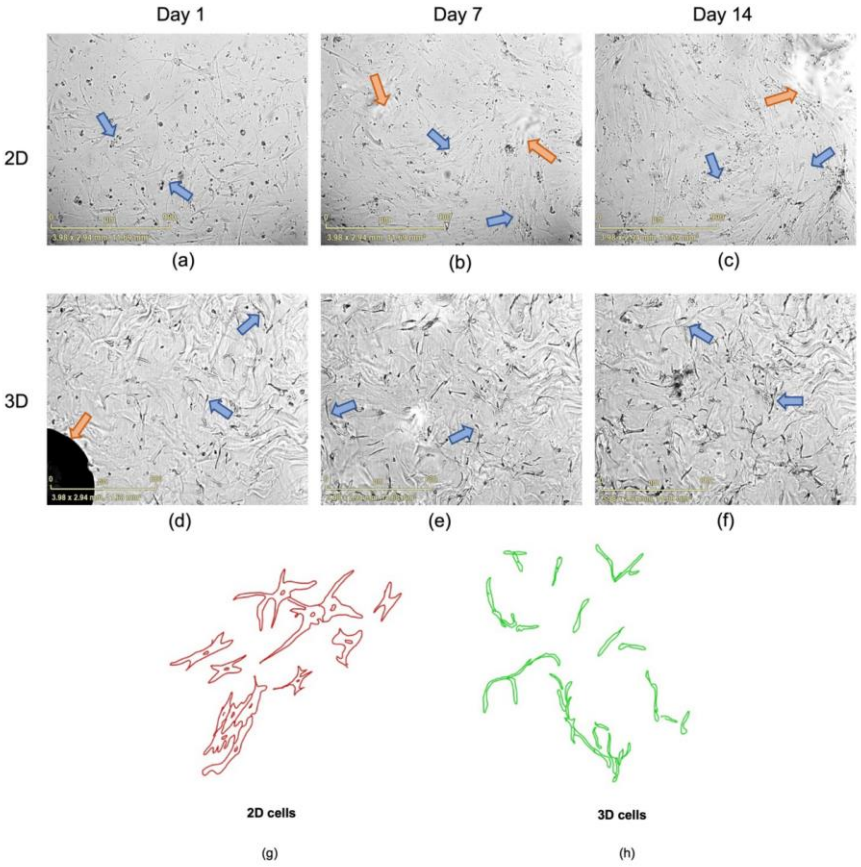


**Figure 4.** (**a**–**f**) Representative live cell images at time points D1, D7 and D14. Blue arrows indicate different cells and show differences between 2D and 3D; orange arrows show artefacts present in the images. The white blurry artefacts are glares and reflections, and the black round artefacts are bubbles; (**g**,**h**) Graphical representation of cell morphology changes between 2D and 3D cells. These were manually drawn by tracing the cell shapes on a digital tablet. Scale bar 800 µm.

### 2.2. Cell Characterisation

#### 2.2.1. Immunocytochemistry

Immunocytochemistry imaging (Figure 5) showed expression of the CNPase marker only in the 3D-grown ADSCs. All other markers remained negative.

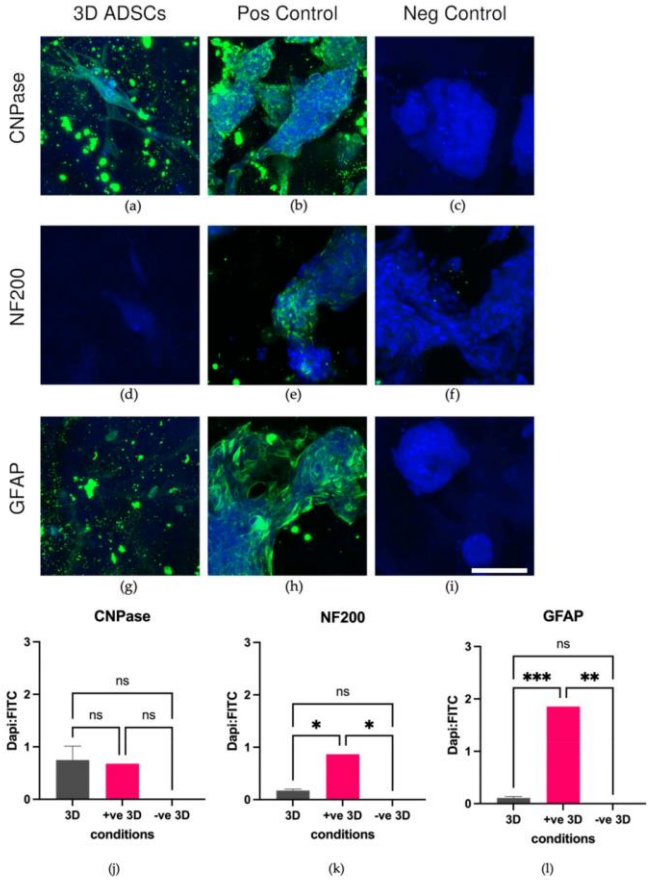


**Figure 5.** (**a**–**i**) Representative maximum intensity projection confocal microscopy images of immunocytochemistry staining of ADSCs in 3D with respective positive and negative staining controls for each antibody marker CNPase, NF200 and GFAP. Cells were imaged with a Nikon A1R inverted microscope using a S Plan Fluor LWD 20× 0.7NA objective. Fluorescence was captured with a laser at 405 nm excitation and PMT detector (425–475 nm) for DAPI (blue), and 488 nm excitation and GaAsP detector (500–550 nm) for AlexaFluor488-conjugated secondary antibodies (green). Scale bar = 100 µm. Please note that control cells are smaller than ADSCs; (**j**–**l**) immunocytochemistry marker expression for 3D cells. Marker expression was measured from sum intensity projections of wide-field fluorescence images of the whole 3D plug and is displayed as the fraction of the percentage area of FITC (AlexaFluor488-conugated secondary antibody) over the percentage area of DAPI-labelled nuclei. No statistical significance $p > 0.05$; statistical significance *, $p \leq 0.05$; statistical significance **, $p \leq 0.01$; statistical significance ***, $p \leq 0.001$; statistical significance, ns: not significant.

2.2.2. Proteomics

Proteomic analysis using MaxQuant and LFQ Analyst revealed clear proteome changes between ADSCs grown in 2D vs. 3D environments.

A total of 2878 proteins were identified, with 218 proteins only present in 2D samples and absent in 3D samples, and 93 present in 3D samples but absent in 2D samples (Figure 6a). Additionally, of the total 2878 proteins identified, 2291 proteins changed in abundance with 439 proteins changed in abundance by >1.5-fold with $p$-value < 0.05 meaning 15% of all proteins detected significantly changed in abundance by at least 1.5-fold (Figure 6b).

Supplementary S1 (Table S1) includes all 439 proteins that changed in abundance with respective log2 fold changes and $p$-values.

While functional enrichment analysis of all 439 significant proteins using StringDB revealed quite broad changes, changes in actin, ribosomal and neural-related functions are notable (Supplementary S2). The heatmap displayed in Figure 7a shows the different functional enrichments of the proteins detected relating to actin, ribosome and neural processes and their respective log2 fold change, and Figure 7b shows in more detail the number of proteins detected involved in each function.

A total of 67 proteins with changed abundance are related to actin; of these 67, 45 are related to both actin and neural processes, of which 36 proteins increased in abundance, and 9 decreased in abundance (Supplementary S2).

Supplementary S2 includes a table with all the proteins and functions included in Figure 7 heatmap and graph (Table S2), the permalink to the StringDB network analysis results and an additional heatmap of all functional enrichment processes detected using StringDB with log2 fold change in all proteins (Figure S1).

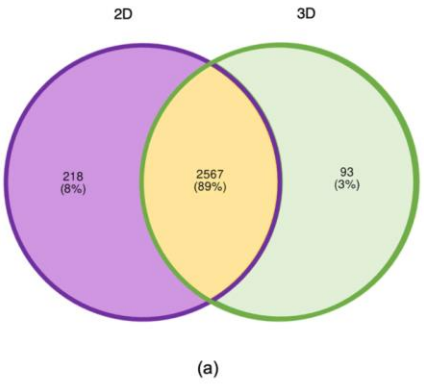


**Figure 6.** *Cont.*

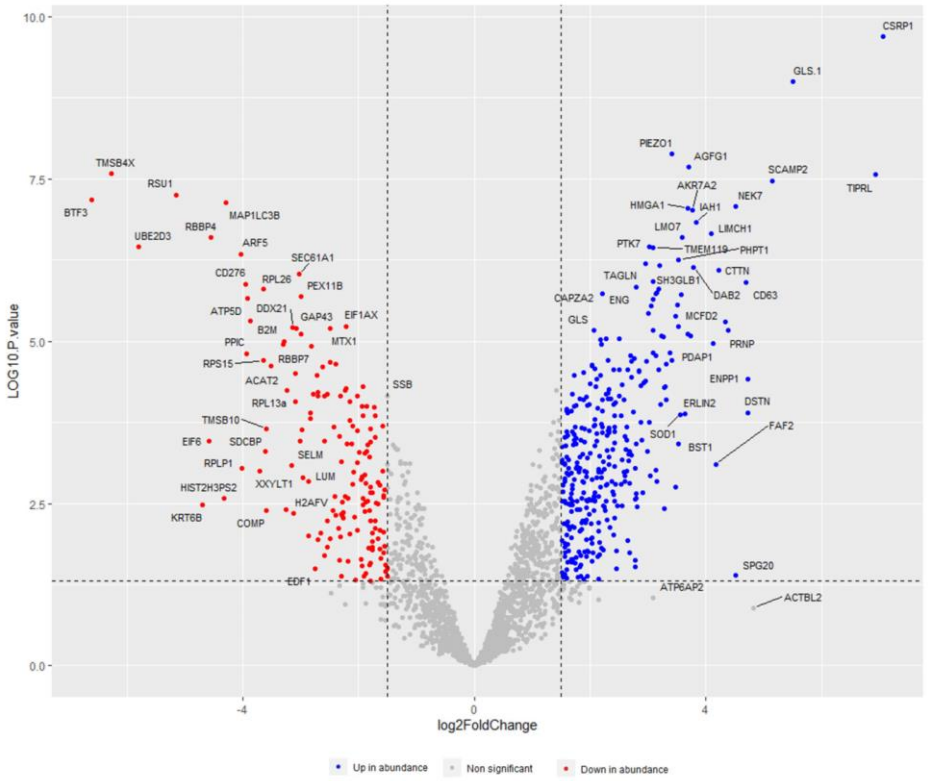


(b)

**Figure 6.** (**a**) Venn diagram showing total number of proteins detected in both 2D and 3D sample groups as well as the total number of proteins that were detectable in 2D sample group and were not in the 3D sample group and all proteins that were detectable in 3D sample group that were not detected in the 2D sample group; (**b**) Volcano plot showing total number of proteins detected with increase or decrease in abundance in 3D samples compared to 2D samples. Blue dots represent proteins that have increased in abundance by >1.5 fold with a *p*-value of <0.05 in 3D samples compared to 2D samples; red dots proteins that have decreased in abundance > 1.5 fold with a *p*-value of <0.05 in 3D samples compared to 2D samples. Gray are all non-significant detected proteins.


**Figure 7.** (**a**) Heatmap showing all proteins involved in neural, actin and ribosomal processes with respective fold change. Hierarchical clustering and further division into similarity groups was conducted. Blue indicates increase in abundance, red decrease in abundance, purple neural functions, green ribosomal functions and yellow actin functions. (**b**) Number of proteins identified with roles in neural functions revealed during functional and network analysis.

## 3. Discussion

The aim of this study was to examine ADSCs' cellular and molecular differences when grown in 2D or 3D environments where the 3D environment is designed to mimic the density and elasticity of brain tissue. It was hypothesised that there would be biological differences at the cellular level in growth patterns and morphology as well as complementary changes in the analysed proteome. The data confirmed the hypothesis that the 3D environment did indeed have a significant effect on the ADSCs morphology and protein abundances when compared to 2D-grown ADSCs.

Cell viability was unchanged between the 2D and the 3D gels, and cells exhibited increased proliferation as shown by an increase in alamar blue fluorescence and by an increase in the area covered by cells in the 3D-grown cells (Figures 2 and 3) compared to the cells in the 2D environment. Furthermore, morphological changes in the cells were clearly seen in the 3D environment compared to the ones in 2D. In the 3D environment, cells became spindle-like and aligned with one another, showing elongation, branching out and a low nuclei-to-cytoplasm ratio, which are key morphological characteristics of neural cells, implying that these cells are differentiating down a neural lineage by just being in a 3D environment.

Immunocytochemistry analysis showed that ADSCs started to express CNPase, a well-known oligodendrocyte marker, in the 3D environment. Structural and neural changes were further confirmed by the proteomics analysis, which showed significant proteome changes between cells grown in 2D and 3D environments. There were over 2870 proteins identified and 439 significantly changing in abundance, with the most striking changes were observed in proteins annotated as being involved in neural, actin and ribosomal processes.

### *3.1. ADSCs in 3D Matrices Show Increased Cell Viability and Morphological Changes Indicative of Neural Differentiation*

It has been previously reported that neural precursor cells grown in PEG-based matrices have a higher metabolic activity, lower apoptotic activity and higher cell proliferation rates [49], as well as enhancing neural stem cell (NSCs) survival, proliferation and differentiation compared to those grown in 2D environments [50]. The alamar blue assay, a widely used viability and proliferation test, showed that the cells remained viable and continued to proliferate over the 14-day period in our study, with the cells grown in 3D conditions having higher proliferation rates than those in 2D conditions (Figure 2). Additionally, cell area coverage analysis showed an increase in coverage over time, with 3D cells having a significantly increased cell coverage between day 1 and day 14 (Figure 3), showing that the cells are thriving in the 3D environment.

It is also widely known that the cell environment plays a key role in many cell functions and influences proliferation, differentiation, migration and morphology [51]. When cells are grown in 2D conditions, they are forced flat onto a hard surface where they are only attached to the XY plane and have no interactions or pressures from the Z plane; therefore, they do not have anything "on top of them" and are forced to extend their cytoplasm in order to have more attachment points [52]. On the other hand, when cells are grown inside a matrix in a 3D conformation, cells start to interact with the matrix in an XYZ axis, having cues all around them. In 3D conditions, the cells are suspended within the matrix, where they can move and migrate and interact with other cells, rather than being forced to attach to a 2D surface that cannot be modified by the cells [52]. Furthermore, the stiffness of polystyrene or glass surfaces used to grow monolayer cultures is multiple orders of magnitude greater than any soft tissues found in the human body. This environment provides atypical stimuli that affect cellular development [53]. This is especially important in the context of neural development, as brain tissue represents one of the softest tissues in the body [54].

3D matrices are known to mimic better in vivo conditions, and cells are known to adopt morphologies more resemblant to those occurring in the body as well as responding to the

mechanical cues of the matrix [36]. The ADSCs grown in the 3D matrices have also shown notable morphological changes, with cells going from large, flat, "fried-egg" like shapes with centrally located nuclei and large cytoplasm-to-nuclei ratio to thin, elongated, spindle-shaped cells with low cytoplasm-to-nuclei ratio and branching out creating networks between cells (Figure 4), which are morphological features usually seen in neural cells. In addition, mechanical cues play an important role in stem cell differentiation. It has been previously shown that substrate stiffness can direct attachment, survival, growth and differentiation of MSCs [44]. For example, MSCs can undergo osteogenesis when placed in stiffer substrates [55–57] and differentiate towards neural lineage when placed in softer matrices [41,44], with MSCs going towards neuronal lineage in ~1 kPa stiffness matrix and towards glial lineage when in ~10 kPa matrices [44]. These results suggest that these cells may be differentiating down a neural lineage by the PEG-based matrices.

### 3.2. Immunocytochemistry and Proteome Changes of ADSCs in 3D Matrices Are Indicative of Neural Differentiation

CNPase is a myelin-associated protein that is expressed in pre-oligodendrocytes and oligodendrocytes and is widely used as a marker for early oligodendrocyte differentiation and myelin formation [58–60]. Furthermore, CNPase has been previously detected in ADSCs undergoing chemical differentiation in 2D environments [61]. In the current study, CNPase was detected in the immunocytochemistry results for the ADSCs grown in 3D only (Figure 5), and it was found to be slightly increased (0.9 log2 fold change) in the proteome findings in the 3D-grown cells suggesting that perhaps the cells are starting to differentiate towards oligodendrocytes or that there may be myelin formation occurring. GFAP and NF-200 immunocytochemistry did not show increases in the ADSCs grown in 3D. However, it should be noted that these are both mature structural cell markers, and the ADSCs may not be at that stage of differentiation yet, given how long neural cells take to differentiate, with cortical neurogenesis taking around 108 embryonic days to complete [62].

### 3.3. Structural Proteins Expression Involved in Neural Differentiation

The proteome analysis showed protein abundance changes related to neural, actin and ribosomal functions. Interestingly, network analysis detected over 250 proteins with statistically significant changes in abundance relating to the nervous system and nervous system processes (Figure 7), of which 45 proteins are also involved in actin-related functions (Supplementary S2 Table S2). Actin is an essential component of cell cytoskeleton; it has an important role in cell survival, morphology and movement. Actin filaments, in conjunction with other proteins, provide mechanical support, assist in sensing environmental cues and tracking the movement of intracellular materials, such as internalised membrane vesicles, and assist in cell migration and division [63]. More specifically, in the neural context, microtubules, neurofilaments and F-actin are the main filaments of the neuronal cytoskeleton. Actin, in particular, is involved in neuronal outgrowth, morphology and synaptic function, playing a key role in establishing and maintaining neuronal polarity with many actin-regulating proteins influencing neuronal morphology and plasticity [64,65]. Neurons' polarised morphology is instrumental to their ability to process and transfer information between dendrites and axons. These are long and highly branched structures extending from the neuronal cell's body and reaching up to hundreds of microns in length, forming a widespread and complex arbour [64,66,67]. Additionally, the growth cones within neurons detect and interpret extracellular signals that guide the growth and elongation of neurons [68]. These findings, supported by the observed neural-like morphological changes in the ADSCs grown in 3D PEG-based matrices (Figure 4), suggest that the cells are going through structural and shape changes indicative of neural differentiation.

Of particular interest is CSRP1 protein, also known as CSP1, it was the protein most increased in abundance detected in the whole dataset. It increased by 7.3 log2 fold change (Figure 6b) in 3D-grown cells. CSRP1 has diverse roles in cellular development, from suppressing cell proliferation, protecting cells from stress-induced death, regulating cell

movement [69,70] and playing a role in actin dynamics by interacting with actin to regulate actin filament bundling [71,72]. In the nervous system context, CRP1 is the only protein of the CRP protein family to be found in the CNS [73]. It colocalizes with actin in growth cone filopodia in neurons playing a role in its formation; increased CRP1 expression has been found to increase filopodia formation and dendritic growth in neurons, and its absence has been found to cause the opposite, with the deletion of CSRP1 gene causing inhibition of filopodia formation and dendritic growth in neurons [73].

Another protein group of interest is the ADF/Cofilin proteins that are well-known regulators of actin dynamics and are highly expressed in growth cones [74,75]. They are involved in growth cone motility, axon growth and neurite extension during early neural development [76–79]. ADF/Cofilin proteins have also been recently recognised as promising target proteins to regenerate axons in the adult nervous system, given their critical role in F-actin binding, severing and depolymerising activities during early neuronal development [80]. Furthermore, cofilin knockdown models resulted in neuron polarity defects [75] and ADF/Cofilin are known to regulate synaptic function through their effect on dendritic spines [81]. Interestingly, our results showed that ADF (labelled as DSTN) was one of our top six proteins increased in abundance in the 3D-grown cells with a log2 fold change of 4.72. Cofilin (labelled as CFL1) was also found to be increased by 2.02 log2 fold.

Another interesting finding is the high increase in the actin-binding protein Cortactin (labelled as CTTN). In our dataset, Cortactin was increased by a log2 fold change of 4.23, making it one of the top 12 most increased proteins in the dataset. CTTN is an actin-binding protein that regulates actin cytoskeletal networks and is essential for endocytosis, cell migration, adhesion, synaptic organisation and cell morphogenesis [82]. It is found in the dendritic spines [83] and more specifically plays an important role in pre- and postsynaptic structures and in neuron-specific functions like axon guidance, synaptogenesis and growth cone formation as well as in functional and structural synaptic plasticity [84–88]. CTTN loss is also associated with a reduction in dendritic spine numbers [83], and it is enriched in both axonal and dendritic growth cones of young neurons [89]. Studies have also found that CTTN is enriched in the central region of all neurite growth cones prior to neurons developing into axons [90].

Several other actin-binding proteins, which are involved in similar pathways, are also increased in abundance in this proteomic data, which further supports our findings. CAP2 increased by 3.16 log2 fold in 3D-grown cells, and it is expressed in growth cones, dendrites and postsynaptic terminals. It is also involved in dendrite morphology regulation, spine development and synaptic plasticity in neurons [91–93]. ADD1, increased by 2.65 log2 fold, is an actin-binding protein of the subcortical neuronal cytoskeleton and plays a role in axonal diameter maintenance [94] and synaptic plasticity [95]. DBN1, also known as drebrin, was increased by 1.59 log2 fold in the 3D-grown cells and has a role in neuron growth and brain development. It is present in the dendritic spines of excitatory synapses, and it is mainly found during early brain development in the dendritic spines of immature neurons [96–98].

Lastly, β3-Tubulin (TUBB3) was found to have increased by 1.51 log2 fold in the 3D-treated cells. TUBB3 is a major component of the neuronal cytoskeleton, and it is highly expressed in microtubule during neural development, playing a critical role in maintenance, maturation and proper axon guidance, and it has been long used as a neuronal marker in [99–103].

These proteome changes, together with the observed morphological changes in Figure 4, suggest that the cells' cytoskeleton is significantly rearranging in response to its environment, and the cells may be differentiating towards neural cells forming axons and dendrites.

### *3.4. Ribosomal Protein Involvement in Neural Differentiation*

The proteomics findings also clearly indicate considerable changes in the abundance of proteins involved in ribosome and translational processes (Figure 7a). Ribosome biogenesis

and regulation of protein synthesis are known to be of major importance when it comes to the modulation of cell behaviour [104]. It is well known that stem cells possess the ability to self-renew and differentiate. However, the self-renewal potential diminishes once the cells start differentiating towards a more specific lineage. The same applies to proliferative capacity. The balance between molecular processes responsible for maintaining pluripotency and directing cell fate rapidly shifts to accommodate these changes [105]. The most striking decrease in abundance out of all proteins in our dataset can be observed in the basic transcription factor 3 (referred to as BTF3). It sustained a −6.61 log2 fold change in proteome of cells grown in 3D environment. BTF3 has been found to be responsible for maintaining stem-like characteristics, and its lowered presence has been linked to loss of self-renewal capacity in differentiating stem cells [106,107]. Additionally, several proteins associated with formation of cytoplasmic ribonucleoprotein granule have been shown to increase in abundance in the 3D environment. One of them was the far upstream element-binding protein 2 (here referred to as KHSRP), which increased by 3.09 log2 fold. It is a KH-type splicing regulatory protein, responsible for RNA binding and the resulting decay of mRNAs with AU-rich elements found in the 3′ untranslated region (UTR) [108]. KHRSP has been shown to be highly expressed in the brain tissue. It plays an important role in neuronal development by regulating axonal branching and elongation, while its deficits were linked to impaired neuronal development [109,110].

Proteome analysis also demonstrated decrease in abundance of several proteins that are known to be components of small and large ribosomal subunits. This indicates that the ribosome biogenesis levels are not what is expected of fully differentiated cells. The 14-day incubation period, without neural induction media or supplements, was not sufficient for the ADSCs to become entirely committed. This was confirmed using the viability (Figure 2) and proliferation (Figure 3) assessments, where slow increase in the parameters are still visible at the time of final measurements for both 2D and 3D cells. If the cells were at a further stage in their differentiation, higher abundance of ribosomal proteins and higher translational efficiency would be expected [105]. Interaction analysis, performed using StringDB, revealed strong associations between the ribosomal subunit proteins and the before-mentioned BTF3 protein. Therefore, the decrease in ribosome biogenesis can be linked to the reduction in BTF3 synthesis, which subsequently can result in lower global biogenesis levels. At the same time, some proteins from the group of eukaryotic translation initiation factors (eIFs), such as EIF4H, EIF3E, EIF3F, and EIF3M, have increased significantly in abundance with log2 fold changes ranging from 1.73 to 3.32 depending on the factor. Translation is highly coordinated by the assembly of eIFs at the 5′ end of mRNAs. The EIF-3 complex has been shown to play a crucial role in regulation of mRNA translation by controlling various steps of protein synthesis including initiation, elongation and termination [111]. The function of EIF4H in protein synthesis is executed by enhancing helicase activity, which facilitates mRNA recruitment process in the ribosome [112]. Increase in abundance of proteins responsible for initiating translation shows that even after the short 14-day incubation time, some alterations in the cellular mechanisms of ADSCs are present. As much as the exact direction of these changes cannot be established with certainty, the 3D environment is most definitely making an impact on the cells.

In summary, this study has shown that ADSCs grown in a PEG-based matrix mimicking brain stiffness underwent significant cytoskeletal changes. Cells started to rearrange, and the formation of dendrites and axons is suspected, given the morphological and proteome changes. Furthermore, early oligodendrocyte marker expression also suggests that the cells are starting to differentiate towards the oligodendrocyte lineage. It is possible that the cells are starting to differentiate into multiple populations of cells rather than just one type of cell, given the multicellular nature of the brain. These findings are promising and set a precedent to explore this area further. The addition of chemical differentiation mixtures as well as longer time periods would be the logical next steps.

## 4. Materials and Methods

ADSCs from a single donor were isolated and expanded as previously described [113] with approval from the UTS Human Research Ethics Committee (Ethics number 2013000437). Written informed consent was acquired for donor lipoaspirate release for research purposes only. After isolation, and prior to experiments, the cells were maintained in DMEM/F12+ Glutamax media (Gibco, Life Technologies, Carlsbad, CA, USA) with 10% heat inactivated FBS (Gibco, Life Technologies, Carlsbad, CA, USA) and incubated at 37 °C at 5% $CO_2$. Cells used for these experiments were between passage ten and twelve.

At passage 10–12, cells were lifted from the tissue culture flasks using TrypLE express (12604 Gibco, Life Technologies, Roskilde, Denmark) and either re-plated into 96-well plates (2D) or prepared for bioprinting (3D) following manufacturer's instructions.

Once the cells were re-plated in 2D or bioprinted, they were maintained in similar conditions as above with the addition of 1% antibiotics/antimycotics (ABAM, Gibco life technologies, Carlsbad, CA, USA) to the media; media was changed every 84 h using the same maintenance media and incubated at 37 °C at 5% $CO_2$.

### *4.1. 3D Bioprinting of ADSCs in PEG-Based Hydrogels*

ADSCs were 3D printed in a PEG-based hydrogel using a RASTRUM bioprinter (Inventia, Sydney, Australia). The cell plugs were printed into 96-well plates following the manufacturer's instructions.

In brief, a large plug and imaging plug were printed at ~1.1 kPa containing RGD and YIGSR peptides (matrix code PX02.21P). RGD and YIGSR were included in the system given that the peptide trimer RGD is found in collagen, laminin and fibronectin, which mediates the adhesion of many cells including neurons [47], and laminin-derived (YIGSR) peptide is known to promote neuronal cell binding [48].

Cells were seeded at a concentration of 10 million/mL. The imaging plug consisted of a small volume of hydrogel with embedded cells in the centre of the well measuring 0.5 mm in height and 2.2 mm in diameter (Figure 8a). The large plug occupied the well completely, measuring 0.5 mm in height and 5 mm in diameter (Figure 8b). Negative controls were included as 2D-seeded cells. Cells were lifted from the tissue culture flasks using TrypLE express (12604 Gibco, Life Technologies, Roskilde, Denmark) and re-plated into 96-well plates in 2D conditions at 10 million/mL, the same concentration as 3D cells. These were grown in parallel and treated the same way. The only difference was the 3D construct vs. 2D environment.

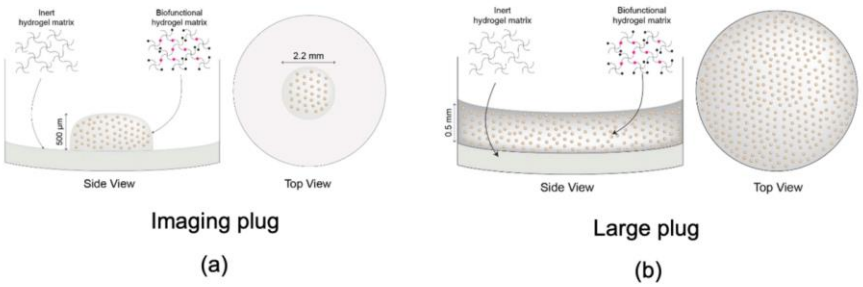


**Figure 8.** Visual representation and dimensions of the different constructs provided by Rastrum. (**a**) Smaller sized plug, referred to as imaging plug used for immunocytochemistry; (**b**) Larger size plug, referred to as large plug (used for viability assays, live cell imaging and proteomics). Diagrams adapted with permission from Inventia Life Science.

Positive controls for immunocytochemistry were included and printed in parallel to the ADSCs following the same method. These are further explained in the immunocytochemistry Section 4.4.1.

### 4.2. Cell Morphology: Incucyte Imaging

Live images of the same Z plane were taken daily using the organoid program in the Incucyte® S3 Live-Cell Analysis Instrument for 14 days, and morphological changes were visually assessed.

Cell confluence was assessed as the area covered by cells in each image ($\mu m^2$/image). This was conducted using the instrument inbuilt analysis software. The parameters used to assess ADSCs confluence were the following: Radius 200; Sensitivity 70; Edge sensitivity 0; Hole fill ($\mu m^2$) 500; Adjust size (pixels) 0. After the initial analysis was finalised by the instrument, all images in all time points were manually checked for artifacts that would not accurately represent the confluence. Common artifacts found in the images were glare (Figure 4C) and bubbles (Figure 4D), which prevented the camera from taking an accurate photo of the cell coverage. Further analysis and graphing were performed using the data exported from the Incucyte® proprietary software version 2022B Rev1. Averages of total area for wells of each cell type and per time point, with associated standard deviations for both for 2D and 3D models, were plotted. The dataset was assessed for normality using Shapiro–Wilk test and statistical significance was subsequently determined using parametric two-way ANOVA with Tukey's multiple comparisons. GraphPad PRISM software version 9.5.0 was used for data visualisation (Figure 4).

### 4.3. Cell Viability and Proliferation: Alamar Blue

Cell viability assay was performed at four different time points: D3.5, D7, D10.5 and D14 using an Alamar blue assay. Alamar blue is a non-toxic cell viability assay that detects metabolically active cells. When Alamar blue is added to cells, if cells are metabolically active, the main active ingredient resazurin is reduced to resorufin, and the solution becomes red in colour and highly fluorescent.

Alamar blue (10% in media) was added to the cells and left to incubate for 16 h to allow enough time to penetrate through the 3D matrices. To keep variables to a minimum, the same was performed on the 2D cells. Negative control wells were included; these only contained the alamar blue and media mixture. After the incubation period, the alamar blue and media mixture was transferred to a different 96-well plate to keep cellular growth environment as undisturbed as possible from outside factors. The collected alamar blue media was then measured using the fluorescence bottom-up mode in a Tecan M200 Plate Reader using 530–560 nm excitation and 590 nm emission wavelengths. The results were averaged across the 96-wells, and data was normalised to the negative controls. The data was analysed as fold change ratio values from D3.5 to standardize and allow for comparison. The dataset was assessed for normality using Shapiro–Wilk test and, due to the assumption not being met, non-parametric Kruskal–Wallis test was performed to determine significance. GraphPad PRISM software version 9.5.0 was used for data visualisation (Figure 2).

### 4.4. Cell Characterization

#### 4.4.1. Immunocytochemistry

Cells from the imaging plug were fixed using 10% formalin for 30 min prior to washing and storing in PBST + 0.1%$w/v$ sodium azide at 4 °C.

For staining, cells were first placed in PBST (0.01M PBS and 0.1% Triton X-100 (BDH #30632) at pH 7.4) for 1 h at room temperature. Primary antibodies were diluted in PBG (0.1M PBS, pH 7.4, 0.1% Triton-X, 2% NGS, 1% BSA (Sigma-Aldrich, St. Louis, MO, USA, #A9647)) and were added to the relevant wells and incubated at 4 °C for 3 days. Primary antibodies were rabbit anti-glial fibrillary acidic protein (GFAP) (1/500, Dako, Glostrup, Denmark #Z0334) as an astrocyte marker; mouse anti-2′,3′ cyclic-nucleotide 3′ phosphodiesterase (CNPase), (1/100 Abcam, Cambridge, UK, #ab6319-100) as an oligodendrocyte

marker; and mouse anti-Neurofilament 200 (1/50, biosensis CM998100) as a mature neuron marker.

After primary antibody incubation was completed, cells were then washed with three changes of PBST for 30 min and incubated with goat anti-mouse AF488 (1/200, Invitrogen, Carlsbad, CA, USA #A11001) or goat anti-rabbit AF488 (1/ 200, Invitrogen, Carlsbad, CA, USA #A11008) secondary antibodies in PBG for another 3 days at 4 °C. Following an additional two 20 min washes with PBST, cells were incubated with Hoechst (1/5000 Invitrogen, Carlsbad, CA, USA) for 30 min to stain the nuclei and finally washed three times with PBST for another 30 min each and stored in antifade/glycerol at 4 °C until imaged.

Positive staining control cells at 10 million/mL conc were included in all staining runs. Glioblastoma U87MG cells were used for GFAP- and CNPase-positive staining controls. Neuroblastoma SHSY-5Y cells were used for NF200-positive staining controls. Both U87MG and SHSY-5Y cells were grown in separate plates to the experimental cells; however, the cells were grown and stained in parallel with the experimental plates for each antibody and were fixed and stained following the same protocol as the experimental cells. In both as 2D and 3D environment, U87MG and SHSY-5Y cells were grown in a 96-well plate with DMEM/F12+Glutamax media (Gibco, Waltham, MA, USA) enriched with 10% heat-inactivated FBS (Sigma-Aldrich, St. Louis, MO, USA) until confluent.

Brightfield and wide-field fluorescence microscopy was performed using a Nikon Ti inverted microscope with a 10× 0.3 numerical aperture Plan Fluor objective, NIS Elements acquisition software (version 5.30.06) with a solid state Lumencor illumination source and a Nikon DS-Qi2 CMOS camera. Six 1024 × 1024 field of views were captured covering the area of each imaging plug and stitched using the NIS Elements acquisition software with default overlap settings. Series of images were captured through the $z$ dimension using a step size of 5.6 µm.

Wide-field fluorescence images were processed using Clarify.ai and Denoise.ai algorithms using the NIS Elements acquisition software. FIJI (FIJI is just ImageJ) version 1.53t [114] was used for image analysis. Where appropriate, z-stacks were corrected for axial drift using the Linear Registration with SIFT plugin with an expected translation transformation. Sum intensity projections for FITC and DAPI channels were thresholded using the default algorithm to create a binary mask and area fraction was measured. For immunolabelled images (FITC channel), binary masks were processed using Smooth and Fill Holes before area fraction was measured. To eliminate non-specific secondary antibody aggregates from measurements, only particles with a pixel size of larger than 100 pixels$^2$ and a circularity of 0–0.8 were quantified. Marker expression was measured from sum intensity projections of wide-field fluorescence images of the whole 3D plug and is displayed as the fraction of percentage area of FITC (AlexaFluor488-conugated secondary antibody) over the percentage area of DAPI-labelled nuclei. One-way ANOVA with multiple comparison was conducted using Bonferroni's multiple comparison test. No statistical significance $p > 0.05$; statistical significance *, $p \leq 0.05$; statistical significance **, $p \leq 0.01$; statistical significance ***, $p \leq 0.001$; statistical significance ****, $p \leq 0.0001$.

Representative images were captured using a Nikon A1R inverted confocal microscope with a 20× 0.7 numerical aperture LWD S Plan Fluor objective and NIS Elements acquisition software. DAPI was imaged with an excitation of 405 nm and emission detected with a PMT detector at 425–475 nm. AF488 was imaged with an excitation of 488 nm and emission detected with a GaAsP detector at 500–550 nm. To account for differences in labelling intensity in these qualitative images, each expression marker was imaged using the following settings: CNPase samples were captured with a 488 nm laser intensity of 4.16, gain of 44 and offset of −3 and a 405 nm laser intensity of 18.95, gain of 150 and offset of −5; NF200 samples were captured with a 488 nm laser intensity of 6.71, gain of 44 and offset of −3 and a 405 nm laser intensity of 13.22, gain of 150 and offset of −2; GFAP samples were captured with a 488 nm laser intensity of 1.75, gain of 39 and offset of −3, and a 405 nm laser intensity of 18.95, gain of 150 and offset of −2. Z-stacks were acquired with a step

size of 3 µm. Fluorescence images were processed using the Denoise.ai algorithm using the NIS Elements acquisition software, and Maximum Intensity Projections were created. In Figure 5, the displayed dynamic range for FITC for 3D samples is 0–550, whilst for positive controls the displayed dynamic range for FITC is 0–1000.

#### 4.4.2. Proteomics

Protein Extraction

Cells were released from the 3D large plugs using Rastrum cell retrieval protocol provided by the company. In brief, media from printed 3D cell models was discarded, cells were washed with PBS and cell retrieval solution was added to the wells. The wells were then incubated at 37 °C for 30 min. Cells were then collected by pipetting up and down in each well and then were transferred to the collection tubes. The wells were then further washed with PBS and remaining cells were combined in the tubes. Cells were then centrifuged, and supernatant was removed. The cell pellets were then frozen until ready to be used for proteomics. Six wells were pooled to make one proteomics sample.

Once ready, samples were defrosted and resuspended in 1% SDC, 5 mM TCEP, 10 mM IAA, 100 mM HEPES pH 8.5, heated to 95 °C for 5 min and incubated for an hour at room temperature. After the incubation, 0.1 µg of trypsin was added to 10 ug of sample and incubated at 37 °C overnight. The peptides were then recovered using SDB-RPS-based stage tip column method, which is a modified protocol from Rappsilber et al., 2007. The digested cell were centrifuged at maximum speed for 5 min to digest any insoluble material, and 10× the volume of digest was the volume of SPE load buffer added (90% acetonitrile, 1% trifluoroacetic acid). The sample was mixed by pipetting up and down and was then added to the stage tip column that contained one disc of SDB-RPS cut with an 18-gauge blunt end needle. The liquid was centrifuged through the disc at 5000 rpm until all liquid moved through. Following this, two washing steps were performed to help wash any contaminants and salts from the column and bound peptides. Firstly, 100 µL of SPE load buffer were passed through at 5000 rpm until all liquid moved through followed by second wash using 100 µL of SPE wash buffer (10% acetonitrile, 0.1% trifluoroacetic acid). After, the peptides were eluted directly into the injection vials by washing the column with 50 µL of SPE elution buffer (71 µL of 1M ammonia solution, 800 µL of 100% acetonitrile, 129 µL of water) and centrifuging at 5000 rpm until all liquid passed through the column into the vials. The vials containing the peptides were then placed into the vacuum centrifuge (Savant DNA 120, SpeedVac Concentrator, Thermo Scientific, Carlsbad, CA, USA) to evaporate all liquid. Once samples were dry, the peptides were resuspended using 25 µL of MS loading solvent (2% acetonitrile, 0.2% trifluoroacetic Acid) and samples were ready to be analysed using LC-MS/MS.

LC-MS/MS Analysis

Using an Acquity M-class nanoLC system (Waters, Milford, MA, USA), 5 µL of the sample was loaded at 15 µL/min for 3 min onto a nanoEase Symmetry C18 trapping column (180 µm × 20 mm) before being washed onto a PicoFrit column (75 µm ID × 350 mm; New Objective, Woburn, MA, USA) packed with SP-120-1.7-ODS-BIO resin (1.7 µm, Osaka Soda Co., Tokyo, Japan) heated to 45 °C at 300 nL/min. Peptides were eluted from the column and into the source of a Q Exactive Plus mass spectrometer (Thermo Scientific, Carlsbad, CA, USA) using the following program: 5–30% MS buffer B (98% acetonitrile + 0.2% formic acid) over 90 min, 30–80% MS buffer B over 3 min, 80% MS buffer B for 2 min, 80–5% for 3 min. The eluting peptides were ionised at 2400 V. A data-dependant MS/MS (dd-MS2) experiment was performed, with a survey scan of 350–1500 Da performed at 70,000 resolution for peptides of charge state 2+ or higher with an AGC target of $3 \times 10^6$ and maximum injection time of 50 ms. The top 12 peptides were selected fragmented in the HCD cell using an isolation window of 1.4 $m/z$, an AGC target of $1 \times 10^5$ and maximum injection time of 100 ms. Fragments were scanned in the Orbitrap analyser at

17,500 resolution, and the product ion fragment were masses measured over a mass range of 120–2000 Da. The mass of the precursor peptide was then excluded for 30 s.

Data Processing and Analysis

The MS/MS data files were searched using MaxQuant (version 2.0.3.0) hosted on the Galaxy Australia platform against the UniProt *Homo sapiens* database (downloaded on 23 March 2023) using the following specific parameters settings. Min. peptide length: 7; Max. peptide mass (Da): 4600; Min. unique peptides: 0; Calculate peak properties: false; Match between runs: True; Match time window (min): 0.7; Match Ion Mobility Window: 0.05; Alignment time window (min): 20; Alignment ion mobility: 1; Match unidentified features: False; Include contaminants: True; Decoy mode: Revert; PSM FDR: 0.01; Protein FDR: 0.01; Min. peptide length for unspecific searches: 8; Max. peptide length for unspecific searches: 25; Peptides for quantification: Unique + razor; Use only unmodified peptides: True; Separate LFQ in parameter groups: false; Stabilize large LFQ ratios: True; Require MS/MS for LFQ comparisons: True; Missed cleavages: 2; Fixed modifications: nothing selected; Variable modifications: Oxidation (M) Carbamidomethyl (C) Deamination (NQ); Enzyme: Trypsin/P; Digestion mode: Semi-specific; Quantitation methods: LFQ; LFQ min. ratio count: 2; LFQ min. number of neighbours: 3; LFQ average number of neighbours: 6; Normalization type: Classic.

The Protein Groups file from the MaxQuant search was then input in LFQ Analyst (Dev.) (https://bioinformatics.erc.monash.edu/apps/LFQ-Analyst/, accessed 10 June 2023 [115]) for further analysis. LFQ analyst was set to 0.05 *p*-value cutoff, 1.5 log2 fold change cut off with Perseus-type imputation, no normalization and Benjamini–Hochberg FDR correction.

StringDB analysis was conducted using String V.11 using the following analysis parameters: Network type: Full string network; Meaning of network edges: evidence; Active interaction sources: Textmining, experiments, databases, co-expression, neighbourhood, gene fusion, co-occurrence; Minimum required interaction score: medium confidence (0.400); Max number of interactors to show: 1st shell—non/query proteins only. 2nd shell—none; Network display mode: interactive svg; and Network display options: disable 3D bubble design and disable structure previews inside network bubbles.

**Supplementary Materials:** The following supporting information can be downloaded at: https://www.mdpi.com/article/10.3390/ijms241512139/s1.

**Author Contributions:** Conceptualization, J.S., N.G.P. and C.A.G.; methodology, J.S., N.G.P., M.P.P. and C.A.G.; formal analysis, N.G.P. and A.L.B.; investigation, N.G.P.; resources, J.S., B.K.M. and M.P.P.; data curation, N.G.P., A.M.S. and A.L.B.; writing—original draft preparation, N.G.P.; writing—review and editing, All; visualization, N.G.P. and A.M.S.; supervision J.S., M.P.P. and C.A.G.; project administration, J.S.; funding acquisition, J.S. and B.K.M. All authors have read and agreed to the published version of the manuscript.

**Funding:** This research was partially funded by the Schwartz Foundation philanthropic donation to support research.

**Institutional Review Board Statement:** The study was conducted according to the guidelines of the Declaration of Helsinki and approved by Human Research Ethics Committee of University of Technology Sydney UTS-HREC Santos-2013000437.

**Informed Consent Statement:** Informed consent was obtained from all subjects involved in the study.

**Data Availability Statement:** The data presented in this study are available in Supplementary S1 and S2 and in supplementary material: String permalink with network functional analysis: https://version-11-5.string-db.org/cgi/network?networkId=bFY8QJcX4JxW accessed on 10 May 2023.

**Acknowledgments:** The authors would like to thank Max L. Cummins for proofreading the article and helping with data visualization. The authors acknowledge the use of the Nikon A1R inverted confocal and Nikon Ti inverted wide-field fluorescence microscopes in the Microbial Imaging Facility at the AIMI in the Faculty of Science, the University of Technology Sydney.

**Conflicts of Interest:** The authors declare no conflict of interest.

## References

1. World Health Organization. What Are Neurological Disorders? 2016. Available online: http://www.who.int/features/qa/55/en/ (accessed on 21 October 2018).
2. Feigin, V.L.; Nichols, E.; Alam, T.; Bannick, M.S.; Beghi, E.; Blake, N.; Culpepper, W.J.; Dorsey, E.R.; Elbaz, A.; Ellenbogen, R.G.J.T.L.N. Global, regional, and national burden of neurological disorders, 1990–2016: A systematic analysis for the Global Burden of Disease Study 2016. *Lancet Neurol.* **2019**, *18*, 459–480. [CrossRef] [PubMed]
3. World Health Organization. *Neurological Disorders: Public Health Challenges*; World Health Organization: Geneva, Switzerland, 2006.
4. Hopkins, A.M.; DeSimone, E.; Chwalek, K.; Kaplan, D.L. 3D in vitro modeling of the central nervous system. *Prog. Neurobiol.* **2015**, *125*, 1–25. [CrossRef] [PubMed]
5. Pankevich, D.E.; Altevogt, B.M.; Dunlop, J.; Gage, F.H.; Hyman, S.E. Improving and Accelerating Drug Development for Nervous System Disorders. *Neuron* **2014**, *84*, 546–553. [CrossRef]
6. Wegener, G.; Rujescu, D. The current development of CNS drug research. *Int. J. Neuropsychopharmacol.* **2013**, *16*, 1687–1693. [CrossRef] [PubMed]
7. Nicholson, C. Diffusion and related transport mechanisms in brain tissue. *Rep. Prog. Phys.* **2001**, *64*, 815. [CrossRef]
8. Syková, E.; Nicholson, C.; Zhao, H.-H.; Du, H.; Cai, Y.; Liu, C.; Xie, Z.; Chen, K.C.; Verkhratsky, A.; Nedergaard, M.; et al. Diffusion in Brain Extracellular Space. *Physiol. Rev.* **2008**, *88*, 1277–1340. [CrossRef]
9. Lam, D.; Enright, H.A.; Cadena, J.; Peters, S.K.G.; Sales, A.P.; Osburn, J.J.; Soscia, D.A.; Kulp, K.S.; Wheeler, E.K.; Fischer, N.O. Tissue-specific extracellular matrix accelerates the formation of neural networks and communities in a neuron-glia co-culture on a multi-electrode array. *Sci. Rep.* **2019**, *9*, 4159. [CrossRef]
10. Nicholson, C.; Syková, E. Extracellular space structure revealed by diffusion analysis. *Trends Neurosci.* **1998**, *21*, 207–215. [CrossRef]
11. Dityatev, A.; Schachner, M.; Sonderegger, P. The dual role of the extracellular matrix in synaptic plasticity and homeostasis. *Nat. Rev. Neurosci.* **2010**, *11*, 735–746. [CrossRef]
12. Song, I.; Dityatev, A. Crosstalk between glia, extracellular matrix and neurons. *Brain Res. Bull.* **2017**, *136*, 101–108. [CrossRef]
13. Burnside, E.R.; Bradbury, E.J. Review: Manipulating the extracellular matrix and its role in brain and spinal cord plasticity and repair. *Neuropathol. Appl. Neurobiol.* **2014**, *40*, 26–59. [CrossRef]
14. Elkin, B.S.; Azeloglu, E.U.; Costa, K.D.; Iii, B.M.; Shafiq, M.; Jung, Y.; Kim, S.H.; Schwarb, H.; Johnson, C.L.; McGarry, M.D.; et al. Mechanical Heterogeneity of the Rat Hippocampus Measured by Atomic Force Microscope Indentation. *J. Neurotrauma* **2007**, *24*, 812–822. [CrossRef]
15. Lu, Y.-B.; Franze, K.; Seifert, G.; Steinhäuser, C.; Kirchhoff, F.; Wolburg, H.; Guck, J.; Janmey, P.; Wei, E.-Q.; Käs, J.; et al. Viscoelastic properties of individual glial cells and neurons in the CNS. *Proc. Natl. Acad. Sci. USA* **2006**, *103*, 17759–17764. [CrossRef]
16. Gimble, J.; Guilak, F. Adipose-derived adult stem cells: Isolation, characterization, and differentiation potential. *Cytotherapy* **2003**, *5*, 362–369. [CrossRef]
17. Woodbury, D.; Schwarz, E.J.; Prockop, D.J.; Black, I.B. Adult rat and human bone marrow stromal cells differentiate into neurons. *J. Neurosci. Res.* **2000**, *61*, 364–370. [CrossRef]
18. Wankhade, U.D.; Shen, M.; Kolhe, R.; Fulzele, S. Advances in Adipose-Derived Stem Cells Isolation, Characterization, and Application in Regenerative Tissue Engineering. *Stem Cells Int.* **2016**, *2016*, 3206807. [CrossRef]
19. Jang, S.; Cho, H.-H.; Cho, Y.-B.; Park, J.-S.; Jeong, H.-S. Functional neural differentiation of human adipose tissue-derived stem cells using bFGF and forskolin. *BMC Cell Biol.* **2010**, *11*, 25. [CrossRef]
20. Park, J.; Lee, N.; Lee, J.; Choe, E.K.; Kim, M.K.; Lee, J.; Byun, M.S.; Chon, M.-W.; Kim, S.W.; Lee, C.J.; et al. Small molecule-based lineage switch of human adipose-derived stem cells into neural stem cells and functional GABAergic neurons. *Sci. Rep.* **2017**, *7*, 10166. [CrossRef]
21. Soheilifar, M.H.; Javeri, A.; Amini, H.; Taha, M.F. Generation of Dopamine-Secreting Cells from Human Adipose Tissue-Derived Stem Cells In Vitro. *Rejuvenation Res.* **2018**, *21*, 360–368. [CrossRef]
22. Faghih, H.; Javeri, A.; Amini, H.; Taha, M.F. Directed differentiation of human adipose tissue-derived stem cells to dopaminergic neurons in low-serum and serum-free conditions. *Neurosci. Lett.* **2019**, *708*, 134353. [CrossRef]
23. Fajardo, J.; Milthorpe, B.K.; Santos, J. Molecular Mechanisms Involved in Neural Substructure Development during Phosphodiesterase Inhibitor Treatment of Mesenchymal Stem Cells. *Int. J. Mol. Sci.* **2020**, *21*, 4867. [CrossRef] [PubMed]
24. Santos, J.; Hubert, T.; Milthorpe, B.K. Valproic Acid Promotes Early Neural Differentiation in Adult Mesenchymal Stem Cells Through Protein Signalling Pathways. *Cells* **2020**, *9*, 619. [CrossRef] [PubMed]

25. Santos, J.; Dalla, P.V.; Milthorpe, B.K. Molecular Dynamics of Cytokine Interactions and Signalling of Mesenchymal Stem Cells Undergoing Directed Neural-like Differentiation. *Life* **2022**, *12*, 392. [CrossRef] [PubMed]
26. Ning, H.; Lin, G.; Lue, T.F.; Lin, C.-S. Neuron-like differentiation of adipose tissue-derived stromal cells and vascular smooth muscle cells. *Differentiation* **2006**, *74*, 510–518. [CrossRef] [PubMed]
27. Ahmadi, N.; Razavi, S.; Kazemi, M.; Oryan, S. Stability of neural differentiation in human adipose-derived stem cells by two induction protocols. *Tissue Cell* **2012**, *44*, 87–94. [CrossRef]
28. Edmondson, R.; Broglie, J.J.; Adcock, A.F.; Yang, L. Three-Dimensional Cell Culture Systems and Their Applications in Drug Discovery and Cell-Based Biosensors. *ASSAY Drug Dev. Technol.* **2014**, *12*, 207–218. [CrossRef]
29. Strioga, M.; Viswanathan, S.; Darinskas, A.; Slaby, O.; Michalek, J.; Maria, O.M.; Kumala, S.; Heravi, M.; Syme, A.; Eliopoulos, N.; et al. Same or Not the Same? Comparison of Adipose Tissue-Derived Versus Bone Marrow-Derived Mesenchymal Stem and Stromal Cells. *Stem Cells Dev.* **2012**, *21*, 2724–2752. [CrossRef]
30. Baharvand, H.; Hashemi, S.M.; Ashtiani, S.K.; Farrokhi, A. Differentiation of human embryonic stem cells into hepatocytes in 2D and 3D culture systems in vitro. *Int. J. Dev. Biol.* **2006**, *50*, 645–652. [CrossRef]
31. Benya, P.D.; Shaffer, J.D. Dedifferentiated chondrocytes reexpress the differentiated collagen phenotype when cultured in agarose gels. *Cell* **1982**, *30*, 215–224. [CrossRef]
32. Zietarska, M.; Maugard, C.M.; Filali-Mouhim, A.; Alam-Fahmy, M.; Tonin, P.N.; Provencher, D.M.; Mes-Masson, A.-M. Molecular description of a 3D in vitro model for the study of epithelial ovarian cancer (EOC). *Mol. Carcinog.* **2007**, *46*, 872–885. [CrossRef]
33. Costa, E.C.; Moreira, A.F.; De Melo-Diogo, D.; Gaspar, V.M.; Carvalho, M.P.; Correia, I.J. 3D tumor spheroids: An overview on the tools and techniques used for their analysis. *Biotechnol. Adv.* **2016**, *34*, 1427–1441. [CrossRef]
34. Langhans, S.A. Three-Dimensional in Vitro Cell Culture Models in Drug Discovery and Drug Repositioning. *Front. Pharmacol.* **2018**, *9*, 6. [CrossRef]
35. Duval, K.; Grover, H.; Han, L.-H.; Mou, Y.; Pegoraro, A.F.; Fredberg, J.; Chen, Z. Modeling Physiological Events in 2D vs. 3D Cell Culture. *Physiology* **2017**, *32*, 266–277. [CrossRef]
36. Antoni, D.; Burckel, H.; Josset, E.; Noel, G. Three-Dimensional Cell Culture: A Breakthrough in Vivo. *Int. J. Mol. Sci.* **2015**, *16*, 5517–5527. [CrossRef]
37. Kim, J.B. Three-dimensional tissue culture models in cancer biology. *Semin. Cancer Biol.* **2005**, *15*, 365–377. [CrossRef]
38. Dhaliwal, A. 3D cell culture: A review. *Mater Methods* **2012**, *2*, 162. [CrossRef]
39. Hongisto, V.; Jernström, S.; Fey, V.; Mpindi, J.-P.; Kleivi Sahlberg, K.; Kallioniemi, O.; Perälä, M. High-Throughput 3D Screening Reveals Differences in Drug Sensitivities between Culture Models of JIMT1 Breast Cancer Cells. *PLoS ONE* **2013**, *8*, e77232. [CrossRef]
40. Ravi, M.; Paramesh, V.; Kaviya, S.R.; Anuradha, E.; Solomon, F.D.P. 3D Cell Culture Systems: Advantages and Applications. *J. Cell. Physiol.* **2015**, *230*, 16–26. [CrossRef]
41. Engler, A.J.; Sen, S.; Sweeney, H.L.; Discher, D.E. Matrix Elasticity Directs Stem Cell Lineage Specification. *Cell* **2006**, *126*, 677–689. [CrossRef]
42. Streuli, C. Extracellular matrix remodelling and cellular differentiation. *Curr. Opin. Cell Biol.* **1999**, *11*, 634–640. [CrossRef]
43. Hopkins, A.M.; De Laporte, L.; Tortelli, F.; Spedden, E.; Staii, C.; Atherton, T.J.; Hubbell, J.A.; Kaplan, D.L. Silk Hydrogels as Soft Substrates for Neural Tissue Engineering. *Adv. Funct. Mater.* **2013**, *23*, 5140–5149. [CrossRef]
44. Her, G.J.; Wu, H.-C.; Chen, M.-H.; Chen, M.-Y.; Chang, S.-C.; Wang, T.-W. Control of three-dimensional substrate stiffness to manipulate mesenchymal stem cell fate toward neuronal or glial lineages. *Acta Biomater.* **2013**, *9*, 5170–5180. [CrossRef] [PubMed]
45. Li, Y.; Huang, G.; Li, M.; Wang, L.; Elson, E.L.; Lu, T.J.; Genin, G.M.; Xu, F. An approach to quantifying 3D responses of cells to extreme strain. *Sci. Rep.* **2016**, *6*, 19550. [CrossRef] [PubMed]
46. Matyash, M.; Despang, F.; Mandal, R.; Fiore, D.; Gelinsky, M.; Ikonomidou, C. Novel Soft Alginate Hydrogel Strongly Supports Neurite Growth and Protects Neurons Against Oxidative Stress. *Tissue Eng. Part A* **2012**, *18*, 55–66. [CrossRef]
47. Rao, S.S.; Winter, J.O. Adhesion molecule-modified biomaterials for neural tissue engineering. *Front. Neuroeng.* **2009**, *2*, 6. [CrossRef] [PubMed]
48. Krishnan, U.M. Biomaterials in the treatment of Parkinson's disease. *Neurochem. Int.* **2021**, *145*, 105003. [CrossRef]
49. Lampe, K.J.; Mooney, R.G.; Bjugstad, K.B.; Mahoney, M.J. Effect of macromer weight percent on neural cell growth in 2D and 3D nondegradable PEG hydrogel culture. *J. Biomed. Mater. Res. Part A* **2010**, *94*, 1162–1171. [CrossRef]
50. Naghdi, P.; Tiraihi, T.; Ganji, F.; Darabi, S.; Taheri, T.; Kazemi, H. Survival, proliferation and differentiation enhancement of neural stem cells cultured in three-dimensional polyethylene glycol-RGD hydrogel with tenascin. *J. Tissue Eng. Regen. Med.* **2016**, *10*, 199–208. [CrossRef]
51. Cretel, E.; Pierres, A.; Benoliel, A.-M.; Bongrand, P. How Cells Feel Their Environment: A Focus on Early Dynamic Events. *Cell. Mol. Bioeng.* **2008**, *1*, 5–14. [CrossRef]
52. Baker, B.M.; Chen, C.S. Deconstructing the third dimension—How 3D culture microenvironments alter cellular cues. *J. Cell Sci.* **2012**, *125*, 3015–3024. [CrossRef]
53. Caliari, S.R.; Burdick, J.A. A practical guide to hydrogels for cell culture. *Nat. Methods* **2016**, *13*, 405–414. [CrossRef]
54. Budday, S.; Ovaert, T.C.; Holzapfel, G.A.; Steinmann, P.; Kuhl, E. Fifty Shades of Brain: A Review on the Mechanical Testing and Modeling of Brain Tissue. *Arch. Comput. Methods Eng.* **2020**, *27*, 1187–1230. [CrossRef]

55. Li, X.; Huang, Y.; Zheng, L.; Liu, H.; Niu, X.; Huang, J.; Zhao, F.; Fan, Y. Effect of substrate stiffness on the functions of rat bone marrow and adipose tissue derived mesenchymal stem cells in vitro. *J. Biomed. Mater. Res. Part A* **2014**, *102*, 1092–1101. [CrossRef]
56. Mao, A.S.; Shin, J.-W.; Mooney, D.J. Effects of substrate stiffness and cell-cell contact on mesenchymal stem cell differentiation. *Biomaterials* **2016**, *98*, 184–191. [CrossRef]
57. Shih, Y.-R.V.; Tseng, K.-F.; Lai, H.-Y.; Lin, C.-H.; Lee, O.K. Matrix stiffness regulation of integrin-mediated mechanotransduction during osteogenic differentiation of human mesenchymal stem cells. *J. Bone Miner. Res.* **2011**, *26*, 730–738. [CrossRef]
58. Kuhn, S.; Gritti, L.; Crooks, D.; Dombrowski, Y. Oligodendrocytes in development, myelin generation and beyond. *Cells* **2019**, *8*, 1424. [CrossRef]
59. Edwards, A.M.; Braun, P.E. Gene Expression of the Central and Peripheral Nervous System Myelin Membrane 2′, 3′-Cyclic Nucleotide 3′-Phosphodiesterase in Development. *Dev. Neurosci.* **1988**, *10*, 75–80. [CrossRef]
60. Braun, P.E.; Sandillon, F.; Edwards, A.; Matthieu, J.M.; Privat, A. Immunocytochemical localization by electron microscopy of 2′3′-cyclic nucleotide 3′-phosphodiesterase in developing oligodendrocytes of normal and mutant brain. *J. Neurosci.* **1988**, *8*, 3057–3066. [CrossRef]
61. Pelegri, N.G.; Milthorpe, B.K.; Gorrie, C.A.; Santos, J. Neurogenic marker expression in differentiating human adipose-derived adult mesenchymal stem cells. *Stem Cell Investig.* **2023**, *10*, 7. [CrossRef]
62. Gulati, A. Understanding neurogenesis in the adult human brain. *Indian J. Pharmacol.* **2015**, *47*, 583–584. [CrossRef]
63. Pollard, T.D.; Cooper, J.A. Actin, a Central Player in Cell Shape and Movement. *Science* **2009**, *326*, 1208–1212. [CrossRef] [PubMed]
64. Konietzny, A.; Bär, J.; Mikhaylova, M. Dendritic Actin Cytoskeleton: Structure, Functions, and Regulations. *Front. Cell. Neurosci.* **2017**, *11*, 147. [CrossRef] [PubMed]
65. Georges, P.C.; Hadzimichalis, N.M.; Sweet, E.S.; Firestein, B.L. The Yin–Yang of Dendrite Morphology: Unity of Actin and Microtubules. *Mol. Neurobiol.* **2008**, *38*, 270–284. [CrossRef] [PubMed]
66. Magee, J.C. Dendritic integration of excitatory synaptic input. *Nat. Rev. Neurosci.* **2000**, *1*, 181–190. [CrossRef]
67. Gulledge, A.T.; Kampa, B.M.; Stuart, G.J. Synaptic integration in dendritic trees. *J. Neurobiol.* **2005**, *64*, 75–90. [CrossRef]
68. Moutin, M.-J.; Bosc, C.; Peris, L.; Andrieux, A. Tubulin post-translational modifications control neuronal development and functions. *Dev. Neurobiol.* **2021**, *81*, 253–272. [CrossRef]
69. Miyasaka, K.Y.; Kida, Y.S.; Sato, T.; Minami, M.; Ogura, T. Csrp1 regulates dynamic cell movements of the mesendoderm and cardiac mesoderm through interactions with Dishevelled and Diversin. *Proc. Natl. Acad. Sci. USA* **2007**, *104*, 11274–11279. [CrossRef]
70. Latonen, L.; Järvinen, P.M.; Laiho, M. Cytoskeleton-interacting LIM-domain protein CRP1 suppresses cell proliferation and protects from stress-induced cell death. *Exp. Cell Res.* **2008**, *314*, 738–747. [CrossRef]
71. Tran, T.C.; Singleton, C.; Fraley, T.S.; Greenwood, J.A. Cysteine-rich protein 1 (CRP1) regulates actin filament bundling. *BMC Cell Biol.* **2005**, *6*, 45. [CrossRef]
72. Jang, H.S.; Greenwood, J.A. Glycine-rich region regulates cysteine-rich protein 1 binding to actin cytoskeleton. *Biochem. Biophys. Res. Commun.* **2009**, *380*, 484–488. [CrossRef]
73. Ma, L.; Greenwood, J.A.; Schachner, M. CRP1, a Protein Localized in Filopodia of Growth Cones, Is Involved in Dendritic Growth. *J. Neurosci.* **2011**, *31*, 16781–16791. [CrossRef]
74. Bamburg, J.R.; Bray, D. Distribution and cellular localization of actin depolymerizing factor. *J. Cell Biol.* **1987**, *105*, 2817–2825. [CrossRef]
75. Garvalov, B.K.; Flynn, K.C.; Neukirchen, D.; Meyn, L.; Teusch, N.; Wu, X.; Brakebusch, C.; Bamburg, J.R.; Bradke, F. Cdc42 Regulates Cofilin during the Establishment of Neuronal Polarity. *J. Neurosci.* **2007**, *27*, 13117–13129. [CrossRef]
76. Flynn, K.C.; Hellal, F.; Neukirchen, D.; Jacob, S.; Tahirovic, S.; Dupraz, S.; Stern, S.; Garvalov, B.K.; Gurniak, C.; Shaw, A.E.; et al. ADF/Cofilin-Mediated Actin Retrograde Flow Directs Neurite Formation in the Developing Brain. *Neuron* **2012**, *76*, 1091–1107. [CrossRef]
77. Endo, M.; Ohashi, K.; Sasaki, Y.; Goshima, Y.; Niwa, R.; Uemura, T.; Mizuno, K. Control of Growth Cone Motility and Morphology by LIM Kinase and Slingshot via Phosphorylation and Dephosphorylation of Cofilin. *J. Neurosci.* **2003**, *23*, 2527–2537. [CrossRef]
78. Kuhn, T.B.; Meberg, P.J.; Brown, M.D.; Bernstein, B.W.; Minamide, L.S.; Jensen, J.R.; Okada, K.; Soda, E.A.; Bamburg, J.R. Regulating actin dynamics in neuronal growth cones by ADF/cofilin and rho family GTPases. *J. Neurobiol.* **2000**, *44*, 126–144. [CrossRef]
79. Meberg, P.J. Signal-Regulated ADF/Cofilin Activity and Growth Cone Motility. *Mol. Neurobiol.* **2000**, *21*, 097–108. [CrossRef]
80. Tedeschi, A.; Dupraz, S.; Curcio, M.; Laskowski, C.J.; Schaffran, B.; Flynn, K.C.; Santos, T.E.; Stern, S.; Hilton, B.J.; Larson, M.J.; et al. ADF/Cofilin-Mediated Actin Turnover Promotes Axon Regeneration in the Adult CNS. *Neuron* **2019**, *103*, 1073–1085.e6. [CrossRef]
81. Ben Zablah, Y.; Merovitch, N.; Jia, Z. The Role of ADF/Cofilin in Synaptic Physiology and Alzheimer's Disease. *Front. Cell Dev. Biol.* **2020**, *8*, 594998. [CrossRef]
82. Lua, B.L.; Low, B.C. Cortactin phosphorylation as a switch for actin cytoskeletal network and cell dynamics control. *FEBS Lett.* **2005**, *579*, 577–585. [CrossRef]
83. Hering, H.; Sheng, M. Activity-Dependent Redistribution and Essential Role of Cortactin in Dendritic Spine Morphogenesis. *J. Neurosci.* **2003**, *23*, 11759–11769. [CrossRef] [PubMed]

84. Cornelius, J.; Rottner, K.; Korte, M.; Michaelsen-Preusse, K. Cortactin Contributes to Activity-Dependent Modulation of Spine Actin Dynamics and Spatial Memory Formation. *Cells* **2021**, *10*, 1835. [CrossRef] [PubMed]
85. Alicea, D.; Perez, M.; Maldonado, C.; Dominicci-Cotto, C.; Marie, B. Cortactin Is a Regulator of Activity-Dependent Synaptic Plasticity Controlled by Wingless. *J. Neurosci.* **2017**, *37*, 2203–2215. [CrossRef] [PubMed]
86. Racz, B.; Weinberg, R.J. The Subcellular Organization of Cortactin in Hippocampus. *J. Neurosci.* **2004**, *24*, 10310–10317. [CrossRef]
87. Chen, Y.-K.; Hsueh, Y.-P. Cortactin-Binding Protein 2 Modulates the Mobility of Cortactin and Regulates Dendritic Spine Formation and Maintenance. *J. Neurosci.* **2012**, *32*, 1043–1055. [CrossRef] [PubMed]
88. Cheng, Y.; Leung, S.; Mangoura, D. Transient suppression of cortactin ectopically induces large telencephalic neurons towards a GABAergic phenotype. *J. Cell Sci.* **2000**, *113*, 3161–3172. [CrossRef]
89. Strasser, G.A.; Rahim, N.A.; VanderWaal, K.E.; Gertler, F.B.; Lanier, L.M. Arp2/3 is a negative regulator of growth cone translocation. *Neuron* **2004**, *43*, 81–94. [CrossRef]
90. Du, Y.; Weed, S.A.; Xiong, W.-C.; Marshall, T.D.; Parsons, J.T. Identification of a Novel Cortactin SH3 Domain-Binding Protein and Its Localization to Growth Cones of Cultured Neurons. *Mol. Cell. Biol.* **1998**, *18*, 5838–5851. [CrossRef]
91. Kumar, A.; Paeger, L.; Kosmas, K.; Kloppenburg, P.; Noegel, A.A.; Peche, V.S. Neuronal Actin Dynamics, Spine Density and Neuronal Dendritic Complexity Are Regulated by CAP2. *Front. Cell. Neurosci.* **2016**, *10*, 180. [CrossRef]
92. Pelucchi, S.; Vandermeulen, L.; Pizzamiglio, L.; Aksan, B.; Yan, J.; Konietzny, A.; Bonomi, E.; Borroni, B.; Rust, M.; Marino, D.D. CAP2 is a novel regulator of Cofilin in synaptic plasticity and Alzheimer's disease. *Brain Commun.* **2019**, 789552. [CrossRef]
93. Schneider, F.; Metz, I.; Khudayberdiev, S.; Rust, M.B. Functional Redundancy of Cyclase-Associated Proteins CAP1 and CAP2 in Differentiating Neurons. *Cells* **2021**, *10*, 1525. [CrossRef] [PubMed]
94. Leite, S.C.; Sampaio, P.; Sousa, V.F.; Nogueira-Rodrigues, J.; Pinto-Costa, R.; Peters, L.L.; Brites, P.; Sousa, M.M. The Actin-Binding Protein α-Adducin Is Required for Maintaining Axon Diameter. *Cell Rep.* **2016**, *15*, 490–498. [CrossRef] [PubMed]
95. Vukojevic, V.; Gschwind, L.; Vogler, C.; Demougin, P.; de Quervain, D.J.F.; Papassotiropoulos, A.; Stetak, A. A role for α-adducin (ADD-1) in nematode and human memory. *EMBO J.* **2012**, *31*, 1453–1466. [CrossRef] [PubMed]
96. Ma, L.; Li, Y.; Wang, R. Drebrin and cognitive impairment. *Clin. Chim. Acta* **2015**, *451*, 121–124. [CrossRef]
97. Nishijima, H.; Arai, A.; Kimura, T.; Mori, F.; Yamada, J.; Migita, K.; Wakabayashi, K.; Baba, M.; Ueno, S.; Tomiyama, M. Drebrin immunoreactivity in the striatum of a rat model of levodopa-induced dyskinesia. *Neuropathology* **2013**, *33*, 391–396. [CrossRef]
98. Mahadomrongkul, V.; Huerta, P.T.; Shirao, T.; Aoki, C. Stability of the distribution of spines containing drebrin A in the sensory cortex layer I of mice expressing mutated APP and PS1 genes. *Brain Res.* **2005**, *1064*, 66–74. [CrossRef]
99. Duly, A.M.; Kao, F.C.; Teo, W.S.; Kavallaris, M. βIII-Tubulin Gene Regulation in Health and Disease. *Front. Cell Dev. Biol.* **2022**, *10*, 851542. [CrossRef]
100. Caccamo, D.; Katsetos, C.D.; Herman, M.M.; Frankfurter, A.; Collins, V.P.; Rubinstein, L.J. Immunohistochemistry of a spontaneous murine ovarian teratoma with neuroepithelial differentiation. Neuron-associated beta-tubulin as a marker for primitive neuroepithelium. *Lab. Investig.* **1989**, *60*, 390–398.
101. Jiang, Y.Q.; Oblinger, M.M. Differential regulation of beta III and other tubulin genes during peripheral and central neuron development. *J. Cell Sci.* **1992**, *103 Pt 3*, 643–651. [CrossRef]
102. Linhartová, I.; Dráber, P.; Dráberová, E.; Viklický, V. Immunological discrimination of β-tubulin isoforms in developing mouse brain. Post-translational modification of non-class-III β-tubulins. *Biochem. J.* **1992**, *288*, 919–924. [CrossRef]
103. Hausrat, T.J.; Radwitz, J.; Lombino, F.L.; Breiden, P.; Kneussel, M. Alpha-and beta-tubulin isotypes are differentially expressed during brain development. *Dev. Neurobiol.* **2021**, *81*, 333–350. [CrossRef] [PubMed]
104. Saba, J.A.; Liakath-Ali, K.; Green, R.; Watt, F.M. Translational control of stem cell function. *Nat. Rev. Mol. Cell Biol.* **2021**, *22*, 671–690. [CrossRef] [PubMed]
105. Gabut, M.; Bourdelais, F.; Durand, S. Ribosome and Translational Control in Stem Cells. *Cells* **2020**, *9*, 497. [CrossRef] [PubMed]
106. Hu, J.; Sun, F.; Chen, W.; Zhang, J.; Zhang, T.; Qi, M.; Feng, T.; Liu, H.; Li, X.; Xing, Y.; et al. BTF3 sustains cancer stem-like phenotype of prostate cancer via stabilization of BMI1. *J. Exp. Clin. Cancer Res.* **2019**, *38*, 227. [CrossRef] [PubMed]
107. Zhou, W.; Yun, Z.; Wang, T.; Li, C.; Zhang, J. BTF3-mediated regulation of BMI1 promotes colorectal cancer through influencing epithelial-mesenchymal transition and stem cell-like traits. *Int. J. Biol. Macromol.* **2021**, *187*, 800–810. [CrossRef] [PubMed]
108. Briata, P.; Bordo, D.; Puppo, M.; Gorlero, F.; Rossi, M.; Perrone-Bizzozero, N.; Gherzi, R. Diverse roles of the nucleic acid-binding protein KHSRP in cell differentiation and disease. *Wiley Interdiscip. Rev. RNA* **2016**, *7*, 227–240. [CrossRef]
109. Bird, C.W.; Gardiner, A.S.; Bolognani, F.; Tanner, D.C.; Chen, C.-Y.; Lin, W.-J.; Yoo, S.; Twiss, J.L.; Perrone-Bizzozero, N.P. KSRP Modulation of GAP-43 mRNA Stability Restricts Axonal Outgrowth in Embryonic Hippocampal Neurons. *PLoS ONE* **2013**, *8*, e79255. [CrossRef]
110. Olguin, S.L.; Patel, P.; Buchanan, C.N.; Dell'orco, M.; Gardiner, A.S.; Cole, R.; Vaughn, L.S.; Sundararajan, A.; Mudge, J.; Allan, A.M.; et al. KHSRP loss increases neuronal growth and synaptic transmission and alters memory consolidation through RNA stabilization. *Commun. Biol.* **2022**, *5*, 672. [CrossRef]
111. Wolf, D.A.; Lin, Y.; Duan, H.; Cheng, Y. eIF-Three to Tango: Emerging functions of translation initiation factor eIF3 in protein synthesis and disease. *J. Mol. Cell Biol.* **2020**, *12*, 403–409. [CrossRef]
112. Mishra, R.K.; Datey, A.; Hussain, T. mRNA Recruiting eIF4 Factors Involved in Protein Synthesis and Its Regulation. *Biochemistry* **2020**, *59*, 34–46. [CrossRef]

113. Santos, J.; Milthorpe, B.K.; Herbert, B.R.; Padula, M.P. Proteomic Analysis of Human Adipose Derived Stem Cells during Small Molecule Chemical Stimulated Pre-neuronal Differentiation. *Int. J. Stem Cells* **2017**, *10*, 193–217. [CrossRef]
114. Schindelin, J.; Arganda-Carreras, I.; Frise, E.; Kaynig, V.; Longair, M.; Pietzsch, T.; Preibisch, S.; Rueden, C.; Saalfeld, S.; Schmid, B.; et al. Fiji: An open-source platform for biological-image analysis. *Nat. Methods* **2012**, *9*, 676–682. [CrossRef]
115. Shah, A.D.; Goode, R.J.A.; Huang, C.; Powell, D.R.; Schittenhelm, R.B. LFQ-Analyst: An Easy-To-Use Interactive Web Platform To Analyze and Visualize Label-Free Proteomics Data Preprocessed with MaxQuant. *J. Proteome Res.* **2019**, *19*, 204–211. [CrossRef]

**Supplementary 1**

**Table S1** All proteins detected with significant change in abundance between treatments, including gene name, protein IDs, p-value and log fold change. Significant p-value < 0.05. The background colors refer to the change in abundance of each protein in the 3D culture as compared to the 2D culture. Increase in abundance was marked by blue, while decrease by red. The intensity of the color is proportional to the magnitude of each change (i.e. the darker the color the larger the fold change). Log2 scale was used.

| Gene Name | Protein IDs | 2D vs 3D Log2 fold change | 2D vs 3D p.value |
|---|---|---|---|
| CSRP1 | P21291 | 7.07 | 2.04E-10 |
| TIPRL | O75663 | 6.94 | 2.70E-08 |
| GLS.1 | O94925-3 | 5.5 | 1.01E-09 |
| SCAMP2 | O15127 | 5.15 | 3.40E-08 |
| ENPP1 | P22413 | 4.73 | 3.84E-05 |
| DSTN | P60981 | 4.72 | 0.000125 |
| CD63 | F8VNT9 | 4.7 | 1.23E-06 |
| NEK7 | Q8TDX7 | 4.52 | 8.38E-08 |
| PRNP | P04156 | 4.38 | 6.89E-06 |
| MCFD2 | Q8NI22 | 4.33 | 5.10E-06 |
| CTTN | Q14247 | 4.23 | 8.12E-07 |
| FAF2 | Q96CS3 | 4.17 | 0.000782 |
| PDAP1 | Q13442 | 4.13 | 1.09E-05 |
| LIMCH1 | Q9UPQ0 | 4.09 | 2.20E-07 |
| IAH1 | H7C5G1 | 3.84 | 1.47E-07 |
| DAB2 | P98082-3 | 3.79 | 7.33E-07 |
| AKR7A2 | O43488 | 3.77 | 9.47E-08 |
| MARCKS | P29966 | 3.74 | 8.22E-06 |
| AGFG1 | P52594-2 | 3.71 | 2.09E-08 |
| FAS | Q59FU8 | 3.69 | 7.85E-06 |
| HMGA1 | P17096 | 3.69 | 8.89E-08 |
| ERLIN2 | O94905 | 3.64 | 0.000133 |
| LMO7 | Q8WWI1-3 | 3.59 | 2.49E-07 |
| TAX1BP3 | O14907 | 3.57 | 1.94E-06 |
| SOD1 | P00441 | 3.56 | 0.000134 |
| HMOX2 | A0A087WT44 | 3.53 | 5.84E-06 |
| PHPT1 | Q9NRX4 | 3.53 | 5.60E-07 |
| BST1 | A6NC48 | 3.52 | 0.000386 |
| GRPEL1 | Q9HAV7 | 3.51 | 2.73E-06 |
| COPZ2 | Q9P299 | 3.48 | 4.13E-06 |
| ALYREF | E9PB61 | 3.47 | 0.00177 |
| CDH2 | C9J126 | 3.41 | 2.00E-05 |

| | | | |
|---|---|---|---|
| PIEZO1 | Q92508 | 3.41 | 1.30E-08 |
| NUTF2 | P61970 | 3.38 | 1.51E-05 |
| COL1A2 | P08123 | 3.32 | 7.96E-05 |
| EIF4H | A0A7I2V4E4 | 3.32 | 2.24E-05 |
| SORBS3 | O60504-2 | 3.3 | 5.08E-05 |
| CARHSP1 | Q9Y2V2 | 3.28 | 0.00373 |
| COL1A1 | P02452 | 3.28 | 5.09E-05 |
| LPXN | O60711 | 3.26 | 8.69E-06 |
| ABR | A0A0G2JQ41 | 3.23 | 8.23E-06 |
| KLC1 | G3V3H3 | 3.21 | 9.39E-05 |
| SH3GLB1 | A0A087WW40 | 3.2 | 6.71E-07 |
| DFFA | O00273 | 3.19 | 1.56E-06 |
| PSMD4 | Q5VWC4 | 3.18 | 2.76E-05 |
| CAP2 | P40123 | 3.16 | 1.77E-06 |
| EIF3E | P60228 | 3.15 | 0.00143 |
| OSTF1 | Q92882 | 3.14 | 1.68E-05 |
| GDI1 | P31150 | 3.13 | 1.85E-06 |
| UFC1 | Q9Y3C8 | 3.13 | 0.000964 |
| KHSRP | M0R0C6 | 3.09 | 2.25E-06 |
| TMEM119 | Q4V9L6 | 3.09 | 3.64E-07 |
| ANXA6 | E5RK69 | 3.08 | 2.27E-06 |
| MAP4K4 | E7ENQ1 | 3.08 | 1.22E-06 |
| RAB1A | P62820 | 3.08 | 6.81E-06 |
| TIMM9 | Q9Y5J7 | 3.08 | 1.53E-05 |
| RAPH1 | C9J164 | 3.05 | 2.85E-06 |
| PDHB | P11177-2 | 3.04 | 0.00117 |
| ACP2 | E9PQY3 | 3.03 | 0.000178 |
| PTK7 | Q13308-4 | 3.03 | 3.47E-07 |
| CALM2 | P0DP25 | 3.01 | 3.70E-06 |
| DDX6 | P26196 | 2.99 | 0.000504 |
| GRAMD3 | Q96HH9-4 | 2.98 | 2.03E-05 |
| ATP2B1 | P20020-1 | 2.96 | 4.13E-05 |
| TAGLN | Q01995 | 2.96 | 6.39E-07 |
| UBQLN2 | Q9UHD9 | 2.93 | 4.31E-05 |
| PDLIM2 | B3KPU0 | 2.91 | 0.00217 |
| CERCAM | Q5T4B2 | 2.89 | 0.000336 |
| AKAP12 | Q02952-3 | 2.88 | 4.90E-05 |
| RAI14 | Q9P0K7-4 | 2.87 | 0.000177 |
| TRIP6 | Q15654 | 2.85 | 2.86E-05 |
| TSNAX | Q99598 | 2.85 | 2.89E-05 |

| | | | |
|---|---|---|---|
| PRKRA | A0A7I2YQ87 | 2.81 | 0.00354 |
| NNMT | P40261 | 2.8 | 0.000381 |
| BAX | Q07812-5 | 2.79 | 0.00221 |
| ENG | P17813 | 2.79 | 1.45E-06 |
| SQSTM1 | Q13501 | 2.79 | 0.00264 |
| LOX | P28300 | 2.78 | 9.00E-04 |
| VAMP3 | Q15836 | 2.78 | 0.00274 |
| AHNAK2 | Q8IVF2 | 2.77 | 1.82E-05 |
| SERPINB1 | P30740 | 2.74 | 0.000122 |
| IFITM3 | E9PS44 | 2.72 | 2.02E-05 |
| DYNLT1 | P63172 | 2.71 | 0.000569 |
| PAFAH1B2 | P68402 | 2.71 | 3.57E-05 |
| LIMA1 | Q9UHB6 | 2.7 | 1.65E-05 |
| HN1 | J3KT51 | 2.69 | 0.000494 |
| SCUBE3 | Q8IX30 | 2.68 | 0.00155 |
| ATP5H | O75947 | 2.67 | 0.000542 |
| C21orf33 | P0DPI2 | 2.67 | 0.000689 |
| ADD1 | E7EV99 | 2.65 | 2.70E-05 |
| ZMPSTE24 | O75844 | 2.65 | 0.0116 |
| CLTA | P09496-2 | 2.64 | 0.000208 |
| PCBP1 | Q15365 | 2.64 | 0.000337 |
| PICALM | Q13492 | 2.64 | 0.000993 |
| CAPNS1 | A0A0C4DGQ5 | 2.61 | 0.000467 |
| CACYBP | Q9HB71 | 2.6 | 0.0012 |
| SLC30A1 | Q9Y6M5 | 2.6 | 0.000293 |
| TPD52L2 | O43399 | 2.6 | 0.00142 |
| BAG2 | O95816 | 2.58 | 7.84E-05 |
| RPL24 | C9JXB8 | 2.58 | 0.00102 |
| DLG1 | Q12959-5 | 2.56 | 4.64E-05 |
| GCC1 | Q96CN9 | 2.56 | 0.000677 |
| ITGA2 | P17301 | 2.55 | 0.0034 |
| FUBP3 | Q96I24 | 2.53 | 0.00157 |
| HERC4 | Q5GLZ8-3 | 2.53 | 0.000138 |
| C1orf198 | Q9H425-3 | 2.51 | 9.23E-06 |
| CTBP1 | Q13363-2 | 2.5 | 6.96E-05 |
| HSPB1 | P04792 | 2.5 | 2.72E-05 |
| ETFA | P13804 | 2.47 | 0.00338 |
| STAT3 | A0A7I2V4R2 | 2.44 | 8.69E-05 |
| TOLLIP | Q9H0E2 | 2.44 | 0.00157 |
| SLK | Q9H2G2 | 2.43 | 0.00527 |

| | | | |
|---|---|---|---|
| HSPB6 | O14558 | 2.42 | 0.000245 |
| PPP1R14B | Q96C90 | 2.42 | 0.000211 |
| PSMD5 | Q16401-2 | 2.42 | 0.000855 |
| SCYL1 | E9PS17 | 2.42 | 0.000139 |
| SORBS2 | O94875-11 | 2.42 | 0.000366 |
| SRP72 | O76094 | 2.42 | 0.00289 |
| BOLA2 | A0A499FJE1 | 2.4 | 0.00231 |
| HADHA | H0YFD6 | 2.4 | 2.77E-05 |
| PTRHD1 | Q6GMV3 | 2.4 | 0.00957 |
| STX4 | Q12846 | 2.4 | 9.44E-05 |
| AIMP2 | Q13155 | 2.39 | 0.00208 |
| PRRC1 | Q96M27 | 2.39 | 0.000461 |
| ZNF207 | J3QRS9 | 2.37 | 0.00142 |
| FKBP1A | P62942 | 2.35 | 7.70E-05 |
| LNP | Q9C0E8-2 | 2.34 | 0.00744 |
| CTNND1 | O60716 | 2.33 | 0.000223 |
| DCTD | P32321 | 2.33 | 0.000254 |
| HSPE1 | P61604 | 2.33 | 0.000215 |
| SPAG9 | O60271-4 | 2.33 | 0.00078 |
| ACAA1 | P09110 | 2.32 | 0.000599 |
| CMPK1 | P30085 | 2.32 | 5.52E-05 |
| IGBP1 | P78318 | 2.32 | 0.000239 |
| AP2A1 | O95782-2 | 2.31 | 0.00024 |
| FTL | P02792 | 2.31 | 7.59E-05 |
| PDLIM7 | Q9NR12 | 2.31 | 6.25E-05 |
| TBC1D2 | Q9BYX2-3 | 2.31 | 1.98E-05 |
| BANF1 | O75531 | 2.3 | 0.000285 |
| CTPS1 | A0A3B3IRI2 | 2.3 | 0.00158 |
| HIBADH | P31937 | 2.3 | 0.00562 |
| STK38L | Q9Y2H1 | 2.29 | 0.000483 |
| DDX42 | Q86XP3 | 2.28 | 9.12E-06 |
| SLC12A4 | Q9UP95 | 2.28 | 0.00167 |
| RAB5C | P51148 | 2.27 | 6.60E-05 |
| SYNPO2 | H0Y9Y3 | 2.27 | 0.00291 |
| SSSCA1 | G3V1B8 | 2.26 | 0.00407 |
| C1orf123 | Q9NWV4 | 2.25 | 0.00355 |
| TBCD | A0A804HLF8 | 2.24 | 0.000931 |
| AP2M1 | A0A8I5KWD3 | 2.23 | 0.00072 |
| GSS | A0A2R8Y430 | 2.23 | 0.0034 |
| CAPZA2 | P47755 | 2.21 | 1.83E-06 |

| | | | |
|---|---|---|---|
| COPS4 | Q9BT78 | 2.21 | 0.000208 |
| PPP1R9B | Q96SB3 | 2.21 | 0.000252 |
| RIC8A | Q9NPQ8-4 | 2.21 | 0.000118 |
| UBAP2L | Q14157-1 | 2.21 | 7.86E-05 |
| EMC8 | M0R1B0 | 2.2 | 0.00126 |
| PDXDC1 | H3BND4 | 2.2 | 1.10E-05 |
| PHLDB1 | Q86UU1-3 | 2.2 | 0.000192 |
| UBE2Z | Q9H832 | 2.2 | 0.00103 |
| NUDC | Q9Y266 | 2.19 | 0.0154 |
| MYL9 | P24844 | 2.18 | 9.36E-06 |
| RPS10 | P46783 | 2.18 | 0.00175 |
| TGM2 | P21980 | 2.18 | 3.36E-05 |
| API5 | Q9BZZ5-2 | 2.17 | 0.0125 |
| YKT6 | A0A7I2V4L6 | 2.16 | 0.000595 |
| CAV1 | Q03135 | 2.15 | 0.00094 |
| SNX1 | Q13596-2 | 2.15 | 0.00243 |
| CIRBP | Q14011 | 2.14 | 0.00104 |
| COMMD4 | A0A0B4J287 | 2.14 | 0.00628 |
| HSD17B10 | Q99714 | 2.14 | 0.00243 |
| RBM3 | P98179 | 2.14 | 0.0083 |
| TNS1 | A0A804HI61 | 2.13 | 0.000109 |
| TTLL12 | Q14166 | 2.12 | 0.00127 |
| AK4 | P27144 | 2.11 | 0.000339 |
| APPL2 | Q8NEU8 | 2.11 | 0.000262 |
| CCDC22 | O60826 | 2.11 | 3.89E-05 |
| CUL4B | A0A7P0T954 | 2.1 | 5.03E-05 |
| ARFGAP2 | Q8N6H7 | 2.09 | 0.00218 |
| EEF1B2 | P24534 | 2.09 | 2.67E-05 |
| ZYX | Q15942 | 2.09 | 0.000193 |
| APOOL | Q6UXV4 | 2.08 | 0.000161 |
| COPS3 | Q9UNS2-2 | 2.08 | 0.00041 |
| MAVS | Q7Z434 | 2.08 | 0.00287 |
| SEC24A | O95486 | 2.08 | 0.00284 |
| GLS | O94925 | 2.07 | 6.80E-06 |
| PPM1F | P49593-2 | 2.07 | 0.000203 |
| TBL2 | E9PF19 | 2.07 | 0.00245 |
| ECH1 | Q13011 | 2.06 | 0.0041 |
| DCTN2 | Q13561 | 2.04 | 0.0105 |
| IPO5 | O00410 | 2.04 | 2.42E-05 |
| RAB31 | Q13636 | 2.04 | 0.00134 |

| | | | |
|---|---|---|---|
| CAPZA1 | P52907 | 2.03 | 2.33E-05 |
| PURA | Q00577 | 2.03 | 0.0132 |
| CFL1 | E9PK25 | 2.02 | 0.00278 |
| IMMT.1 | Q16891-4 | 2.01 | 0.0111 |
| YBX3.1 | P16989-2 | 2.01 | 0.00642 |
| EHD1 | A0A024R571 | 2 | 4.49E-05 |
| EXOC2 | Q96KP1 | 2 | 0.000534 |
| B3GALTL | Q6Y288 | 1.99 | 0.000237 |
| YAP1 | P46937-5 | 1.99 | 0.00271 |
| MXRA7 | P84157-2 | 1.98 | 0.0046 |
| TMPO | P42167 | 1.98 | 9.51E-05 |
| EXOC1 | Q9NV70-2 | 1.95 | 0.000637 |
| SH3BGRL3 | Q9H299 | 1.95 | 9.83E-05 |
| SNAP23 | O00161 | 1.95 | 0.00287 |
| CYBRD1 | Q53TN4-3 | 1.94 | 0.00369 |
| SCAMP1 | A0A087WXB0 | 1.94 | 0.00277 |
| SMS | P52788 | 1.94 | 0.0114 |
| C14orf166 | Q9Y224 | 1.93 | 7.27E-05 |
| CACNA2D1 | P54289-4 | 1.93 | 0.00105 |
| MRPL50 | Q8N5N7 | 1.93 | 0.00123 |
| TMEM214 | Q6NUQ4 | 1.93 | 0.00558 |
| UBXN6 | Q9BZV1-2 | 1.92 | 0.00628 |
| PAWR | Q96IZ0 | 1.91 | 0.000362 |
| C12orf75 | F8VQD4 | 1.9 | 0.000997 |
| EIF3F | H0YDT6 | 1.9 | 0.00022 |
| PPME1 | Q9Y570 | 1.89 | 0.00147 |
| CD81 | E9PJK1 | 1.88 | 8.02E-05 |
| CUL4A | Q13619 | 1.88 | 0.00215 |
| FXR2 | P51116 | 1.88 | 3.08E-05 |
| ALCAM | Q13740 | 1.87 | 0.000546 |
| PDCD5 | O14737 | 1.87 | 0.00585 |
| PFDN2 | Q9UHV9 | 1.87 | 0.00142 |
| LAMTOR3 | Q9UHA4-2 | 1.86 | 0.00626 |
| ZC3HAV1 | Q7Z2W4 | 1.86 | 0.00783 |
| CARS | P49589 | 1.85 | 0.000213 |
| PRPSAP1 | Q14558 | 1.85 | 0.00261 |
| STRN | O43815-2 | 1.84 | 0.000332 |
| IMMT | Q16891-2 | 1.83 | 7.60E-05 |
| M6PR | H0YGT2 | 1.83 | 0.00831 |
| PRKCDBP | Q969G5 | 1.83 | 0.000896 |

| | | | |
|---|---|---|---|
| GSK3B | P49841 | 1.82 | 0.000612 |
| UNC45A | A0A1W2PNX8 | 1.82 | 0.0039 |
| LAMTOR1 | Q6IAA8 | 1.8 | 0.00102 |
| WDR44 | Q5JSH3-4 | 1.78 | 0.00393 |
| DBNL | Q9UJU6 | 1.77 | 0.000856 |
| GALK1 | P51570 | 1.77 | 0.00291 |
| SFXN1 | Q9H9B4 | 1.77 | 0.000734 |
| ATP6V1C1 | P21283 | 1.76 | 0.000381 |
| MT-CO2 | P00403 | 1.76 | 9.58E-05 |
| EEF1D | P29692-2 | 1.75 | 0.000316 |
| ERGIC1 | Q969X5-2 | 1.75 | 0.000905 |
| CCDC80 | Q76M96-2 | 1.74 | 0.000206 |
| EIF3M | Q7L2H7 | 1.73 | 0.00746 |
| PAICS | P22234 | 1.73 | 0.000102 |
| PEA15 | Q15121 | 1.73 | 0.000334 |
| AAK1 | A0A096LP25 | 1.72 | 0.000274 |
| ARSB | P15848 | 1.72 | 0.00134 |
| SPATS2L | B8ZZZ7 | 1.72 | 3.33E-05 |
| PDIA6 | Q15084-3 | 1.71 | 0.000393 |
| ASAP2 | O43150 | 1.7 | 0.00287 |
| PNN | Q9H307 | 1.7 | 0.00329 |
| SEC16A | A0A8I5KPG1 | 1.7 | 0.00186 |
| GYG1 | P46976-2 | 1.69 | 6.50E-05 |
| HSPB2 | Q16082 | 1.69 | 0.00704 |
| TAGLN2 | P37802 | 1.69 | 0.00025 |
| UQCRC1 | P31930 | 1.69 | 0.00166 |
| BAG3 | O95817 | 1.68 | 0.00106 |
| TUBB4A | P04350 | 1.68 | 0.0106 |
| CORO1C | Q9ULV4-3 | 1.67 | 0.00221 |
| NPM1 | P06748 | 1.67 | 0.00415 |
| UAP1 | Q16222-3 | 1.67 | 0.000117 |
| NEU1 | Q99519 | 1.66 | 0.00266 |
| PLIN3 | O60664 | 1.66 | 0.00336 |
| CKAP5 | Q14008-2 | 1.65 | 0.00796 |
| STXBP1 | A0A1B0GWF2 | 1.63 | 0.00113 |
| BSG | P35613-2 | 1.62 | 0.000908 |
| CLTB | P09497-2 | 1.62 | 0.000672 |
| CNN2 | B4DDF4 | 1.62 | 0.000675 |
| PGM1 | A0A3B3ITK7 | 1.62 | 0.00317 |
| ARHGEF10 | H0YAN8 | 1.61 | 0.00596 |

| | | | |
|---|---|---|---|
| IFI16 | Q16666-3 | 1.61 | 0.00684 |
| PPM1G | O15355 | 1.61 | 0.0136 |
| STAT1 | P42224 | 1.61 | 0.000129 |
| UBA1 | P22314-2 | 1.61 | 0.000278 |
| THY1 | E9PIM6 | 1.6 | 0.00011 |
| TWF2 | Q6IBS0 | 1.6 | 0.000602 |
| CCT2 | P78371 | 1.59 | 0.00029 |
| DBN1 | Q16643 | 1.59 | 0.00025 |
| EPB41L2 | O43491 | 1.59 | 0.00107 |
| HNRNPM | A0A087X0X3 | 1.59 | 0.000119 |
| LAMP2 | P13473-2 | 1.59 | 0.00949 |
| CSRP2 | Q16527 | 1.58 | 0.000413 |
| HDGFRP2 | Q7Z4V5-2 | 1.58 | 0.00308 |
| DNAJB1 | M0QXK0 | 1.57 | 0.000299 |
| ENDOD1 | O94919 | 1.57 | 0.00077 |
| S100A10 | P60903 | 1.57 | 0.000783 |
| CCT6A | P40227 | 1.56 | 0.00286 |
| DDX19A | I3L0H8 | 1.56 | 0.0013 |
| NDRG1 | Q92597 | 1.56 | 0.00143 |
| PPP3CA | Q08209-3 | 1.56 | 0.015 |
| SH3KBP1 | Q5JPT2 | 1.56 | 0.013 |
| COL5A2 | P05997 | 1.54 | 0.00646 |
| ARL6IP5 | O75915 | 1.53 | 0.00165 |
| PPP1R18 | A0A0G2JHC2 | 1.53 | 0.00208 |
| CMAS | Q8NFW8 | 1.52 | 0.0118 |
| MYL12B | O14950 | 1.52 | 0.000426 |
| C9orf89 | Q96LW7-2 | 1.51 | 0.00294 |
| SEMA7A | O75326 | 1.51 | 0.00074 |
| TUBB3 | Q13509 | 1.51 | 0.000672 |
| HIST1H3A | P68431 | -1.55 | 0.0144 |
| PSPH | C9JBI3 | -1.55 | 0.00195 |
| ASMTL | O95671-3 | -1.57 | 0.00237 |
| CCAR1 | Q8IX12-2 | -1.57 | 0.00879 |
| CRLF1 | O75462 | -1.57 | 0.00251 |
| HSD17B12 | Q53GQ0 | -1.59 | 0.000201 |
| SAR1A | Q9NR31 | -1.59 | 0.000988 |
| PSMB5 | P28074 | -1.63 | 0.00166 |
| UBTF | E9PKP7 | -1.64 | 0.00808 |
| NAA25 | Q14CX7-2 | -1.66 | 0.011 |
| SYNE3 | Q6ZMZ3-2 | -1.66 | 0.00151 |

| | | | |
|---|---|---|---|
| NDUFA9 | Q16795 | -1.67 | 0.00323 |
| RRAGD | Q9NQL2-2 | -1.69 | 0.00311 |
| JUP | P14923 | -1.71 | 0.00756 |
| SUN2 | B0QY64 | -1.71 | 0.000302 |
| FXR1 | E7EU85 | -1.72 | 0.000139 |
| TUBB8 | Q3ZCM7 | -1.72 | 0.00576 |
| TPM4 | P67936 | -1.73 | 0.000104 |
| ARPC5L | Q9BPX5 | -1.76 | 0.0146 |
| PRKG1 | Q13976 | -1.76 | 0.00216 |
| RPS4X | P62701 | -1.76 | 0.0123 |
| SERBP1 | Q8NC51 | -1.77 | 0.009 |
| COG2 | B7Z2Y2 | -1.79 | 0.00576 |
| UQCRFS1 | P47985 | -1.79 | 0.00218 |
| PSAT1 | Q9Y617 | -1.8 | 0.000223 |
| RPL23A | P62750 | -1.8 | 0.00177 |
| TMED10 | P49755 | -1.8 | 0.000361 |
| HIST1H4A | P62805 | -1.81 | 0.000599 |
| PRMT5 | O14744-2 | -1.81 | 0.00406 |
| EIF4B | E7EX17 | -1.84 | 0.000388 |
| NDUFC2 | O95298-2 | -1.85 | 0.00288 |
| BLMH | Q13867 | -1.86 | 0.000498 |
| COL6A3 | P12111-2 | -1.86 | 0.000102 |
| BASP1 | P80723 | -1.87 | 0.00297 |
| FKBP9 | O95302 | -1.87 | 0.00153 |
| NQO1 | P15559-2 | -1.89 | 0.000525 |
| RPS5 | M0R0F0 | -1.89 | 0.00413 |
| SRSF3 | P84103 | -1.89 | 0.00113 |
| PTGES3L-AARSD1 | C9J5N1 | -1.92 | 4.92E-05 |
| PWP1 | Q13610 | -1.92 | 0.0033 |
| RECQL | P46063 | -1.92 | 0.00262 |
| TMED4 | Q7Z7H5-3 | -1.93 | 0.000142 |
| DCPS | Q96C86 | -1.94 | 0.00128 |
| FKBP7 | Q9Y680-3 | -1.94 | 0.00123 |
| LMNB1 | P20700 | -1.94 | 9.98E-05 |
| TJP1 | A0A0G2JNH2 | -1.96 | 0.00135 |
| CDH13 | P55290 | -1.99 | 0.000522 |
| CCDC47 | Q96A33 | -2.02 | 0.00808 |
| SNX18 | Q96RF0-2 | -2.02 | 0.000751 |
| SCPEP1 | Q9HB40 | -2.03 | 6.86E-05 |
| YWHAE | P62258 | -2.03 | 0.00024 |

| | | | |
|---|---|---|---|
| SRRT | Q9BXP5-5 | -2.07 | 0.0051 |
| SF1 | A0A7P0T9U7 | -2.09 | 0.00103 |
| DHX29 | Q7Z478 | -2.1 | 0.000199 |
| RASA4B | F8W6L0 | -2.11 | 0.00161 |
| RSL1D1 | J3QSV6 | -2.12 | 0.000383 |
| BZW1 | C9IZ80 | -2.15 | 0.00918 |
| CTSL | P07711-3 | -2.16 | 8.41E-05 |
| PSMA7 | O14818 | -2.16 | 0.000164 |
| RPL15 | A0A2R8YEM3 | -2.18 | 0.00263 |
| UBLCP1 | Q8WVY7 | -2.2 | 0.000385 |
| EIF1AX | P47813 | -2.21 | 5.91E-06 |
| SLC16A3 | J3QQV2 | -2.22 | 5.39E-05 |
| LRRFIP2 | Q9Y608-4 | -2.24 | 0.00242 |
| SZRD1 | Q7Z422-2 | -2.24 | 5.74E-05 |
| ACSL3 | A0A7P0TA76 | -2.27 | 0.00529 |
| ENAH | Q8N8S7-3 | -2.27 | 0.00426 |
| SNRPD1 | J3QLI9 | -2.28 | 0.00488 |
| UBE2K | P61086 | -2.28 | 0.00305 |
| CRYZ | Q08257 | -2.29 | 0.00464 |
| RANBP1 | P43487-2 | -2.3 | 0.000726 |
| IDE | A0A7I2V3E3 | -2.31 | 6.96E-05 |
| MAGOHB | F5H6N1 | -2.31 | 0.0104 |
| MAN2A1 | Q16706 | -2.33 | 0.000289 |
| PRKAG1 | P54619-3 | -2.35 | 0.00763 |
| HIST1H1E | P10412 | -2.39 | 2.28E-05 |
| ILVBL | A1L0T0 | -2.4 | 0.00474 |
| RPS11 | P62280 | -2.41 | 0.00247 |
| FAU | E9PR30 | -2.43 | 0.000207 |
| COL15A1 | A0A087X0K0 | -2.45 | 0.00404 |
| HTRA1 | Q92743 | -2.49 | 0.0109 |
| MTX1 | Q13505-3 | -2.49 | 6.25E-06 |
| PSMB6 | P28072 | -2.49 | 2.09E-05 |
| HSDL2 | Q6YN16-2 | -2.54 | 6.62E-05 |
| MGST3 | O14880 | -2.54 | 0.0146 |
| NQO2 | Q5TD07 | -2.54 | 0.00577 |
| PPT1 | A0A2C9F2P4 | -2.59 | 0.000345 |
| RDX | A0A2R8Y5S7 | -2.59 | 7.07E-05 |
| RPS6 | P62753 | -2.63 | 2.51E-05 |
| SSR2 | P43308 | -2.65 | 0.00891 |
| WDR61 | H0YN81 | -2.7 | 6.06E-05 |

| | | | |
|---|---|---|---|
| RPA1 | P27694 | -2.71 | 7.03E-05 |
| UBE2I | H3BQQ9 | -2.71 | 0.0115 |
| AKR1C2 | P52895 | -2.72 | 3.39E-05 |
| RPL35 | P42766 | -2.79 | 6.63E-05 |
| NIPSNAP3A | Q9UFN0 | -2.82 | 1.20E-05 |
| LGMN | Q99538-3 | -2.83 | 0.000155 |
| NACA | F8W0W4 | -2.83 | 0.000127 |
| MTHFD2 | A0A7I2V2U6 | -2.87 | 0.00146 |
| PSMA2 | A0A024RA52 | -2.87 | 0.0101 |
| LUM | P51884 | -2.97 | 0.00128 |
| EWSR1 | B0QYK0 | -2.98 | 0.000228 |
| NOP56 | O00567 | -2.99 | 7.79E-06 |
| PEX11B | O96011 | -2.99 | 2.05E-06 |
| CD151 | K4DIA7 | -3.01 | 0.000345 |
| SEC61A1 | B4DR61 | -3.03 | 9.06E-07 |
| GAP43 | P17677 | -3.08 | 6.30E-06 |
| SRP68 | Q9UHB9-4 | -3.09 | 8.62E-05 |
| PSMA3 | P25788-2 | -3.1 | 3.11E-05 |
| GSTM3 | P21266 | -3.12 | 0.00448 |
| DDX21 | A0A8I5KNP3 | -3.14 | 6.13E-06 |
| SELM | Q8WWX9 | -3.16 | 0.000812 |
| RPL13a | Q8J015 | -3.24 | 5.71E-05 |
| H2AFV | Q71UI9 | -3.26 | 0.00389 |
| ALDH3A2 | P51648-2 | -3.29 | 1.02E-05 |
| RBBP7 | E9PC52 | -3.3 | 1.11E-05 |
| ACAT2 | Q9BWD1 | -3.52 | 2.43E-05 |
| COMP | G3XAP6 | -3.59 | 0.00399 |
| TMSB10 | P63313 | -3.59 | 0.000222 |
| SDCBP | O00560-3 | -3.61 | 0.000492 |
| RPL26 | P61254 | -3.64 | 1.58E-06 |
| RPS15 | K7ELC2 | -3.65 | 2.00E-05 |
| XXYLT1 | A0A140T9D0 | -3.71 | 0.00101 |
| B2M | P61769 | -3.87 | 4.93E-06 |
| ATP5D | P30049 | -3.92 | 2.16E-06 |
| PPIC | P45877 | -3.94 | 1.54E-05 |
| CD276 | A0A0C4DGH0 | -3.95 | 1.31E-06 |
| RPLP1 | P05386 | -4.02 | 0.000912 |
| ARF5 | P84085 | -4.04 | 4.50E-07 |
| MAP1LC3B | H3BTL1 | -4.29 | 7.26E-08 |
| HIST2H3PS2 | Q5TEC6 | -4.33 | 0.00262 |

| | | | |
|---|---|---|---|
| RBBP4 | Q09028-4 | -4.56 | 2.51E-07 |
| EIF6 | P56537 | -4.58 | 0.000345 |
| KRT6B | CON_P04259 | -4.7 | 0.00328 |
| RSU1 | Q15404 | -5.15 | 5.52E-08 |
| UBE2D3 | P61077-2 | -5.8 | 3.52E-07 |
| TMSB4X | P62328 | -6.28 | 2.63E-08 |
| BTF3 | P20290-2 | -6.61 | 6.64E-08 |

**Supplementary S2**

**Table S2.** All proteins involved in processes and functions of actin, ribosomal and neural. including fold change. With blue representing an increase in abundance in 3D compared to 2D and red representing a decrease in abundance in 3D compared to 2D.

| Protein | Log2 Fold change | Functions | Involvement |
|---|---|---|---|
| DAB2 | 3.79 | Actin cytoskeleton | actin |
| TAX1BP3 | 3.57 | Actin cytoskeleton, Actin cytoskeleton | actin |
| BST1 | 3.52 | Regulation of actin filament-based process, Regulation of actin cytoskeleton organization | actin |
| LPXN | 3.26 | Actin cytoskeleton, Actin cytoskeleton | actin |
| TAGLN | 2.96 | Actin binding, Actin filament binding, Actin-binding | actin |
| PDLIM2 | 2.91 | Actin cytoskeleton organization, Actin filament-based process, Actin binding, Actin cytoskeleton, Actin filament bundle, Mixed, incl. actin filament organization, and filamentous actin | actin |
| TRIP6 | 2.85 | Actin cytoskeleton, Actin filament bundle, Actin cytoskeleton, Actin filament bundle | actin |
| STK38L | 2.29 | Actin binding, Actin cytoskeleton, Actin cytoskeleton, Actin-binding | actin |
| SYNPO2 | 2.27 | Regulation of actin filament-based process, Regulation of actin filament organization, Regulation of actin cytoskeleton organization, Actin binding, Actin cytoskeleton, Actin filament bundle, Actin cytoskeleton, Actin filament bundle, Actin-binding | actin |
| TNS1 | 2.13 | Actin binding, Mixed, incl. actin filament organization, and filamentous actin, Mixed, incl. regulation of actin polymerization or depolymerization, and Calponin homology (CH) domain, RHO GTPases Activate WASPs and WAVEs, and actin filament organization, Actin-binding | actin |
| ZYX | 2.09 | Actin cytoskeleton organization, Actin filament-based process, Actin filament organization, Actin cytoskeleton, Actin filament bundle, Mixed, incl. actin filament organization, and filamentous actin, Mixed, incl. regulation of actin polymerization or depolymerization, and Calponin homology (CH) domain, RHO GTPases Activate WASPs and WAVEs, and actin filament organization, Actin cytoskeleton, Actin filament bundle | actin |
| CAPZA1 | 2.03 | Actin cytoskeleton organization, Actin filament-based process, Regulation of actin filament-based process, Regulation of actin filament organization, Regulation of actin cytoskeleton organization, Regulation of actin filament depolymerization, Regulation of actin polymerization or depolymerization, Barbed-end actin filament capping, Negative regulation of actin filament depolymerization, Negative regulation of actin filament polymerization, Regulation of actin filament polymerization, Actin binding, Actin filament binding, Actin cytoskeleton, F-actin capping protein complex, Actin cytoskeleton, F-actin capping protein complex, Actin-binding | actin |

| | | | |
|---|---|---|---|
| PAWR | 1.91 | Actin cytoskeleton organization, Actin filament-based process, Actin filament organization, Actin binding, Actin cytoskeleton, Actin cytoskeleton | actin |
| PRKCDBP | 1.83 | Actin cytoskeleton organization, Actin filament-based process | actin |
| TAGLN2 | 1.69 | Mixed, incl. actin filament organization, and filamentous actin, Mixed, incl. regulation of actin polymerization or depolymerization, and Calponin homology (CH) domain, RHO GTPases Activate WASPs and WAVEs, and actin filament organization | actin |
| CNN2 | 1.62 | Actin cytoskeleton organization, Actin filament-based process, Regulation of actin filament-based process, Actin binding, Actin cytoskeleton, Actin filament bundle, Actin cytoskeleton, Actin filament bundle, Actin-binding | actin |
| CSRP2 | 1.58 | Actin cytoskeleton organization, Actin filament-based process | actin |
| PPP1R18 | 1.53 | Actin binding, Actin-binding | actin |
| SYNE3 | -1.66 | Actin binding, Actin filament binding | actin |
| JUP | -1.71 | Regulation of actin filament-based process, Actin cytoskeleton | actin |
| PRKG1 | -1.76 | Actin cytoskeleton organization, Actin filament-based process | actin |
| CSRP1 | 7.07 | Actin cytoskeleton organization, Actin filament-based process, Nervous system, Central nervous system, Brain, Forebrain | actin, neural |
| DSTN | 4.72 | Actin cytoskeleton organization, Actin filament-based process, Actin filament organization, Regulation of actin filament-based process, Regulation of actin filament organization, Regulation of actin cytoskeleton organization, Regulation of actin filament depolymerization, Regulation of actin polymerization or depolymerization, Actin filament depolymerization, Actin polymerization or depolymerization, Actin binding, Actin filament binding, Actin cytoskeleton, Cortical actin cytoskeleton, Mixed, incl. actin filament organization, and filamentous actin, Mixed, incl. regulation of actin polymerization or depolymerization, and Calponin homology (CH) domain, RHO GTPases Activate WASPs and WAVEs, and actin filament organization, Actin-binding, Nervous system, Central nervous system, Brain | actin, neural |
| CTTN | 4.23 | Actin cytoskeleton organization, Actin filament-based process, Actin filament organization, Regulation of actin filament-based process, Regulation of actin filament organization, Regulation of actin cytoskeleton organization, Regulation of actin polymerization or depolymerization, Actin polymerization or depolymerization, Regulation of actin filament polymerization, Actin binding, Actin filament binding, Actin cytoskeleton, Cortical actin cytoskeleton, Actin cytoskeleton, Positive regulation of axon extension, Neuron projection, Somatodendritic compartment, Dendrite, Postsynapse organization, Synapse, Postsynaptic density, Postsynapse | actin, neural |

| | | | |
|---|---|---|---|
| LIMCH1 | 4.09 | Actin cytoskeleton organization, Actin filament-based process, Regulation of actin filament-based process, Regulation of actin filament organization, Regulation of actin cytoskeleton organization, Actin binding, Actin cytoskeleton, Actin filament bundle, Actin cytoskeleton, Actin filament bundle, Nervous system, Central nervous system, Brain | actin, neural |
| MARCKS | 3.74 | Actin cytoskeleton organization, Actin filament-based process, Actin filament organization, Actin binding, Actin filament binding, Actin cytoskeleton, Actin filament bundle, Actin cytoskeleton, Actin-binding, Nervous system, Central nervous system, Brain | actin, neural |
| PHPT1 | 3.53 | Regulation of actin filament-based process, Regulation of actin cytoskeleton organization, Nervous system, Central nervous system, Brain | actin, neural |
| SORBS3 | 3.3 | Actin cytoskeleton organization, Actin filament-based process, Actin filament organization, Regulation of actin filament-based process, Regulation of actin filament organization, Regulation of actin cytoskeleton organization, Nervous system | actin, neural |
| ABR | 3.23 | Actin cytoskeleton organization, Actin filament-based process, Axon, Neuron projection, Somatodendritic compartment, Dendrite, Synapse, Postsynaptic density, Postsynapse, Glutamatergic synapse, Nervous system, Central nervous system, Brain, Forebrain, Cerebral cortex | actin, neural |
| CAP2 | 3.16 | Actin cytoskeleton organization, Actin filament-based process, Actin filament organization, Actin polymerization or depolymerization, Actin binding, Actin cytoskeleton, Cortical actin cytoskeleton, Mixed, incl. actin filament organization, and filamentous actin, Mixed, incl. regulation of actin polymerization or depolymerization, and Calponin homology (CH) domain, RHO GTPases Activate WASPs and WAVEs, and actin filament organization, Axon guidance, Synapse, Postsynaptic density, Postsynapse, Nervous system development, Nervous system, Central nervous system, Brain, Forebrain, Cerebral cortex, Amygdala, Basal ganglion, Ganglion | actin, neural |
| ANXA6 | 3.08 | Actin binding, Actin filament binding, Nervous system, Central nervous system, Brain, Forebrain, Cerebral cortex, Amygdala, Basal ganglion, Ganglion | actin, neural |
| PTK7 | 3.03 | Actin cytoskeleton organization, Actin filament-based process, Wnt signaling pathway, planar cell polarity pathway | actin, neural |
| RAI14 | 2.87 | Actin binding, Nervous system, Central nervous system, Brain | actin, neural |

| | | | |
|---|---|---|---|
| LIMA1 | 2.7 | Actin cytoskeleton organization, Actin filament-based process, Actin filament organization, Regulation of actin filament-based process, Regulation of actin filament organization, Regulation of actin cytoskeleton organization, Regulation of actin filament depolymerization, Regulation of actin polymerization or depolymerization, Negative regulation of actin filament depolymerization, Actin binding, Actin filament binding, Actin cytoskeleton, Actin filament bundle, Actin cytoskeleton, Actin filament bundle, Actin-binding, Nervous system, Central nervous system, Brain, Forebrain | actin, neural |
| ADD1 | 2.65 | Actin cytoskeleton organization, Actin filament-based process, Actin filament organization, Regulation of actin filament-based process, Regulation of actin filament organization, Regulation of actin cytoskeleton organization, Regulation of actin filament depolymerization, Regulation of actin polymerization or depolymerization, Barbed-end actin filament capping, Negative regulation of actin filament depolymerization, Negative regulation of actin filament polymerization, Regulation of actin filament polymerization, Actin binding, Actin filament binding, Actin cytoskeleton, F-actin capping protein complex, Actin cytoskeleton, F-actin capping protein complex, Actin-binding, Synapse, Postsynaptic density, Postsynapse, Nervous system, Central nervous system, Brain, Forebrain, Cerebral cortex | actin, neural |
| DLG1 | 2.56 | Actin cytoskeleton organization, Actin filament-based process, Actin filament organization, Regulation of actin filament-based process, Regulation of actin filament organization, Regulation of actin cytoskeleton organization, Regulation of actin polymerization or depolymerization, Regulation of actin filament polymerization, Axon, Axon guidance, Neuron projection, Postsynapse organization, Synapse, Postsynaptic density, Postsynapse, Glutamatergic synapse, Nervous system development, Nervous system, Central nervous system, Brain | actin, neural |
| SORBS2 | 2.42 | Actin cytoskeleton organization, Actin filament-based process, Actin filament organization, Actin cytoskeleton, Actin cytoskeleton, Nervous system, Central nervous system, Brain, Forebrain | actin, neural |
| PDLIM7 | 2.31 | Actin cytoskeleton organization, Actin filament-based process, Actin binding, Actin cytoskeleton, Actin filament bundle, Mixed, incl. actin filament organization, and filamentous actin, Actin cytoskeleton, Axon guidance, Nervous system development, Nervous system, Central nervous system, Brain | actin, neural |

| | | | |
|---|---|---|---|
| CAPZA2 | 2.21 | Actin cytoskeleton organization, Actin filament-based process, Regulation of actin filament-based process, Regulation of actin filament organization, Regulation of actin cytoskeleton organization, Regulation of actin filament depolymerization, Regulation of actin polymerization or depolymerization, Barbed-end actin filament capping, Negative regulation of actin filament depolymerization, Negative regulation of actin filament polymerization, Regulation of actin filament polymerization, Actin binding, Actin filament binding, Actin cytoskeleton, F-actin capping protein complex, Actin cytoskeleton, F-actin capping protein complex, Actin-binding, Nervous system, Central nervous system, Brain, Forebrain, Cerebral cortex, Amygdala, Basal ganglion, Ganglion | actin, neural |
| PPP1R9B | 2.21 | Actin cytoskeleton organization, Actin filament-based process, Actin filament organization, Actin filament depolymerization, Actin polymerization or depolymerization, Actin binding, Actin filament binding, Actin cytoskeleton, Cortical actin cytoskeleton, Actin-binding, Filopodium, Filopodium, Growth cone, Axon, Distal axon, Neuron projection, Neuronal cell body, Somatodendritic compartment, Dendritic spine neck, Dendrite, Synapse, Postsynaptic density, Postsynapse, Nervous system, Central nervous system, Brain, Forebrain, Cerebral cortex, Amygdala, Basal ganglion, Ganglion | actin, neural |
| MYL9 | 2.18 | Actin cytoskeleton, Actin filament bundle, Actin cytoskeleton, Axon guidance, Nervous system development | actin, neural |
| CAV1 | 2.15 | Regulation of actin filament-based process, Nervous system, Central nervous system, Brain | actin, neural |
| PPM1F | 2.07 | Regulation of actin filament-based process, Regulation of actin filament organization, Regulation of actin cytoskeleton organization, Nervous system, Central nervous system, Brain | actin, neural |
| DCTN2 | 2.04 | Actin cytoskeleton, Actin cytoskeleton, Growth cone, Axon, Distal axon, Neuron projection, Nervous system, Central nervous system, Brain | actin, neural |
| CFL1 | 2.02 | Actin cytoskeleton organization, Actin filament-based process, Actin filament organization, Regulation of actin filament-based process, Regulation of actin filament organization, Regulation of actin cytoskeleton organization, Regulation of actin filament depolymerization, Regulation of actin polymerization or depolymerization, Actin filament depolymerization, Actin polymerization or depolymerization, Actin binding, Actin filament binding, Actin cytoskeleton, Cortical actin cytoskeleton, Mixed, incl. actin filament organization, and filamentous actin, Mixed, incl. regulation of actin polymerization or depolymerization, and Calponin homology (CH) domain, Actin cytoskeleton, Actin filament bundle, Actin-binding, Axon guidance, Nervous system development, Nervous system, Central nervous system, Brain, Brain cell line | actin, neural |
| CACNA2D1 | 1.93 | Actin filament-based process, Nervous system, Central nervous system, Brain | actin, neural |

| | | | |
|---|---|---|---|
| DBNL | 1.77 | Actin cytoskeleton organization, Actin filament-based process, Regulation of actin filament-based process, Regulation of actin filament organization, Regulation of actin cytoskeleton organization, Regulation of actin polymerization or depolymerization, Regulation of actin filament polymerization, Actin binding, Actin filament binding, Actin cytoskeleton, Cortical actin cytoskeleton, Actin cytoskeleton, Actin-binding, Positive regulation of axon extension, Neuron projection, Neuronal cell body, Somatodendritic compartment, Dendrite, Postsynapse organization, Synapse, Postsynaptic density, Postsynapse, Nervous system, Central nervous system, Brain | actin, neural |
| BAG3 | 1.68 | Actin cytoskeleton, Actin filament bundle, Neuron projection, Nervous system, Central nervous system, Brain | actin, neural |
| CORO1C | 1.67 | Actin cytoskeleton organization, Actin filament-based process, Actin filament organization, Actin binding, Actin filament binding, Actin cytoskeleton, Mixed, incl. actin filament organization, and filamentous actin, Mixed, incl. regulation of actin polymerization or depolymerization, and Calponin homology (CH) domain, RHO GTPases Activate WASPs and WAVEs, and actin filament organization, Actin cytoskeleton, Actin-binding, Synapse, Nervous system, Central nervous system, Brain | actin, neural |
| ARHGEF10 | 1.61 | Actin cytoskeleton organization, Actin filament-based process, Regulation of actin filament-based process, Regulation of actin filament organization, Regulation of actin cytoskeleton organization, Nervous system, Central nervous system, Brain | actin, neural |
| TWF2 | 1.6 | Actin cytoskeleton organization, Actin filament-based process, Actin filament organization, Regulation of actin filament-based process, Regulation of actin filament organization, Regulation of actin cytoskeleton organization, Regulation of actin filament depolymerization, Regulation of actin polymerization or depolymerization, Barbed-end actin filament capping, Actin filament depolymerization, Negative regulation of actin filament depolymerization, Negative regulation of actin filament polymerization, Actin polymerization or depolymerization, Regulation of actin filament polymerization, Actin binding, Actin filament binding, Actin cytoskeleton, Mixed, incl. actin filament organization, and filamentous actin, Mixed, incl. regulation of actin polymerization or depolymerization, and Calponin homology (CH) domain, RHO GTPases Activate WASPs and WAVEs, and actin filament organization, Actin-binding, Filopodium, Growth cone, Positive regulation of axon extension, Axon, Distal axon, Neuron projection | actin, neural |

| | | | |
|---|---|---|---|
| DBN1 | 1.59 | Actin cytoskeleton organization, Actin filament-based process, Actin filament organization, Regulation of actin filament-based process, Regulation of actin filament organization, Regulation of actin cytoskeleton organization, Regulation of actin polymerization or depolymerization, Regulation of actin filament polymerization, Actin binding, Actin filament binding, Actin cytoskeleton, Cortical actin cytoskeleton, Mixed, incl. actin filament organization, and filamentous actin, Actin cytoskeleton, Actin-binding, Growth cone, Positive regulation of axon extension, Axon, Distal axon, Neuron projection, Somatodendritic compartment, Dendrite, Postsynapse organization, Synapse, Postsynaptic density, Postsynapse, Glutamatergic synapse, Nervous system, Central nervous system, Brain | actin, neural |
| EPB41L2 | 1.59 | Actin cytoskeleton organization, Actin filament-based process, Actin binding, Actin cytoskeleton, Cortical actin cytoskeleton, Actin cytoskeleton, Actin-binding, Nervous system, Central nervous system, Brain | actin, neural |
| ENDOD1 | 1.57 | Mixed, incl. actin filament organization, and filamentous actin, Mixed, incl. regulation of actin polymerization or depolymerization, and Calponin homology (CH) domain, RHO GTPases Activate WASPs and WAVEs, and actin filament organization, Nervous system, Central nervous system, Brain | actin, neural |
| S100A10 | 1.57 | Regulation of actin filament-based process, Regulation of actin filament organization, Regulation of actin cytoskeleton organization, Nervous system, Central nervous system, Brain | actin, neural |
| SH3KBP1 | 1.56 | Actin cytoskeleton organization, Actin filament-based process, Actin filament organization, Axon guidance, Neuron projection, Synapse, Nervous system development | actin, neural |
| MYL12B | 1.52 | Actin cytoskeleton, Actin filament bundle, Actin cytoskeleton, Axon guidance, Nervous system development, Nervous system, Central nervous system, Brain | actin, neural |
| SUN2 | -1.71 | Actin filament-based process, Nervous system, Central nervous system, Brain | actin, neural |
| TPM4 | -1.73 | Actin cytoskeleton organization, Actin filament-based process, Actin filament organization, Actin binding, Actin filament binding, Actin cytoskeleton, Actin filament bundle, Actin cytoskeleton, Actin filament bundle, Actin-binding, Nervous system, Central nervous system, Brain | actin, neural |

| | | | |
|---|---|---|---|
| ARPC5L | -1.76 | Actin cytoskeleton organization, Actin filament-based process, Actin filament organization, Regulation of actin filament-based process, Regulation of actin filament organization, Regulation of actin cytoskeleton organization, Regulation of actin polymerization or depolymerization, Regulation of actin filament polymerization, Actin binding, Actin filament binding, Actin cytoskeleton, Mixed, incl. actin filament organization, and filamentous actin, Mixed, incl. regulation of actin polymerization or depolymerization, and Calponin homology (CH) domain, RHO GTPases Activate WASPs and WAVEs, and actin filament organization, Actin cytoskeleton, Actin-binding, Synapse, Glutamatergic synapse | actin, neural |
| TJP1 | -1.96 | Actin cytoskeleton organization, Actin filament-based process, Regulation of actin filament-based process, Regulation of actin filament organization, Regulation of actin cytoskeleton organization, Actin cytoskeleton, Actin cytoskeleton, Nervous system, Central nervous system, Brain | actin, neural |
| ENAH | -2.27 | Actin cytoskeleton organization, Actin filament-based process, Actin filament organization, Actin polymerization or depolymerization, Actin binding, Mixed, incl. actin filament organization, and filamentous actin, Mixed, incl. regulation of actin polymerization or depolymerization, and Calponin homology (CH) domain, RHO GTPases Activate WASPs and WAVEs, and actin filament organization, Actin-binding, Filopodium, Axon guidance, Synapse, Nervous system development | actin, neural |
| RDX | -2.59 | Regulation of actin filament-based process, Regulation of actin filament organization, Regulation of actin cytoskeleton organization, Regulation of actin filament depolymerization, Regulation of actin polymerization or depolymerization, Barbed-end actin filament capping, Negative regulation of actin filament depolymerization, Negative regulation of actin filament polymerization, Regulation of actin filament polymerization, Actin binding, Actin cytoskeleton, Cortical actin cytoskeleton, Actin cytoskeleton, Actin-binding, Filopodium, Filopodium, Axon guidance, Neuron projection, Nervous system development, Nervous system, Central nervous system, Brain, Forebrain, Cerebral cortex | actin, neural |
| TMSB10 | -3.59 | Actin cytoskeleton organization, Actin filament-based process, Actin filament organization, Regulation of actin filament-based process, Regulation of actin filament organization, Regulation of actin cytoskeleton organization, Regulation of actin polymerization or depolymerization, Negative regulation of actin filament polymerization, Regulation of actin filament polymerization, Actin binding, Actin-binding, Nervous system, Central nervous system, Brain | actin, neural |
| SDCBP | -3.61 | Actin cytoskeleton organization, Actin filament-based process, Axon guidance, Synapse, Nervous system development, Nervous system, Central nervous system, Brain | actin, neural |

| | | | |
|---|---|---|---|
| TMSB4X | -6.28 | Actin cytoskeleton organization, Actin filament-based process, Actin filament organization, Regulation of actin filament-based process, Regulation of actin filament organization, Regulation of actin cytoskeleton organization, Regulation of actin polymerization or depolymerization, Negative regulation of actin filament polymerization, Regulation of actin filament polymerization, Actin binding, Mixed, incl. actin filament organization, and filamentous actin, Mixed, incl. regulation of actin polymerization or depolymerization, and Calponin homology (CH) domain, RHO GTPases Activate WASPs and WAVEs, and actin filament organization, Actin-binding, Nervous system, Central nervous system, Brain | actin, neural |
| CD63 | 4.7 | Nervous system, Central nervous system, Brain | neural |
| PRNP | 4.38 | Axon, Distal axon, Axon guidance, Neuron projection, Somatodendritic compartment, Dendrite, Postsynapse organization, Synapse, Postsynaptic density, Postsynapse, Nervous system development, Nervous system, Central nervous system, Brain, Forebrain, Cerebral cortex | neural |
| MCFD2 | 4.33 | Nervous system, Central nervous system, Brain | neural |
| FAF2 | 4.17 | Nervous system, Central nervous system, Brain | neural |
| AKR7A2 | 3.77 | Nervous system, Central nervous system, Brain | neural |
| AGFG1 | 3.71 | Neuronal cell body, Somatodendritic compartment | neural |
| HMGA1 | 3.69 | Nervous system, Central nervous system, Brain | neural |
| LMO7 | 3.59 | Nervous system, Central nervous system, Brain | neural |
| SOD1 | 3.56 | Axon, Neuron projection, Neuronal cell body, Somatodendritic compartment, Dendrite, Nervous system, Central nervous system, Brain, Brain cell line, Forebrain, Cerebral cortex | neural |
| GRPEL1 | 3.51 | Nervous system, Central nervous system, Brain | neural |
| CDH2 | 3.41 | Neuron projection, Postsynapse organization, Synapse, Postsynaptic density, Postsynapse, Nervous system, Central nervous system, Brain | neural |
| COL1A1 | 3.28 | Nervous system, Central nervous system, Brain, Brain cell line | neural |
| SH3GLB1 | 3.2 | Nervous system, Central nervous system, Brain | neural |
| PSMD4 | 3.18 | Axon guidance, Nervous system development, Nervous system, Central nervous system, Brain, Wnt signaling pathway, planar cell polarity pathway | neural |
| GDI1 | 3.13 | Positive regulation of axon extension, Axon, Neuron projection, Neuronal cell body, Somatodendritic compartment, Nervous system, Central nervous system, Brain | neural |
| MAP4K4 | 3.08 | Nervous system, Central nervous system, Brain | neural |
| RAB1A | 3.08 | Nervous system, Central nervous system, Brain | neural |
| RAPH1 | 3.05 | Filopodium, Filopodium | neural |
| PDHB | 3.04 | Nervous system, Central nervous system, Brain, Forebrain, Cerebral cortex | neural |
| ACP2 | 3.03 | Nervous system, Central nervous system, Brain, Forebrain | neural |
| CALM2 | 3.01 | Nervous system, Central nervous system, Brain, Forebrain, Cerebral cortex, Basal ganglion, Ganglion | neural |

| | | | |
|---|---|---|---|
| GRAMD3 | 2.98 | Nervous system, Central nervous system, Brain | neural |
| ATP2B1 | 2.96 | Neuron projection, Neuronal cell body, Somatodendritic compartment, Synapse, Glutamatergic synapse, Nervous system, Central nervous system, Brain, Forebrain, Cerebral cortex | neural |
| UBQLN2 | 2.93 | Nervous system, Central nervous system, Brain, Forebrain, Cerebral cortex, Amygdala, Basal ganglion, Ganglion | neural |
| CERCAM | 2.89 | Nervous system, Central nervous system, Brain, Brain cell line | neural |
| AKAP12 | 2.88 | Neuronal cell body, Somatodendritic compartment, Synapse, Nervous system, Central nervous system, Brain | neural |
| TSNAX | 2.85 | Nervous system, Central nervous system, Brain, Forebrain, Cerebral cortex, Basal ganglion, Ganglion | neural |
| PRKRA | 2.81 | Nervous system, Central nervous system, Brain | neural |
| ENG | 2.79 | Nervous system, Central nervous system, Brain | neural |
| VAMP3 | 2.78 | Neuron projection, Synapse, Nervous system, Central nervous system, Brain | neural |
| AHNAK2 | 2.77 | Nervous system, Central nervous system, Brain, Forebrain, Cerebral cortex | neural |
| IFITM3 | 2.72 | Nervous system, Central nervous system, Brain | neural |
| DYNLT1 | 2.71 | Growth cone, Axon, Distal axon, Neuron projection, Neuronal cell body, Somatodendritic compartment, Nervous system, Central nervous system, Brain | neural |
| PAFAH1B2 | 2.71 | Nervous system, Central nervous system, Brain | neural |
| HN1 | 2.69 | Nervous system, Central nervous system, Brain | neural |
| ATP5H | 2.67 | Nervous system, Central nervous system, Brain | neural |
| ZMPSTE24 | 2.65 | Nervous system, Central nervous system, Brain | neural |
| CLTA | 2.64 | Axon guidance, Synapse, Postsynapse, Presynaptic endocytic zone membrane, Postsynaptic endocytic zone cytoplasmic component, Nervous system development, Nervous system, Central nervous system, Brain, Forebrain, Cerebral cortex | neural |
| PICALM | 2.64 | Neuronal cell body, Somatodendritic compartment, Synapse, Postsynapse, Presynaptic endocytic zone membrane, Nervous system, Central nervous system, Brain | neural |
| CACYBP | 2.6 | Neuron projection, Nervous system, Central nervous system, Brain | neural |
| SLC30A1 | 2.6 | Synapse, Postsynaptic density, Postsynapse | neural |
| TPD52L2 | 2.6 | Nervous system, Central nervous system, Brain | neural |
| BAG2 | 2.58 | Axon, Neuron projection, Somatodendritic compartment, Dendrite, Nervous system | neural |
| GCC1 | 2.56 | Nervous system, Central nervous system | neural |
| ITGA2 | 2.55 | Axon, Distal axon, Axon guidance, Neuron projection, Synapse, Nervous system development | neural |
| HERC4 | 2.53 | Nervous system, Central nervous system, Brain | neural |
| CTBP1 | 2.5 | Synapse, Glutamatergic synapse, Nervous system, Central nervous system, Brain | neural |
| HSPB1 | 2.5 | Axon, Neuron projection, Nervous system, Central nervous system, Brain | neural |
| ETFA | 2.47 | Brain cell line | neural |

| | | | |
|---|---|---|---|
| STAT3 | 2.44 | Synapse, Postsynaptic density, Postsynapse, Glutamatergic synapse, Nervous system, Central nervous system, Brain | neural |
| TOLLIP | 2.44 | Nervous system, Central nervous system, Brain | neural |
| PSMD5 | 2.42 | Axon guidance, Nervous system development, Wnt signaling pathway, planar cell polarity pathway | neural |
| SCYL1 | 2.42 | Nervous system, Central nervous system, Brain, Forebrain | neural |
| BOLA2 | 2.4 | Nervous system, Central nervous system, Brain | neural |
| HADHA | 2.4 | Nervous system, Central nervous system, Brain, Forebrain, Cerebral cortex | neural |
| STX4 | 2.4 | Neuron projection, Somatodendritic compartment, Dendrite, Synapse, Postsynapse, Glutamatergic synapse | neural |
| PRRC1 | 2.39 | Nervous system, Central nervous system | neural |
| ZNF207 | 2.37 | Nervous system, Central nervous system, Brain | neural |
| FKBP1A | 2.35 | Nervous system, Central nervous system, Brain | neural |
| KIAA1715 | 2.34 | Nervous system, Central nervous system, Brain | neural |
| CTNND1 | 2.33 | Growth cone, Axon, Distal axon, Neuron projection, Somatodendritic compartment, Dendrite, Synapse, Postsynaptic density, Postsynapse, Glutamatergic synapse, Nervous system, Central nervous system, Brain | neural |
| HSPE1 | 2.33 | Nervous system, Central nervous system, Brain | neural |
| SPAG9 | 2.33 | Nervous system, Central nervous system, Brain | neural |
| CMPK1 | 2.32 | Nervous system, Central nervous system, Brain, Forebrain | neural |
| AP2A1 | 2.31 | Filopodium, Axon guidance, Nervous system development, Wnt signaling pathway, planar cell polarity pathway | neural |
| FTL | 2.31 | Nervous system, Central nervous system, Brain | neural |
| BANF1 | 2.3 | Nervous system, Central nervous system, Brain | neural |
| SLC12A4 | 2.28 | Synapse, Nervous system, Central nervous system, Brain | neural |
| RAB5C | 2.27 | Nervous system, Central nervous system, Brain | neural |
| C1orf123 | 2.25 | Nervous system, Central nervous system, Brain | neural |
| TBCD | 2.24 | Nervous system, Central nervous system, Brain | neural |
| AP2M1 | 2.23 | Axon guidance, Nervous system development, Nervous system, Central nervous system, Brain, Wnt signaling pathway, planar cell polarity pathway | neural |
| GSS | 2.23 | Nervous system, Central nervous system, Brain, Forebrain, Cerebral cortex, Basal ganglion, Ganglion | neural |
| COPS4 | 2.21 | Synapse, Nervous system, Central nervous system, Brain | neural |
| RIC8A | 2.21 | Nervous system, Central nervous system, Brain | neural |
| PDXDC1 | 2.2 | Nervous system, Central nervous system, Brain | neural |
| PHLDB1 | 2.2 | Nervous system, Central nervous system, Brain | neural |
| UBE2Z | 2.2 | Nervous system, Central nervous system, Brain | neural |
| NUDC | 2.19 | Nervous system, Central nervous system, Brain | neural |
| TGM2 | 2.18 | Nervous system, Central nervous system, Brain | neural |
| YKT6 | 2.16 | Neuron projection, Neuronal cell body, Somatodendritic compartment, Dendrite, Nervous system | neural |
| AK4 | 2.11 | Nervous system, Central nervous system, Brain | neural |
| ARFGAP2 | 2.09 | Nervous system, Central nervous system, Brain | neural |

| | | | |
|---|---|---|---|
| EEF1B2 | 2.09 | Nervous system, Central nervous system, Brain | neural |
| COPS3 | 2.08 | Nervous system, Central nervous system, Brain, Forebrain, Cerebral cortex | neural |
| MAVS | 2.08 | Nervous system, Central nervous system, Brain | neural |
| SEC24A | 2.08 | Nervous system, Central nervous system, Brain | neural |
| GLS | 2.07 | Synapse, Nervous system, Central nervous system, Brain | neural |
| ECH1 | 2.06 | Nervous system, Central nervous system, Brain | neural |
| IPO5 | 2.04 | Nervous system, Central nervous system, Brain | neural |
| RAB31 | 2.04 | Nervous system, Central nervous system, Brain | neural |
| PURA | 2.03 | Neuron projection, Neuronal cell body, Somatodendritic compartment, Dendrite, Synapse, Postsynapse, Glutamatergic synapse | neural |
| EHD1 | 2 | Nervous system, Central nervous system, Brain | neural |
| EXOC2 | 2 | Nervous system, Central nervous system, Brain | neural |
| YAP1 | 1.99 | Nervous system development, Nervous system, Central nervous system, Brain, Forebrain | neural |
| TMPO | 1.98 | Nervous system, Central nervous system, Brain | neural |
| SNAP23 | 1.95 | Neuron projection, Synapse | neural |
| CYBRD1 | 1.94 | Nervous system, Central nervous system, Brain | neural |
| SCAMP1 | 1.94 | Synapse | neural |
| C14orf166 | 1.93 | Nervous system, Central nervous system, Brain | neural |
| TMEM214 | 1.93 | Nervous system, Central nervous system, Brain, Forebrain, Cerebral cortex, Amygdala, Basal ganglion, Ganglion | neural |
| PPME1 | 1.89 | Nervous system, Central nervous system, Brain, Forebrain, Cerebral cortex, Basal ganglion, Ganglion | neural |
| CD81 | 1.88 | Nervous system, Central nervous system, Brain | neural |
| ALCAM | 1.87 | Axon, Axon guidance, Neuron projection, Neuronal cell body, Somatodendritic compartment, Dendrite, Nervous system development, Nervous system, Central nervous system, Brain | neural |
| CARS | 1.85 | Nervous system, Central nervous system, Brain | neural |
| PRPSAP1 | 1.85 | Nervous system, Central nervous system, Brain | neural |
| STRN | 1.84 | Neuron projection, Neuronal cell body, Somatodendritic compartment, Dendrite, Synapse, Postsynaptic density, Postsynapse | neural |
| IMMT | 1.83 | Nervous system, Central nervous system, Brain, Brain cell line | neural |
| M6PR | 1.83 | Nervous system, Central nervous system, Brain | neural |
| GSK3B | 1.82 | Axon, Axon guidance, Neuron projection, Somatodendritic compartment, Dendrite, Synapse, Postsynapse, Glutamatergic synapse, Nervous system development | neural |
| UNC45A | 1.82 | Nervous system, Central nervous system, Brain | neural |
| WDR44 | 1.78 | Nervous system, Central nervous system, Brain | neural |
| GALK1 | 1.77 | Nervous system, Central nervous system, Brain | neural |
| ATP6V1C1 | 1.76 | Nervous system, Central nervous system, Brain | neural |
| EEF1D | 1.75 | Nervous system, Central nervous system, Brain | neural |
| ERGIC1 | 1.75 | Nervous system, Central nervous system, Brain, Forebrain | neural |
| CCDC80 | 1.74 | Nervous system, Central nervous system, Brain | neural |

| | | | |
|---|---|---|---|
| PAICS | 1.73 | Nervous system, Central nervous system, Brain | neural |
| PEA15 | 1.73 | Nervous system, Central nervous system, Brain, Brain cell line | neural |
| AAK1 | 1.72 | Axon, Distal axon, Neuron projection, Synapse, Nervous system, Central nervous system, Brain | neural |
| SPATS2L | 1.72 | Nervous system, Central nervous system, Brain, Ganglion | neural |
| PDIA6 | 1.71 | Nervous system, Central nervous system, Brain, Forebrain, Cerebral cortex, Amygdala, Basal ganglion, Ganglion | neural |
| ASAP2 | 1.7 | Nervous system, Central nervous system, Brain | neural |
| SEC16A | 1.7 | Nervous system, Central nervous system, Brain | neural |
| UQCRC1 | 1.69 | Nervous system, Central nervous system, Brain, Forebrain, Cerebral cortex, Basal ganglion, Ganglion | neural |
| TUBB4A | 1.68 | Axon, Axon guidance, Neuron projection, Neuronal cell body, Somatodendritic compartment, Nervous system development, Nervous system, Central nervous system, Brain | neural |
| NEU1 | 1.66 | Nervous system, Central nervous system, Brain | neural |
| STXBP1 | 1.63 | Axon, Neuron projection, Synapse, Postsynapse, Glutamatergic synapse, Nervous system, Central nervous system, Brain, Forebrain, Cerebral cortex | neural |
| BSG | 1.62 | Axon, Neuron projection, Nervous system, Central nervous system, Brain | neural |
| CLTB | 1.62 | Axon guidance, Synapse, Postsynapse, Presynaptic endocytic zone membrane, Postsynaptic endocytic zone cytoplasmic component, Nervous system development | neural |
| PGM1 | 1.62 | Nervous system, Central nervous system, Brain, Forebrain | neural |
| IFI16 | 1.61 | Nervous system, Central nervous system, Brain, Forebrain | neural |
| PPM1G | 1.61 | Nervous system, Central nervous system, Brain | neural |
| STAT1 | 1.61 | Axon, Neuron projection, Somatodendritic compartment, Dendrite, Nervous system, Central nervous system, Brain | neural |
| UBA1 | 1.61 | Nervous system, Central nervous system, Brain | neural |
| THY1 | 1.6 | Growth cone, Axon, Distal axon, Neuron projection, Neuronal cell body, Somatodendritic compartment, Dendrite, Nervous system, Central nervous system, Brain, Forebrain, Cerebral cortex, Amygdala, Basal ganglion, Ganglion | neural |
| CCT2 | 1.59 | Nervous system, Central nervous system, Brain, Brain cell line, Forebrain, Cerebral cortex, Amygdala, Basal ganglion, Ganglion | neural |
| LAMP2 | 1.59 | Nervous system, Central nervous system, Brain | neural |
| DNAJB1 | 1.57 | Neuron projection, Neuronal cell body, Somatodendritic compartment, Dendrite, Synapse, Postsynaptic density, Postsynapse, Glutamatergic synapse, Nervous system, Central nervous system, Brain | neural |
| CCT6A | 1.56 | Nervous system, Central nervous system, Brain | neural |
| NDRG1 | 1.56 | Postsynapse organization, Synapse, Glutamatergic synapse, Nervous system, Central nervous system, Brain, Brain cell line | neural |

| | | | |
|---|---|---|---|
| PPP3CA | 1.56 | Neuron projection, Somatodendritic compartment, Dendrite, Synapse, Postsynapse, Glutamatergic synapse, Nervous system, Central nervous system, Brain, Forebrain, Cerebral cortex, Amygdala, Basal ganglion, Ganglion | neural |
| COL5A2 | 1.54 | Axon guidance, Nervous system development, Nervous system, Central nervous system, Brain | neural |
| ARL6IP5 | 1.53 | Nervous system, Central nervous system, Brain | neural |
| SEMA7A | 1.51 | Positive regulation of axon extension, Axon guidance, Nervous system development, Nervous system, Central nervous system, Brain, Forebrain, Cerebral cortex | neural |
| TUBB3 | 1.51 | Filopodium, Filopodium, Growth cone, Axon, Distal axon, Axon guidance, Neuron projection, Somatodendritic compartment, Dendrite, Nervous system development, Brain cell line | neural |
| HIST1H3A | -1.55 | Nervous system, Central nervous system, Brain, Forebrain, Cerebral cortex, Basal ganglion, Ganglion | neural |
| PSPH | -1.55 | Neuron projection | neural |
| ASMTL | -1.57 | Nervous system, Central nervous system, Brain | neural |
| CCAR1 | -1.57 | Nervous system, Central nervous system, Brain | neural |
| HSD17B12 | -1.59 | Nervous system, Central nervous system, Brain | neural |
| PSMB5 | -1.63 | Axon guidance, Nervous system development, Nervous system, Central nervous system, Brain, Forebrain, Wnt signaling pathway, planar cell polarity pathway | neural |
| RRAGD | -1.69 | Nervous system, Central nervous system, Brain | neural |
| TUBB8 | -1.72 | Axon guidance, Nervous system development | neural |
| SERBP1 | -1.77 | Nervous system, Central nervous system, Brain | neural |
| UQCRFS1 | -1.79 | Nervous system, Central nervous system, Brain | neural |
| PSAT1 | -1.8 | Nervous system, Central nervous system, Brain | neural |
| TMED10 | -1.8 | Nervous system, Central nervous system, Brain, Forebrain, Cerebral cortex, Amygdala, Basal ganglion, Ganglion | neural |
| HIST1H4A | -1.81 | Nervous system, Central nervous system, Brain | neural |
| BLMH | -1.86 | Nervous system, Central nervous system, Brain | neural |
| COL6A3 | -1.86 | Axon guidance, Nervous system development | neural |
| BASP1 | -1.87 | Growth cone, Axon, Distal axon, Neuron projection, Nervous system, Central nervous system, Brain, Forebrain, Cerebral cortex, Basal ganglion, Ganglion | neural |
| FKBP9 | -1.87 | Nervous system | neural |
| NQO1 | -1.89 | Neuron projection, Neuronal cell body, Somatodendritic compartment, Dendrite, Synapse, Nervous system, Central nervous system, Brain, Forebrain, Cerebral cortex, Basal ganglion, Ganglion | neural |
| SRSF3 | -1.89 | Nervous system, Central nervous system, Brain | neural |
| TMED4 | -1.93 | Nervous system, Central nervous system, Brain | neural |
| FKBP7 | -1.94 | Nervous system, Central nervous system, Brain | neural |
| LMNB1 | -1.94 | Nervous system, Central nervous system, Brain, Brain cell line | neural |
| CDH13 | -1.99 | Neuron projection, Synapse, Nervous system, Central nervous system, Brain | neural |

| | | | |
|---|---|---|---|
| YWHAE | -2.03 | Growth cone, Axon, Distal axon, Neuron projection, Synapse, Glutamatergic synapse, Nervous system, Central nervous system, Brain, Forebrain, Cerebral cortex, Basal ganglion, Ganglion | neural |
| BZW1 | -2.15 | Nervous system, Central nervous system, Brain | neural |
| PSMA7 | -2.16 | Axon guidance, Synapse, Postsynapse, Nervous system development, Nervous system, Central nervous system, Brain, Wnt signaling pathway, planar cell polarity pathway | neural |
| UBLCP1 | -2.2 | Nervous system, Central nervous system, Brain | neural |
| SLC16A3 | -2.22 | Synapse, Postsynaptic density, Postsynapse, Nervous system, Central nervous system, Brain, Forebrain, Cerebral cortex | neural |
| ACSL3 | -2.27 | Nervous system, Central nervous system, Brain | neural |
| UBE2K | -2.28 | Filopodium, Nervous system, Central nervous system, Brain | neural |
| CRYZ | -2.29 | Nervous system, Central nervous system, Brain, Forebrain | neural |
| ILVBL | -2.4 | Nervous system, Central nervous system, Brain | neural |
| PSMB6 | -2.49 | Axon guidance, Nervous system development, Nervous system, Central nervous system, Brain, Wnt signaling pathway, planar cell polarity pathway | neural |
| HSDL2 | -2.54 | Nervous system, Central nervous system, Brain | neural |
| MGST3 | -2.54 | Nervous system, Central nervous system, Brain | neural |
| NQO2 | -2.54 | Nervous system, Central nervous system, Brain | neural |
| PPT1 | -2.59 | Axon, Neuron projection, Neuronal cell body, Somatodendritic compartment, Dendrite, Synapse, Nervous system, Central nervous system, Brain | neural |
| SSR2 | -2.65 | Nervous system, Central nervous system, Brain | neural |
| RPA1 | -2.71 | Nervous system, Central nervous system, Brain | neural |
| UBE2I | -2.71 | Nervous system, Central nervous system, Brain | neural |
| NIPSNAP3A | -2.82 | Nervous system, Central nervous system, Brain | neural |
| LGMN | -2.83 | Postsynapse organization | neural |
| NACA | -2.83 | Nervous system, Central nervous system, Brain | neural |
| MTHFD2 | -2.87 | Nervous system, Central nervous system, Brain | neural |
| EWSR1 | -2.98 | Nervous system, Central nervous system, Brain | neural |
| GAP43 | -3.08 | Filopodium, Filopodium, Growth cone, Axon, Distal axon, Axon guidance, Neuron projection, Neuronal cell body, Somatodendritic compartment, Dendrite, Synapse, Postsynaptic density, Postsynapse, Nervous system development, Nervous system, Central nervous system, Brain, Forebrain, Cerebral cortex, Basal ganglion, Ganglion | neural |
| PSMA3 | -3.1 | Axon guidance, Synapse, Nervous system development, Wnt signaling pathway, planar cell polarity pathway | neural |
| GSTM3 | -3.12 | Nervous system, Central nervous system, Brain | neural |
| H2AFV | -3.26 | Nervous system, Central nervous system, Brain | neural |
| ACAT2 | -3.52 | Nervous system, Central nervous system, Brain, Forebrain, Cerebral cortex, Amygdala, Basal ganglion, Ganglion | neural |
| XXYLT1 | -3.71 | Nervous system | neural |
| B2M | -3.87 | Nervous system, Central nervous system, Brain | neural |
| ATP5D | -3.92 | Nervous system, Central nervous system, Brain | neural |

| | | | |
|---|---|---|---|
| ARF5 | -4.04 | Nervous system, Central nervous system, Brain | neural |
| MAP1LC3B | -4.29 | Nervous system, Central nervous system, Brain | neural |
| RBBP4 | -4.56 | Nervous system, Central nervous system, Brain | neural |
| RSU1 | -5.15 | Nervous system, Central nervous system, Brain, Brain cell line, Forebrain | neural |
| UBE2D3 | -5.8 | Nervous system, Central nervous system, Brain | neural |
| EIF4H | 3.32 | Nervous system, Central nervous system, Brain, Ribonucleoprotein complex, GTP hydrolysis and joining of the 60S ribosomal subunit, Ribosomal scanning and start codon recognition | neural, ribosome |
| CARHSP1 | 3.28 | Nervous system, Central nervous system, Brain, Cytoplasmic ribonucleoprotein granule | neural, ribosome |
| KLC1 | 3.21 | Growth cone, Axon, Distal axon, Neuron projection, Nervous system, Central nervous system, Brain, Ribonucleoprotein complex subunit organization | neural, ribosome |
| EIF3E | 3.15 | Nervous system, Central nervous system, Brain, Ribonucleoprotein complex biogenesis, Ribonucleoprotein complex subunit organization, Ribonucleoprotein complex assembly, Ribonucleoprotein complex, GTP hydrolysis and joining of the 60S ribosomal subunit, Ribosomal scanning and start codon recognition, Ribonucleoprotein complex | neural, ribosome |
| KHSRP | 3.09 | Nervous system, Central nervous system, Brain, Brain cell line, Cytoplasmic ribonucleoprotein granule | neural, ribosome |
| SQSTM1 | 2.79 | Nervous system, Central nervous system, Brain, Forebrain, Cerebral cortex, Basal ganglion, Ganglion, Cytoplasmic ribonucleoprotein granule | neural, ribosome |
| PCBP1 | 2.64 | Nervous system, Central nervous system, Brain, Cytoplasmic ribonucleoprotein granule, Ribonucleoprotein | neural, ribosome |
| RPL24 | 2.58 | Axon guidance, Nervous system development, Ribosome assembly, Ribonucleoprotein complex biogenesis, Ribonucleoprotein complex subunit organization, Ribonucleoprotein complex assembly, Ribosome biogenesis, Structural constituent of ribosome, Cytosolic ribosome, Ribonucleoprotein complex, Ribosome, Ribosomal subunit, Cytosolic large ribosomal subunit, Large ribosomal subunit, Cytoplasmic ribosomal proteins, Cytoplasmic ribosomal proteins, Cytoplasmic ribosomal proteins, Ribosome, GTP hydrolysis and joining of the 60S ribosomal subunit, Cytoplasmic ribosomal proteins, Cytosolic ribosome, Ribonucleoprotein complex, Ribosome, Ribosomal subunit, Cytosolic large ribosomal subunit, Large ribosomal subunit, Ribonucleoprotein, Ribosomal protein | neural, ribosome |
| UBAP2L | 2.21 | Nervous system, Central nervous system, Brain, Cytoplasmic ribonucleoprotein granule | neural, ribosome |

| | | | |
|---|---|---|---|
| RPS10 | 2.18 | Axon guidance, Nervous system development, Nervous system, Central nervous system, Brain, Ribosome assembly, Ribonucleoprotein complex biogenesis, Ribonucleoprotein complex subunit organization, Ribonucleoprotein complex assembly, Ribosome biogenesis, Structural constituent of ribosome, Cytosolic ribosome, Ribonucleoprotein complex, Ribosome, Ribosomal subunit, Cytosolic small ribosomal subunit, Cytoplasmic ribosomal proteins, Cytoplasmic ribosomal proteins, Cytoplasmic ribosomal proteins, Ribosome, GTP hydrolysis and joining of the 60S ribosomal subunit, Ribosomal scanning and start codon recognition, Cytoplasmic ribosomal proteins, Cytosolic ribosome, Ribonucleoprotein complex, Ribosome, Ribosomal subunit, Cytosolic small ribosomal subunit, Ribonucleoprotein, Ribosomal protein | neural, ribosome |
| API5 | 2.17 | Nervous system, Central nervous system, Brain, Ribonucleoprotein complex, Ribonucleoprotein complex | neural, ribosome |
| CIRBP | 2.14 | Nervous system, Central nervous system, Brain, Ribonucleoprotein complex, Cytoplasmic ribonucleoprotein granule | neural, ribosome |
| HSD17B10 | 2.14 | Nervous system, Central nervous system, Brain, Ribonucleoprotein complex, Ribonucleoprotein complex | neural, ribosome |
| RBM3 | 2.14 | Neuron projection, Somatodendritic compartment, Dendrite, Nervous system, Central nervous system, Brain, Ribonucleoprotein complex binding, Ribonucleoprotein complex | neural, ribosome |
| CUL4B | 2.1 | Nervous system, Central nervous system, Brain, Ribonucleoprotein complex biogenesis, Ribosome biogenesis | neural, ribosome |
| MRPL50 | 1.93 | Nervous system, Central nervous system, Brain, Forebrain, Cerebral cortex, Ribonucleoprotein complex, Ribosome, Ribosomal subunit, Large ribosomal subunit, Ribonucleoprotein complex, Ribosome, Ribosomal subunit, Large ribosomal subunit, Ribonucleoprotein, Ribosomal protein | neural, ribosome |
| EIF3F | 1.9 | Nervous system, Central nervous system, Brain, Forebrain, Cerebral cortex, Amygdala, Basal ganglion, Ganglion, Ribonucleoprotein complex biogenesis, Ribonucleoprotein complex subunit organization, Ribonucleoprotein complex assembly, Ribonucleoprotein complex, GTP hydrolysis and joining of the 60S ribosomal subunit, Ribosomal scanning and start codon recognition, Ribonucleoprotein complex | neural, ribosome |
| FXR2 | 1.88 | Filopodium, Filopodium, Growth cone, Axon, Distal axon, Neuron projection, Neuronal cell body, Somatodendritic compartment, Dendritic spine neck, Dendrite, Synapse, Postsynaptic density, Postsynapse, Nervous system, Central nervous system, Brain, Cytosolic ribosome, Ribonucleoprotein complex, Ribosome, Ribosomal subunit, Cytosolic large ribosomal subunit, Cytoplasmic ribonucleoprotein granule, Large ribosomal subunit, Cytosolic ribosome, Ribonucleoprotein complex, Ribosome, Ribosomal subunit, Cytosolic large ribosomal subunit, Large ribosomal subunit | neural, ribosome |

| | | | |
|---|---|---|---|
| EIF3M | 1.73 | Nervous system, Central nervous system, Brain, Forebrain, Ribonucleoprotein complex biogenesis, Ribonucleoprotein complex subunit organization, Ribonucleoprotein complex assembly, Ribonucleoprotein complex, GTP hydrolysis and joining of the 60S ribosomal subunit, Ribosomal scanning and start codon recognition | neural, ribosome |
| PNN | 1.7 | Nervous system, Central nervous system, Brain, Ribonucleoprotein complex, Ribonucleoprotein complex | neural, ribosome |
| NPM1 | 1.67 | Nervous system, Central nervous system, Brain, Ribosome assembly, Ribonucleoprotein complex biogenesis, Ribosome biogenesis, Ribonucleoprotein complex binding, Ribonucleoprotein complex, Ribonucleoprotein complex | neural, ribosome |
| CKAP5 | 1.65 | Nervous system, Ribonucleoprotein complex binding | neural, ribosome |
| HNRNPM | 1.59 | Nervous system, Central nervous system, Brain, Ribonucleoprotein complex, Ribonucleoprotein complex, Ribonucleoprotein | neural, ribosome |
| DDX19A | 1.56 | Nervous system, Central nervous system, Brain, Cytoplasmic ribonucleoprotein granule | neural, ribosome |
| FXR1 | -1.72 | Filopodium, Filopodium, Growth cone, Axon, Distal axon, Neuron projection, Neuronal cell body, Somatodendritic compartment, Dendritic spine neck, Dendrite, Synapse, Postsynaptic density, Postsynapse, Glutamatergic synapse, Nervous system, Central nervous system, Brain, Ribonucleoprotein complex, Cytoplasmic ribonucleoprotein granule, Ribonucleoprotein complex | neural, ribosome |
| RPS4X | -1.76 | Axon guidance, Synapse, Nervous system development, Nervous system, Central nervous system, Brain, Structural constituent of ribosome, Cytosolic ribosome, Ribonucleoprotein complex, Ribosome, Ribosomal subunit, Cytosolic small ribosomal subunit, Cytoplasmic ribonucleoprotein granule, Cytoplasmic ribosomal proteins, Cytoplasmic ribosomal proteins, Cytoplasmic ribosomal proteins, Ribosome, GTP hydrolysis and joining of the 60S ribosomal subunit, Ribosomal scanning and start codon recognition, Cytoplasmic ribosomal proteins, Cytosolic ribosome, Ribonucleoprotein complex, Ribosome, Ribosomal subunit, Cytosolic small ribosomal subunit, Ribonucleoprotein, Ribosomal protein | neural, ribosome |

| | | | |
|---|---|---|---|
| RPL23A | -1.8 | Axon guidance, Nervous system development, Nervous system, Central nervous system, Brain, Ribosome assembly, Ribonucleoprotein complex biogenesis, Ribonucleoprotein complex subunit organization, Ribonucleoprotein complex assembly, Ribosome biogenesis, Structural constituent of ribosome, Cytosolic ribosome, Ribonucleoprotein complex, Ribosome, Ribosomal subunit, Cytosolic large ribosomal subunit, Large ribosomal subunit, Cytoplasmic ribosomal proteins, Cytoplasmic ribosomal proteins, Cytoplasmic ribosomal proteins, Ribosome, GTP hydrolysis and joining of the 60S ribosomal subunit, Cytoplasmic ribosomal proteins, Cytosolic ribosome, Ribonucleoprotein complex, Ribosome, Ribosomal subunit, Cytosolic large ribosomal subunit, Large ribosomal subunit, Ribonucleoprotein, Ribosomal protein | neural, ribosome |
| PRMT5 | -1.81 | Nervous system, Central nervous system, Brain, Ribonucleoprotein complex biogenesis, Ribonucleoprotein complex subunit organization, Ribonucleoprotein complex assembly, Ribonucleoprotein complex binding | neural, ribosome |
| EIF4B | -1.84 | Nervous system, Central nervous system, Brain, Ribonucleoprotein complex, GTP hydrolysis and joining of the 60S ribosomal subunit, Ribosomal scanning and start codon recognition, Ribonucleoprotein complex | neural, ribosome |
| RPS5 | -1.89 | Axon guidance, Nervous system development, Nervous system, Central nervous system, Brain, Ribosome assembly, Ribonucleoprotein complex biogenesis, Ribonucleoprotein complex subunit organization, Ribonucleoprotein complex assembly, Ribosome biogenesis, Structural constituent of ribosome, Cytosolic ribosome, Ribonucleoprotein complex, Ribosome, Ribosomal subunit, Cytosolic small ribosomal subunit, Cytoplasmic ribosomal proteins, Cytoplasmic ribosomal proteins, Cytoplasmic ribosomal proteins, Ribosome, GTP hydrolysis and joining of the 60S ribosomal subunit, Ribosomal scanning and start codon recognition, Cytoplasmic ribosomal proteins, Cytosolic ribosome, Ribonucleoprotein complex, Ribosome, Ribosomal subunit, Cytosolic small ribosomal subunit, Ribonucleoprotein, Ribosomal protein | neural, ribosome |
| SRRT | -2.07 | Nervous system, Central nervous system, Brain, Forebrain, Ribonucleoprotein complex | neural, ribosome |
| SF1 | -2.09 | Nervous system, Central nervous system, Brain, Forebrain, Cerebral cortex, Ribonucleoprotein complex biogenesis, Ribonucleoprotein complex subunit organization, Ribonucleoprotein complex assembly, Ribonucleoprotein complex, Ribosome, Ribonucleoprotein complex, Ribosome | neural, ribosome |

| | | | |
|---|---|---|---|
| DHX29 | -2.1 | Nervous system, Central nervous system, Brain, Ribosome assembly, Ribonucleoprotein complex biogenesis, Ribonucleoprotein complex subunit organization, Ribonucleoprotein complex assembly, Ribosome biogenesis, Ribonucleoprotein complex binding, Cytosolic ribosome, Ribonucleoprotein complex, Ribosome, Ribosomal subunit, Cytosolic small ribosomal subunit, Cytosolic ribosome, Ribonucleoprotein complex, Ribosome, Ribosomal subunit, Cytosolic small ribosomal subunit | neural, ribosome |
| RSL1D1 | -2.12 | Nervous system, Central nervous system, Brain, Forebrain, Cerebral cortex, Basal ganglion, Ganglion, Ribonucleoprotein complex biogenesis, Ribosome biogenesis, Ribonucleoprotein complex, Ribonucleoprotein complex | neural, ribosome |
| RPL15 | -2.18 | Axon guidance, Nervous system development, Nervous system, Central nervous system, Brain, Structural constituent of ribosome, Cytosolic ribosome, Ribonucleoprotein complex, Ribosome, Ribosomal subunit, Cytosolic large ribosomal subunit, Large ribosomal subunit, Cytoplasmic ribosomal proteins, Cytoplasmic ribosomal proteins, Cytoplasmic ribosomal proteins, Ribosome, GTP hydrolysis and joining of the 60S ribosomal subunit, Cytoplasmic ribosomal proteins, Cytosolic ribosome, Ribonucleoprotein complex, Ribosome, Ribosomal subunit, Cytosolic large ribosomal subunit, Large ribosomal subunit, Ribonucleoprotein, Ribosomal protein | neural, ribosome |
| EIF1AX | -2.21 | Nervous system, Central nervous system, Brain, Forebrain, GTP hydrolysis and joining of the 60S ribosomal subunit, Ribosomal scanning and start codon recognition | neural, ribosome |
| MAGOHB | -2.31 | Axon guidance, Neuronal cell body, Somatodendritic compartment, Nervous system development, Nervous system, Central nervous system, Brain, Ribonucleoprotein complex, Ribonucleoprotein complex | neural, ribosome |
| RPS11 | -2.41 | Axon guidance, Nervous system development, Nervous system, Central nervous system, Brain, Structural constituent of ribosome, Cytosolic ribosome, Ribonucleoprotein complex, Ribosome, Ribosomal subunit, Cytosolic small ribosomal subunit, Cytoplasmic ribosomal proteins, Ribosome, GTP hydrolysis and joining of the 60S ribosomal subunit, Ribosomal scanning and start codon recognition, Cytoplasmic ribosomal proteins, Cytosolic ribosome, Ribonucleoprotein complex, Ribosome, Ribosomal subunit, Cytosolic small ribosomal subunit, Ribonucleoprotein, Ribosomal protein | neural, ribosome |

| | | | |
|---|---|---|---|
| RPS6 | -2.63 | Axon guidance, Neuron projection, Somatodendritic compartment, Dendrite, Nervous system development, Nervous system, Central nervous system, Brain, Ribonucleoprotein complex biogenesis, Ribosome biogenesis, Structural constituent of ribosome, Cytosolic ribosome, Ribonucleoprotein complex, Ribosome, Ribosomal subunit, Cytosolic small ribosomal subunit, Cytoplasmic ribonucleoprotein granule, Cytoplasmic ribosomal proteins, Ribosome, GTP hydrolysis and joining of the 60S ribosomal subunit, Ribosomal scanning and start codon recognition, Cytoplasmic ribosomal proteins, Cytosolic ribosome, Ribonucleoprotein complex, Ribosome, Ribosomal subunit, Cytosolic small ribosomal subunit, Ribonucleoprotein, Ribosomal protein | neural, ribosome |
| RPL35 | -2.79 | Axon guidance, Nervous system development, Nervous system, Central nervous system, Brain, Ribonucleoprotein complex biogenesis, Ribosome biogenesis, Structural constituent of ribosome, Cytosolic ribosome, Ribonucleoprotein complex, Ribosome, Ribosomal subunit, Cytosolic large ribosomal subunit, Large ribosomal subunit, Cytoplasmic ribosomal proteins, Ribosome, GTP hydrolysis and joining of the 60S ribosomal subunit, Cytoplasmic ribosomal proteins, Cytosolic ribosome, Ribonucleoprotein complex, Ribosome, Ribosomal subunit, Cytosolic large ribosomal subunit, Large ribosomal subunit, Ribonucleoprotein, Ribosomal protein | neural, ribosome |
| PSMA2 | -2.87 | Axon guidance, Nervous system development, Nervous system, Central nervous system, Brain, Wnt signaling pathway, planar cell polarity pathway, Cytoplasmic ribonucleoprotein granule | neural, ribosome |
| NOP56 | -2.99 | Nervous system, Central nervous system, Brain, Ribonucleoprotein complex biogenesis, Ribosome biogenesis, Ribonucleoprotein complex, Ribonucleoprotein complex, Ribonucleoprotein | neural, ribosome |
| SEC61A1 | -3.03 | Nervous system, Central nervous system, Brain, Ribonucleoprotein complex binding, Ribonucleoprotein complex | neural, ribosome |
| RPL13A | -3.24 | Axon guidance, Nervous system development, Nervous system, Central nervous system, Brain, Structural constituent of ribosome, Cytosolic ribosome, Ribonucleoprotein complex, Ribosome, Ribosomal subunit, Cytosolic large ribosomal subunit, Large ribosomal subunit, Ribosome, GTP hydrolysis and joining of the 60S ribosomal subunit, Cytoplasmic ribosomal proteins, Cytosolic ribosome, Ribonucleoprotein complex, Ribosome, Ribosomal subunit, Cytosolic large ribosomal subunit, Large ribosomal subunit, Ribonucleoprotein, Ribosomal protein | neural, ribosome |

| | | | |
|---|---|---|---|
| RPL26 | -3.64 | Axon guidance, Nervous system development, Nervous system, Central nervous system, Brain, Ribonucleoprotein complex biogenesis, Ribosome biogenesis, Structural constituent of ribosome, Cytosolic ribosome, Ribonucleoprotein complex, Ribosome, Ribosomal subunit, Cytosolic large ribosomal subunit, Large ribosomal subunit, Cytoplasmic ribosomal proteins, Cytoplasmic ribosomal proteins, Cytoplasmic ribosomal proteins, Ribosome, GTP hydrolysis and joining of the 60S ribosomal subunit, Cytoplasmic ribosomal proteins, Cytosolic ribosome, Ribonucleoprotein complex, Ribosome, Ribosomal subunit, Cytosolic large ribosomal subunit, Large ribosomal subunit, Ribonucleoprotein, Ribosomal protein | neural, ribosome |
| RPS15 | -3.65 | Axon guidance, Nervous system development, Nervous system, Central nervous system, Brain, Ribosome assembly, Ribonucleoprotein complex biogenesis, Ribonucleoprotein complex subunit organization, Ribonucleoprotein complex assembly, Ribosome biogenesis, Structural constituent of ribosome, Cytosolic ribosome, Ribonucleoprotein complex, Ribosome, Ribosomal subunit, Cytosolic small ribosomal subunit, Cytoplasmic ribosomal proteins, Cytoplasmic ribosomal proteins, Cytoplasmic ribosomal proteins, Ribosome, GTP hydrolysis and joining of the 60S ribosomal subunit, Ribosomal scanning and start codon recognition, Cytoplasmic ribosomal proteins, Cytosolic ribosome, Ribonucleoprotein complex, Ribosome, Ribosomal subunit, Cytosolic small ribosomal subunit, Ribonucleoprotein, Ribosomal protein | neural, ribosome |
| RPLP1 | -4.02 | Axon guidance, Nervous system development, Nervous system, Central nervous system, Brain, Structural constituent of ribosome, Ribonucleoprotein complex binding, Cytosolic ribosome, Ribonucleoprotein complex, Ribosome, Ribosomal subunit, Cytosolic large ribosomal subunit, Large ribosomal subunit, Cytoplasmic ribosomal proteins, Cytoplasmic ribosomal proteins, Ribosome, GTP hydrolysis and joining of the 60S ribosomal subunit, Cytoplasmic ribosomal proteins, Cytosolic ribosome, Ribonucleoprotein complex, Ribosome, Ribosomal subunit, Cytosolic large ribosomal subunit, Large ribosomal subunit, Ribonucleoprotein, Ribosomal protein | neural, ribosome |
| EIF6 | -4.58 | Nervous system, Central nervous system, Brain, Ribosome assembly, Ribonucleoprotein complex biogenesis, Ribonucleoprotein complex subunit organization, Ribonucleoprotein complex assembly, Ribosome biogenesis, Ribonucleoprotein complex binding, Ribonucleoprotein complex, Ribonucleoprotein complex | neural, ribosome |
| BTF3 | -6.61 | Nervous system, Central nervous system, Brain, Ribonucleoprotein complex, Ribosome | neural, ribosome |
| ALYREF | 3.47 | Ribonucleoprotein complex, Ribonucleoprotein complex | ribosome |
| DDX6 | 2.99 | Ribonucleoprotein complex, Cytoplasmic ribonucleoprotein granule, Ribonucleoprotein complex | ribosome |
| SERPINB1 | 2.74 | Cytoplasmic ribonucleoprotein granule | ribosome |

| | | | |
|---|---|---|---|
| SRP72 | 2.42 | Ribonucleoprotein complex binding, Ribonucleoprotein complex, Ribonucleoprotein complex, Ribonucleoprotein | ribosome |
| CUL4A | 1.88 | Ribonucleoprotein complex biogenesis, Ribosome biogenesis | ribosome |
| PWP1 | -1.92 | Ribonucleoprotein complex biogenesis, Ribosome biogenesis | ribosome |
| DCPS | -1.94 | Cytoplasmic ribonucleoprotein granule | ribosome |
| SNRPD1 | -2.28 | Ribonucleoprotein complex biogenesis, Ribonucleoprotein complex subunit organization, Ribonucleoprotein complex assembly, Ribonucleoprotein complex binding, Ribonucleoprotein complex, Ribonucleoprotein complex, Ribonucleoprotein | ribosome |
| FAU | -2.43 | Structural constituent of ribosome, Cytosolic ribosome, Ribonucleoprotein complex, Ribosome, Ribosomal subunit, Cytosolic small ribosomal subunit, Cytoplasmic ribosomal proteins, Ribosome, Cytoplasmic ribosomal proteins, Cytosolic ribosome, Ribonucleoprotein complex, Ribosome, Ribosomal subunit, Cytosolic small ribosomal subunit | ribosome |
| SRP68 | -3.09 | Ribonucleoprotein complex binding, Ribonucleoprotein complex, Ribosome, Ribonucleoprotein complex, Ribosome, Ribonucleoprotein | ribosome |
| DDX21 | -3.14 | Ribonucleoprotein complex biogenesis, Ribosome biogenesis | ribosome |

String permalink with network functional analysis: https://version-11-5.string-db.org/cgi/network?networkId=bFY8QJcX4JxW

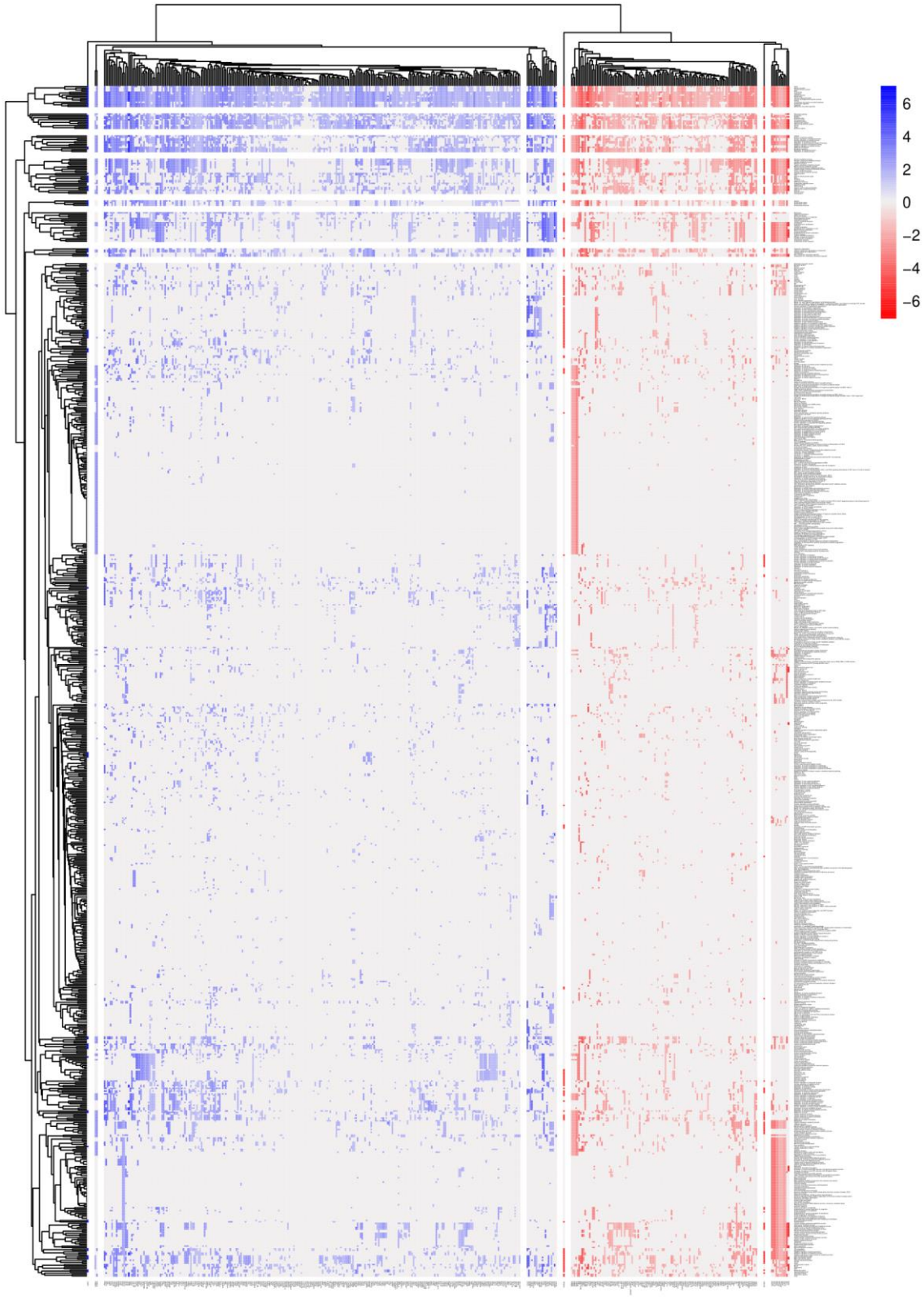
6
4
2
0
−2
−4
−6

**Figure S1** Heatmap showing all significant proteins, fold change and their correlation with the string functional network analysis. Blue increase in abundance in 3D samples compared to 2D samples. Red decrease in abundance in 3D samples compared to 2D samples.

After successfully creating a 3D model using PEG-based hydrogels where the cells survived and even showed signs of neural differentiation, the next step was to introduce the differentiation supplements utilised in Chapter Two. Chapter Five will explore the combination of supplements used in Chapter Two together with the 3D model developed in Chapter Four.

# Chapter Five: Neural marker expression in adipose-derived stem cells grown in PEG-based 3D matrix is enhanced in the presence of B27 and CultureOne supplements.

**Submitted as:**
*Gomila Pelegri, N.; Stanczak, A.M.; Bottomley, A.L.; Cummins M.L; Milthorpe, B.K.; Gorrie, C.A.; Padula, M.P.; Santos, J*
*Neural marker expression in adipose-derived stem cells grown in PEG-based 3D matrix is enhanced in the presence of B27 and CultureOne supplements.*

Under review - submitted to the International Journal of Molecular Sciences on 11th October 2023

I certify that the work present in chapter five of this thesis has not been previously submitted as part of the requirements for a degree. I also certify that I carried out over 70% of the experimental work, analysis and interpretation of the data presented in this paper.

**Author's contributions:**
Conceptualisation, JS, NGP and C.G.; methodology, JS, NGP, MP and C.G.; formal analysis, NGP, AB; investigation, NGP and AS.; resources, JS, BM, MP; data curation, NGP and AS; writing—original draft preparation, NGP; writing—review and editing, All.; visualisation, NGP, AS and MLC; supervision JS, MP and CG.; project administration, JS.; funding acquisition, JS and BM. All authors have read and agreed to the published version of the manuscript.

| | |
|---|---|
| Neus Gomila Pelegri | Production Note: Signature removed prior to publication. |
| Aleksandra M. Stanczak | Production Note: Signature removed prior to publication. |
| Amy L. Bottomley | Production Note: Signature removed prior to publication. |
| Max L. Cummins | Production Note: Signature removed prior to publication. |
| Bruce K. Milthorpe | Production Note: Signature removed prior to publication. |
| Catherine A. Gorrie | Production Note: Signature removed prior to publication. |
| Matthew P. Padula | Production Note: Signature removed prior to publication. |
| Jerran Santos | Production Note: Signature removed prior to publication. |

International Journal of
*Molecular Sciences*

MDPI

*Article*

# Neural Marker Expression in Adipose-Derived Stem Cells Grown in PEG-Based 3D Matrix Is Enhanced in the Presence of B27 and CultureOne Supplements

**Neus Gomila Pelegri [1,2], Aleksandra M. Stanczak [3], Amy L. Bottomley [4], Max L. Cummins [5,6], Bruce K. Milthorpe [1], Catherine A. Gorrie [2], Matthew P. Padula [3] and Jerran Santos [1,*]**

[1] Advanced Tissue Engineering and Stem Cell Biology Group, School of Life Sciences, University of Technology Sydney, Ultimo, NSW 2007, Australia; neus.gomilapelegri@uts.edu.au (N.G.P.); bruce.milthorpe@uts.edu.au (B.K.M.)
[2] Neural Injury Research Unit, School of Life Sciences, University of Technology Sydney, Ultimo, NSW 2007, Australia; catherine.gorrie@uts.edu.au
[3] School of Life Sciences, University of Technology Sydney, Ultimo, NSW 2007, Australia; aleksandra.m.stanczak@student.uts.edu.au (A.M.S.); matthew.padula@uts.edu.au (M.P.P.)
[4] Microbial Imaging Facility, University of Technology Sydney, Ultimo, NSW 2007, Australia; amy.bottomley@uts.edu.au
[5] Australian Institute for Microbiology and Infection, University of Technology Sydney, Ultimo, NSW 2007, Australia; max.cummins@uts.edu.au
[6] The Australian Centre for Genomic Epidemiological Microbiology, University of Technology Sydney, Ultimo, NSW 2007, Australia
* Correspondence: jerran.santos@uts.edu.au

**Abstract:** Adipose-derived stem cells (ADSCs) have incredible potential as an avenue to better understand and treat neurological disorders. While they have been successfully differentiated into neural stem cells and neurons, most such protocols involve 2D environments, which are not representative of in vivo physiology. In this study, human ADSCs were cultured in 1.1 kPa polyethylene-glycol 3D hydrogels for 10 days with B27, CultureOne (C1), and N2 neural supplements to examine the neural differentiation potential of ADSCs using both chemical and mechanical cues. Following treatment, cell viability, proliferation, morphology, and proteome changes were assessed. Results showed that cell viability was maintained during treatments, and while cells continued to proliferate over time, proliferation slowed down. Morphological changes between 3D untreated cells and treated cells were not observed. However, they were observed among 2D treatments, which exhibited cellular elongation and co-alignment. Proteome analysis showed changes consistent with early neural differentiation for B27 and C1 but not N2. No significant changes were detected using immunocytochemistry, potentially indicating a greater differentiation period was required. In conclusion, treatment of 3D-cultured ADSCs in PEG-based hydrogels with B27 and C1 further enhances neural marker expression, however, this was not observed using supplementation with N2.

**Keywords:** tissue engineering; bioprinting; neural differentiation; proteomics; 3D tissue culture; immunocytochemistry; polyethylene glycol; neuroregeneration; neural development; regenerative medicine



**Citation:** Gomila Pelegri, N.; Stanczak, A.M.; Bottomley, A.L.; Cummins, M.L.; Milthorpe, B.K.; Gorrie, C.A.; Padula, M.P.; Santos, J. Neural Marker Expression in Adipose-Derived Stem Cells Grown in PEG-Based 3D Matrix Is Enhanced in the Presence of B27 and CultureOne Supplements. *Int. J. Mol. Sci.* **2023**, *24*, 16269. https://doi.org/10.3390/ijms242216269

Academic Editor: Marco Tatullo

Received: 11 October 2023
Revised: 3 November 2023
Accepted: 8 November 2023
Published: 13 November 2023



## 1. Introduction

Adipose-derived stem cells (ADSCs) have been at the forefront of regenerative medicine, given their potential to differentiate into adipogenic, chondrogenic, osteogenic, myogenic, and neurogenic-like cell lineages [1–4]. These qualities make them suitable for many applications, and in the context of neuroregeneration, ADSCs are a desirable source of cells due to their neurogenic differentiation potential [2–4] and their availability [5,6]. Autologous ADSCs can be easily obtained in high numbers via subcutaneous adipose

liposuction, which is a significantly less invasive procedure when compared to other collection methods like bone marrow aspirates [5–7].

ADSCs have been successfully differentiated into neural-like cells using different growth factors and chemicals [8–14]. Rodent ADSCs have been successfully differentiated into neural stem cells and dopaminergic neurons [8], while human ADSCs (hADSCs) have also shown neurogenic potential and have been successfully differentiated into neurospheres [9], neuron-like cells [9], and dopamine-secreting cells [10,11]. Furthermore, transplantation of ADSCs has shown positive effects in animal models of neurological disorders such as Parkinson's disease [15], peripheral nerve injury [16], epilepsy [17], and stroke [18].

These findings are promising and show ADSCs' potential as a tool to understand neural development and find potential treatments for neurological disorders. However, the most common methods of differentiation are usually solely chemically induced, using multistep protocols with many chemical mixtures, and performed in 2D cell culture environments [2,3,8–14,19]. These monolayer cellular models are not representative of human tissue structure and do not consider any of the crucial 3D interactions that affect stem cells during differentiation [20,21]. Some of these chemical inductions have proven to be transient and reversible when conducted in a 2D environment alone; Ahmadi et al. demonstrated that a neurosphere formation protocol, while slower than chemical inductions, had better cell viability, and the neural differentiation was more stable than in 2D constructs [9].

In recent years, research has shown that cells grown in a 3D environment that mimics their native tissue are more comparable to in vivo behaviour and present distinctive morphological changes compared to their 2D-grown counterparts [20–23]. In a 3D environment, cells can arrange themselves in more natural conformations. They can aggregate themselves into multiple layers where cell exposure to nutrients and waste products is similar to in vitro conditions [21,22,24]. These arrangements provide insights into drug treatments and cell proliferation rates that are more realistic than those observed in 2D cultures [25]. Furthermore, it has been shown that cells respond to the mechanical stimuli of their environment, such as pressure, and interact with ECM proteins and scaffold composition, mimicking the natural interactions between the cells and their ECM and directing cellular differentiation [26–29]. Of particular interest, human-derived mesenchymal stem cells (hMSCs) have been shown to differentiate towards a neural lineage when grown in scaffolds resembling a brain stiffness of 1 kPa [28]. Additionally, our previous work showed that hADSCs spontaneously express neural markers when grown in PEG-based hydrogels of 1.1 kPa stiffness [30], further highlighting the importance of growth matrices and cell growth environment when conducting neural differentiation of hADSCs.

This study builds upon our previous work, where we used the readily available media supplements B27, C1, and N2 for neural induction of ADSCs in 2D matrices [31], and on our most recent investigation of the effects of mechanical properties of 3D polyethylene glycol (PEG)-based hydrogels containing RGD and YIGSR peptides to initiate neural differentiation of hADSCs [30]. This work merges both concepts and explores the effects of treatment and matrix combined using cost-effective and standardised supplements together with the reproducibility of commercially available system rastrum bioprinting (Inventia, Sydney, Australia). This is necessary to progress the development of treatments for a range of conditions where neuronal tissue is compromised.

## 2. Results

### *2.1. Cell Proliferation, Viability, and Morphology*

#### 2.1.1. Cell Proliferation and Viability

Cell treatment began on day 3.5, 84 h after the cells were plated. The Alamar blue measurement on day 3.5 was the last measurement before cells started treatment and therefore serves as a control. Increases or decreases in fold change and hence cell metabolic activity were measured from that time point. An increase in fold change is indicative

of cells showing an increase in cell metabolic activity, while a decrease in fold change is indicative of a decrease in metabolic activity (Figure 1).

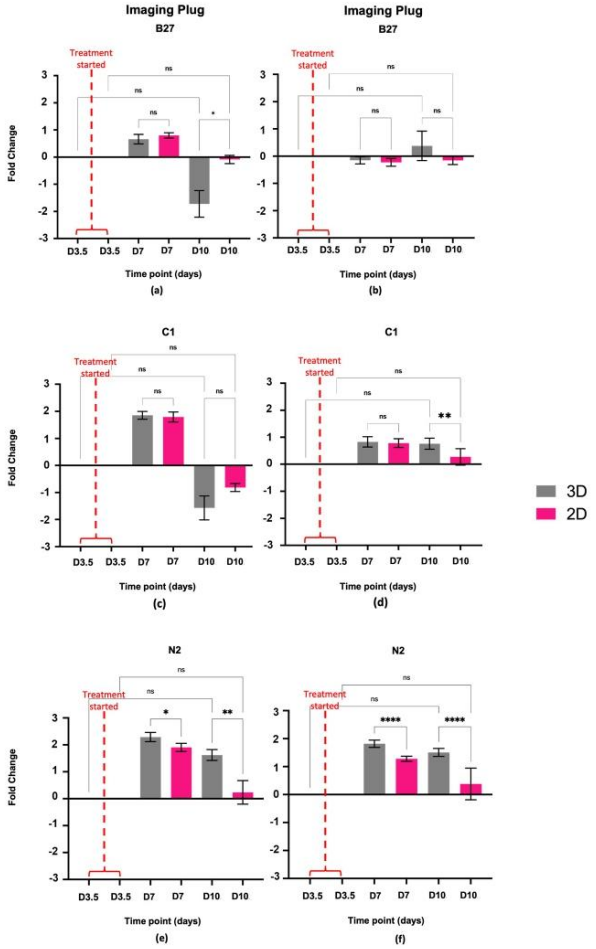


**Figure 1.** Alamar blue cell viability. Fold change activity measured over treatment course using Alamar blue assay. Fold change is relative to day 3.5 prior to cell treatment, marked by the red line. A Log2 scale has been used where the initial measurement obtained on day 3.5 equals zero, and the increase or decrease in measured parameters falls on the respective side of the x-axis. (**a**) Imaging plug treated with B27, (**b**) large plug treated with B27, (**c**) imaging plug treated with C1, (**d**) large plug treated with C1, (**e**) imaging plug treated with N2, (**f**) large plug treated with N2. No statistical significance $p > 0.05$; statistical significance *, $p \leq 0.05$; statistical significance **, $p \leq 0.01$; statistical significance ****, $p \leq 0.0001$; ns: not significant.

Alamar blue results for cells treated with B27 show very little change in metabolic activity for both 3D and 2D samples (Figure 1a,b). In the imaging plug, metabolic activity

decreased in the 3D samples compared to the 2D samples at D10 (Figure 1a) but no statistically significant changes were detected in the 3D plug (Figure 1b).

For the cells treated with C1, Alamar blue results show that metabolic activity decreased in the imaging plug for both 3D and 2D samples from D3 to D10 (Figure 1c), however, no statistical significance was detected. In the large plug, metabolic activity increased in both the 3D and the 2D samples compared to the control, with 2D samples showing significantly lower metabolic activity at D10 compared to the 3D samples (Figure 1d) ($p \leq 0.05$; statistical significance **).

Alamar blue results indicate that N2 treatment causes metabolic activity to increase at the beginning of treatment and then decrease by day 10 in the imaging and large plugs for both 3D and 2D samples (Figure 1e,f), with 3D samples having overall higher metabolic activity compared to 2D samples (*, $p \leq 0.05$; statistical significance **, $p \leq 0.01$; statistical significance for imaging plug, and statistical significance ****, $p \leq 0.0001$).

Live cell imaging analysis (Figure 2) shows that the cell confluence in the DMEM control group for both 3D and 2D steadily increases over time, while treatments cause a decrease in this variable over the treatment course (Figure 2a,c,e). The 3D samples overall show higher confluence than the 2D counterparts in all instances, with cell confluence being significantly higher in the 3D samples than in the 2D samples in all treatments (Figure 2b,d,f) (parametric two-way ANOVA with Tukey's multiple comparisons: $p \leq 0.05$ for B27, $p \leq 0.05$ for C1 and ****, $p \leq 0.0001$ for N2).

#### 2.1.2. Cell Morphology

Live cell imaging (Figure 3) showed changes in cell morphology and alignment in all 2D samples, with all treatments showing greater cell alignment compared to the usual disorganised arrangement of DMEM control cells. The 2D-treated cells became more polarised and aligned with one another (Figure 3d–f,j–l,p–r,s,u,w). Despite the imaging data for the 2D samples providing insight into alterations in cellular morphology, the interpretation of the images of the cells grown in 3D culture has proven challenging. No obvious morphological and cellular arrangement changes can be seen in the 3D samples (Figure 3a–c,g–i,m–o,t,v,x,z). The 3D morphology and arrangement changes are harder to visually assess, given the nature of 3D constructs and images only showing one slice of the Z plane. Therefore, morphology cannot effectively be visually assessed by imaging in the same way that morphology changes in the 2D samples can be, highlighting the need for more robust and accessible protocols.

### *2.2. Cell Characterisation*

#### 2.2.1. Immunocytochemistry

The staining of positive control cells (Figure 4e,k,q) showed robust positivity for all antibodies and negative control cells (Figure 4f,l,r) showed no signal as expected. There were high levels of fluorescent debris in all samples stained in 3D plugs, and these were unable to be removed despite multiple washing steps. Therefore, 'speckles' were removed during analysis based on size and staining intensity. This is further explained in Section 4.4.1.

Immunocytochemistry analysis revealed that incubation of cells with B27, C1, and N2 supplements while suspended in PEG-based 3D matrices did not significantly increase the specific markers for neurons (NF200), oligodendrocytes (CPNase), or astrocytes (GFAP) compared to the DMEM controls. C1 was observed to have the greatest increases for CPNase and GFAP and N2 had the greatest increase in NF200 but these were not statistically significant.

#### 2.2.2. Proteomics

Proteomics analysis revealed distinct changes between each 3D treatment and the 3D DMEM control and between the 3D treatments themselves (Figure 5). When compared to the DMEM control, 18 proteins decreased and 62 proteins increased (Log2 fold change of $+/-1.5$) with B27 treatment, 38 decreased and 30 increased with C1 treatment, and 107

decreased and 28 increased with N2 treatment, with only 6 decreased and 3 increased proteins common to all treatments (Figure 5).

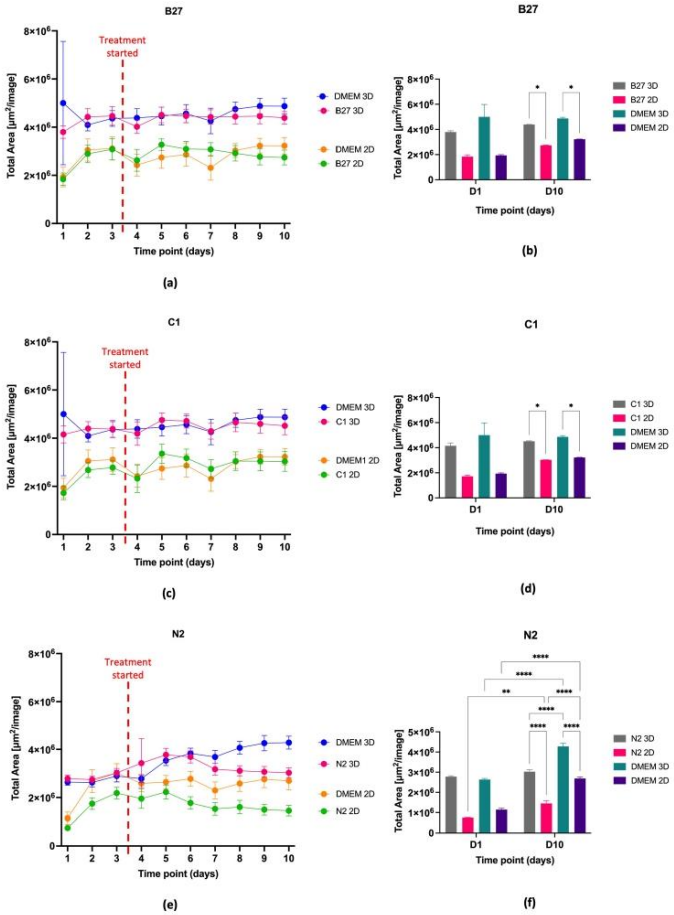


**Figure 2.** Cell confluence and proliferation over treatment course. Dot graphs show cell confluence and proliferation over time as measured by total cell area in 2D and 3D (large plug) culture for cells treated with (**a**) B27; (**c**) C1; and (**e**) N2. Bar graphs show the proliferation changes of the cells measured as total cell area comparing D1 and D10 in both 2D and 3D (large plug) for (**b**) B27; (**d**) C1; and (**f**) N2. No statistical significance $p > 0.05$; statistical significance *, $p \leq 0.05$; statistical significance **, $p \leq 0.01$; statistical significance ****, $p \leq 0.0001$; interactions not shown in bar graph are not significant.

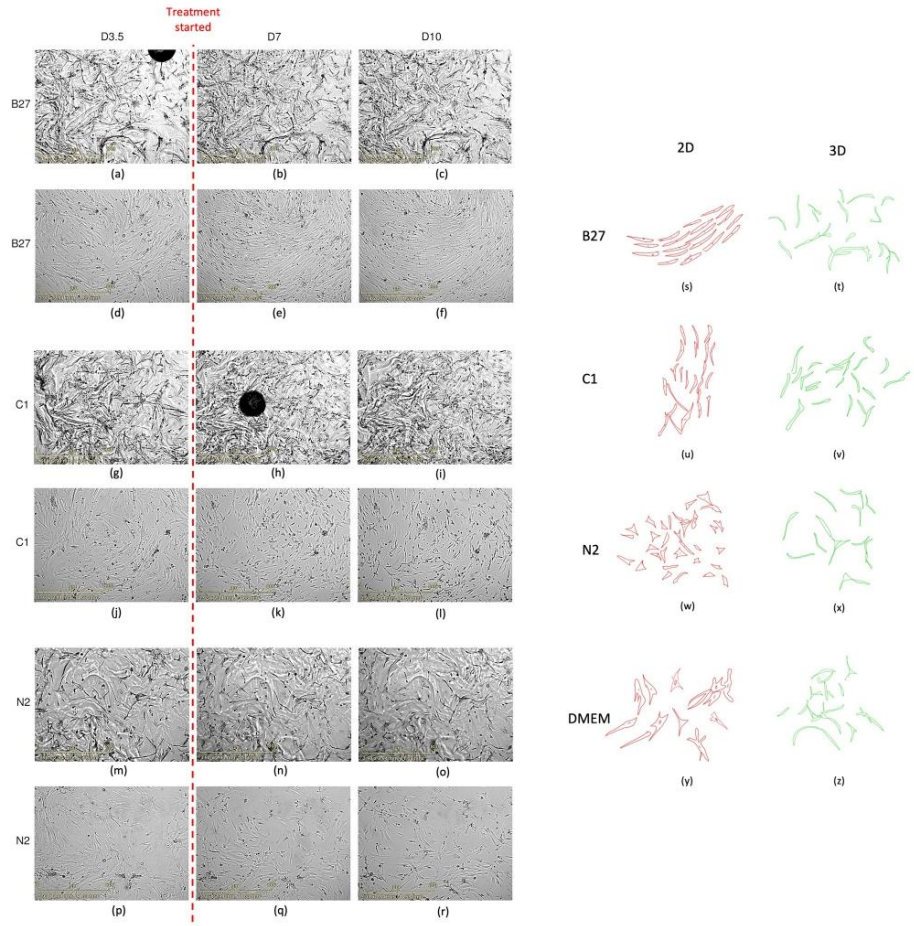


**Figure 3.** Live cell imaging over course of treatment. (**a**–**r**) Representative live cell images at time points D3.5, D7, and D10 for both 2D- and 3D-cultured cells. (**a**–**c**) B27 3D; (**d**–**f**) B27 2D; (**g**–**i**) C1 3D; (**j**–**l**) C1 2D; (**m**–**o**) N2 2D; and (**p**–**r**) N2 3D. The black round artefacts are bubbles. (**s**–**z**) Graphical representation of cell morphology changes between 2D and 3D cells in each treatment. These were manually drawn by tracing the cell shapes on a digital tablet. Scale bar in yellow is 800 µm.

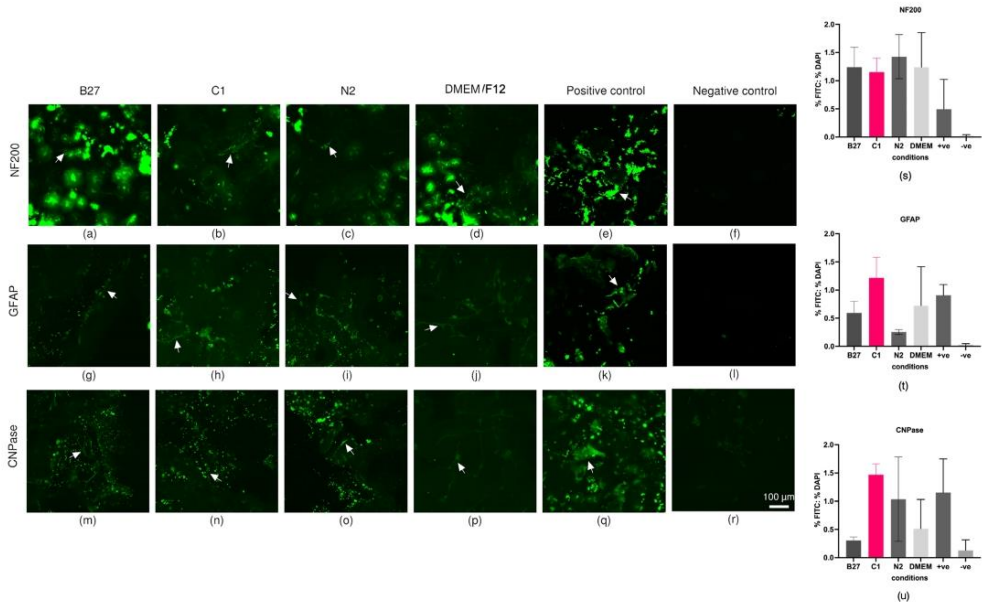


**Figure 4.** (**a**–**r**) Immunocytochemistry imaging. Representative maximum intensity projection confocal microscopy images of immunocytochemistry staining of ADSCs treated with either B27, C1, N2, or DMEM in 3D with respective positive and negative staining controls for antibody markers CNPase, NF200, and GFAP. Cells were imaged with a Nikon A1R inverted microscope using an S Plan Fluor LWD 20× 0.7NA objective. Fluorescence was captured with a laser at 488 nm excitation and GaAsP detector (500–550 nm) for AlexaFluor488-conjugated secondary antibodies (green). Scale bar = 100 µm. Note that control cells are smaller than ADSCs. Green speckles are unspecific staining and were excluded during analysis. White arrows show examples of positive cell staining. (**s**–**u**) Immunocytochemistry marker expression for 3D cells in each treatment with B27, C1, N2, and DMEM. Marker expression was measured from sum intensity projections of wide-field fluorescence images of the whole 3D plug and is displayed as the fraction of the percentage area of FITC (AlexaFluor488-conjugated secondary antibody) over the percentage area of DAPI-labelled nuclei. One-way ANOVA with multiple comparison was conducted using Bonferroni's multiple comparison test. No statistical significance ($\alpha = 0.05$) was detected.

Notably, StringDB analysis for the proteins identified for each treatment and treatment overlap revealed a range of identified proteins that were related to neural functions (Figure 6).

StringDB analysis of B27-treated cells revealed 91 proteins annotated as involved in functions associated with the brain, 14 proteins involved in brain cell lines, and 10 proteins in axon guidance, with more than half of these increasing in abundance (Figure 7a). C1 treatment String analysis revealed 87 proteins annotated as involved in the brain, 6 proteins involved in brain cell lines, and 14 proteins involved in the forebrain, with more than half of these increasing in abundance (Figure 7b). N2 treatment String analysis revealed 82 proteins annotated as involved in the brain, 83 proteins involved in the nervous system, and 16 involved in axon guidance, with more than half of these decreasing in abundance (Figure 7c).

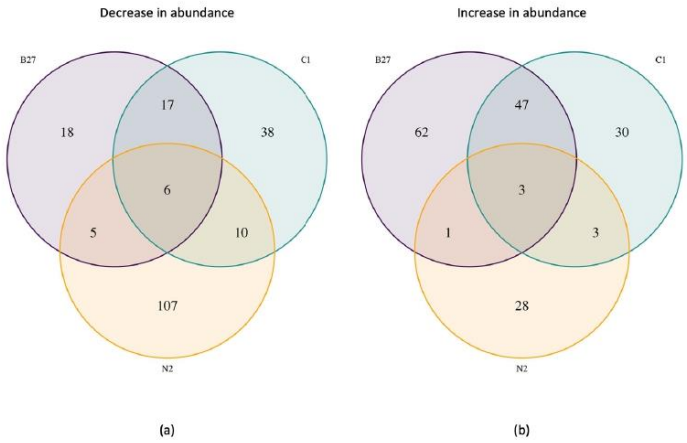


**Figure 5.** Count of proteins that have (**a**) decreased or (**b**) increased in each treatment (3D) compared to the DMEM control (3D).

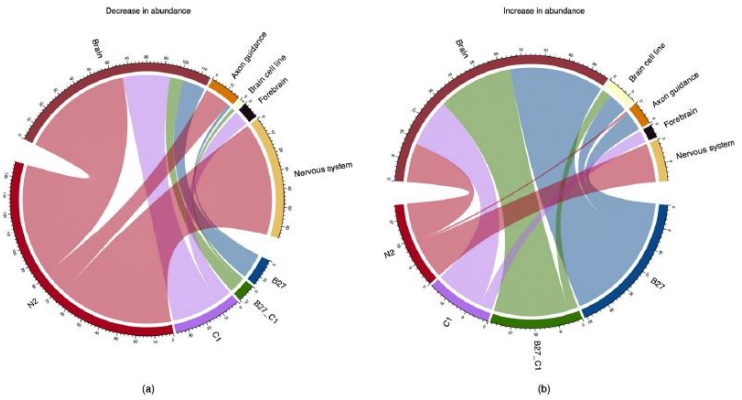


**Figure 6.** Chord diagram visualising the total number of proteins involved in different neural processes in each treatment with (**a**) being proteins with fold changes $\leq -1.5$ and (**b**) being proteins with fold changes $\geq 1.5$. Numbers associated with the neural function segments (top) indicate the count of proteins associated with the given neural function. Numbers associated with treatment segments (bottom) should be interpreted with caution; these indicate the count of neural functions within a given treatment (a protein corresponding to multiple neural functions will be counted multiple times accordingly).

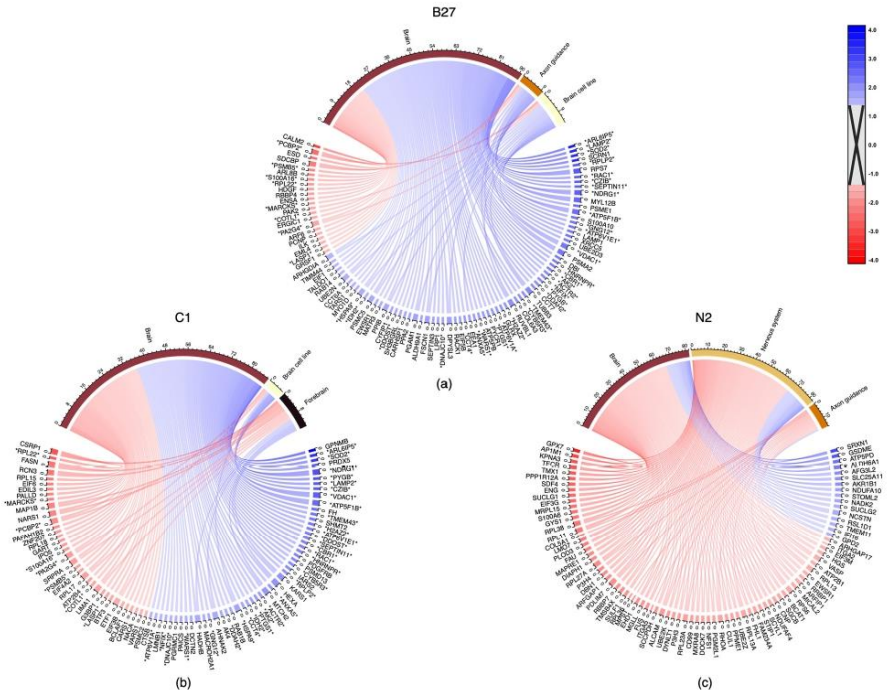


**Figure 7.** Names of proteins associated with ≥1.5-fold change or ≤−1.5-fold change (bottom) and implicated in potential neural functions by 3D treatment (top) with (**a**) B27, (**b**) C1, and (**c**) N2. Colours for a given gene indicate the relative fold change in comparison to the negative control (3D DMEM), where red indicates a negative fold change and blue indicates a positive fold change. Where a protein has a wider section allocated, this protein can be seen linked to multiple functions (e.g., CRSP1, the first protein (clockwise) in C1 treatment). * Asterisks appending and prepending protein names indicate those which that are present in both C1 and B27 (no overlap of proteins was detected among other treatment combinations).

## 3. Discussion

The aim of this study was to examine the effects of the neural culture supplements B27, C1, and N2 on ADSCs grown in a 3D environment. Our previous work and the literature more broadly demonstrate that ADSCs grown in traditional 2D culture with neural culture supplements exhibit changes consistent with neural differentiation [31]. Similarly, ADSCs grown in a 3D culture system have shown a degree of differentiation toward neural cell subtypes with the expression of neural markers [30]. Thus, it was hypothesised that the supplements would further enhance neural differentiation of the ADSCs grown in 3D and there would be biological differences and changes in the expressed proteome indicative of this. The data obtained support the hypothesis that the supplements enhanced neural differentiation in the ADSCs grown in 3D compared to the untreated 3D cells. The supplements had a range of observable effects on the ADSCs with changes in proliferation, surface marker expression, and the wider proteome.

### 3.1. Cell Viability and Confluence during Supplement Treatment

Similarly, to our previous work [30], the cells grown in PEG-based 3D matrices did not experience a statistically significant decrease in viability or proliferation. In addition, treatment with either B27, C1, or N2 had no statistically significant effect on the viability and proliferation of the 3D-grown cells over the treatment course. Cell viability and confluence remained unchanged for B27- (Figures 1a,b and 2a,b), C1- (Figures 1c,d and 2c,d), and N2-treated (Figures 1e,f and 2e,f) cells in 3D when compared to the beginning of treatment. While cell coverage fluctuated over time, there was no difference between beginning and end time points, indicating that the treatments have not compromised cell health and are not negatively impacting cell growth. It is important to note, however, that while there is no statistically significant decrease or increase in cell confluence, supplements have slowed down cell growth. It is known that as stem cells start to differentiate, proliferation decreases, and as neural cells mature, they reach the $G_0$ cell cycle stage, where division stops [32]. When looking at DMEM 3D control cells, these have shown a significant increase in confluence over time (Figure 2e,f), similar to that previously reported [30]. While the treated cells' proliferation may not have significantly decreased from when treatment started, no increase in proliferation is a sign of metabolic activity slowing down. Furthermore, the proteomics data showed that proliferating cell nuclear antigen (PCNA), a protein that regulates proliferation throughout the cell cycle [33], decreased in 3D B27 ($-0.54$-fold) and in 3D C1 ($-0.777$-fold) compared to the DMEM 3D control, supporting that the cell proliferation is slowing down in B27 and C1 compared to the DMEM 3D control.

In summary, Alamar blue and cell confluence results suggest that cell treatment has not caused significant cell loss. Still, the cell proliferation is slowing down compared to DMEM 3D control counterparts after 10 days of treatment, which may be a sign of cells starting to commit to a lineage.

### 3.2. Morphological Changes during Supplement Treatment

Cell morphology is an important aspect to consider in cell culture as it provides important information on cell changes and health [34]. Furthermore, the cell environment also plays an important role in cell functions, differentiation, migration, and morphology [35].

While no distinct morphological changes can be observed between treatments and the 3D DMEM control, cell morphology did change in 3D compared to 2D grown samples, similar to our previous work [30]. It is known that cells in 3D growth environments differ significantly morphologically and physiologically from their 2D-grown counterparts, with spatial and physical aspects of 3D cultures influencing gene expression and cellular behaviour through signal transduction from the outside in rather than inside out [22]. Two-dimensionally grown untreated ADSCs normally present an irregular fibroblastic-like morphology appearing as large, flattened cells with centrally located nuclei (Figure 3d,j,p). When these cells are placed in a PEG-based 3D matrix, their cytoskeleton rearranges [30]; cells become elongated, with a more condensed cytoplasm, lower nuclei-to-cytoplasm ratio, and spindle-like morphology. They also present clear networks and branch out; morphological features normally seen in neural cells. These morphological changes have also been observed in 2D-grown ADSCs treated with B27, C1, and N2 [31].

We previously showed that the PEG-based matrix alone started to direct cells towards a neural pathway with significant structural changes [30], suggesting that the exposure of ADSCs to supplements in the current study did not further enhance the neural morphological changes. This may be due to the timeframe used in these experiments, and more time points for 3D need to be explored. Additionally, morphological changes between treatments in 3D are likely more subtle than those observed between 2D and 3D treatments we have previously undertaken [30].

Additionally, it is important to note that 3D morphology and arrangement changes are harder to visually assess, given the nature of 3D constructs and images only showing one slice of the Z plane. Therefore, more subtle morphology changes potentially induced by the treatments cannot effectively be visually assessed by imaging in the same way that

morphology changes in the 2D samples can be. Equipment limitations may also impact the ability to obtain more robust images for morphology assessment. The microscope available for high-content live cell imaging in this work is not able to perform Z-stacks, and higher-magnification images were not able to be obtained due to the working distance of the objectives and the height of the gels. This highlights the need for more robust and accessible protocols and equipment in live microscopy for 3D tissue culture.

### 3.3. Neural Surface Marker Expression Changes

The nature of the hydrogels presented difficulties in minimising non-specific staining. Despite many optimisation steps and added washing steps to the protocol, unbound antibodies are likely to be retained within the gel during staining. These presented as speckles within the images and were removed during analysis based on size and staining intensity (see Section 4.1), however, it further highlights the need for more robust staining protocols for 3D samples.

Immunocytochemistry results showed that treatment of ADSCs in PEG-based 3D matrices with B27, C1, and N2 did not significantly increase neural marker expression in the time frame they were treated.

While not statistically significant, it is important to note that C1 treatment caused the greatest increase in CNPase and GFAP marker levels that are biologically relevant and in line with that previously reported in the 2D experiments [31]. Similarly, N2 had the greatest increase in the NF200 neuronal marker and showed increased levels of CNPase and GFAP, analogous to previous 2D experiments [31], indicating that C1 cells may be differentiating towards a glial lineage. Additionally, proteomics data detected CNPase in the samples, however, the amounts detected were not significant when compared to the 3D DMEM controls.

Three-dimensional environments provide a more realistic and heterogeneous growth and unequal cell exposure to oxygen, nutrients, and treatments, creating a gradient of medium availability completely different to that in 2D environments [21,36,37]. This means that cells grown in 3D are potentially exposed to different amounts of treatments depending on their location within the gels and depending on the treatment's ability to diffuse through the gel effectively [21,36,37]. It is likely that the effects on the cells from the treatments have been less/slower due to the nature of the 3D environment, and treatment diffusion through the matrix may mean that cells in 3D matrices require longer exposure times. It is also possible that the unequal cell exposure to the treatments may have created different cell populations at different stages of growth and differentiation. In 2D cultures, cells proliferate at similar rates, while in 3D cultures, it is normal to have a mixture of cells at different stages in the cell cycle [22] and the low numbers of markers detected may be due to only certain cell populations expressing them. In the future, single-cell proteomics methodologies will shed more light on cell-to-cell differences due to their location in the 3D environment.

Additionally, GFAP and NF200 are mature cell markers, and the ADSCs may not yet be at a differentiation stage where they are abundantly expressed and detectable by untargeted proteomics methodologies, given that neural cells take up to 108 embryonic days to differentiate into cortical neurons [38]. Nevertheless, these findings, while not statistically significant, are of biological significance in understanding how cells change and respond to treatment in 3D environments.

### 3.4. Analysis of Proteome Changes across Supplement Cells

Proteome analysis showed that all treatments caused changes in the cells, including changes in abundance of proteins annotated as being involved in neural processes (Figures 6 and 7). Interestingly, most proteins involved in these processes were unique for each treatment. B27 and C1 treatments caused abundance changes in the same 39 proteins involved in neural processes by ±1.5-fold (Log2). Additionally, B27 treatment caused abundance changes in an additional 57 proteins involved in neural processes by ±1.5-fold

(Log2) and C1 treatment caused ±1.5-fold (Log2) abundance changes in an additional 49 proteins involved in neural processes. N2 treatment caused changes in the abundance of 86 unique proteins involved in neural processes by at least ±1.5-fold (Log2) with no other neural-related proteins shared with any other treatment (Figures 6 and 7).

#### 3.4.1. Proteome Changes Common in B27 and C1

B27 and C1 treatment proteome analysis revealed similar proteins increasing and decreasing in abundance that are annotated as being related to neural processes, suggesting changes are occurring in similar pathways.

Of particular interest is ARL6IP5 which increased in abundance with B27 by 3.71-fold (Log2) and with C1 by 3.40-fold (Log2). ARL6IP5 is a protein involved in the neurotransmitter release cycle and regulates intracellular concentrations of taurine and glutamate via SLC1A1/EAAC1 [39]. Taurine plays a role in neural development, osmoregulation, and neural protection with taurine transporters found in glutaminergic neurons [40–42]. Glutamate is the most abundant free amino acid in the brain and the major excitatory neurotransmitter in the central nervous system (CNS) [43], and it plays an important role in memory, neuronal development, and synaptic plasticity [44,45] Furthermore, increased expression of ARL6IP5 has been shown to induce neuronal differentiation and has been found to increase neurite length [46].

RAC1 is a neural surface antigen involved in the nerve growth factor receptor signalling pathway. It regulates many cellular responses, such as proliferation differentiation and neuronal maturation during hippocampus development [47]. It also plays a role in neuron adhesion, migration, and differentiation, dendritic spine formation, and synaptic plasticity in neurons [48] and was also found to be increased in abundance in both B27 and C1 treatments; it increased by 2.79-fold (Log2) in B27 and by 2.24-fold in C1. RAC1 is known to also play a role in regulating GABA (A) receptor synaptic stability through its role in PAK1 activation [48] and has a crucial role in dendritic growth and dendritic spine maturation through the Cdc42/Rac pathway [47,49]. Additionally, SEPTIN11, also known to be involved in neuronal cytoarchitecture for its role in dendritic arborisation and dendritic spines and GABAergic synaptic connectivity [50,51], was also increased with both B27 and C1 by 2.75-fold (Log2) and 2.25-fold (Log2), respectively. ATP6V1A protein also plays a role in neurite development and synaptic connectivity [52] and increased by 1.93-fold (Log2) with B27 and by 1.51-fold (Log2) with C1.

Lastly, NDRG1 protein, known to have a role in hormone responses, cell growth, and differentiation [53], was also found to be increased in both treatments, increasing by 2.66-fold (Log2) with B27 and by 2.94-fold (Log2) with C1. Furthermore, it has a role in cell trafficking in Schwann cells, and it is an essential protein for the maintenance and development of the peripheral nerve myelin sheath [53].

In summary, the identification of these proteins in both B27- and C1-treated cells suggests that the treatments have enhanced neural marker expression further than just the 3D environment alone in the given time frame. Furthermore, these proteins have the potential to be utilised as markers for neural differentiation of ADSCs.

#### 3.4.2. Proteome Changes Unique to B27 Treatment

In B27-treated cells, β3-tubulin (TUBB3) increased by 2.08-fold (Log2) from the 3D DMEM control. This is particularly interesting given that TUBB3 had been previously seen to increase in 3D DMEM when compared to 2D DMEM cells, showing that the environment alone increased the marker [30]. The further increase in TUBB3 observed in the 3D B27-treated cells in this study suggests that B27 treatment had a further effect on TUBB3 protein levels in the cells. β3-Tubulin is a well-known marker for early neural development; it is a major component in the neuronal cytoskeleton and is highly expressed during neural development, playing a role in maintenance, maturation, and proper axon guidance [54–58]. Similarly, DPYSL3, a necessary protein for signalling and cytoskeleton remodelling, was found to increase by 1.8-fold (Log2) with B27. It also plays a role in

axon guidance, neuronal growth, cone collapse, and cell migration [59]. Furthermore, FSCN1 is an actin-bundling protein that is involved in the reorganisation of the actin cytoskeleton filopodia formation and axon growth cone collapse in response to nerve growth factor [60,61]. In the B27 treatment, FSCN1 increased by 1.76-fold (Log2) and its expression in the nervous system is known to increase during development and decrease after maturation [62], suggesting that the cells may be in an early neural developmental stage. CYFIP1 was also found to be increased by 1.67-fold (Log2) in B27 treatment. This particular protein plays a role in lamellipodia formation and axon outgrowth, and it is part of the WAVE complex, which regulates actin filament reorganization, also regulated by RAC1 [63] (which is also increased with B27 and C1 and addressed above). The increase in abundance of these proteins suggests that there are notable changes occurring in the cytoskeleton of the cells towards the formation of axons and that similar pathways for axon formation and cytoskeleton remodelling are being activated by B27 treatment in the ADSCs in the 3D environment.

Additionally, the increase in SEPTIN proteins in B27 treatment suggests changes in the neurodevelopment realm. SEPTIN proteins contribute to neurodevelopment and neuronal functions in the mammalian nervous system [64], with SEPTIN3 being highly expressed in the brain [65]. SEPTIN3 protein is involved in presynaptic plasticity via the cGMP/PKG pathway, and its expression is developmentally regulated as nervous system development increases [65] and it is predominantly abundant in nerve terminals and presynaptic and synaptic vesicles [65,66]. SEPTIN3 increased in abundance by 1.77-fold (Log2) with B27 together with SEPTIN11. As previously mentioned, SEPTIN11 increased with both B27 and C1, and it plays an important role in neuroarchitecture and dendrite formation [50,51]. Furthermore, LRP1 also increased by 1.79-fold (Log2) and is a membrane receptor found in neurons. It is involved in calcium signalling and neurotransmission [67] and is essential in neural development through extracellular signal transduction and intracellular signal propagation modulation [68], suggesting further development of the cytoarchitecture of neurons.

Lastly, COL6A3 (collagen VI) also increased by 2.03-fold (Log2). Collagen IV is a major protein found in the nervous system; it acts as a regulator for Schwann cell differentiation and is essential for nerve myelination preservation, function and structure, and for assisting in nerve regeneration after injury [69]. Immunocytochemistry analysis detected the CNPase marker, a well-known oligodendrocyte and myelin marker [70], suggesting the cells may start to express myelination markers.

In summary, the proteomics data for B27-treated cells suggest that B27 treatment did enhance the neural marker expression further than just the 3D environment alone in the given time frame.

#### 3.4.3. Proteome Changes Unique to C1 Treatment

In addition to the above-mentioned proteins found to be increased with both B27 and C1, C1 treatment was also associated with an increase in some proteins of interest not observed in other treatments.

PDGFRB increased in abundance by 2.18-fold (Log2) in C1-treated cells. Platelet-derived growth factors (PDGFs) and their receptors (PDGFRs) are essential proteins expressed in embryonic and mature nervous systems in neural progenitor cells, neurons, astrocytes, and oligodendrocytes [71]. They play a role in neural development and cell maintenance in the nervous system [71]. PDGF-mediated signalling has a role in regulating CNS functions such as neurogenesis, cell survival, synaptogenesis, and neuronal development [72]. Specifically, PDGFRB plays a crucial role in neuroprotection, tissue repair, and functional recovery through signalling neurons and astrocytes, as well as a role in CNS development and vascularisation [72], further supporting that the cells are committing to a neural lineage.

Additionally, DCTN2 increased in C1-treated cells by 1.61-fold (Log2), a protein that has been found to play a key role in brain development, specifically in synapse

formation [73,74], further supporting changes towards synapse and dendrite formations in the cells.

In summary, the proteomics data for C1-treated cells suggest that C1 treatment did enhance the neural marker expression further than just the 3D environment alone in the given time frame. It is important to remember that C1 is a commercially available supplement designed to enhance the support of NSCs to neurons whilst minimising the persistence of progenitor cells, and when used with ADSCs it may promote the maturation of the cells.

#### 3.4.4. Proteome Changes Unique to N2

N2 proteome analysis showed a different proteome profile with no overlap with the other treatments in proteins related to neural processes, with most neural-related proteins decreasing in abundance, indicative that the treatment may not be enhancing neural development like the other treatments are. Furthermore, some of the proteins enhanced by the treatment seem to be involved in neurodegeneration. For example, GSDME was increased in abundance by 2.61-fold (Log2) and is a protein involved in mitochondrial dysfunction, axon loss, and neurite retraction and is thought to contribute to neurodegeneration [75]. Furthermore, mutations to AFG3L2 are associated with spinocerebellar ataxia involving loss of Purkinje cells [76]. Another protein which was found to increase by 2.06-fold (Log2) in N2 treatment is NCSTN, which has been linked to Alzheimer's disease through its involvement in amyloid formation [77].

Nevertheless, it is important to note that these were short experiments with non-neuronal cells. The protein abundance profile should be further assessed for longer periods of time. Furthermore, these supplements are intended to support mature neuronal cells, and those mechanisms may be suppressing differentiation in these cells. N2, particularly, is designed for long-term support of differentiated cells, so longer time periods may be required to see more definitive changes.

In conclusion, cell proliferation, viability, immunocytochemistry, and proteomics analysis looking specifically at proteins related to neuronal processes in ADSCs treated with B27 and C1 indicates that those supplements are pushing them further down a neuronal pathway, suggesting that supplementation is a useful addition to 3D culture for the neural differentiation of ADSCs. On the other hand, however, N2 treatment did not reduce cell proliferation or show proteome changes indicative of enhanced neural marker expression similar to B27 and C1 in that short time. Ideally, these experiments should be repeated for a longer period with treatment combinations also being explored.

## 4. Materials and Methods

hADSCs from a single donor were isolated and expanded as previously described [12] with approval from the UTS Human Research Ethics Committee (ethics number 2013000437). Written informed consent was acquired for donor lipoaspirate release for research purposes only. After isolation, and prior to experiments, the cells were maintained in DMEM/F12 + Glutamax media (Gibco, Life Technologies, Carlsbad, CA, USA) with 10% heat inactivated FBS (Gibco, Life Technologies, Carlsbad, CA, USA) and incubated at 37 °C at 5% $CO_2$. Cells used for these experiments were between passages five and ten.

At passage five to ten, cells were lifted from the tissue culture flasks using TrypLE express (12604 Gibco, Life Technologies, Roskilde, Denmark) and prepared for bioprinting following the manufacturer's instructions.

Once the cells were replated in 2D or bioprinted, they were maintained in similar conditions as above for 84 h before treatment, starting with the addition of 1% antibiotics/antimycotics (ABAM, Gibco life technologies, Carlsbad, CA, USA) to maintenance media and treatments. There were a total of three experimental groups and one undifferentiated control group. The groups consisted of hADSCs treated with the treatments B27, N2, CultureOne (C1), and DMEM (undifferentiated control), respectively (Table 1). Control cells were also included. The experimental design is outlined in more depth in

Table 1. Media were changed every 84 h following the experimental design from Table 1 and incubated at 37 °C at 5% $CO_2$. The 2D cells were added as a viability control.

**Table 1.** Outline of experimental treatments and cell types.

| Treatment | Cell Type | Base Media | Supplement |
|---|---|---|---|
| B27 | hADSC | Neurobasal media | 1% B27 supplement |
| CultureOne | hADSC | Neurobasal media | 1% CultureOne (C1) |
| N2 | hADSC | Neurobasal media | 1% N2 supplement |
| DMEM (undifferentiated control) | hADSC | DMEM/F12 + Glutamax—control media | 10% FBS |
| Positive Staining controls | SHSY-5Y or U87MG | DMEM/F12 + Glutamax—control media | 10% FBS |
| Negative staining controls | hADSC | DMEM/F12 + Glutamax—control media | 10% FBS |

*4.1. The 3D Bioprinting of hADSCs in PEG-Based Hydrogels*

hADSCs were 3D printed in a PEG-based hydrogel using a RASTRUM bioprinter (Inventia, Sydney, Australia). The cell plugs were printed into 96-well plates following the manufacturer's instructions using the same protocol and matrices as previously described in Pelegri et al., 2023, with 24 plugs printed for each treatment for downstream analysis [30].

In brief, a large plug and imaging plug were printed at ~1.1 kPa containing RGD and YIGSR peptides (matrix code PX02.21P). RGD and YIGSR were included in the system given that the peptide trimer RGD is found in collagen, laminin, and fibronectin, which mediates the adhesion of many cells, including neurons [78], and laminin-derived (YIGSR) peptide is known to promote neuronal cell binding [79].

Cells were seeded at a concentration of 10 million/mL. The imaging plug consisted of a small volume of hydrogel with embedded cells in the centre of the well measuring 0.5 mm in height and 2.2 mm in diameter (Figure 8a). The large plug occupied the well completely, measuring 0.5 mm in height and 5 mm in diameter (Figure 8b). The 2D-seeded cells were also included as morphology and viability controls. Cells were lifted from the tissue culture flasks using TrypLE express (12604 Gibco, Life Technologies, Roskilde, Denmark) and replated into 96-well plates in 2D conditions at 10 million/mL, the same concentration as 3D cells. These were grown in parallel and treated the same way. The only difference was the 3D construct vs. 2D environment.

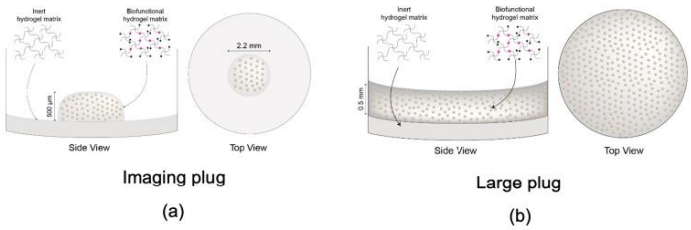


**Figure 8.** Visual representation and dimensions of the different constructs provided by Rastrum. (**a**) Smaller plug, referred to as imaging plug used for immunocytochemistry; (**b**) Larger plug, referred to as large plug (used for viability assays, live cell imaging, and proteomics. Graphics reproduced from Pelegri et al., 2023.

Positive controls for immunocytochemistry were included and printed in parallel to the ADSCs following the same method. These are further explained in Immunocytochemistry Section 4.4.1.

### 4.2. Cell Morphology: Incucyte Imaging

Live images were taken every 24 h using the organoid programme in the Incucyte® S3 Live-Cell Analysis Instrument (Sartorius, Göttingen, Germany) for 10 days following the same methods as Pelegri et al., 2023 [30].

In brief, cell confluence was assessed as the area covered by cells in each image ($um^2$/image). This was conducted using the instrument's inbuilt analysis software. Parameters were set to: radius 200; sensitivity 70; edge sensitivity 0; hole fill ($um^2$) 500; adjust size (pixels) 0. After the initial analysis was finalised by the instrument, all images at all time points were manually checked for artifacts that would not accurately represent the confluence. Common artifacts found in the images were glares and bubbles which prevented the camera from taking an accurate photo of the cell coverage. Further analysis and graphing were performed using the data exported from the Incucyte® proprietary software (version 2022B Rev2). Averages of total area for wells of each cell type and per time point, with associated standard deviations for both for 2D and 3D models, were plotted. The dataset was assessed for normality using Shapiro–Wilk test and statistical significance was subsequently determined using parametric two-way ANOVA with Tukey's multiple comparisons. GraphPad PRISM software (version 10.0.3) was used for data visualisation (Figure 3).

### 4.3. Cell Viability and Proliferation: Alamar Blue

Cell viability assay was performed at 3 different time points: D3.5, D7, and D10.5, using an Alamar blue assay. Alamar blue is a non-toxic cell viability assay that detects metabolically active cells. When Alamar blue is added to cells, if cells are metabolically active, the main active ingredient, resazurin, is reduced to resorufin, and the solution becomes red in colour and highly fluorescent.

Alamar blue (10% in media) was added to the cells and left to incubate for 16 h to allow enough time to penetrate through the 3D matrices. To keep variables to a minimum, the same was carried out on the 2D cells. Negative control wells were included; these only contained the Alamar blue and clean media mixture. After the incubation period, the Alamar blue and media mixture was transferred to a different 96-well plate to keep the cellular growth environment as undisturbed as possible from outside factors. The collected Alamar blue media were measured using the fluorescence bottom-up mode in a Tecan M200Plate Reader (Tecan, Männedorf, Switzerland) using 530–560 nm excitation and 590 nm emission wavelengths. The results were averaged across the 96 wells, and data were normalised to the negative controls. The data were analysed as fold change ratio values from D3.5. The dataset was assessed for normality using the Shapiro–Wilk test, and due to the assumption not being met, a non-parametric Kruskal–Wallis test was performed to determine significance. GraphPad PRISM software was used for data visualisation (Figure 1).

### 4.4. Cell Characterisation

#### 4.4.1. Immunocytochemistry

Cells from the imaging plug were fixed using 10% formalin for 30 min prior to washing and storing in PBST + 0.1% $w/v$ sodium azide at 4 °C. For staining, cells were first placed in PBST (0.01 M PBS and 0.1% Triton X-100 (BDH #30632) at pH 7.4) for 1 h at room temperature. Primary antibodies were diluted in PBG (0.1 M PBS, pH 7.4, 0.1% Triton-X, 2% NGS, 1% BSA (Sigma Aldrich, St. Louis, MO, USA, #A9647)) and were added to the relevant wells and incubated at 4 °C for 3 days. Primary antibodies were rabbit anti-glial fibrillary acidic protein (GFAP) (1/500, Dako, Glostrup, Denmark #Z0334) as an astrocyte marker; mouse anti-2′,3′ cyclic-nucleotide 3′ phosphodiesterase (CNPase) (1/100 Abcam, Cambridge, UK #ab6319-100) as an oligodendrocyte marker; and mouse anti-neurofilament 200 (1/50, biosensis CM998100) as a mature neuron marker.

After primary antibody incubation was completed, cells were then washed with three changes of PBST for 30 min and incubated with goat anti-mouse AF488 (1/200,

Invitrogen, Carlsbad, CA, USA #A11001) or goat anti-rabbit AF488 (1/200, Invitrogen, #A11008) secondary antibodies in PBG for another 3 days at 4 °C. Following an additional two 20 min washes with PBST, cells were incubated with Hoechst (1/5000 Invitrogen) for 30 min to stain the nuclei and finally washed three times with PBST for another 30 min each and stored in antifade/glycerol at 4 °C until imaged.

Positive staining control cells at 10 million/mL conc were included in all staining runs. Glioblastoma U87MG cells were used for GFAP and CNPase positive staining controls. Neuroblastoma SHSY-5Y cells were used for NF200 positive staining controls. Both U87MG and SHSY-5Y cells were grown in separate plates to the experimental cells; however, the cells were grown and stained in parallel with the experimental plates for each antibody and were fixed and stained following the same protocol as the experimental cells. U87MG and SHSY-5Y cells were grown in a 96-well plate with DMEM/F12 + Glutamax media (Gibco, Baltimore, MA, USA) enriched with 10% heat-inactivated FBS (Sigma Aldrich) until confluent.

Wide-field fluorescence microscopy was performed using a Nikon Ti inverted microscope with a ×10 0.3 numerical aperture Plan Fluor objective, NIS Elements acquisition software (version 5.30.06) with a solid state Lumencor illumination source, and a Nikon DS-Qi2 CMOS camera. Six 1024 × 1024 fields of view were captured, covering the area of each imaging plug and stitched using the NIS Elements acquisition software with default overlap settings. Series of images were captured through the z dimension using a step size of 5.6 µm.

Wide-field fluorescence images were processed using the Clarify.ai algorithm using the NIS Elements acquisition software. FIJI (FIJI is just ImageJ) version 1.53 t [108] was used for image analysis. Where appropriate, Z-stacks were corrected for axial drift using the Linear Registration with SIFT plugin with an expected translation transformation. Sum intensity projections for FITC and DAPI channels were subjected to background subtraction with a rolling ball of 50 pixels, before being thresholded using the Li (FITC) or Triangle (DAPI) algorithm to create a binary mask and area fraction was measured. To eliminate non-specific secondary antibody aggregates from measurements, only particles with a pixel size larger than 100 pixels2 and a circularity of 0–0.8 were quantified. Marker expression was measured from sum intensity projections of wide-field fluorescence images of the whole 3D plug and is displayed as the fraction of the percentage area of FITC (AlexaFluor488-conjugated secondary antibody) over the percentage area of DAPI-labelled nuclei. One-way ANOVA with multiple comparisons was conducted using Bonferroni's multiple comparison test. No statistical significance $p > 0.05$; statistical significance *, $p \leq 0.05$; statistical significance **, $p \leq 0.01$; statistical significance ***, $p \leq 0.001$; statistical significance ****, $p \leq 0.0001$.

Representative images were captured using a Nikon A1R inverted confocal microscope (Nikon, Tokyo, Japan) with a ×20 0.7 numerical aperture LWD S Plan Fluor objective and NIS Elements acquisition software. AF488 was imaged with an excitation of 488 nm, and emission detected with a GaAsP detector at 500–550 nm. FITC was captured with a 488 nm laser intensity of 3.5, gain of 40, and offset of—3. Z-stacks were acquired with a step size of 3 µm. Fluorescence images were processed using the denoise.ai algorithm using the NIS Elements acquisition software, and maximum intensity projections were created. In Figure 4, the displayed dynamic range for FITC for 3D samples is 0–175, whilst for positive controls, the displayed dynamic range for FITC is 0–2000.

#### 4.4.2. Proteomics

Protein Extraction

Cells were released from the 3D large plugs using the Rastrum cell retrieval protocol provided by the company. In brief, media from printed 3D cell models were discarded, cells were washed with PBS, and cell retrieval solution was added to the wells. The wells were then incubated at 37 °C for 30 min. Cells were then collected by pipetting up and down in each well and then were transferred to the collection tubes. The wells were then

further washed with PBS and the remaining cells were combined in the tubes. Cells were then centrifuged and supernatant was removed. The cell pellets were then frozen until ready to be used for proteomics. Six wells were pooled to make one proteomics sample.

Once ready, samples were defrosted and resuspended in 1% SDC, 5 mM TCEP, 10 mM IAA, 100 mM HEPES pH 8.5, heated to 95 °C for 5 min, and incubated for an hour at room temperature. After the incubation, 0.1 ug of trypsin was added to 10 ug of sample and incubated at 37 °C overnight. The peptides were then recovered using the SDB-RPS-based stage tip column method, which is a modified protocol from Rappsilber et al. (2007). The cell digests were centrifuged at maximum speed for 5 min to digest any insoluble material. Then, 10× the volume of digest was added of SPE load buffer (90% acetonitrile, 1% trifluoroacetic acid). The sample was mixed by trituation and was then added to the stage tip column which contained 1 disc of SDB-RPS cut with an 18-gauge blunt-end needle. The liquid was centrifuged through the disc at 5000 rpm until all liquid moved through. Following this, two washing steps were performed to help wash any contaminants and salts from the column and bound peptides. Firstly, 100 µL of SPE load buffer was passed through at 5000 rpm until all liquid moved through followed by a second wash using 100 µL of SPE wash buffer (10% acetonitrile, 0.1% trifluoroacetic acid). After, the peptides were eluted directly into the injection vials by washing the column with 50 µL of SPE elution buffer (71 µL of 1 M ammonia solution, 800 µL of 100% acetonitrile, 129 µL of water) and centrifuging at 5000 rpm until all liquid passed through the column into the vials. The vials containing the peptides were then placed into a vacuum centrifuge (Savant DNA 120, SpeedVac Concentrator, Thermo Scientific, Carlsbad, CA, USA) to evaporate all liquid. Once samples were dry, the peptides were resuspended using 25 µL of MS loading solvent (2% acetonitrile, 0.2% trifluoroacetic acid) and samples were ready to be analysed by LC-MS/MS.

LC-MS/MS Analysis

Using an Acquity M-class nanoLC system (Waters, Milford, MA, USA), 5 µL of the sample was loaded at 15 µL/min for 3 min onto a nanoEase Symmetry C18 trapping column (180 µm × 20 mm) before being washed onto a PicoFrit column (75 µm × 350 mm; New Objective, Woburn, MA, USA) packed with SP-120-1.7-ODS-BIO resin (1.7 µm, Osaka Soda Co., Osaka, Japan) heated to 45 C at 300 nL/min. Peptides were eluted from the column and into the source of a Q Exactive Plus mass spectrometer (Thermo Scientific) using the following program: 5–30% MS buffer B (98% acetonitrile + 0.2% formic acid) over 90 min, 30–80% MS buffer B over 3 min, 80% MS buffer B for 2 min, 80–85% for 3 min. The eluting peptides were ionised at 2400 V. A data-dependent MS/MS (dd-MS2) experiment was performed, with a survey scan of 350–1500 Da performed at 70,000 resolution for peptides of charge state of 2+ or higher with an AGC target of $3 \times 10^6$ and maximum injection time of 50 ms. The top 12 peptides were selected and fragmented in the HCD cell using an isolation window of 1.4 $m/z$, an AGC target of $1 \times 10^5$, and maximum injection time of 100 ms. Fragments were scanned in the Orbitrap analyser at 17,500 resolution and the product ion fragment masses measured over a mass range of 120–2000 Da. The mass of the precursor peptide was then excluded for 30 s.

Data Processing and Analysis

Raw files from the Q Exactive Plus were searched using MaxQuant (version 2.0.3.0) hosted on the Galaxy Australia platform against the UniProt *Homo sapiens* database (downloaded on 23 March 2023) using the following specific parameters settings. Min. peptide length: 7. Max. peptide mass (Da): 4600. Min. unique peptides: 0. Calculate peak properties: false. Match between runs: true. Match time window (min): 0.7. Match ion mobility window: 0.05. Alignment time window (min): 20. Alignment ion mobility: 1. Match unidentified features: false. Include contaminants: true. Decoy mode: revert. PSM FDR: 0.01. Protein FDR: 0.01. Min. peptide length for unspecific searches: 8. Max. peptide length for unspecific searches: 25. Peptides for quantification: unique + razor. Use only

unmodified peptides: true. Separate LFQ in parameter groups: false. Stabilize large LFQ ratios: true. Require MS/MS for LFQ comparisons: true. Missed cleavages: 2. Fixed modifications: nothing selected. Variable modifications: oxidation (M) carbamidomethyl (C) deamination (NQ). Enzyme: trypsin/P. Digestion mode: semi-specific. Quantitation methods: LFQ. LFQ min. ratio count: 2. LFQ min. number of neighbours: 3. LFQ average number of neighbours: 6. Normalization type: classic.

The Protein Groups file from the MaxQuant search was then input in LFQ Analyst (Dev.) (https://bioinformatics.erc.monash.edu/apps/LFQ-Analyst/; accessed on 1 September 2023 [80]) for further analysis. LFQ analyst was set to a 0.05 *p*-value cutoff, 1.5 Log2 fold change cutoff with Perseus-type imputation, no normalization, and Benjamini–Hochberg FDR correction.

StringDB analysis was conducted using String V.11 using the following analysis parameters: Network type: full string network; meaning of network edges: evidence; active interaction sources: textmining, experiments, databases, co-expression, neighbourhood, gene fusion, co-occurrence; minimum required interaction score: medium confidence (0.400); max number of interactors to show: 1st shell—non/query proteins only. 2nd shell—none; network display mode: interactive SVG; network display options: disable 3D bubble design, disable structure previews inside network bubbles. Scripts used for data processing and visualisation of proteomic data are available on GitHub (https://github.com/maxlcummins/Pelegri_et_al_2023; accessed on 6 October 2023).

**Author Contributions:** Conceptualisation, J.S., N.G.P. and C.A.G.; methodology, J.S., N.G.P., M.P.P. and C.A.G.; formal analysis, N.G.P. and A.L.B.; investigation, N.G.P. and A.M.S.; resources, J.S., B.K.M. and M.P.P.; data curation, N.G.P. and A.M.S.; writing—original draft preparation, N.G.P.; writing—review and editing, all; visualisation, N.G.P., A.M.S. and M.L.C.; supervision J.S., M.P.P. and C.A.G.; project administration, J.S.; funding acquisition, J.S. and B.K.M. All authors have read and agreed to the published version of the manuscript.

**Funding:** This research was partially funded by the Schwartz Foundation philanthropic donation to support research.

**Institutional Review Board Statement:** The study was conducted according to the guidelines of the Declaration of Helsinki and approved by Human Research Ethics Committee of University of Technology Sydney UTS-HREC Santos-2013000437, 21 June 2013.

**Informed Consent Statement:** Informed consent was obtained from all subjects involved in the study.

**Data Availability Statement:** Proteomics LFQ analyst data, String data, and scripts used for data processing and visualization of the proteomics experiments are available on GitHub (https://github.com/maxlcummins/Pelegri_et_al_2023; accessed on 6 October 2023).

**Acknowledgments:** The authors acknowledge the use of the Nikon A1R inverted confocal and Nikon Ti inverted wide-field fluorescence microscopes in the Microbial Imaging Facility at the AIMI in the Faculty of Science, the University of Technology Sydney.

**Conflicts of Interest:** The authors declare no conflict of interest.

## References

1. Gimble, J.; Guilak, F. Adipose-derived adult stem cells: Isolation, characterization, and differentiation potential. *Cytotherapy* **2003**, *5*, 362–369. [CrossRef] [PubMed]
2. Jang, S.; Cho, H.H.; Cho, Y.B.; Park, J.S.; Jeong, H.S. Functional neural differentiation of human adipose tissue-derived stem cells using bFGF and forskolin. *BMC Cell Biol.* **2010**, *11*, 25. [CrossRef]
3. Park, J.; Lee, N.; Lee, J.; Choe, E.K.; Kim, M.K.; Lee, J.; Byun, M.S.; Chon, M.W.; Kim, S.W.; Lee, C.J.; et al. Small molecule-based lineage switch of human adipose-derived stem cells into neural stem cells and functional GABAergic neurons. *Sci. Rep.* **2017**, *7*, 10166. [CrossRef] [PubMed]
4. Wislet-Gendebien, S.; Wautier, F.; Leprince, P.; Rogister, B. Astrocytic and neuronal fate of mesenchymal stem cells expressing nestin. *Brain Res. Bull.* **2005**, *68*, 95–102. [CrossRef]
5. Tsuji, W.; Rubin, J.P.; Marra, K.G. Adipose-derived stem cells: Implications in tissue regeneration. *World J. Stem Cells* **2014**, *6*, 312–321. [CrossRef]

6. Wankhade, U.D.; Shen, M.; Kolhe, R.; Fulzele, S. Advances in Adipose-Derived Stem Cells Isolation, Characterization, and Application in Regenerative Tissue Engineering. *Stem Cells Int.* **2016**, *2016*, 3206807. [CrossRef] [PubMed]
7. Strioga, M.; Viswanathan, S.; Darinskas, A.; Slaby, O.; Michalek, J. Same or not the same? Comparison of adipose tissue-derived versus bone marrow-derived mesenchymal stem and stromal cells. *Stem Cells Dev.* **2012**, *21*, 2724–2752. [CrossRef]
8. Rad, A.A.; Heidari, M.H.; Aliaghaei, A.; Broujeni, M.E.; Shojaei, A.; Abbaszadeh, H.-A. In vitro differentiation of adipose derived stem cells into functional dopaminergic neurons. *Biomed. Pharmacol. J.* **2017**, *10*, 595–605.
9. Ahmadi, N.; Razavi, S.; Kazemi, M.; Oryan, S. Stability of neural differentiation in human adipose derived stem cells by two induction protocols. *Tissue Cell* **2012**, *44*, 87–94. [CrossRef]
10. Soheilifar, M.H.; Javeri, A.; Amini, H.; Taha, M.F. Generation of Dopamine-Secreting Cells from Human Adipose Tissue-Derived Stem Cells In Vitro. *Rejuvenation Res.* **2018**, *21*, 360–368. [CrossRef]
11. Faghih, H.; Javeri, A.; Amini, H.; Taha, M.F. Directed differentiation of human adipose tissue-derived stem cells to dopaminergic neurons in low-serum and serum-free conditions. *Neurosci. Lett.* **2019**, *708*, 134353. [CrossRef] [PubMed]
12. Santos, J.; Milthorpe, B.K.; Herbert, B.R.; Padula, M.P. Proteomic Analysis of Human Adipose Derived Stem Cells during Small Molecule Chemical Stimulated Pre-neuronal Differentiation. *Int. J. Stem Cells* **2017**, *10*, 193–217. [CrossRef] [PubMed]
13. Santos, J.; Hubert, T.; Milthorpe, B.K. Valproic Acid Promotes Early Neural Differentiation in Adult Mesenchymal Stem Cells Through Protein Signalling Pathways. *Cells* **2020**, *9*, 619. [CrossRef]
14. Santos, J.; Dalla, P.V.; Milthorpe, B.K. Molecular Dynamics of Cytokine Interactions and Signalling of Mesenchymal Stem Cells Undergoing Directed Neural-like Differentiation. *Life* **2022**, *12*, 392. [CrossRef] [PubMed]
15. Chi, K.; Fu, R.H.; Huang, Y.C.; Chen, S.Y.; Hsu, C.J.; Lin, S.Z.; Tu, C.T.; Chang, L.H.; Wu, P.A.; Liu, S.P. Adipose-derived Stem Cells Stimulated with n-Butylidenephthalide Exhibit Therapeutic Effects in a Mouse Model of Parkinson's Disease. *Cell Transplant.* **2018**, *27*, 456–470. [CrossRef] [PubMed]
16. Carlson, K.B.; Singh, P.; Feaster, M.M.; Ramnarain, A.; Pavlides, C.; Chen, Z.L.; Yu, W.M.; Feltri, M.L.; Strickland, S. Mesenchymal stem cells facilitate axon sorting, myelination, and functional recovery in paralyzed mice deficient in Schwann cell-derived laminin. *Glia* **2011**, *59*, 267–277. [CrossRef]
17. Wang, L.; Zhao, Y.; Pan, X.; Zhang, Y.; Lin, L.; Wu, Y.; Huang, Y.; He, H. Adipose-derived stem cell transplantation improves learning and memory via releasing neurotrophins in rat model of temporal lobe epilepsy. *Brain Res.* **2021**, *1750*, 147121. [CrossRef]
18. Zhou, F.; Gao, S.; Wang, L.; Sun, C.; Chen, L.; Yuan, P.; Zhao, H.; Yi, Y.; Qin, Y.; Dong, Z.; et al. Human adipose-derived stem cells partially rescue the stroke syndromes by promoting spatial learning and memory in mouse middle cerebral artery occlusion model. *Stem Cell Res. Ther.* **2015**, *6*, 92. [CrossRef]
19. Ning, H.; Lin, G.; Lue, T.F.; Lin, C.S. Neuron-like differentiation of adipose tissue-derived stromal cells and vascular smooth muscle cells. *Differentiation* **2006**, *74*, 510–518. [CrossRef]
20. Langhans, S.A. Three-dimensional in vitro cell culture models in drug discovery and drug repositioning. *Front. Pharmacol.* **2018**, *9*, 6. [CrossRef]
21. Duval, K.; Grover, H.; Han, L.H.; Mou, Y.; Pegoraro, A.F.; Fredberg, J.; Chen, Z. Modeling Physiological Events in 2D vs. 3D Cell Culture. *Physiology* **2017**, *32*, 266–277. [CrossRef] [PubMed]
22. Edmondson, R.; Broglie, J.J.; Adcock, A.F.; Yang, L. Three-dimensional cell culture systems and their applications in drug discovery and cell-based biosensors. *Assay Drug Dev. Technol.* **2014**, *12*, 207–218. [CrossRef] [PubMed]
23. Benya, P.D.; Shaffer, J.D. Dedifferentiated chondrocytes reexpress the differentiated collagen phenotype when cultured in agarose gels. *Cell* **1982**, *30*, 215–224. [CrossRef] [PubMed]
24. Costa, E.C.; Moreira, A.F.; de Melo-Diogo, D.; Gaspar, V.M.; Carvalho, M.P.; Correia, I. 3D tumor spheroids: An overview on the tools and techniques used for their analysis. *Biotechnol. Adv.* **2016**, *34*, 1427–1441. [CrossRef]
25. Hongisto, V.; Jernstrom, S.; Fey, V.; Mpindi, J.P.; Kleivi Sahlberg, K.; Kallioniemi, O.; Perala, M. High-throughput 3D screening reveals differences in drug sensitivities between culture models of JIMT1 breast cancer cells. *PLoS ONE* **2013**, *8*, e77232. [CrossRef]
26. Engler, A.J.; Sen, S.; Sweeney, H.L.; Discher, D.E. Matrix elasticity directs stem cell lineage specification. *Cell* **2006**, *126*, 677–689. [CrossRef]
27. Hopkins, A.M.; De Laporte, L.; Tortelli, F.; Spedden, E.; Staii, C.; Atherton, T.J.; Hubbell, J.A.; Kaplan, D.L.J. Silk hydrogels as soft substrates for neural tissue engineering. *Adv. Funct. Mater.* **2013**, *23*, 5140–5149. [CrossRef]
28. Her, G.J.; Wu, H.C.; Chen, M.H.; Chen, M.Y.; Chang, S.C.; Wang, T.W. Control of three-dimensional substrate stiffness to manipulate mesenchymal stem cell fate toward neuronal or glial lineages. *Acta Biomater.* **2013**, *9*, 5170–5180. [CrossRef]
29. Li, Y.; Huang, G.; Li, M.; Wang, L.; Elson, E.L.; Lu, T.J.; Genin, G.M.; Xu, F. An approach to quantifying 3D responses of cells to extreme strain. *Sci. Rep.* **2016**, *6*, 19550. [CrossRef]
30. Gomila Pelegri, N.; Stanczak, A.M.; Bottomley, A.L.; Milthorpe, B.K.; Gorrie, C.A.; Padula, M.P.; Santos, J. Adipose-Derived Stem Cells Spontaneously Express Neural Markers When Grown in a PEG-Based 3D Matrix. *Int. J. Mol. Sci.* **2023**, *24*, 12139. [CrossRef]
31. Pelegri, N.G.; Milthorpe, B.K.; Gorrie, C.A.; Santos, J. Neurogenic marker expression in differentiating human adipose derived adult mesenchymal stem cells. *Stem Cell Investig.* **2023**, *10*, 7. [CrossRef] [PubMed]
32. Cooper, G. Cell proliferation in development and differentiation. In *The Cell: A Molecular Approach*, 2nd ed.; Sinauer Associates: Sunderland, MA, USA, 2000.
33. De Biasio, A.; Sánchez, R.; Prieto, J.; Villate, M.; Campos-Olivas, R.; Blanco, F.J. Reduced stability and increased dynamics in the human proliferating cell nuclear antigen (PCNA) relative to the yeast homolog. *PLoS ONE* **2011**, *6*, e16600. [CrossRef] [PubMed]

34. Folkman, J.; Moscona, A. Role of cell shape in growth control. *Nature* **1978**, *273*, 345–349. [CrossRef] [PubMed]
35. Baker, B.M.; Chen, C.S. Deconstructing the third dimension: How 3D culture microenvironments alter cellular cues. *J. Cell Sci.* **2012**, *125*, 3015–3024. [CrossRef]
36. Antoni, D.; Burckel, H.; Josset, E.; Noel, G. Three-dimensional cell culture: A breakthrough in vivo. *Int. J. Mol. Sci.* **2015**, *16*, 5517–5527. [CrossRef]
37. Kim, J.B. Three-dimensional tissue culture models in cancer biology. *Semin. Cancer Biol.* **2005**, *15*, 365–377. [CrossRef]
38. Gulati, A. Understanding neurogenesis in the adult human brain. *Indian J. Pharmacol.* **2015**, *47*, 583. [CrossRef]
39. UniProt. O75915·PRAF3_HUMAN. 2023. Available online: https://www.uniprot.org/uniprotkb/O75915/entry (accessed on 5 October 2023).
40. Jia, F.; Yue, M.; Chandra, D.; Keramidas, A.; Goldstein, P.A.; Homanics, G.E.; Harrison, N.L. Taurine is a potent activator of extrasynaptic GABAA receptors in the thalamus. *J. Neurosci.* **2008**, *28*, 106–115. [CrossRef]
41. Sturman, J.A. Taurine in development. *J. Nutr.* **1988**, *118*, 1169–1176. [CrossRef]
42. Xu, H.; Zhou, K.-Q.; Huang, Y.-N.; Chen, L.; Xu, T.-L. Taurine activates strychnine-sensitive glycine receptors in neurons of the rat inferior colliculus. *Brain Res.* **2004**, *1021*, 232–240. [CrossRef]
43. Zhou, Y.; Danbolt, N.C. Glutamate as a neurotransmitter in the healthy brain. *J. Neural Transm.* **2014**, *121*, 799–817. [CrossRef]
44. Pal, M.M. Glutamate: The master neurotransmitter and its implications in chronic stress and mood disorders. *Front. Hum. Neurosci.* **2021**, *15*, 722323. [CrossRef] [PubMed]
45. Crupi, R.; Impellizzeri, D.; Cuzzocrea, S. Role of metabotropic glutamate receptors in neurological disorders. *Front. Mol. Neurosci.* **2019**, *12*, 20. [CrossRef] [PubMed]
46. Siddique, I.; Kamble, K.; Gupta, S.; Solanki, K.; Bhola, S.; Ahsan, N.; Gupta, S. ARL6IP5 Ameliorates α-Synuclein Burden by Inducing Autophagy via Preventing Ubiquitination and Degradation of ATG12. *Int. J. Mol. Sci.* **2023**, *24*, 499. [CrossRef] [PubMed]
47. Vadodaria, K.C.; Brakebusch, C.; Suter, U.; Jessberger, S. Stage-specific functions of the small Rho GTPases Cdc42 and Rac1 for adult hippocampal neurogenesis. *J. Neurosci.* **2013**, *33*, 1179–1189. [CrossRef] [PubMed]
48. UniProt. P63000·RAC1_HUMAN. 2023. Available online: https://www.uniprot.org/uniprotkb/P63000/entry (accessed on 5 October 2023).
49. Gualdoni, S.; Albertinazzi, C.; Corbetta, S.; Valtorta, F.; de Curtis, I. Normal levels of Rac1 are important for dendritic but not axonal development in hippocampal neurons. *Biol. Cell* **2007**, *99*, 455–464. [CrossRef] [PubMed]
50. Li, X.; Serwanski, D.R.; Miralles, C.P.; Nagata, K.-i.; De Blas, A.L. Septin 11 is present in GABAergic synapses and plays a functional role in the cytoarchitecture of neurons and GABAergic synaptic connectivity. *J. Biol. Chem.* **2009**, *284*, 17253–17265. [CrossRef] [PubMed]
51. UniProt. Q9NVA2·SEP11_HUMAN. 2023. Available online: https://www.uniprot.org/uniprotkb/Q9NVA2/entry (accessed on 5 October 2023).
52. UniProt. P38606·VATA_HUMAN. 2023. Available online: https://www.uniprot.org/uniprotkb/P38606/entry (accessed on 6 October 2023).
53. UniProt. Q92597·NDRG1_HUMAN. 2023. Available online: https://www.uniprot.org/uniprotkb/Q92597/entry (accessed on 6 October 2023).
54. Duly, A.M.; Kao, F.C.; Teo, W.S.; Kavallaris, M. βIII-Tubulin Gene Regulation in Health and Disease. *Front. Cell Dev. Biol.* **2022**, *10*, 851542. [CrossRef]
55. Caccamo, D.; Katsetos, C.; Herman, M.; Frankfurter, A.; Collins, V.; Rubinstein, L. Immunohistochemistry of a spontaneous murine ovarian teratoma with neuroepithelial differentiation. Neuron-associated beta-tubulin as a marker for primitive neuroepithelium. *Lab. Investig.* **1989**, *60*, 390–398.
56. Jiang, Y.Q.; Oblinger, M.M. Differential regulation of beta III and other tubulin genes during peripheral and central neuron development. *J. Cell Sci.* **1992**, *103*, 643–651. [CrossRef]
57. Linhartová, I.; Dráber, P.; Dráberová, E.; Viklický, V. Immunological discrimination of β-tubulin isoforms in developing mouse brain. Post-translational modification of non-class-III β-tubulins. *Biochem. J.* **1992**, *288*, 919–924. [CrossRef] [PubMed]
58. Hausrat, T.J.; Radwitz, J.; Lombino, F.L.; Breiden, P.; Kneussel, M. Alpha-and beta-tubulin isotypes are differentially expressed during brain development. *Dev. Neurobiol.* **2021**, *81*, 333–350. [CrossRef] [PubMed]
59. UniProt. Q14195·DPYL3_HUMAN. 2023. Available online: https://www.uniprot.org/uniprotkb/Q14195/entry (accessed on 6 October 2023).
60. Deinhardt, K.; Kim, T.; Spellman, D.S.; Mains, R.E.; Eipper, B.A.; Neubert, T.A.; Chao, M.V.; Hempstead, B.L. Neuronal growth cone retraction relies on proneurotrophin receptor signaling through Rac. *Sci. Signal* **2011**, *4*, ra82. [CrossRef]
61. UniProt. Q16658·FSCN1_HUMAN. 2023. Available online: https://www.uniprot.org/uniprotkb/Q16658/entry (accessed on 7 October 2023).
62. Zhang, F.-R.; Tao, L.-H.; Shen, Z.-Y.; Lv, Z.; Xu, L.-Y.; Li, E.-M. Fascin expression in human embryonic, fetal, and normal adult tissue. *J. Histochem. Cytochem.* **2008**, *56*, 193–199. [CrossRef] [PubMed]
63. UniProt. Q7L576·CYFP1_HUMAN. 2023. Available online: https://www.uniprot.org/uniprotkb/Q7L576/entry (accessed on 7 October 2023).

64. Werner, B.; Yadav, S. Phosphoregulation of the septin cytoskeleton in neuronal development and disease. *Cytoskeleton* **2022**, *80*, 275–289. [CrossRef]
65. Xue, J.; Tsang, C.W.; Gai, W.P.; Malladi, C.S.; Trimble, W.S.; Rostas, J.A.; Robinson, P.J. Septin 3 (G-septin) is a developmentally regulated phosphoprotein enriched in presynaptic nerve terminals. *J. Neurochem.* **2004**, *91*, 579–590. [CrossRef]
66. Tsang, C.W.; Fedchyshyn, M.; Harrison, J.; Xie, H.; Xue, J.; Robinson, P.J.; Wang, L.-Y.; Trimble, W.S. Superfluous role of mammalian septins 3 and 5 in neuronal development and synaptic transmission. *Mol. Cell. Biol.* **2008**, *28*, 7012–7029. [CrossRef]
67. Kinoshita, A.; Shah, T.; Tangredi, M.M.; Strickland, D.K.; Hyman, B.T. The intracellular domain of the low density lipoprotein receptor-related protein modulates transactivation mediated by amyloid precursor protein and Fe65. *J. Biol. Chem.* **2003**, *278*, 41182–41188. [CrossRef]
68. May, P.; Herz, J. LDL receptor-related proteins in neurodevelopment. *Traffic* **2003**, *4*, 291–301. [CrossRef]
69. Gregorio, I.; Braghetta, P.; Bonaldo, P.; Cescon, M. Collagen VI in healthy and diseased nervous system. *Dis. Models Mech.* **2018**, *11*, dmm032946. [CrossRef]
70. Raasakka, A.; Kursula, P. The myelin membrane-associated enzyme 2′,3′-cyclic nucleotide 3′-phosphodiesterase: On a highway to structure and function. *Neurosci. Bull.* **2014**, *30*, 956–966. [CrossRef] [PubMed]
71. Funa, K.; Sasahara, M. The roles of PDGF in development and during neurogenesis in the normal and diseased nervous system. *J. Neuroimmune Pharmacol.* **2014**, *9*, 168–181. [CrossRef] [PubMed]
72. Sil, S.; Periyasamy, P.; Thangaraj, A.; Chivero, E.T.; Buch, S. PDGF/PDGFR axis in the neural systems. *Mol. Aspects Med.* **2018**, *62*, 63–74. [CrossRef] [PubMed]
73. Abe, T.K.; Tanaka, H.; Iwanaga, T.; Odani, S.; Kuwano, R. The presence of the 50-kDa subunit of dynactin complex in the nerve growth cone. *Biochem. Biophys. Res. Commun.* **1997**, *233*, 295–299. [CrossRef]
74. UniProt. Q13561·DCTN2_HUMAN. 2023. Available online: https://www.uniprot.org/uniprotkb/Q13561/entry (accessed on 7 October 2023).
75. Neel, D.V.; Basu, H.; Gunner, G.; Bergstresser, M.D.; Giadone, R.M.; Chung, H.; Miao, R.; Chou, V.; Brody, E.; Jiang, X.; et al. Gasdermin-E mediates mitochondrial damage in axons and neurodegeneration. *Neuron* **2023**, *111*, 1222–1240.e1229. [CrossRef]
76. Patron, M.; Sprenger, H.-G.; Langer, T. m-AAA proteases, mitochondrial calcium homeostasis and neurodegeneration. *Cell Res.* **2018**, *28*, 296–306. [CrossRef]
77. Li, Z.; Qiu, D.-h.; Liu, H.-Y.; Lei, Q.-F. Analysis of the nicastrin promoter rs10752637 polymorphism and its association with Alzheimer's disease. *Eur. J. Neurosci.* **2009**, *30*, 1831–1836.
78. Rao, S.S.; Winter, J.O. Adhesion molecule-modified biomaterials for neural tissue engineering. *Front. Neuroeng.* **2009**, *2*, 6. [CrossRef]
79. Krishnan, U.M. Biomaterials in the treatment of Parkinson's disease. *Neurochem. Int.* **2021**, *145*, 105003. [CrossRef]
80. Shah, A.D.; Goode, R.J.; Huang, C.; Powell, D.R.; Schittenhelm, R.B. LFQ-analyst: An easy-to-use interactive web platform to analyze and visualize label-free proteomics data preprocessed with MaxQuant. *J. Proteome Res.* **2019**, *19*, 204–211. [CrossRef]

# Chapter Six: Concluding remarks and Future Directions.

## 6.1. Conclusions

Neurological disorders account for over 9 million deaths per annum globally and are the leading cause of disability and death worldwide [1-3]. Despite significant efforts to understand and treat the different disorders, most remain poorly understood, incurable and difficult to treat [4-6]. These treatment difficulties can be attributed to the limited self-repair capacity of the nervous system as well as its complex and inaccessible nature, with research translation being limited by the lack of more representative nervous system models to test treatments and better understand disease [7-9]. Traditional 2D tissue culture has been one of the more widely used techniques to understand cell interactions and test drugs; however, it has proven not to be representative of *in vivo* conditions as the cell architecture and arrangement are far from that of the tissue of origin [10-12]. Tissue engineering and 3D tissue culture offer a new avenue to research neurological conditions in environments that better mimic the brain [13]. ADSCs have previously been identified as a suitable candidate to create models to further understand nervous system disorders as well as potential therapeutics for neuroregeneration, given their neurogenic differentiation potential and their sourcing ease [14-16].

In this project, a new model to differentiate ADSCs towards neural lineage in 3D culture was tested based on our hypothesis that ‘ADSCs will show enhanced neural differentiation in 3D environments that mimic neural tissue stiffness, and that differentiation will be enhanced by the addition of neural growth supplements in the 3D environments’.

Prior to creating 3D models, **Chapter Two** explored the effects of commercially available neural support supplements B27, C1 and N2 on hADSCs. Cells were to be treated for 42 days using those supplements, however, due to the cells lifting

from the 2D plastic surfaces, downstream analysis was only able to be performed on the cells treated for 7 days. The neural differentiation potential of those treatments over 7 days was then assessed using cell morphology, immunocytochemistry, cytokine analysis and a CNPase functional assay. The results showed that even at a short time frame of 7 days, cells treated with C1 and N2 showed significant changes in neural marker expression, with C1 expressing high levels of functional CNPase, while B27 did not show significant changes in the same period of time. This chapter reiterated the need for more robust tissue culture models that better support cells undergoing neural differentiation, as exemplified by the cell monolayer lifting, and confirmed that B27, C1 and N2 should be further explored as potential neural differentiation mixtures.

Chapter Two has been published and can be found here:
https://www.ncbi.nlm.nih.gov/pmc/articles/PMC10076228/
*Pelegri NG, Milthorpe BK, Gorrie CA, Santos J. Neurogenic marker expression in differentiating human adipose derived adult mesenchymal stem cells. Stem Cell Investigation 2023 Mar 23;10:7. doi: 10.21037/sci-2022-015. PMID: 37034185; PMCID: PMC10076228.*

**Chapter three** sought to develop a more suitable environment to further assess neural differentiation of hADSCs using those treatments. The use of GelMa, a commonly used biomaterial, was explored as a matrix to create a 3D model to mimic the brain environment to assess ADSCs neural differentiation. However, GelMa matrix experiments were not able to reproduce what appears in the published literature, and therefore the work moved on to use other 3D matrices that proved to be much more successful and user-friendly.

**Chapter four** explored the suitability of a PEG-based 3D matrix as a model to mimic the brain environment. The model was developed using the RASTRUM bioprinter (Inventia, Sydney, Australia), where RGB and YIGSR peptides, a feature of the mammalian extracellular matrix, were added to the matrix for cell

adhesion, and the cell/matrix printed at a 1.1kPa stiffness. Cells were maintained in the gel for 14 days, and cell morphology, viability, proteome changes and immunocytochemistry neural marker expression were assessed. Results showed that cells continued to proliferate over time, meaning the matrix did not negatively impact cell health. Furthermore, cells showed significant cytoskeletal changes, with the morphological and proteome changes suggesting that the cells started to form dendrites and axons. CNPase was also detected in the cells, further suggesting the initiation of neural differentiation of the cells by the 3D environment alone. The findings of this chapter are promising and suggest that PEG-based hydrogels with RGB and YIGSR peptides at 1.1kPa are a 3D model worth further investigating for neural differentiation of hADSCs.

The work that resulted from chapter four has been published in the International Journal of Molecular Sciences and received the paper of the month award at UTS Science faculty. It can be found here:
https://www.mdpi.com/1422-0067/24/15/12139
*Gomila Pelegri, N.; Stanczak, A.M.; Bottomley, A.L.; Milthorpe, B.K.; Gorrie, C.A.; Padula, M.P.; Santos, J. Adipose-Derived Stem Cells Spontaneously Express Neural Markers When Grown in a PEG-Based 3D Matrix. Int. J. Mol. Sci. 2023, 24, 12139. https://doi.org/10.3390/ijms241512139*

**Chapter 5** followed on from the findings in Chapter 4 and explored the combination of the PEG-based 3D matrix developed in Chapter 4 together with the neural support supplements B27, C1 and N2 used in Chapter 2 to assess the differentiation potential of the combined 3D environment and chemical environment on hADSCs. Cells were grown for a total of 10 days and treated for 7 days with B27, C1 and N2, similarly to Chapter 2. Following cell culture, cell morphology, viability, proteome changes and immunocytochemistry of neural marker expression were assessed using similar methodologies used in Chapter 4. Results showed that B27 and C1 supplements further enhanced neural differentiation of the ADSCs and pushed them down neuronal pathways.

The work that resulted from chapter five has been published to the International Journal of Molecular Sciences. It can be found here:
https://www.mdpi.com/2558502
*Gomila Pelegri, N.; Stanczak, A.M.; Bottomley, A.L.; Cummins, M.L.; Milthorpe, B.K.; Gorrie, C.A.; Padula, M.P.; Santos, J. Neural Marker Expression in Adipose-Derived Stem Cells Grown in PEG-Based 3D Matrix Is Enhanced in the Presence of B27 and CultureOne Supplements. Int. J. Mol. Sci. 2023, 24, 16269. https://doi.org/10.3390/ijms242216269*

In conclusion, this thesis details proof of concept experiments that identified and assessed potential 3D matrices suitable to create more physiologically relevant models for the neural differentiation of hADSCs. The results suggest that PEG-based hydrogels with RGB and YIGSR at 1.1kPa, combined with commercially available neural supplements B27, C1 and N2, are a promising model for neural differentiation of hADSCs. While additional research needs to be conducted to further confirm the suitability of this model as a neural differentiation model for ADSCs, the results presented in this dissertation show that it is an area of research worth further attention.

## 6.2. Limitations and Future Directions

There are various future directions that need to be explored for this research to become more robust and overcome some of the limitations encountered in this project.

Firstly, experiments to maintain the differentiating ADSCs in the 3D PEG-based matrix with and without treatments should be conducted for longer periods of time. Due to the difficulties encountered in Chapter 3 when exploring GelMa hydrogels, time constraints and limitations in resources became a drawback in this project, and biological time frames were not reflected appropriately. Cortical neurogenesis in the human brain takes up to 108 embryonic days [17]. GABAergic neurons formed from ESCs protocols are run from 20 days [18] to

over two months for oligodendrocytes, astrocytes and glial cells [19]. However, ADSCs differentiation protocols in 2D range between 7 to 14 days only [20-25] showing the need for longer experiments in more suitable environments. It is certain that cells will show a different phenotype if left for longer and that the ultimate fate of the cells can be determined, with the potential for different cells to differentiate down different lineages, which should be further explored in future research.

Ideally, Chapter 4 and 5 experiments should be conducted for up to 42 days, similar to what was conducted for Chapter 2, if not more, given the time required for cells to differentiate. Furthermore, during the treatment course, multiple time points should be included where cell viability via Alamar blue, live/dead cell staining, proteomics and immunocytochemistry analyses are performed. For example, cells should be grown for up to 42 days and analysed at 7 days, 14 days, 30 days, and 42 days. This would give better insight into the effects of the matrix alone on the cells as well as better assess the supplements' role in enhancing neural differentiation.

Additionally, the PEG-based matrix could be further modified to include more of the now available peptides to better mimic the brain ECM. Some examples that could be added and are available via Rastrum are hyaluronic acid, a key component of the brain ECM [26], GFOGER as a biomimetic component for collagens and known part of the brain ECM [27, 28], as well as Fibronectin and IKVAV given the role of fibronectin and laminin in the brain ECM [27, 29, 30]. These would need to be optimised and used in combination as well as individually to conclude which matrix would be ultimately the best to direct ADSCs differentiation towards neural cells.

Treatment-wise, it may be interesting to explore the supplements in combination, given that different supplements support different cells. C1 is designed to support the differentiation of neural stem cells (NSCs) to neurons [31], while B27 and N2 are designed to support mature cells [32, 33]. It would be interesting to see if

combining, for example, C1 and N2 would provide an environment that better supports heterogeneous growth rather than one with homogeneous cell growth.

To better phenotype the cells, using more immunocytochemistry markers at each time point, as well as including functional assays, would allow for a more robust assessment of the cell differentiation stages. Immunocytochemistry markers that could be included to further assess the different cell lineage as well as cell differentiation stages are Nestin, NCAM, NeuN, Double cortin, NeuroD1, PDGFR alpha, OSP, SOX10, Olig2, EAAT1, EAAT2.

Furthermore, as technology matures, it would also be interesting to examine individual cellular phenotypes within the hydrogel and at a proteomic level [34]. This would answer questions such as:

- Are all the ADSCs becoming the same cell type?
- Are cells differentiating towards multiple cell populations?
- Are all cells at the same stage of differentiation?

Single-cell proteomics would allow exploration of these questions. Single-cell transcriptomics would also be a useful tool to assess what individual cellular phenotypes; however, it should be companioned with proteomics to examine the mature proteome of those cells [35]. Targeted proteomics would also be useful as it offers an alternative method to detect protein groups and proteoforms of interest with high sensitivity, quantitative accuracy and reproducibility [36, 37], making the data more specific.

Additionally, to properly assess hADSCs differentiation and neural similarity, the use of normal brain cell lines as positive controls would be highly desirable instead of using cancer cell lines. Healthy human brain tissue and cells are hard to source and expensive. However, it would still be beneficial to include them in future research to properly assess the degree of differentiation of ADSCs and their similarity to the native tissue.

Another important challenge to mention is the difficulties faced when adapting 2D analysis methods to 3D models. An example is live imaging performed during the duration of the experiment. Many microscopes could not be used due to the objective working distance, and the ones that were able to be utilised had to be used at low magnification, meaning that getting high-resolution live cell images was not possible. Additionally, we also encountered significant challenges in conducting immunocytochemistry imaging. The biggest barrier to data interpretation has been the inability to get high-quality microscopy images using traditional imaging techniques and staining techniques. It seems to be apparent that antibodies diffuse poorly through the matrices, creating difficulty in removing any unbound antibody and causing speckling in the images. Inventia Life Sciences does not provide the pore size of the gels (proprietary information), making it hard to know what the best solution for this would be. A potential solution would be using mass spectrometry imaging techniques to maintain spatial organisation and overcome antibody labelling issues, given its ability to image thousands of molecules and maintain spatial distribution without labelling [38]. This would require sequential sectioning for imaging and then in silico reconstruction of the 3D image. Another option would be retrieving the gels, slicing them, staining them using immunohistochemistry and reconstructing the plug afterwards. However, for this thesis, we wanted to explore the cells within their 3D environment as much as possible. Tissue clearing and light sheet microscopes are also alternative options worth exploring if one wants to assess the entire plug. Unfortunately, we did not have access to that technology at the time.

During immunocytochemistry imaging, interference from out-of-plane light also made data analysis more complicated, and data storage also became a challenge; when we imaged in Z-stacks, the imaging files went from 2-3 GBs each to over 10GB per replicate, making it difficult for everyday computers to open the files, let alone analyse the data.

Lastly, it is worth mentioning that while the 3D modelling that has been used in this research was to specifically investigate hADSCs neural differentiation potential, other researchers could apply these condition to iPSC or other cell types in the future.

## 6.3. Significance

My research has furthered our understanding of hADSCs and their potential for growth and neural differentiation in 3D environments, which is the first step in using hADSCs in the autologous treatment of neurological conditions. While well outside the scope of the current project, the potential applications of these strategies for regenerative medicine have a bright future.

## 6.4. References


1. Carroll, W.M., *The global burden of neurological disorders.* The Lancet. Neurology, 2019. **18**(5): p. 418-19.
2. Feigin, V.L., et al., *Global, regional, and national burden of neurological disorders, 1990–2016: a systematic analysis for the Global Burden of Disease Study 2016.* The Lancet. Neurology, 2019. **18**(5): p. 459-80.
3. Feigin, V.L., et al., *The global burden of neurological disorders: translating evidence into policy.* The Lancet. Neurology, 2020. **19**(3): p. 255-65.
4. Organization, W.H. *Mental Health: Neurological disorders*. 2016 May 2016 [cited 2018 21st of October]; Available from: http://www.who.int/features/qa/55/en/.
5. Organization, W.H., *Neurological disorders: public health challenges*. 2006: World Health Organization.
6. Hopkins, A.M., et al., *3D in vitro modeling of the central nervous system.* Progress in neurobiology, 2015. **125**: p. 1-25.
7. Pankevich, D.E., et al., *Improving and accelerating drug development for nervous system disorders.* Neuron, 2014. **84**(3): p. 546-53.
8. Wegener, G. and D. Rujescu, *The current development of CNS drug research.* The international journal of neuropsychopharmacology, 2013. **16**(7): p. 1687-93.
9. Hongisto, V., et al., *High-throughput 3D screening reveals differences in drug sensitivities between culture models of JIMT1 breast cancer cells.* PLoS One, 2013. **8**(10): p. e77232.
10. Duval, K., et al., *Modeling Physiological Events in 2D vs. 3D Cell Culture.* Physiology, 2017. **32**(4): p. 266-77.
11. Antoni, D., et al., *Three-dimensional cell culture: a breakthrough in vivo.* International Journal of Molecular Sciences, 2015. **16**(3): p. 5517-27.

12. Muncie, J.M. and V.M. Weaver, *The Physical and Biochemical Properties of the Extracellular Matrix Regulate Cell Fate.* Current topics in developmental biology, 2018. **130**: p. 1-37.
13. Baker, B.M. and C.S. Chen, *Deconstructing the third dimension: how 3D culture microenvironments alter cellular cues.* Journal of Cell Science, 2012. **125**(13): p. 3015-24.
14. Jang, S., et al., *Functional neural differentiation of human adipose tissue-derived stem cells using bFGF and forskolin.* BMC Cell Biology, 2010. **11**: p. 25.
15. Park, J., et al., *Small molecule-based lineage switch of human adipose-derived stem cells into neural stem cells and functional GABAergic neurons.* Scientific reports, 2017. **7**(1): p. 10166.
16. Wislet-Gendebien, S., et al., *Astrocytic and neuronal fate of mesenchymal stem cells expressing nestin.* Brain research bulletin, 2005. **68**(1-2): p. 95-102.
17. Gulati, A., *Understanding neurogenesis in the adult human brain.* Indian Journal of Pharmacolgy, 2015. **47**(6): p. 583-4.
18. Addae, C., et al., *All-trans-retinoid acid induces the differentiation of encapsulated mouse embryonic stem cells into GABAergic neurons.* Differentiation, 2012. **83**(5): p. 233-241.
19. Hu, B.-Y., et al., *Neural differentiation of human induced pluripotent stem cells follows developmental principles but with variable potency.* Proceedings of the National Academy of Sciences, 2010. **107**(9): p. 4335-4340.
20. Ahmadi, N., et al., *Stability of neural differentiation in human adipose derived stem cells by two induction protocols.* Tissue Cell, 2012. **44**(2): p. 87-94.
21. Soheilifar, M.H., et al., *Generation of Dopamine-Secreting Cells from Human Adipose Tissue-Derived Stem Cells In Vitro.* Rejuvenation Res, 2018. **21**(4): p. 360-368.
22. Faghih, H., et al., *Directed differentiation of human adipose tissue-derived stem cells to dopaminergic neurons in low-serum and serum-free conditions.* Neurosci Lett, 2019. **708**: p. 134353.
23. Lo Furno, D., et al., *Neural differentiation of human adipose-derived mesenchymal stem cells induced by glial cell conditioned media.* Journal of Cellular Physiology, 2018. **233**(10): p. 7091-7100.
24. Cardozo, A.J., D.E. Gómez, and P.F. Argibay, *Neurogenic differentiation of human adipose-derived stem cells: Relevance of different signaling molecules, transcription factors, and key marker genes.* Gene, 2012. **511**(2): p. 427-436.
25. Selaru, A., S. Dinescu, and M. Costache, *The cellular and molecular patterns involved in the neural differentiation of adipose-derived stem cells.* Cell Biology and Translational Medicine, Volume 10: Stem Cells in Tissue Regeneration, 2020: p. 23-41.
26. Bignami, A., M. Hosley, and D. Dahl, *Hyaluronic acid and hyaluronic acid-binding proteins in brain extracellular matrix.* Anatomy and embryology, 1993. **188**(5): p. 419-433.

27. Morwood, A.J., et al., *The Role of Extracellular Matrix (ECM) Adhesion Motifs in Functionalised Hydrogels.* Molecules, 2023. **28**(12).
28. Lam, D., et al., *Tissue-specific extracellular matrix accelerates the formation of neural networks and communities in a neuron-glia co-culture on a multi-electrode array.* Scientific Reports, 2019. **9**(1): p. 4159.
29. Patel, R., et al., *Ile-Lys-Val-ala-Val (IKVAV) peptide for neuronal tissue engineering.* Polymers for Advanced Technologies, 2019. **30**(1): p. 4-12.
30. Song, I. and A. Dityatev, *Crosstalk between glia, extracellular matrix and neurons.* Brain research bulletin, 2018. **136**: p. 101-108.
31. Scientific, T.F. *CultureOne™ Supplement (100X)*. 2023 [cited 2023 10th October]; Available from: https://www.thermofisher.com/order/catalog/product/A3320201.
32. Scientific, T.F. *B-27™ Supplement (50X), serum free*. 2023 [cited 2023 10th October]; Available from: https://www.thermofisher.com/order/catalog/product/17504044.
33. Scientific, T.F. *N-2 Supplement (100X)*. 2023 [cited 2023 10th October]; Available from: https://www.thermofisher.com/order/catalog/product/17502048.
34. Vistain, L.F. and S. Tay, *Single-cell proteomics.* Trends in biochemical sciences, 2021. **46**(8): p. 661-672.
35. Kulkarni, A., et al., *Beyond bulk: a review of single cell transcriptomics methodologies and applications.* Current opinion in biotechnology, 2019. **58**: p. 129-136.
36. Borràs, E. and E. Sabido, *What is targeted proteomics? A concise revision of targeted acquisition and targeted data analysis in mass spectrometry.* Proteomics, 2017. **17**(17-18): p. 1700180.
37. Marx, V., *Targeted proteomics.* Nature methods, 2013. **10**(1): p. 19.
38. Buchberger, A.R., et al., *Mass Spectrometry Imaging: A Review of Emerging Advancements and Future Insights.* Analytical Chemistry, 2018. **90**(1): p. 240-265.